

Modelling, Simulation, and Optimisation of Reverse Osmosis Process with Application in Wastewater Treatment and Food Processing

Item Type	Thesis
Authors	Al-Obaidi, Mudhar A.A.R.; Al-Obaidi, Mudhar A.A.R.
Publisher	University of Bradford
Rights	<pre> The University of Bradford theses are licenced under a Creative Commons Licence.</pre>
Download date	03/05/2022 00:05:09
Link to Item	http://hdl.handle.net/10454/17345

Modelling, Simulation, and Optimisation of Reverse Osmosis Process with Application in Wastewater Treatment and Food Processing

Investigates Reverse Osmosis processes for separating toxic contaminant from wastewater and for concentrating fruit juices under different design and operating conditions using modelling, simulation and optimisation techniques.

MAA. AI-OBAIDI

BSc Chem. Eng., MSc Chem. Eng.
Submitted for the Degree of
Doctor of Philosophy

Chemical Engineering, School of Engineering, Faculty of Engineering, and Informatics.

University of Bradford

United Kingdom

2018

Modelling, Simulation, and Optimisation of Reverse Osmosis Process with Application in Wastewater Treatment and Food Processing Mudhar A. Alwahab Rajib Al-Obaidi

Key words: Wastewater Treatment; Spiral Wound Module; Distributed Modeling; Simulation; Optimisation; Parameter Estimation; Energy Consumption; Phenolic and N-nitrosamine; Apple Juice Concentration.

Abstract

Reverse Osmosis (RO) is a membrane-based separation process applied in several industrial and food processing applications. In this research, performance of RO process is investigated in respect of two applications (a) wastewater treatment (b) concentration fruit juices using model-based techniques. For this purpose, a number of models (both 1 and 2-dimensional steady state and dynamic) for spiral wound RO process are developed based on Solution-Diffusion model and Irreversible Thermodynamic model. The models are validated against actual experimental data reported in the literature before being used in further simulation and optimisation studies for both wastewater treatment and fruit juice concentration. Wastewater effluents of many industrial applications contain a variety of micro-pollutants and highlytoxic compounds, which are released into a variety of water resources. Such pollutants not only disrupt the biological ecosystem, but they also pose a real threat to the water supply for human consumption and to the aquatic ecosystems. The earlier chapters of the thesis evaluate the performance of RO process in terms of removal efficiency of toxic compounds such as chlorophenol, N-nitrosamine, etc. from wastewater. The effect of several operating parameters such as feed pressure, concentration, flow rate and temperature, on the performance of RO process are evaluated. Also, suitability of a number of different RO configurations for efficient removal of toxic compounds are evaluated. For example, (a) two-stage/two-pass RO design synthesis of RO network for the removal of chlorophenol (b) multistage multipass RO process with and without energy recovery option for the removal of N-nitrosamine are investigated. The dynamic response of the RO process for step changes in the operating parameters is investigated for the removal of phenolic compounds. Finally, in the context of wastewater treatment, a case study with multi compounds contaminants is suggested where a multiobjective optimisation problem has achieved the optimum rejection of all the compounds and recovery rate. In respect of food processing, RO has been considered as a prominent process in fruit juice concentration due to its ability to effectively retain the flavour, sensory, aroma and nutritional characteristics and concentrate the juice. This research elucidates one example of apple juice concentration process and focuses on highlighting successful modelling and optimisation methodology. This in turn provides an efficient method of RO process for concentrating apple juice by improving the reliability and efficiency of the underlying separation and concentration process.

Acknowledgment

I would like to express my deepest appreciation to my supervisors Professor Iqbal M. Mujtaba and Dr. Chakib Kara-Zaïtri who have given of their time and consideration in helping and encouraging me carry out this research.

Special thanks to my Iraqi Government and especially the Ministry of High Education and Scientific Research for their funding of my PhD journey based on their premium program of scholarships.

On top of that, I want to warmly dedicate this work to my father and mother for all their unlimited love, and consistent support from birth to this hour and for their strong belief in me. Without them this thesis would never have been possible. Also, my profound thanks to my wife for her assistance, encouragement, patience, love, and prayers for my progress. My special gratitude also goes out to my daughters Malak and Tiba who have made my life full of excitement, contentment, and pleasure. Lastly, my sincere thanks to my brothers, sisters, and friends as well as anyone who have helped me in one way or another during my PhD study.

Table of contents

Abstract	ii
Acknowledgment	. iii
Table of contents	. iv
List of Tables	xvi
Nomenclaturex	viii
Chapter 1	1
Introduction	1
1.1 Reverse Osmosis (RO) process	1
1.2 Measurement of RO process performance	2
1.3 Types of RO membrane modules	2
1.3.1 Spiral wound	3
1.4 Limitations of RO membrane process	5
1.4.1 Concentration polarisation theory	5
1.4.2 Membrane fouling	6
1.5 Application of RO in wastewater treatment	6
1.5.1 The origin of wastewater	7
1.5.2 Importance and applications of reuse water	7
1.5.3 Wastewater and associated challenges	8
1.6 Pollutants	9
1.6.1 Phenolic compounds	9
1.6.2 N-nitrosamine	10
1.7 Rationale for selection the RO process in wastewater treatment	. 11
1.8 Application of RO in food industries	. 13
1.9 Scope of this research	. 14
1.12 Research aim and objectives	. 15
1 12 1 Aim of research	15

1.12.2 Objectives of research	
1.13 Thesis outline 17	
Chapter 2 19	
Literature Review 19	
2.1 Introduction	
2.2 Feasibility of RO process in wastewater 19	
2.3 Phenolic compounds21	
2.4 N-nitrosamine compounds22	
2.5 Experimentation of RO wastewater treatment process 24	
2.5.1 Phenolic compounds	
2.5.2 N-nitrosamine compounds	
2.6 Feasibility of RO process in apple juice concentration	
2.7 Experimentation of RO apple juice concentration	
2.8 Modelling of RO process	
2.8.1 Steady state and dynamic modelling31	
2.8.2 Membrane transport theories	
2.8.3 Overview of the spiral wound RO modelling34	
2.8.4 Modelling of spiral wound RO based on phenolic and N-nitrosamine	
compounds37	
2.8.5 Overview of the spiral wound RO modelling of phenolic and N-	
nitrosamine compounds 40	
2.8.6 Modelling of spiral wound RO based apple juice concentration 41	
2.8.7 Overview of the spiral wound RO modelling of apple juice concentration	
2.9 RO performance enhancements	
2.9.1 Operating parameters43	
2.9.2 RO energy consumption45	
2.9.3 Multi-stage and multi-pass RO design	

2.9.4 Simulation of apple juice concentration by spiral wound RO p	process
	47
2.9.5 Enhancement of apple juice concentration process	47
2.10 Conclusions	49
Chapter 3	50
Spiral Wound Reverse Osmosis Process Modelling and Validation	n 50
3.1 Introduction	50
3.2 Solution diffusion model	51
3.2.1 Distributed models	51
3.2.2 Lumped models	72
3.3 Irreversible thermodynamic model	78
3.3.1 Distributed models	78
3.4 Mass transfer equations of organic compounds	84
3.4.1 Chlorophenol and dimethylphenol	84
3.4.2 N-nitrosamine	85
3.5 The physical properties equations	85
3.6 RO models for apple juice concentration process	86
3.6.1 Distributed model	86
3.6.2 Lumped model	98
3.7 gPROMS software for modelling, simulation and optimisation	102
3.7.1 gPROMS model builder platform	102
3.8 Simulation solver	105
3.9 Parameter estimation	106
3.10 Model validation	108
3.11 Optimisation	109
3.11.1 NLP solution technique	109
2.11 Conclusions	110

Chapter 4	111
Removal of Chlorophenol from Wastewater: Steady State Simulation	
4.1 Introduction	111
4.2 Case 1: Sensitivity analysis of the operating parameters	111
4.2.1 Effect of operating parameters on the spiral wound RO proceperformance	
4.3 Case 2: Simulation and optimisation of a two-stage/two-pass sp wound RO process	
4.3.1 Description of the two stage/two pass RO process	118
4.3.2 Simulation of the two Stage/two pass spiral wound RO process	119
4.3.3 Optimisation of the two-stage/two-pass spiral wound process	
4.4 Conclusions	122
Chapter 5	124
Removal of Dimethylphenol from Wastewater: Dynamic Simulation	124
5.1 Introduction	124
5.2 Dynamic simulation	124
5.2.1 The inlet feed pressure	125
5.2.2 The inlet feed flow rate	129
5.2.3 The inlet feed concentration	134
5.2.4 The inlet feed temperature	137
5.3 Conclusions	139
Chapter 6	141
Removal of N-Nitrosamine from Wastewater: Simulation, Netwo	
Design, and Optimisation	141
6.1 Introduction	141

6.2 Case 1: Simulation of spiral wound RO process for the removal of N-
nitrosamine from wastewater 141
6.2.1 Proposed spiral wound RO configuration
6.2.2 Model equations
6.2.3 Simulation: Effect of operating parameters
6.2.4 Process optimisation
6.3 Case 2: Performance evaluation of multi-stage and multi pass RO networks for the removal of N-nitrosodimethylamine (NDMA) from wastewater
6.3.1 Modelling of a spiral wound RO process
6.3.2 Multi-stage (retentate reprocessing) spiral wound RO networks description
6.3.3 Multi pass (permeate reprocessing) RO networks description 166
6.3.4 Predictive permeate reprocessing multi pass RO process design
6.3.5 Optimisation of predictive multi pass permeate reprocessing RO process design
6.4 Conclusions 177
Chapter 7 179
Simultaneous Removal of Organic and Non-organic Compounds from Wastewater Using RO Process: Modelling, Simulation, and Optimisation
7.1 Introduction
7.3 Process simulation: Effect of operating parameters 180
7.4 Process optimisation 184
7.5 Conclusions 185
Chapter 8 186
Applications of Spiral Wound Reverse Osmosis for the Apple Juice
Concentration: Simulation, and Optimisation

8.1 Introduction	186
8.2 Case 1: Analysis the apple juice concentration using a spi	ral wound
RO process	186
8.2.1 Impact of operating parameters	187
8.3 Case 2: Optimum design of a multi-stage spiral wound RO) process
for the production of highly concentrated apple Juice	189
8.3.1 Apple juice concentration plant description	190
8.3.2 Optimisation technique	192
8.3.3 Analysing the impact of operating parameters on th	e product
concentration	195
8.4 Conclusions	201
Chapter 9	202
Conclusions and Recommendations for Future Research	202
9.1 Conclusions	202
9.2 Recommendations for future research	206
References	208
Appendix (A)	a
List of publications out of the author's PhD project	L

List of Figures

Fig. 1.1. Scenario A: Osmosis, Scenario B: Osmotic Equilibrium and Scenario
C: Reverse Osmosis
Fig. 1.2. Schematic configuration of the spiral wound module (Adapted from:
https://www.complete-water.com/reverse-osmosis-theory-of-operation) 3
4
Fig. 1.3. Schematic diagram of the spiral wound membrane module and flow
directions4
Fig. 1.4. Schematic diagram of concentration polarisation theory 6
Fig. 2.1. Schematic diagram of an individual RO process (Adapted from
Srinivasan et al. (2011))
Fig. 2.2. Schematic diagram of full-scale three elements RO plant 28
Fig. 2.3. Schematic diagram of full-scale seven elements RO plant 28
Fig. 3.1. The model validation results
Fig. 3.2. Comparison of theoretical and experimental values of [a: Retentate
flow rate, b: Permeate flow rate, c: Retentate pressure, d: Total permeate
recovery and e: Dimethylphenol rejection]76
Fig. 3.3. Observed and modeled feed pressure versus the membrane length
for three different average permeate fluxes (initial conditions of NDMA,
3.3761x10 ⁻⁹ kmol/m³, 2.43x10 ⁻³ m³/s, and 20 °C)
Fig. 3.4. Observed and modeled average permeate flux and retentate flow rate
versus inlet feed pressure (initial conditions, $3.3761x10^{-9}$ kmol/m³, $2.43x10^{-3}$
m³/s, and 20 °C)
Fig. 3.5. Experimental and modelled rejections of eight N-nitrosamine solutes
at three average permeate fluxes of (2.78x10 $^{-6}$, 5.56x10 $^{-6}$ and 8.33x10 $^{-6}$ m/s)
(initial conditions, $2.43x10^{-3}$ m³/s and 20 °C)
Fig. 3.6. Experimental and model rejections of the two selected aroma
compounds versus average operating temperature for two different inlet feed
flow rates at inlet conditions (°Brix = 10.5, TMP = 34.542 atm) 96
Fig. 3.7. Experimental and model Isopentyl acetate rejection versus operating
trans-membrane pressure for three different inlet feed flow rates at inlet
conditions (°Brix = 10.5, Tb = 20 °C)

Fig. 3.8. Experimental and model outlet water flux versus operating trans-
membrane pressure for two different inlet feed flow rates at inlet conditions
(°Brix = 10.5, Tb = 20 °C)
Fig. 3.9. Experimental and model retentate flow rate versus operating trans-
membrane pressure for three different inlet feed flow rates at inlet conditions
(°Brix = 10.5, Tb = 20 °C)
Fig. 3.10. Experimental and predicted aroma compounds rejection at inlet
conditions (°Brix = 10.5, Tb = 20 °C, TMP = 34.542 atm, Fb(0) = 1.6667x10 $-$
4 m³/s)
Fig. 3.11. Screenshot of the project entities for the gPROMS 104
Fig. 3.12. Screenshot of the model entity
Fig. 3.13. Screenshot of the optimisation entity
Fig. 4.1. Steady state feed flow rate along the membrane length of different
inlet feed flow rates (inlet feed conditions, $2.335 \times 10^{-3} \text{ kmol/m}^3$, 7.77 atm , and
32 °C)
Fig. 4.2: Steady state feed concentration along the membrane length of
different inlet feed flow rates (inlet feed conditions, 2.335x10 ⁻³ kmol/m³, 7.77
atm, and 32 °C)
Fig. 4.3. Steady state total water recovery along the membrane length of
different inlet feed flow rates (inlet feed conditions, 6.226x10 ⁻³ kmol/m3, 13.58
atm, and 31 °C)113
Fig. 4.4. Steady state solute rejection versus inlet feed flow rates of different
inlet feed pressures (inlet feed conditions, 6.226x10 ⁻³ kmol/m³, and 31
°C)114
Fig. 4.5. Steady state total water recovery versus inlet feed pressures of
different inlet feed concentrations (inlet feed conditions, 2.583x10 ⁻⁴ m³/s, and
32 °C)
Fig. 4.6. Steady state average permeate concentration versus inlet feed
pressures of different inlet feed concentrations (inlet feed conditions 2.583x10
⁴ m³/s and 32 °C)
Fig. 4.7. Steady state solute rejection versus inlet feed temperatures of
different inlet feed pressures (inlet feed conditions, 2.335x10 ⁻³ kmol/m³ and
2.166x10 ⁻⁴ m ³ /s)

Fig. 4.8. Steady state membrane solute rejection intensity versus inlet feed
concentrations of different points along the membrane length (inlet feed
conditions, 2.166x10 ⁻⁴ m ³ /s, 11.64 atm, and 32 °C)
Fig. 4.9. Steady state solute rejection versus inlet feed concentrations of
different inlet feed pressures (inlet feed conditions, 2.166x10 ⁻⁴ m³/s, and 31
°C)117
Fig. 4.10. Schematic diagram of the proposed two-stage/two-pass RO process
119
Fig. 5.1. The result of the step change of operating pressure on retentate
concentration for several operating concentrations at operating conditions of
2.583x10 ⁻⁴ m³/s, and 31.5 °C
Fig. 5.2. The result of the step change of operating pressure on mean
permeate concentration for several operating concentrations at operating
conditions of 2.583x10 ⁻⁴ m ³ /s, and 31.5 °C
Fig. 5.3. The result of the step change of operating pressure on solute rejection
for several operating concentrations at operating conditions of 2.583x10 ⁻⁴
m³/s, and 31.5 °C
Fig. 5.4. The result of the multiple change of operating pressure on solute
rejection for operating conditions of 6.548x10 ⁻³ kmol/m³, 2.166x10 ⁻⁴ m³/s, and
31.5 °C
Fig. 5.5. The result of the multiple change of operating pressure on average
permeate concentration for operating conditions of 6.548x10 ⁻³ kmol/m³,
2.166x10 ⁻⁴ m³/s, and 31.5 °C
Fig. 5.6. The influence of the step change of operating feed flow rate on
retentate concentration for several operating pressures at operating conditions
of 6.548x10 ⁻³ kmol/m³, and 31.5 °C
Fig. 5.7. The influence of the step change of operating feed flow rate on
average permeate concentration for several operating pressures at operating
conditions of 6.548x10 ⁻³ kmol/m³, and 31.5 °C
Fig. 5.8. The influence of the step change of operating feed flow rate on
rejection parameter for several operating pressures at operating conditions of
6.548x10 ⁻³ kmol/m³, and 31.5 °C

Fig. 5.9. The result of the multiple change of feed flow rate on retentate
concentration for operating conditions of 6.548x10 ⁻³ kmol/m³, 10 atm, and 31.5
°C133
Fig. 5.10. The result of the multiple change of feed flow rate on average
permeate concentration for operating conditions of 6.548x10 ⁻³ kmol/m³, 10
atm, and 31.5 °C
Fig. 5.11. The result of the multiple change of feed flow rate on solute rejection
for operating conditions of 6.548x10 ⁻³ kmol/m³, 10 atm, and 31.5 °C 134
Fig. 5.12. The result of the step change of operating concentration on retentate
concentration for several operating pressures at operating conditions of
2.583x10 ⁻⁴ m³/s, and 31.5 °C
Fig. 5.13. The result of the step change of operating concentration on average
permeate concentration for several operating pressures at operating
conditions of 2.583x10 ⁻⁴ m ³ /s, and 31.5 °C
Fig. 5.14. The result of the step change of operating concentration on rejection
parameter for several operating pressures at operating conditions of 2.583x10
⁴ m³/s, and 31.5 °C
Fig. 5.15. The result the step change of operating temperature on retentate
concentration for several operating pressures at operating conditions of
2.583x10 ⁻⁴ m³/s, and 6.548x10 ⁻³ kmol/m³
Fig. 5.16. The effects of the step change in operating temperature to mean
permeate concentration for several operating pressures at operating
conditions of 2.583x10 ⁻⁴ m³/s, and 6.548x10 ⁻³ kmol/m³
Fig. 5.17. The result of the step change of operating temperature on rejection
parameter for several operating pressures at operating conditions of 2.583x10
⁴ m³/s, and 6.548x10 ⁻³ kmol/m³
Fig. 6.1. Schematic diagram of a conventional RO pilot-scale plant 143
Fig. 6.2. Friction parameter versus inlet feed pressure for module type ESPA2-
4040 (initial conditions 2.43x10 ⁻³ m³/s, and 20 °C)
Fig. 6.3. Dependence of N-nitrosamine rejection on inlet feed pressure at inlet
feed conditions of 2.43x10 ⁻³ m³/s, and 20 °C
Fig. 6.4. Specific energy consumption of two types RO pilot-plants with and
without ERD (Figs. 6.1 and 2.2 in Section 2.5.2 in Chapter 2) and total recovery

versus inlet feed pressure at inlet feed conditions of 2.43x10 ⁻³ m ³ /s, and 20 °C	С
14	8
Fig. 6.5. The relation between the inlet feed pressure and the pressur	е
difference at inlet and outlet edges at inlet conditions of 2.43x10 ⁻³ m³/s, an	d
20 °C14	8
Fig. 6.6. Dependence of N-nitrosamine rejection on inlet feed flow rate at inle	et
feed conditions of 10.1 atm, and 20 °C	9
Fig. 6.7. Specific energy consumption of two types RO pilot-plants with an	d
without ERD and total recovery versus inlet feed flow rate at inlet fee	d
conditions of 10.1 atm, and 20 °C	0
Fig. 6.8. Dependence of N-nitrosamine rejection on inlet feed temperature a	at
inlet feed conditions of 2.43x10 ⁻³ m³/s, and 10.1 atm	1
Fig. 6.9. Specific energy consumption of two types RO pilot-plants with an	d
without ERD and ERD with Boiler and total recovery versus inlet fee	d
temperature at inlet conditions of 2.43x10 ⁻³ m/s, and 10.1 atm 15	2
Fig. 6.10. The tested configurations of retentate reprocessing RO networks of	of
six pressure vessels	3
Fig. 6.11. The tested configurations of retentate reprocessing RO networks of	of
six pressure vessels (F: Feed, P: permeate, R: Retentate)	4
Fig. 6.12. Tested configuration of permeate reprocessing RO network of thre	е
stages	6
Fig. 6.13. Tested configuration of permeate reprocessing RO network of tw	O
stages	7
Fig. 6.14. Tested two configurations of retentate and permeate reprocessing	g
RO network of four stages	8
Fig. 6.15. Six stages RO network with permeate reprocessing, P: Pump, S	3:
Stage, ERD: Energy recovery device	2
Fig. 7.1. The variation of operating parameters along the membran	е
length	1
Fig. 7.2. Effect of compound concentration on rejection and recovery rat	е
(operating conditions: 2.583x10 ⁻⁴ m³/s, 10 atm, and 30 °C)	2
Fig. 7.3. Effect of operating temperature on rejection and recovery rat	е
(operating conditions: 2.583x10 ⁻⁴ m ³ /s, 10 atm, and 350 ppm)	2

Fig. 7.4. Operating pressure verses rejection and recovery rate (operating
conditions: 2.583x10 ⁻⁴ m³/s, 30 °C, 350 ppm)
Fig. 7.5. Effect of operating feed flow rate on rejection and recovery rate
(operating conditions: 10 atm, 30 °C, 350 ppm)
Fig. 8.1. Outlet Brix variation as a function of operating trans-membrane
pressure at different inlet feed flow rates at inlet conditions ($^{\circ}$ Brix = 10.5, Tb =
20 °C)
Fig. 8.2. Outlet Brix variation as a function of operating temperature at different
inlet feed flow rates at inlet conditions (°Brix = 10.5 , TMP = 34.542 atm) 189
Fig. 8.3. Five different tested RO networks
Fig. 8.4. Sugar species rejection as a function of operating pressure at inlet
feed flow rate and temperature of $1x10^{-3}$ m³/s, and 40 °C, respectively 196
Fig. 8.5. Sugar species rejection as function of operating pressure at inlet feed
flow rate and temperature of $1x10^{-4}$ m³/s, and 40 °C, respectively 196
Fig. 8.6. Sugar species rejection as a function of operating pressure at inlet
feed flow rate and temperature of 3.7x10 $^{-5}$ m³/s, and 40 °C, respectively 197
Fig. 8.7. Impact of variation in inlet feed pressure and flow rate on product
concentration at fixed inlet feed concentration and temperature of 10.5 °Brix,
and 40 °C, respectively
Fig. 8.8. Sugar species retention concentration verse operating pressure at
two inlet feed flow rates and inlet feed concentration and temperature of
3.68x10 ⁻⁵ and 1x10 ⁻³ m³/s, 10.5 °Brix, and 40 °C
Fig. 8.9. Impact of variation in inlet feed pressure and temperature on product
concentration at fixed inlet feed concentration and flow rate of 10.5 °Brix, and
4x10 ⁻⁵ m ³ /s
Fig. 8.10. Sugar species rejection as a function to operating feed temperature
at inlet feed concentration and flow rate of 10.5 Brix, and 3.68x10 ⁻⁵ 200
Fig. 8.11. Sugar species rejection as a function to operating feed temperature
at inlet feed concentration and flow rate of 10.5 Brix, and 1x10-3 201

List of Tables

Table 1.1. Purposes and rates of using wastewater in some countries
(Adapted from (Jiménez and Asano 2008)
Table 2.1. Membrane characteristics and geometry
Table 2.2. Membrane characteristics and geometry
Table 2.3. Physical and transport parameters of the eight N-nitrosamines 27
Table 2.4. Specifications of the spiral wound membrane element
Table 2.5. Specifications of spiral wound membrane element and module
constraints (Álvarez et al. 2002)
Table 2.6. Characteristics of the sugar and aroma compounds and inlet
concentration in the model solution of 10.5 °Brix (Matsuura et al. 1976;
Malaiyandi et al. 1982; Álvarez et al. 1998; Álvarez et al. 2002); (parameter
estimation, Model Type_6)30
Table 2.7. Results of parameter estimation
Table 2.8. Results of parameter estimation measured at 30 – 32 °C 39
Table 3.1. Model Type_1 validation with experimental results for inlet feed flow
rate of $(Fb(0) = 2.166x10^{-4} \text{ m}^3/\text{s})$
Table 3.2. Model Type_1 validation with experimental results for inlet feed flow
rate of $(Fb(0) = 2.33x10^{-4} \text{ m}^3/\text{s})$
Table 3.3. Model Type_1 validation with experimental results for inlet feed flow
rate of (Fb(0) 2.583x10 ⁻⁴ m ³ /s)
Table 3.4. Results of parameter estimation
Table 3.5. Model Type_2 validation with experimental results for inlet feed flow
rate of $(Fb(0, y) = 2.166x10^{-4} \text{ m}^3/\text{s})$ 64
Table 3.6. Model Type_2 validation with experimental results for inlet feed flow
rate of $(Fb(0, y) = 2.33x10^{-4} \text{ m}^3/\text{s})$ 65
Table 3.7. Model Type_2 validation with experimental results for inlet feed flow
rate of $(Fb(0, y) = 2.583x10^{-4} \text{ m}^3/\text{s})$
Table 3.8. Comparison of 1D and 2D models predictions against experimental
data of (Srinivasan et al. 2011) for dimethylphenol removal from
wastewater
Table 3.9. Physical and transport parameters of the eight selected organic
compounds
76

Table 3.10. Model validation results against chlorophenol removal
Rej
Table 3.11. Results of parameter estimation
Table 3.12. Results of relative errors and sum of square errors 82
Table 4.1. Summary of the impact of operating parameters on the performance
of RO process
Table 4.2. Simulation results at initial chlorophenol concentration of 6.226E-3
kmol/m ³
Table 4.3. Optimisation results at inlet chlorophenol concentration of 6.226x10
³ kmol/m ³
Table 6.1. Summary of the impact of operating parameters on the performance
of RO process
Table 6.2. The optimisation results
Table 6.3. The parameter estimation results
Table 6.4. The model validation results
Table 6.5. Specifications of the spiral wound membrane element (Abbas 2005)
Table 6.6. Simulation results of seventeen scenarios of retentate reprocessing
RO networks
Table 6.7. Simulation results of permeate reprocessing RO networks 168
Table 6.8. The limits of operation of the spiral-wound membrane element
(Abbas 2005)
Table 6.9. Optimisation results of configuration U
Table 7.1. Physical and transport parameters of the eight selected organic and
non-organic compounds
Table 8.1. Comparison of outlet apple juice concentration for five cases of RO
networks

Nomenclature

A: The effective area of the membrane (m²)

A_s: Feed cross section open area (m²)

 $A_{\rm w}$: Water transport coefficient of the membrane for solution diffusion model (m/atm s)

A *: Parameter defined in Eq. (M.6.45) in Chapter 3

A': Characteristic parameter of the feed spacer (dimensionless)

b : Feed channel friction parameter (atm s/m⁴)

 B_s : Solute transport parameter of the membrane for solution-diffusion model (m/s)

B_{s(i)}: Sugar species transport parameter of the membrane (m/s)

 $B_{s\left(T_{b}\right)}$: Solute transport parameter of the membrane at any temperature (m/s)

°Brix_{in}: Concentration of apple juice at the inlet edge of the membrane (°Brix)

°Brix_{out}: Concentration of apple juice at the outlet edge of the membrane (°Brix)

 ${}^\circ \mathrm{Brix}_{(x)}$: Concentration of apple juice at any point along x-axis of the feed channel (${}^\circ \mathrm{Brix}$)

B*: Parameter defined in Eq. (M.6.46) in Chapter 3

C_b: Bulk feed solute concentrations at the feed channel (kmol/m³)

 $C_{b(x)}$: Fluid solute concentration at any point along x-axis (kmol/m³)

 $C_{b(x,y)}$: Fluid solute concentration at any point along x and y-axes (kmol/m³)

C_{b(0)}: Inlet solute concentration of the feed channel (kmol/m³)

C_{b(L)}: Outlet solute concentration of the feed channel (kmol/m³)

C_{b(i)}: Sugar species concentration of the feed channel (kmol/m³)

 $C_{b(x)}^{\sim}$: Mean solute concentration at any point along x-axis of the membrane (kmol/m³)

 $C_{b(0)}^{\sim}$: Mean solute concentration at the inlet edge of the membrane (kmol/m³)

 $C_{b(L)}^{\sim}$: Mean solute concentration at the outlet edge of the membrane (kmol/m³)

C_f: Inlet feed solute concentrations at the feed channel (kmol/m³)

C_{f(i)}: Inlet feed sugar species concentrations at the feed channel (kmol/m³)

C_m: Dimensionless solute concentration (dimensionless)

 $C_{\rm p}$: Specific heat capacity of water (4181 j/kg K)

C_p: Permeate solute concentration in the permeate channel (kmol/m³)

 $C_{p(i)}$: Permeate sugar species concentration at the permeate channel (kmol/m³)

 $C_{p(x)}$: Permeate concentration at any point along x-axis of the permeate channel (kmol/m³)

 $C_{p(x,y)}$: Permeate concentration at any point along x and y-axes of the permeate channel (kmol/m³)

 $C_{p(av)}$: Average permeate solute concentration in the permeate channel (kmol/m³)

 $C_{\mathrm{p}(0)}$: Inlet permeate solute concentration of the permeate channel (kmol/m³)

 $C_{p(L)}$: Outlet permeate solute concentration of the permeate channel (kmol/m³)

C_r: Retentate solute concentration (kmol/m³)

 $C_{r(i)}$: Retentate sugar species concentration (kmol/m³)

C_w: Solute concentration at the membrane wall (kmol/m³)

C_{w(i)}: Sugar species concentration at the membrane wall (kmol/m³)

 $C_{w(x)}$: Solute concentration at the membrane wall at any point along x-axis (kmol/m³)

 $C_{w(x,y)}$: Solute concentration at the membrane wall at any point along x and y-axes (kmol/m³)

 $C_{m(x)}$: Dimensionless solute concentration at any point along x-axis (dimensionless)

 $C_{m(x,y)}$: Dimensionless solute concentration at any point along x and y-axes (dimensionless)

C_{td}: Total drag coefficient (dimensionless)

D_b: Diffusivity of solute in the feed channel (m²/s)

 $D_{b(x)}$: Diffusivity of solute at any point along x-axis of the feed channel (m²/s)

 $D_{b(x,y)}$: Diffusivity of solute at any point along x and y-axes of the feed channel (m²/s)

 $D_{\rm p}$: Diffusivity of permeate in the permeate channel (m²/s)

 $D_{p(x)}$: Diffusivity of permeate at any point along x-axis of the permeate channel (m²/s)

 $D_{p(x,y)}$: Diffusivity of permeate at any point along x-y axes of the permeate channel (m²/s)

d_h: Hydraulic diameter (m)

de_b: Equivalent diameter of the feed channel (m)

de_p: Equivalent diameter of the permeate channel (m)

D_(i): Diffusion coefficient of any sugar species (m²/s)

D_a: Diffusion coefficient of any sugar species in a very dilute solution (m²/s)

D_s: Diffusion coefficient of any aroma species in a very dilute solution (m²/s)

 $D_{SU(x)}$: Diffusion coefficient of any sugar species at any point along x-axis (m²/s)

 $D_{AR(x)}$: Diffusion coefficient of any aroma compound at any point along x-axis (m²/s)

E: Specific energy consumption of the high-pressure pump (kWh/m³)

E1: Specific energy consumption of the high-pressure pump without ERD (kWh/m³)

E2: Specific energy consumption of the high-pressure pump with ERD (kWh/m³)

E3 : Specific energy consumption of the boiler (kWh/m³)

E4: Total specific energy consumption of the conventional reverse osmosis plant configuration (kWh/m³)

E_(Total): Total energy consumption (kWh/m³)

ERD: Energy recovery device

E_{pump}: The energy consumption of high pressure pump (kWh/m³)

E_{ERD}: The recovered energy of by turbine (kWh/m³)

F_b: Feed flow rate (m³/s)

 $F_{b(x)}$: Feed flow rate at any point along x-axis of the feed channel (m³/s)

 $F_{b(x,y)}$: Feed flow rate at any point along x and y-axes of the feed channel (m³/s)

 $F_{b(0)}$: Inlet feed flow rate of the feed channel (m³/s)

F_{b(L)}: Outlet feed flow rate of the feed channel (m³/s)

F_p: Permeate flow rate (m³/s)

 $F_{p(\boldsymbol{x})}$: Permeate flow rate at any point along x-axis of the permeate channel $\mbox{(m}^{3}\!/\!s)$

 $F_{p(0)}$: Permeate flow rate at the inlet edge of the permeate channel (m³/s)

 $F_{p(L)}$: Permeated flow rate at the outlet edge of the permeate channel (m³/s)

 $F_{p(x,y)}$: Permeate flow rate at any point along x and y-axes of the permeate channel (m³/s)

F_{p(Total)}: Total permeated flow rate at the permeate channel (m³/s)

 $F_{s(x)}$: Solute molar flux in the x-axis of the membrane (kmol/m² s)

 $F_{s(v)}$: Solute molar flux in the y-axis of the membrane (kmol/m² s)

J_s: Solute molar flux through the membrane (kmol/m² s)

 $J_{s(i)}$: Solute molar flux through the membrane of any sugar species (kmol/m² s)

 $J_{s(x)}$: Solute molar flux through the membrane at any point along x-axis (kmol/m² s)

 $J_{s(x,y)}$: Solute molar flux through membrane at any point along x and y-axes (kmol/m² s)

J_w: Water flux at the feed channel (m/s)

 $J_{w(x)}$: Water flux at any point along x-axis of the feed channel (m/s)

 $J_{w(0)}$: Water flux at the inlet edge of the feed channel (m/s)

 $J_{w(L)}$: Water flux at the outlet edge of the feed channel (m/s)

 $J_{w(x,y)}$: Water flux at any point along x and y-axes of the feed channel (m/s)

K: Efficiency of mixing net (i.e. spacer) (K = 0.5) (dimensionless)

k: Mass transfer coefficient in the feed channel (m/s)

 $\mathbf{k}_{(x)}$: Mass transfer coefficient at any point along x-axis of the feed channel (m/s)

 $k_{(x,y)}$: Mass transfer coefficient at any point along x and y-axes of the feed channel (m/s)

 $\mathbf{k}_{(i)}$: Mass transfer coefficient of any sugar species at the feed channel (m/s)

L: Length of the membrane (m)

 L_p : Solvent transport parameter for the irreversible thermodynamic model (m/atm s).

 $\ln C^*_{NaCl}$: Constant related to the chemical nature of the membrane and the effective pore size (dimensionless)

M_{wb}: Molecular weight of bulk water (kg/kmol)

M_{wp}: Molecular weight of permeate (kg/kmol)

M_(i): Molecular weight of any sugar species (kg/kmol)

M_m: Molecular weight of malic acid (kg/kmol)

M_g: Molecular weight of glucose (kg/kmol)

M_{su}: Molecular weight of sucrose (kg/kmol)

M_{so}: Molecular weight of sorbitol (kg/kmol)

M_f: Molecular weight of fructose (kg/kmol)

 $m_{f(x)}$: Parameter defined in sweater density equation calculated at any point along x-axis

 $\ensuremath{m_{p(x)}}$: Parameter defined sweater density equation calculated at any point along x-axis

n: Characteristic parameter of the feed spacer (dimensionless)

 $P_{f(Bp)}$: Supplied pressure of the booster pump (atm)

P_b: Feed pressure at the feed channel (atm)

 $P_{b(x)}$: Feed channel pressure at any point along x-axis of the feed channel (atm)

 $P_{b(x,y)}$: Feed channel pressure at any point along x and y-axes of the feed channel (atm)

 $P_{b(0)}$: Inlet feed pressure of the feed channel (atm)

P_{b(L)}: Outlet feed pressure of the feed channel (atm)

 $P_{f(plant)}$: Operating pressure of the plant (atm)

 $P_{f(Bp)}$: Supplied pressure of the booster pump (atm)

P_{f(out)(ERD)}: Retentate pressure of energy recovery device (atm)

P_{f(in)(ERD)}: Supplied pressure of energy recovery device (atm)

P_n: Permeate pressure in the permeate channel (atm)

 $P_{p(x)}$: Permeate pressure at any point along x-axis of the permeate channel (atm)

 $P_{p(x,y)}$: Permeate pressure at any point along x and y-axes of the permeate channel (atm)

P_{loss}: Pressure loss along the membrane length (atm)

 P_{loss}^{d}: Permissible recommended pressure loss per each module (atm)

Q : Supplied heat by the boiler (j/s)

Q_b: Bulk feed flow rate at the feed channel (m³/s)

Q_p: Permeate flow rate at the permeate channel (m³/s)

Q_f: Inlet feed flow rate at the feed channel (m³/s)

 $Q_{p(plant)}$: Plant product flow rate (m³/s)

Q_{f(plant)}: Plant feed flow rate (m³/s)

 $Q_{r(plant)}$: Plant retentate flow rate (m³/s)

Q_r: Retentate flow rate at the feed channel (m³/s)

 $Q_{f(ERD)}$: Inlet feed flow rate of energy recovery device (m³/s)

 $Q_{r(ERD)}$: retentate flow rate of energy recovery device (m³/s)

 $Q_{f(Bp)}$: Inlet feed flow rate of booster pump (m³/s)

Q_{f(HPP)}: Feed flow rate of high-pressure pump (m³/s)

R: Gas low constant $\left(R = 0.082 \frac{\text{atm m}^3}{^{\circ}\text{K kmol}}\right)$, $\left(8.314 \frac{\text{J}}{\text{mol K}}\right)$

Rec: Water recovery coefficient (dimensionless)

Rec_(plant): Total plant water recovery (dimensionless)

Rej: Solute rejection coefficient of the membrane (dimensionless)

Rej_(i): Sugar speices rejection coefficient of the membrane (dimensionless)

Rej_(av): Average solute rejection coefficient (dimensionless)

 $Re_{b(x)}$: Reynold number at any point along x-axis of the feed channel (dimensionless)

 $Re_{b(x,y)}$: Reynold number at any point along x and y-axes of the feed channel (dimensionless)

Re_b: Reynold number at the feed channel (dimensionless)

Re_p: Reynold number at the permeate channel (dimensionless)

 $\text{Re}_{p(x)}$: Reynolds number at any point along x-axis of the permeate channel (dimensionless)

 $\mbox{Re}_{p(x,y)}$: Reynolds number at any point along x and y-axes of the permeate channel (dimensionless)

Re_{mix}: Reynolds number of the apple juice (dimensionless)

r: Parameter defined in Eq. (M.5.18) in Chapter 3

 $Sc_{b(x)}$: The feed Schmidt number at any point along x-axis of the feed channel (dimensionless)

Sc_i: Schmidt number of any sugar or aroma compound (dimensionless)

 $Sc_{p(x)}$: Permeate Schmidt number at any point along x-axis of the permeate channel (dimensionless)

SSE: Sum of square errors (dimensionless)

T_b: Fluid temperature at the feed channel (°C)

 $T_{b(x)}$: Fluid temperature at any point along x-axis of the feed channel (°C)

 $T_{b(x,y)}$: Fluid temperature at any point along x and y-axes of the feed channel (°C)

T_p: Permeate temperature at the permeate channel (°C)

 $T_{p(\boldsymbol{x})}$: Permeate temperature at any point along x-axis of the permeate channel (°C)

 $T_{p(x,y)}$: Permeate temperature at any point along x and y-axes of the permeate channel (°C)

T_{Ref}: Reference temperature of 25 °C

t_f: Height of the feed channel (m)

t_p: Height of permeate channel (m)

T_{ref}, T_o: Reference temperature of experimental work (°C)

T_{Tank}: Ttemperature accumulated at the tank (°K)

T_{RO}: Feed temperature of RO process (°C)

TMP: Trans-membrane pressure (atm)

 $U_{b(x)}$: Bulk feed velocity at any point along x-axis of the feed channel (m/s)

U_b: Bulk feed velocity at the feed channel (m/s)

V_w: Molar volume of water (m³/kmol)

V_{bp,A}: Molar volume of the solute at its normal boiling point (m³/kmol)

V: The volume of feed tank (m3)

W: Width of the membrane (m)

x: The coordinate of x-axis under consideration (m)

Z: Parameter defined in Eq. (M.5.17) in Chapter 3

 Δx : Length of sub-section in x-axis of the membrane (m)

 Δy : Length of sub-section in y-axis of the membrane (m)

ΔL: Characteristic length of mixing net (m)

 ΔP_b : Total trans-membrane pressure of the membrane (atm)

 $\Delta P_{b_{\left(x\right)}}$: Trans-membrane pressure at any point along x-axis of the membrane (atm)

 $\Delta P_{b_{\left(x,y\right)}}$: Trans-membrane pressure at any point along x and y-axes of the membrane (atm)

 ΔP_{drop} : Pressure drop of the membrane (atm, kpa)

Greek letters

μ_b: Feed viscosity at the feed channel (kg/m s)

 $\mu_{b(x)}$: Feed viscosity at any point along x-axis of the feed channel (kg/m s)

 $\mu_{b(x,y)}$: Feed viscosity at any point along x and y-axes of the feed channel (kg/m s)

 μ_p : Permeate viscosity at the permeate channel (kg/m s)

 $\mu_{p(x)}$: Feed viscosity at any point along x-axis of the permeate channel (kg/m s)

 $\mu_{p(x,y)}$: Feed viscosity at any point along x and y-axes of the permeate channel (kg/m s)

 μ_w : Water viscosity (8.94x10⁻⁴ kg/m s)

 μ_{mix} : Viscosity of apple juice (kg/m s)

 μ_{in} : Viscosity of apple juice at the inlet edge of the membrane (kg/m s)

 μ_{out} : Viscosity of apple juice at the outlet edge of the membrane (kg/m s)

 ρ : Density of water (1000 kg/m³)

ρ_b: Feed density at the feed channel (kg/m³)

 $\rho_{\rm w}$: Molal density of water (55.56 kmol/m³)

 $\rho_{b(x)}$: Feed density at any point along x-axis of the feed channel (kg/m³)

 $\rho_{b(x,y)}\colon \mbox{Feed density at any point along } x$ and y-axes of the feed channel (kg/m³)

 ρ_{mix} : Density of apple juice (kg/m³)

 $\rho_{\rm p}$: Permeate density at the permeate channel (kg/m³)

 $\rho_{p(x)}$: Permeate density at any point along x-axis of permeate channel (kg/m³)

 $\rho_{p(x,y)}$: Permeate density at any point along x and y-axes of permeate channel (kg/m³)

 $\Delta\pi$: Total osmotic pressure difference of the membrane (atm)

 $\Delta\pi_{(x)}$: Omotic pressure difference at any point along x-axis of the membrane (atm)

 $\Delta\pi_{(x,y)}$: Osmotic pressure difference at any point along x and y-axes of membrane (atm)

 $\pi_{\rm w}$: Osmotic pressure of solute regarding the membrane wall concentration $C_{\rm w}$ (atm)

 $\pi_{(i)Cw(x)} .$ Osmotic pressure of any sugar species at membrane wall concentration C_w (atm)

 π_p : Osmotic pressure at permeate channel regarding the permeate concentration C_p (atm)

 $\pi_{(i)Cp(av)}$: Osmotic pressure of any sugar species corresponding the average permeate concentration C_p (atm)

 $\pi_{su(0)}$: Osmotic pressure of sucrose at the inlet edge of the membrane (atm)

 $\pi_{su(x)}$: Osmotic pressure of sucrose at any point along x-axis (atm)

 $\pi_{g(0)}$: Osmotic pressure of glucose at the inlet edge of the membrane (atm)

 $\pi_{g(x)}$: Osmotic pressure of glucose at any point along x-axis (atm)

 $\pi_{m(0)}$: Osmotic pressure of malic acid at the inlet edge of the membrane (atm)

 $\pi_{m(x)}$: Osmotic pressure of malic acid at any point along x-axis (atm)

 $\pi_{f(0)}$: Osmotic pressure of fructose at the inlet edge of the membrane (atm)

 $\pi_{f(\boldsymbol{x})}$: Osmotic pressure of fructose at any point along x-axis (atm)

 $\pi_{so(0)}$: Osmotic pressure of sorbitol at the inlet edge of the membrane (atm)

 $\pi_{so(x)}$: Osmotic pressure of sorbitol at any point along x-axis (atm)

 $\Delta\pi_{Total\;(x)}$: Osmotic pressure difference of sugar species at any point along x-axis (atm)

 $\pi_{w\,(i)}$: Osmotic pressure of the sugar species at the membrane wall $C_{w\,(i)}$ (kpa)

 $\pi_{p\;(i)}$: Osmotic pressure at the permeate channel regarding the sugar species permeate concentration $C_{p\;(i)}$ (kpa)

 $\Delta\pi_{(i)(x)}$: Osmotic pressure difference of any sugar species at any point along x-axis (atm)

σ : Reflection coefficient (dimensionless)

 ω : Solute permeability constant of the membrane for the irreversible thermodynamic model (kmol/m² s atm)

Ø: Parameter defined in Eq. (M.4.13) in Chapter 3

 $\vartheta_{(i)}$: Parameter defined in Eq. (M.6.19) in Chapter 3

 $\vartheta_{(mix)}$: Parameter defined in Eq. (M.6.20) in Chapter 3

 ϵ : Void fraction of the spacer (dimensionless)

δ*Es*: Steric Taft number (dimensionless)

 $(-\Delta\Delta G/RT)$: Concept of free energy parameter (dimensionless)

 ε_{pump} : Pump efficiency (dimensionless)

 ϵ_{Bp} : Booster pump efficiency (dimensionless)

 ϵ_{motor} : Motor efficiency (dimensionless)

 ϵ_{ERD} : Energy recovery device efficiency (dimensionless)

Chapter 1

Introduction

1.1 Reverse Osmosis (RO) process

RO is a pressure driven process which can be specifically characterised by the idea of using a semi-permeable membrane (permeable to solvent, impermeable to solute) to separate two mediums of different solute concentration. In other words, RO unit is a process used to remove undesirable species (salts, pollutants, etc.) from liquid solutions (seawater, wastewater, etc.) by pumping the solution at higher pressure than the osmotic pressure within a closed vessel, which facilitates the solvent to flow from the concentrated side to the diluted side. The portion of water that passes through the membrane is called permeate while the other discharged portion is called retentate of high concentration. When RO is applied for fruit juice concentration, this process used to produce high concentrated stream of fruit juice (retentate) by removing excess water as permeate, which in turn enhances the product stability.

The theory of solute and solvent flow through semi-permeable membranes can be schematically presented in three scenarios as shown in Fig. 1.1, which shows two solutions of different concentrations being separated by a semi-permeable membrane. Scenario A represents a natural phenomenon of water diffusion from the low concentration solution in to the high concentration solution, which is called osmosis. This process continues until osmotic equilibrium is achieved and which is characterised by the equivalent chemical potential of both solutions. The pressure difference between the two solutions is known as the osmotic pressure difference and from this point onward, no further solvent flow takes place. This state is known as the osmotic equilibrium state, i.e. Scenario B. Lastly, for desalination of the concentrated salt water, the procedure can be reversed by applying higher pressure than the solution osmotic pressure, which forces water to pass over the membrane towards the low concentration solution side accompanied by salt rejection, i.e. Scenario C. Usually, this process can happen under ambient temperature and without any phase change (Jain and Gupta 2004).

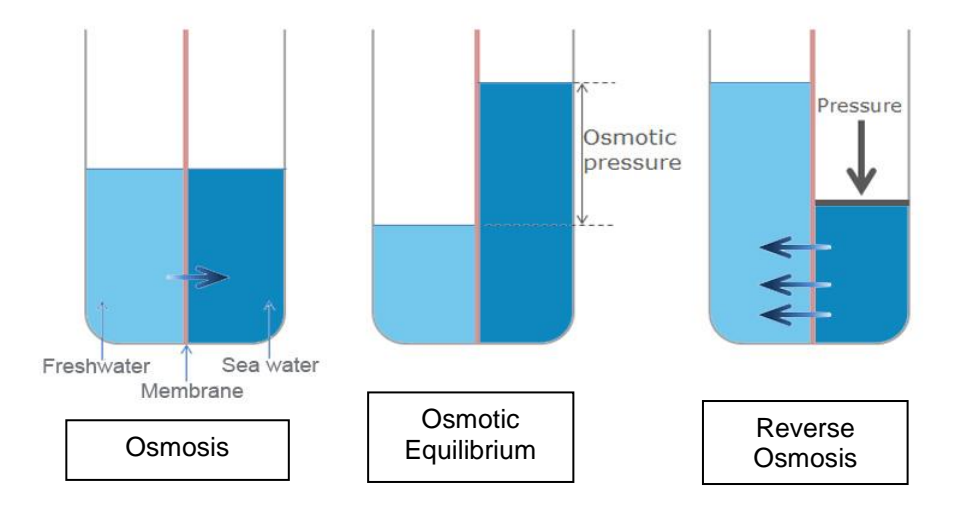


Fig. 1.1. Scenario A: Osmosis, Scenario B: Osmotic Equilibrium and Scenario C: Reverse Osmosis

1.2 Measurement of RO process performance

The key design parameters used to predict the performance of RO process are listed below:

- Trans-membrane pressure and osmotic pressure: The total operating
 pressure that adjusted to overcome the osmotic pressure, permeate
 pressure, friction losses and membrane resistance is called the transmembrane pressure, which is designed to fulfil an economical passage of
 water through the membrane. Specifically, the osmotic pressure is mainly
 dependent on the salt concentration of the fluid.
- Permeate recovery: This term finds the percentage value of total volumetric permeate flow rate per the volumetric feed flow rate.
- Solute rejection: The rejection characteristics of the membrane illustrates the ability of separate solute from aqueous solution system without phase change.

Specifically, the performance of RO process is critically measured in terms of sugar species rejection and the retentate fruit juice concentration measured in Brix when applied for fruit juice concentration.

1.3 Types of RO membrane modules

The RO membranes are placed in several types of modules of different configurations, such as spiral wound, hollow fiber, tubular and plate and frame. The attention of this research will be focused on spiral wound module, which can be considered as the most familiarly used.

1.3.1 Spiral wound

The spiral wound membrane module is made from layers of glued flat rolled membrane sheets wrapped around a central perforated tube designed to collect permeate (Fig. 1.2). The sheets are bound together around three edges with an opening fourth edge connected with a central perforated pipe where the permeated water is collected. Therefore, the sheets are essentially containing product water side and a spacer for the flowing of the feed. These sheets are separated by using a very thin fibers mesh (highly porous spacer), which are wrapped around the permeated pipe. The advantages of inserting the mesh can be assigned through increasing the rate of turbulence inside the unit and enhance the mass transport with decreasing the concentration polarisation impact by minimising the boundary layer at the membrane without excessive pressure drop. In addition, the mesh works as a barrier to keep the membrane parts apart. Then, the spiral wound membranes were fitted in either a plastic or stainless-steel tube to be pressurized. The process of fluid separation starts by pumping the fluid under pressure to enforce permeate flowing through the pores and then collected at the end of the tube at the permeate side.

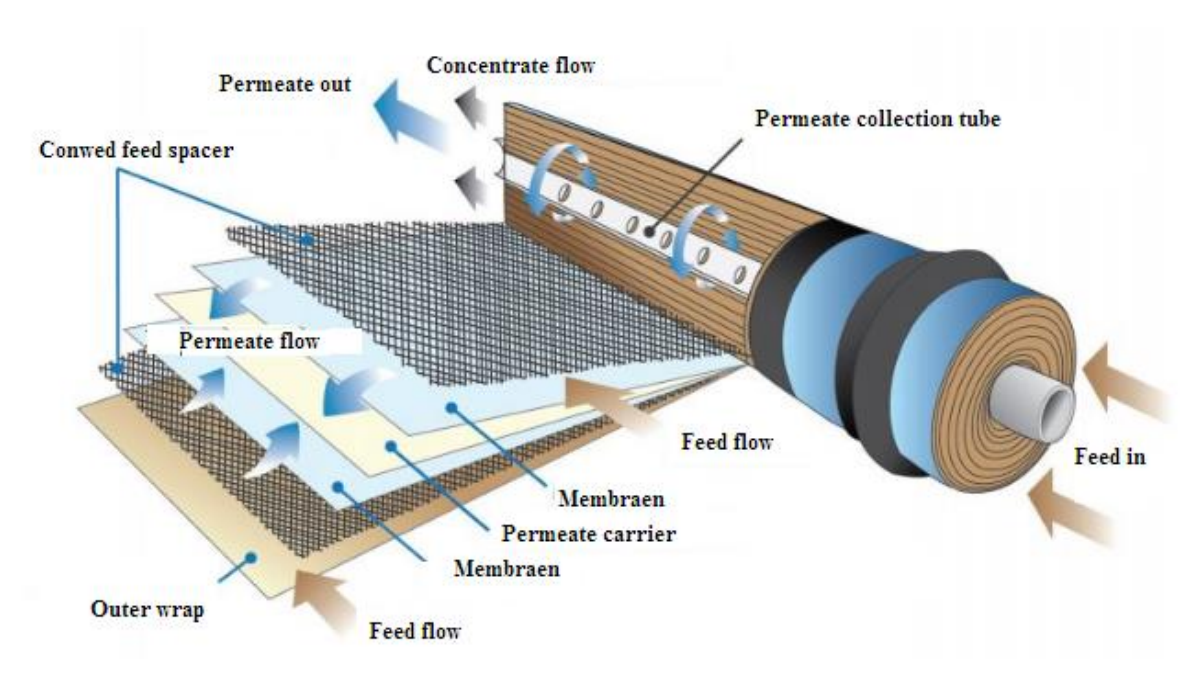


Fig. 1.2. Schematic configuration of the spiral wound module (Adapted from: https://www.complete-water.com/reverse-osmosis-theory-of-operation)

1.3.1.1 Configuration of spiral wound module

Fig. 1.3 shows a schematic view of spiral wound membrane element presented as a flat sheet membrane including the directions of flow inside the module. The specific dimensions of the module are length L and width W. x denotes the axial coordinate along the membrane length, while y denotes the tangential coordinate in the spiral direction starting from the sealed end of the leaf to the end of membrane width. The feed and permeate spacers channels are t_f and t_p , respectively. The effective membrane area can be calculated as $A_m = LW$. Specifically, the spiral wound RO module is composed of two sides, the feed side and the permeate side. The accumulated permeate water flows in the same direction of feed and then flows in the spiral direction into a central perforated pipe. However, the fresh water is flowing perpendicular from the feed side to the permeate side through the membrane region.

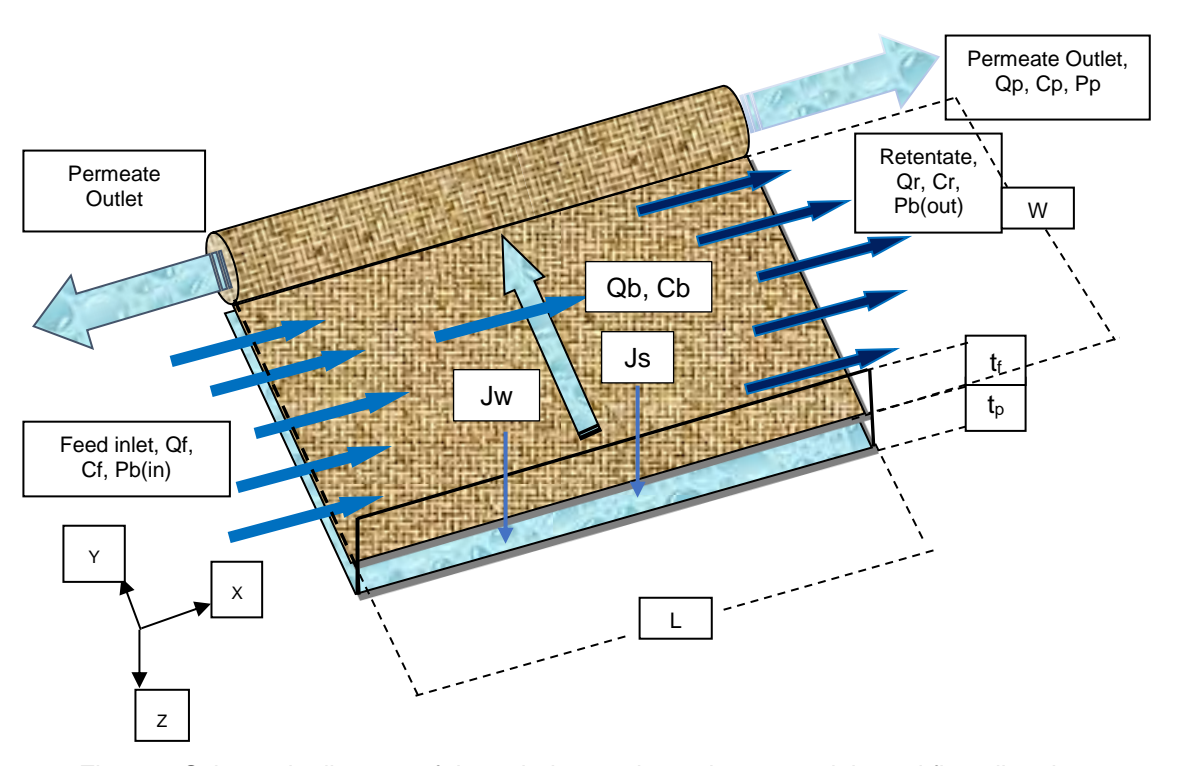


Fig. 1.3. Schematic diagram of the spiral wound membrane module and flow directions

1.3.1.2 Characteristics of spiral wound RO process

The characteristics of spiral wound membranes are a compact design of a high packing density (large membrane area per unit module volume) with high mass transfer and low energy consumption of economical shape. Interestingly, among the other types of RO modules, spiral wound membrane modules are the most popular and often preferred in both desalination and industrial processes. This is

due to offering specific characteristics of ease of operation, replace with low cost and accepted permeation rates with low fouling levels (compared to hollow fiber module), easier to clean and low water production costs (Evangelista, 1988; Baker, 2004). This type of membranes has achieved the highest rates of separation in different fields like water drinking, wastewater treatment, dairy, etc.

1.4 Limitations of RO membrane process

1.4.1 Concentration polarisation theory

Concentration polarisation can be considered as one of the imperfections of RO process, which is caused by the accumulation of solutes on the membrane surface (exceeds the concentration in the bulk liquid) by continuous rejection of solutes. Consequently, this phenomenon can decrease the flux of solvent by reducing the potential of pressure difference along the two sides and increasing the value of osmotic pressure (Sutzkover et al. 2000). In other words, the accumulation of the rejected solute on the membrane surface leads to a reduced convective permeate flux (due to the pressure) and the solute diffusion (from the membrane wall to the bulk side due to the concentration gradient). This in turn has a passive impact on the performance of RO process due to increasing solute flux through the membrane, which decreases the solute rejection.

The schematic diagram of Fig. 1.4 shows the stagnant polarisation layer (δ) . In this respect, the bulk concentration (C_b) , concentration at the membrane surface (C_w) , permeate concentration (C_p) , water flux (I_w) , solute flux (I_s) , and osmotic pressure $(\Delta\pi)$ are represented in Fig. 1.4. Increasing the feed flow rate along the membrane feed channel can increase the wall shear stress, which minimises the width of the boundary layer over the membrane surface (Schwinge et al. 2002). This can be considered as one of the possible solutions of concentration polarisation phenomenon. Moreover, the presence of feed spacers can reduce the formation of concentration polarisation by disrupting the fluid flow and enhancing the mass transfer coefficient. This is because that the spacer consists of several strands where the feed flows above and below the subsequent filaments. However, this may lead to increase the energy consumption due to increase the pressure drop along the membrane feed channel (Da Costa et al. 1993).

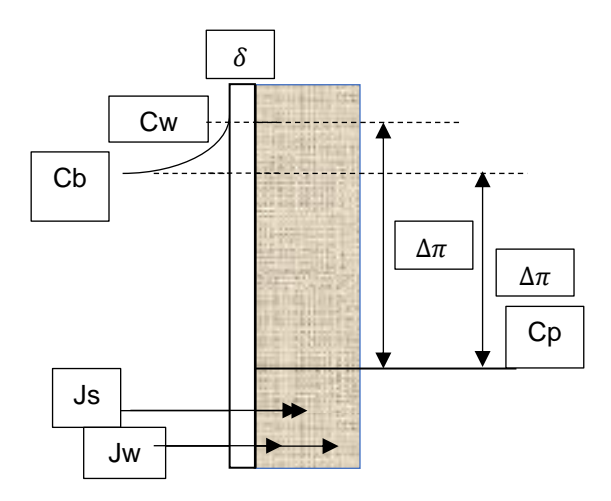


Fig. 1.4. Schematic diagram of concentration polarisation theory

1.4.2 Membrane fouling

The membrane fouling is considered as a critical phenomenon occurred in the membrane technology due to the accumulation of undesirable materials, colloids, and salts on the membrane surface (Chen et al. 2004). This in turn causes an inevitably decline of water permeation through the membrane especially for seawater desalination (Barger and Carnahan 1991). Specifically, this is because of increasing the osmotic pressure that commensurate with an increase of pressure drop through the feed channel, which ultimately to degrade the membrane performance. This in addition to increase the necessity of higher operating pressures, which means higher energy consumption. Pre-treatment methods can be an effective solution of fouling including coagulation, flocculation followed by filtration technology (Sassi 2012).

1.5 Application of RO in wastewater treatment

RO process has been extended to different types of industrial applications in addition to water desalination. Significantly, it shows a growth in water recycling and wastewater treatment in several industries (Lee and Lueptow 2001). The semi-permeable membrane facilitates the removal of undesirable particles and pollutants (Akin and Temelli 2011). This is mainly including the effluent treatments of several applications such as (a) textile industry (Amar et al. 2009), (b) dairy industry (Koyuncu et al. 2000; Álvarez et al. 2002), (c) tannery industry (Bhattacharya et al. 2013) and (d) pharmaceutical industry (Gholami et al. 2012). The performance of individual and multi-stage spiral wound RO modules in terms of industrial wastewater treatment has already been studied by considering a

range of different operating conditions and different pollutants, such as copper (Xijun et al. 1997), nitrate (Schoeman and Steyn 2003); secondary treated sewage effluent (Qin et al. 2005), a synthetic effluent stream of acrylonitrile, sulphate, ammonium, cyanide, and sodium (Bódalo-Santoyo et al. 2004b); copper, and nickel (Mohsen-Nia et al. 2007); chromium (Mohammadi et al. 2009); di-hydrogen phosphate, sulphite, nitrate, and nitrite (Madaeni and Koocheki 2010); and bisphenol A (Khazaali et al. 2014). Therefore, the ongoing research is mainly dependent on the use of spiral wound RO process for the removal of highly-toxic organic phenolic and N-nitrosamine compounds from wastewater.

1.5.1 The origin of wastewater

The fast-growing population and the associated increase in industrialisation have resulted in a significant increase in the production of wastewater. Unquestionably, this production from industry activities is unavoidable. The trend of disposing large volumes of industrial effluents and sewage into rivers and oceans is set to increase in the short and long terms (Wade Miller 2006; Henze et al. 2008). Moreover, many factors determine the quantity and quality of wastewater depending on the industry itself, despite the fact that some areas are not committed with the standards and regulations. Therefore, it is not surprising to see that there have been various initiatives for implementing sustainable alternative solutions by recycling, reclaiming, and reusing of different types of water. Water reuse is on the increase even in countries (such as London) with little or no water shortage (Wade Miller 2006) thus reducing the quantity of wastewater disposed to surface water.

1.5.2 Importance and applications of reuse water

Reclaimed and reused waters have been used in several industries (Wade Miller 2006) as follows;

Industrial reuse: Reuse water of low quality is utilised in cooling towers and power plants due to high-water demand.

Agricultural and irrigation reuse: These are considered as the highest consumers of recycled water for irrigating edible and non-edible agricultural crops. This is due to low cost of wastewater with nutrient content that eliminates the use of fertilizers.

Table 1.1 shows the tendency and the purpose of using recycling/reclaiming water in some countries (Jiménez and Asano 2008).

Table 1.1. Purposes and rates of using wastewater in some countries (Adapted from (Jiménez and Asano 2008)

Country	Purpose	Rate	Notes
Pakistan	Agricultural	96%	Non-treated wastewater
Tunisia	Agricultural	86%	Treated wastewater
Namibia	Municipal	29%	Namibia and Singapore have the most important water reuse for human consumption reclamation projects
Singapore	Municipal	45%	
	Industrial	51%	
Germany	Industrial	69%	USA and Germany have a larger number of recycling
USA	Industrial	45%	and reuse projects across various industries

1.5.3 Wastewater and associated challenges

Apparently, there are a huge amount of wastewater effluents and sewage are disposed into rivers and oceans, which harmfully impact the ecosystem. A significant volume of research continues to focus on the removal of micropollutants from wastewater as these adversely affect the natural ecosystem and human health. However, this is a great challenge because the organic pollutants found in wastewater can neither be easily nor cheaply removed. In general, wastewater treatment is a much more difficult process than water desalination, not only because of the complex toxicological compounds, which exist in the wastewater, but also because such treatment would require advanced and integrated technologies (Henze et al. 2008).

The key challenges for removing pollutants from wastewater are listed below (Bolong et al. 2009):

- The unique regulation of restricted concentration of new organic compounds such as N-nitrosamine in wastewater is complex.
- A variety of organic compounds can be found in wastewater, which can lead to harmful chemical reactions and therefore high toxicological products.
- The existence of some chemicals in the secondary treatment process of effluents with a very low concentration creates more complications during the removal process due to complex analytical determination.

Extensive research work has been performed to solve the above challenges by developing complex treatment systems based on several technologies used alone or in combination.

1.6 Pollutants

The transformed development of resources and technologies has produced different organic and non-organic chemical compounds (Bolong et al. 2009). Therefore, wastewater effluents of many industrial applications contain a variety of micro-pollutants, which are released into a variety of water resources. Such micro-pollutants not only disrupt the biological ecosystem, but they also pose real threat to the water supply for human consumption and to the aquatic ecosystems (Pomiès et al. 2013).

Despite the wide variety of organic compounds that can be found in wastewater, this research focuses on the phenolic and Nitrosamine compounds due to its significant relation to the water and wastewater treatment industry and involves a variety of compounds with a complex function that are in an increased awareness and tighter legislation.

1.6.1 Phenolic compounds

Phenol (C₆H₅OH) and phenolic compounds (aromatic compounds), which are colorless (in room temperature) crystalline substances, consisting of hydroxyl and aromatic hydrocarbon group, are considered as micro-pollutants that can be found in a variety of concentrations in wastewater effluents of many industrial processes such as refineries (6-500 ppm), coal (9-6800 ppm), petrochemical (28-1220 ppm), pharmaceutical, wood products, paint, and pulp productions (0.1-1600 ppm). More importantly, the existence of a stable benzene ring in phenol and phenolic derivatives has increased their resistance to biological decomposition (Kujawski et al. 2004; Karigar et al. 2006; Busca et al. 2008; Ahmed et al. 2010; Mohammed et al. 2016). Much recent research has focused on the removal of chlorophenol, which is formed following the release of phenol into the environment (especially water). This is because it undergoes an active reaction with chlorine to form chlorophenol, which is more persistent than phenol and has a higher toxicity level (Gami et al. 2014; Irfanudeen et al. 2015). These organic compounds are particularly the most common and indeed the most harmful micro-pollutants that cause adverse impact on human health due to high

toxicity even at low concentrations (suspected carcinogen) (Busca et al. 2008; Ahmed et al. 2010; Gami et al. 2014). Therefore, the United States Environmental Protection Agency (US EPA) has classified phenolic compounds as highly toxic compounds (Hsieh et al. 2008). For example, the oral recently tolerable daily intake of phenols has been limited down 0.5 mg/kg/day as confirmed by the European Food Standards Agency (EFSA) (EFSA 2013). Also, phenol brings intolerable tastes to drinking water at about 0.5 ppm (Jiang et al. 2003). Specifically, the removal of these compounds from industrial effluents is critical for the safe discharge into surface water. Therefore, much attention has already been paid by health agencies around the world to establish tight targets for removing these harmful pollutants from industrial effluents before discharging them to surface water. For example, the Agency of Toxic Substances and Disease Registry (ATSDR) limited the concentration of dimethylphenol to a maximum of 0.05 ppm in surface water (ATSDR 2015). The World Health Organization (WHO) has set the phenol concentration to 1 µg/L in drinking water (Hsieh et al. 2008). Water U.K. regulators have set the maximum concentration of phenol in the discharge wastewater of hospitals to be within 10 ppm (Water U.K. 2011). However, the European Union (EU) has regulated total phenols in drinking water to be less than 0.0005 ppm. Broadly speaking, the existence of trace amounts of phenol in industrial effluents can prevent the reuse of water in many applications (Kamble et al. 2008).

1.6.2 N-nitrosamine

N-nitrosamines are one of the trace organic chemicals found in reclaimed water, which considered as one of the by-products of disinfection process of secondary-treated wastewater effluent with chloramines, chlorines, and ozone (inhibitors) (Charrois et al. 2007; Bond et al. 2011; Brisson et al. 2013). The mechanism of N-nitrosamine formation is quite complex due to several reasons including; the possibility that many reactions occur simultaneously in addition to the dependence of reactant concentration and the existence of inhibitors (Charrois et al. 2007). Farré et al. (2011) illustrated the proposed two steps of NDMA (N-nitrosodimethylamine-D6) (C₂H₆N₂O) (the most dangerous compound in N-nitrosamine family) formation in reclaimed water as: a) the reaction of monochloramine (NH₂Cl) with unsymmetrical dimethylhydrazine (UDMH), b) NH₂Cl oxidizes the UDMH intermediate to form NDMA. Also, they concluded that the

rate of NDMA formation increases with the supplied disinfectant dose. Another mechanism of NDMA formation is proposed by the reaction of chloroamines with dimethylamine during chlorine disinfection (Choi and Valentine 2002). NDMA has the lowest molecular weight in the N-nitrosamine family of 74.05, is one of the most concerning (most toxic) compounds in N-nitrosamine family, which can pose toxicological threats to wildlife and its formation can exceed 100 ng/L during chlorination of secondary wastewater effluent (Najm and Trussell 2001). Unfortunately, NDMA is found more often with a rate above legal limits in treated water supply systems including drinking water and wastewater facilities. Therefore, many water authorities around the globe are now regulated against a strict allowable N-nitrosamine concentration level in drinking water and recycled water (US EPA 2009a). For example, the International Agency for Research on Cancer has classified N-nitrosamine as a probably carcinogenic compound to human where a cancer risk level is exhibited at 0.7 ng/L concentration. The US Environmental Protection Agency (US EPA) has restricted the concentration of N-nitrosamine in recycled water to this same level (US EPA 2009b).

1.7 Rationale for selection the RO process in wastewater treatment

Specifically, the most successful treatment processes of phenol compounds removal from wastewater include catalytic wet air oxidation (CWAO), UV/H₂O₂ and RO. CWAO used trickle bed reactor using CUO, Zn, CO oxides as a heterogeneous catalyst and pure oxygen as oxidant of phenol (Mohammed et al. 2016). However, the UV/H₂O₂ technology not only consumes a lot of energy, but it also potentially increases the risk of increasing the carbon concentration of the reused water (Fujioka 2014a).

In the same context, to minimise the risk of releasing NDMA into the recycled water, several treatment approaches have been implemented in indirect potable water reuse schemes. Sharma (2012) reviewed many N-nitrosamine treatment processes and illustrated the specification of each one. It is concluded that UV oxidation is regarded to be the most efficient method. Resin and zeolites adsorption, activated carbon adsorption, sand filtration and ozonation have a little effect in removing NDMA (Krauss et al. 2010). However, an effective and advanced treatment method of effluents coming from wastewater treatment plants, is the combination of several treatment technologies including coagulation with ferric chloride, disinfection by chloramination, ultrafiltration (UF), RO, and an

ultraviolet radiation-hydrogen peroxide advanced oxidation process UV/H₂O₂ (Steinle-Darling et al. 2007; Fujioka et al. 2012). However, the main drawback of this advanced technology is the requirements of high energy (high expensive) due to the requirements of high dose of UV radiation to achieve acceptable levels of NDMA removal in comparison to lower dose used for other organic impurities of wastewater (Fujioka 2014a). This resulted in diverting much attention to membrane technology for reducing treatment costs. Also, the interest scientist to use the RO as a projecting approach is increased in response to avoid the need for costly conventional methods in addition to satisfy the increasingly stringent limits of N-nitrosamine concentration. This methodology has many immediate advantages, including minimum thermal damage, no chemical reactions, high packing density, low energy consumption and high rate of contaminant removal (Fritzmann et al. 2007; Reverberi et al. 2014). In other words, RO offers both a sustainable and economical solution for water treatment with low capital and operating costs and good product recovery and quality (low pollutant concentration) (Marcovecchio et al. 2005), which enhances the use of reclaimed water in different industrial applications (Blandin et al. 2016).

To the best of author's knowledge, a limited number of published models describing RO process, especially for wastewater treatment is available in the public domain. Additionally, it is proved that the available literature includes a few attempts, which explored the distributed modeling of spiral wound RO process used especially for wastewater treatment regarding the removal of high-toxic pollutants from wastewater including the phenolic and N-nitrosamine compounds. These models are developed under critical assumptions. It is therefore essential to generate an accurate model with a reliable process design, which can describe the process more accurately.

The literature contains a few attempts of simulation studies considering the aspect of phenolic and N-nitrosamine compounds. In fact, the available simulation studies are carried out under implementing simple design of the RO process and limited range of operating conditions. Therefore, it is important to investigate the performance of spiral wound RO process for a wide range of operating parameters and complex design of RO process with analysing the complex interaction between them. Also, a number of operating parameters must be controlled within the process constraints to achieve an efficient removal of such pollutants. Understanding the process dynamics is absolutely essential and

is a pre-step for designing any effective controllers. However, there is no any attempt to analyse the dynamic behavior and the sensitivity of the unit performance to a variety of operating parameters.

The process optimisation is to locate the best operating parameters that can achieve the objective functions of maximising the process performance and energy consumption with considering the manufacturer's specification. The literature confirms the lack of optimisation studies especially considering the removal of phenolic and N-nitrosamine compounds from wastewater. To the best of author's knowledge, no studies have been reported for optimising the operating parameters to ensure high removal of these compounds from wastewater.

Finally, exploring the feasibility of complex design including permeate and retentate reprocessing in multi-stage and multi-pass RO process has not explored yet.

1.8 Application of RO in food industries

The membrane technology including RO process is widely used as a potential technique in food industries such as dairy and beverage industries. Significant sales of RO equipment into the food started in 1970s (Pepper 1990). However, the effluents of food industries are more complex compared to seawater, which required the knowledge to select the best membrane type. The treatment of effluents of food industry serve to produce purified and reuse water that reduces the production cost and lowering the effluent volume. Specifically, the hybrid process of several stages of ultrafiltration, nanofiltration and RO has been proposed for the treatment of dairy effluents (Balannec et al. 2005). Also, RO process is used in milk industry as a pre-concentrator before an evaporator to reduce its volume for improving the quality of yoghurt (Jiao et al. 2004).

In this respect, the fruit juice industry concentrates juices to remove excess water, enhance product stability. This has many advantages, including easier and cheaper conservation, storage, transportation, and distribution of the extracted juice. Conventional methods of fruit juices concentration are usually conducted using a high temperature multi-stage vacuum evaporation process. This process usually results in significant losses of nutritional compounds, such as vitamin C, as well as associated thermal effects (Pozderović et al. 2006a). Many experimental studies reported that the process of fruit juice evaporation has a negative impact on taste compound's retention by losing a 90% of volatile aroma

compounds (Olsson and Trägårdh 1999; Pozderović et al. 2006b). As a result, RO has become an alternative process to the conventional methods for removing water from fruit juices and other liquid foods (Girard et al. 2000a). Specifically, RO can be counted as a prominent process in fruit juice concentration due to its ability to effectively retain the flavour, sensory, aroma and nutritional characteristics and concentrate the juice (Alvarez et al. 1997; Kozák et al. 2008). Also, this process minimises the thermal damage of fruit juice due to using low temperature (4 to 50 °C) operation (Girard et al. 2000a). Specifically, the RO process has disadvantage of incapacity to concentrate the standard products compared to evaporation because of high osmotic pressure limitation.

To the best of author's knowledge, no attempt has considered the distributed modelling of spiral wound RO for apple juice concentration. Indeed, there appears to be a gap in the use of an optimisation of the spiral wound RO network for apple juice concentration.

1.9 Scope of this research

RO is a key treatment process in water reclamation applications for the removal of organic chemicals. Also, RO is extensively used in food processing. The research conducted in this study serves these precise purposes and explores the spiral wound RO process as an alternative approach for concentration reduction of high-toxic impurities in industrial wastewater and concentration of apple juice. The investigated pollutants were phenolic and N-nitrosamine compounds, which are considered as extremely toxic compounds with several harmful effects for humans, the environment, and the aquatic life.

Due to the presented backdrop presented in Sections 1.7 and 1.8, the recent research focuses on exploring several strategies to improve the removal of the highly toxic compounds from wastewater including phenolic and N-nitrosamine compounds. These methods are mainly included feasible ideas of optimising the performance of the RO process. The research delivers several attempts of modelling the removal of high-toxic compounds using a spiral wound RO process. Also, the RO enhancement including the optimisation of operating parameters, permeate and retentate reprocessing methodology, and multi-pass design is achieved. Also, a case study of modelling, simulation, optimisation of simultaneous removal of organic and non-organic compounds from wastewater is delivered. This in turn reflects high contributions to the literature and refine the

reliability of removal the highly toxic selected pollutants from wastewater. The recent research also investigated the distributed modelling of spiral wound RO process for apple juice concentration and optimisation methodology. Despite many innovative ideas on the enhancement of the RO process for the removal of high-toxic compounds from wastewater are assembled in the recent research, the research shortcoming is projected in the following:

- The models developed have not referred to the fouling impact on the process performance and consideration of this aspect is also beyond the scope of this work. This is because there is no attempt in the literature to implement experimental research for a long time of operation for the removal of both the selected phenolic and N-nitrosamine compounds from wastewater. These experiments are readily required to investigate the process performance under the impact of fouling.
- The developed models are essentially characterised for the phenolic and N-nitrosamine due to the high passive impact of these compounds on the ecosystem. However, the models can be amended in case of offering the solute transport parameter and the mass transfer coefficient models for any prospected pollutant.

1.12 Research aim and objectives

1.12.1 Aim of research

The overall aim of this research is to develop comprehensive mathematical modelling for the spiral wound RO process based on the removal of highly toxic phenolic and N-nitrosamine compounds from wastewater and apple juice concentration process. The developed models will be used to investigate a reliable operation for the RO process via simulation and optimisation studies using the gPROMS (general Process Modelling System) software.

1.12.2 Objectives of research

- To carry out a literature survey on the modelling based on the solution diffusion model and irreversible thermodynamic model to represent the conceptual performance of each model.
- 2. To carry out a literature survey on the simulation and optimisation of the RO based wastewater and apple juice concentration.

- 3. To develop several lumped and distributed (one and two-dimensional) steady state and dynamic models for spiral wound RO process for analysing the separation mechanism of toxic compounds. This also includes the process of apple juice concentration.
- 4. To carry out a parameter estimation to estimate the best values of the separation membrane parameters and the friction parameter.
- 5. To validate the developed models against the experimental data picked from the literature before doing further simulation and optimisation studies.
- To carry out comprehensive simulation studies to investigate the impact of operating parameters on the performance of spiral wound RO process including wastewater and apple juice concentration.
- 7. To analyse the dynamic behaviour and the sensitivity analysis of the unit performance to a variety of operating parameters.
- To carry out an optimisation study to investigate an optimal multi-stage RO
 process for a specified apple juice product of high concentration measured
 in °Brix.
- To evaluate the merit of a two-stage/two-pass RO process design for removing chlorophenol from water considering model-based techniques with embedding the model within an optimisation framework for maximising the removal of chlorophenol.
- 10.To carry out a comprehensive simulation and optimisation studies to explore several conceptual designs of multi-stage and multi-pass RO processes for N-nitrosamine removal considering model-based techniques and compute the total recovery rate and energy consumption for different configurations of retentate and permeate reprocessing techniques.
- 11.To explore a new conceptual multi-pass RO predictive design of RO process for the removal of N-nitrosamine from wastewater and evaluate the possibility of permeate-reprocessing in multi-stage RO process to enhance the removal of N-nitrosamine from wastewater.
- 12.To model the spiral wound RO process and examine the rejection of organic and non-organic multi compounds of wastewater under various operating parameters. Also, to maximise the rejection and the total permeate recovery via a multi-objective optimisation.

1.13 Thesis outline

The layout of the thesis is highlighted in the following.

Chapter 1: Introduction

General background of wastewater and the associated high-toxic compounds. A brief description of spiral wound RO process and its application in wastewater and apple juice concentration.

Chapter 2: Literature Review

A brief description of the feasibility of RO in wastewater and apple juice concentration process. The literature of experimental past work and membrane theory including overview of the spiral wound RO modelling and simulation of phenolic and N-nitrosamine compounds and apple juice process. Several methods of RO enhancement are addressed.

<u>Chapter 3</u>: Spiral Wound Reverse Osmosis Process Modelling and Validation This chapter presents all the new mathematical model developed for an individual and multistage RO process for the removal of phenolic and N-nitrosamine compounds from wastewater. This also includes the apple juice concentration process. The models' validation and parameter estimation are also provided. Finally, this chapter introduces the gPROMS software which is already used for modelling, simulation, and optimisation of the RO process for both wastewater treatment and apple juice concentration processes.

<u>Chapter 4</u>: Removal of Chlorophenol from Wastewater: Steady State Simulation, and Optimisation

This chapter presents an analysis study for the RO process under variable operating parameters at steady state conditions. Also, a case of two stage/two pass RO process to enhance the removal of chlorophenol is presented.

<u>Chapter 5</u>: Removal of Dimethylphenol from Wastewater: Dynamic Simulation The dynamic simulation of the RO process for the removal of dimethylphenol from wastewater is highlighted in this chapter.

<u>Chapter 6</u>: Removal of N Nitrosamine from Wastewater: Simulation, Network Design, and Optimisation.

This chapter is mainly focused on N-nitrosamine removal from wastewater using a single and multistage spiral wound RO process. This include the simulation and optimisation of NDMA rejection and energy consumption of different configurations. The performance of several configurations of multistage and

multi-pass RO process are evaluated. Moreover, the merits of a new conceptual design of multistage and multi-pass is assessed and optimised.

<u>Chapter 7</u>: Simultaneous Removal of Organic and Non-organic Compounds from Wastewater Using RO Process: Modelling, Simulation, and Optimisation

This chapter presents the simultaneous removal of organic and non-organic multi component wastewater using a spiral wound RO process. Also, the rejection and total recovery rate are optimised.

<u>Chapter 8</u>: Applications of Spiral Wound Reverse Osmosis for the Apple Juice Concentration: Simulation, and Optimisation

This chapter considers the apple juice concentration process using a single and multistage spiral wound RO process. The performance of membrane rejection at different concentrations, temperatures, and pressures is presented with maximising the apple juice concentration using different RO networks configurations via optimisation technique.

<u>Chapter 9</u>: Conclusions and Recommendations for Further Research

This chapter presents the conclusions extracted from the thesis and the recommendations for future research work.

Chapter 2

Literature Review

2.1 Introduction

Reverse osmosis (RO) has been widely used in water treatment to remove several pollutants, such as harmful trace organics, viruses, and dissolved organic matter and also in many other applications. This chapter presents the scope and limitation of the RO process in wastewater treatment and apple juice concentration as an example of food processing. This is carried out by reviewing the feasibility and reliability of RO process for the removal of several organic compounds include the phenolic and N-nitrosamine compounds (the scope of this research) from wastewater and including the apple juice concentration. A thorough literature review indicates that there are various models available, and it is therefore more appropriate to examine the most popular models, particularly those that accurately relate to the removal of organic and non-organic compounds. This chapter looks into a state-of-the art of the modelling of spiral wound RO process for the removal of organic and non-organic from water including the one developed for the removal of phenolic and N-nitrosamine compounds from wastewater and based on the two main models (the irreversible thermodynamics model and solution diffusion model) used in the past by several researchers.

Furthermore, this chapter presents a critical review of the experimental past work for the removal of phenolic and N-Nitrosamine compounds from wastewater. Overview the basic simulation for these compounds is presented briefly. In this respect, this chapter illustrates some literature relevant enhancement and optimisation methods for RO process with presenting the limited research of RO wastewater treatment process.

Finally, this chapter explores the application of RO process in apple juice concentration by illustrating the past work of process experimentation, modelling, and performance enhancement.

2.2 Feasibility of RO process in wastewater

The RO process is extensively used in a wide range of industrial application. Several researchers have explored the feasibility of the process. This in turn investigates the scope and limitation of the RO process for the removal of

different type of pollutants including the highly toxic compounds. Xijun et al. (1997) used a filtration system of two spiral wound non-cellulose composite membranes (total area of 10 m²) type ATFRO (APV, Denmark) linked in a series configuration in addition to a UF membrane for the pre-treatment of an original electroplating wastewater containing copper. Experimental results showed that the maximum copper rejection was around 96.4%.

Bódalo et al. (2004a) used a pilot-scale filtration batch system of an individual flat cell RO module supplied by INDEVEN (Spain) to treat a multi-component synthetic effluent stream of inorganic species of sulphate, ammonium, and cyanide compounds and to test the performance of membrane DESAL-3 (polyethersulfone) of 3x10⁻³ m². The results showed that the rejection of ammonium, cyanide, and sulphate in the range of 92.7-93.5%, 88-90% and 93.8-93.9% respectively, which were dependent on the use of different feed concentrations.

Qdais and Moussa (2004) tested the performance of a bench scale membrane module containing tubular spiral wound RO membrane of 2.5 m² to treat synthetic wastewater samples of different concentrations of copper and cadmium. The process efficiencies of removing Cu and Cd pollutants from wastewater were 98 and 99%, respectively.

Mohsen-Nia et al. (2007) studied the performance of a laboratory scale RO thin film (1.95 m²) composite spiral wound membrane type (RE2012-100) for removing copper and nickel from mixed salt system. The rejection values were around 98% with slightly higher removal of copper due to its larger size.

Gómez et al. (2009) investigated the impact of nature of membrane and operational variables on the performance of a bench scale of flat sheet membrane (3x10⁻³ m²) for removing aniline from aqueous solutions. This study concluded that membrane type (HR98PP) has the highest rejection of 91.8%, while the lowest rejection of 79% was obtained with membrane type MS05. Also, the aniline rejection was slightly increased due to an increase in operating pressure.

The pilot-plant scale of the RO process of a spiral wound module type 2521 TF (Korean CSM company) was used by Mohammadi et al. (2009) to study the performance of the process for removing chromium (Cr⁺⁶) from electroplating industry's effluents. Under optimum operating conditions, the highest removal of chromium was about 99%.

Sagne et al. (2010) investigated the impact of operating variables and membrane type (CPA2 and ESPA2 from Hydanautics and BW30 from DOW) (2.6 m²) for eliminating small organic solutes of carboxylic acids and alcohols from distillery condensates using a recycle mode RO pilot-plant of an individual spiral wound module. The experiments showed that caproic acid and 2.3-butanediol were completely removed. Moreover, the membrane type BW30 achieved maximum removal of more than 80% of butyric acid, valeric acid and 2-phenylethanol solutes compared to other membranes tested.

Madaeni and Koocheki (2010) studied the efficiency of the cross-flow filtration system of two thin film composite spiral wound membranes type Filmtec TW30HP-4641 (11.89 m²) in a series configuration to remove phosphate, sulfite, nitrite, and nitrate from wastewater. The experiment results showed maximum rejection of 91, 93, 95 and 98-99% for nitrite, nitrate, sulfite, and phosphate ions, respectively. However, the rejection of nitrite and nitrate ions can be improved to 99% by the addition of Monopotassium phosphate (KH₂PO₄) into the solution.

Thirugnanasambandham et al. (2016) evaluated the performance of a bench scale filtration system of a spiral wound membrane (2 m²) to treat wine industry wastewater under several operating conditions. The results revealed that all the operating conditions have a significant impact on the process performance and the optimum conditions, were explored for the maximum rejections of 91, 93 and 97% of color, COD¹, and Total Dissolved Salts (TDS), respectively.

The next section focuses on the state-of-art of the feasibility of the RO process for the removal of phenolic compounds and N-nitrosamine from wastewater (the scope of this research) as described below.

2.3 Phenolic compounds

The laboratory investigation of Sundaramoorthy et al. (2011b) confirms that the efficiency of eliminating chlorophenol from wastewater using a pilot-scale of an individual spiral wound RO process is around 83%, compared to 97% for dimethylphenol (Srinivasan et al. 2011). The 83% chlorophenol rejection rate is obtained using 13.58 atm, 2.583x10⁻⁴ m³/s, and 31 °C of operating pressure, flow rate, and temperature, respectively, with 22% total water recovery at an energy

¹ COD is an indicative measure of the amount of oxygen that can be consumed by reactions in a measured solution, which expressed in mass of oxygen consumed over volume of solution (mg/L). Therefore, COD can be used to quantify the amount of organics in water.

consumption of 2.034 kWh/m³ (pump efficiency=85%). The relatively low chlorophenol rejection rate is probably attributed to its high hydrophobicity properties in water (slightly dissolved in water) (20 g/L at 20 °C) in addition to its high activity due to the presence of hydroxyl group, which makes it easily penetrable through the membrane (Gami et al. 2014). Moreover, the experimental results of Srinivasan et al. (2010) confirmed a range of phenol rejection rate of 64 to 87 %.

Tabassi et al. (2014) investigated the performance of a pilot plant for an individual commercial polyamide thin film composite RO membrane spiral wound type SG 2514TF (Osmonics company) of 0.6 m² in removing phenol from synthetic aqueous solutions of different concentrations. The effect of the operating parameters on the process performance was studied where the maximum achieved phenol rejection exceeded to 80%.

Khazaali et al. (2014) confirmed that the maximum rejection of bisphenol A (BPA) from aqueous solutions using cross-flow filtration system of a low-pressure polyamide thin film composite spiral wound RO membrane type TW30-1812-100 (0.446 m²) was around 87%. The research was directed to pin-point the optimum operating pressure that commensurate with the highest rejection.

Occasionally, Li et al. (2010) have examined different types of NF nanofiltration and RO flat sheet membranes (0.072 m²) of plate and frame module to remove phenol from wastewater at a wide range of operating conditions. The results confirmed that phenol rejection of RO membrane type (RO99) is between 76 – 86% at operating pressure varies between 4.9 – 29.6 atm at constant feed concentration, velocity, and temperature of 500 ppm, 0.58 m/s, 25 °C, respectively. Moreover, the experimental work of Arsuaga et al. (2011) showed that a commercial flat sheet RO membranes (139 cm²) types TFC-HR and BW-30 were rejected 75% of phenol due to solute-membrane steric interactions compared to pyrogallol of 96% and 94%, respectively. The above illustrates that phenol and phenolic derivatives are not efficiently removed by RO membranes.

2.4 N-nitrosamine compounds

The efficacy of the RO process specifically for N-nitrosamine and more importantly for NDMA (N-nitrosodimethylamine-D6) ($C_2H_6N_2O$) removal continues to be a challenge as evidenced by a brief state-of-art review in the following.

Steinle-Darling et al. (2007) tested the rejection of seven N-nitrosoalkylamines using a flat-sheet of three commercial RO membranes. The results showed that NDMA rejection was restricted to 54-70% efficiency. Plumlee et al. (2008) tested the performance of the RO process to remove NDMA and concluded that the rejection varied from 24 to 56%. Krauss et al. (2010) confirmed that RO can remove NDMA to about 40-70%. The reason of different efficiencies for the removal of NDMA is attributed to the membrane type where different membranes have different efficiencies.

Fujioka et al. (2012) and Fujioka et al. (2013) used a laboratory-scale system of low pressure NF/RO membranes to investigate the rejection of eight compounds of N-nitrosamine. The results showed that the rejection of NDMA under the same operating conditions ranged between 8 – 80% depending on the type of membrane. Fujioka et al. (2014b) studied the rejection of N-nitrosamine using full-scale spiral wound RO membrane filtration systems with three and seven pressure vessels (PV) connected in series, respectively (one membrane of 7.9 m² per each PV). The study showed that NDMA rejection varies between 40 to 61% and 49 to 35%, respectively. However, a maximum rejection of eight N-nitrosamine compounds between 62% and 99% has been obtained by the experiments at 10.1 atm pressure, 2.43x10⁻³ m³/s of feed flow rate and 20 °C temperature

Schäfer et al. (2010) claimed that NDMA (uncharged and quite hydrophilic) does not stuck to the membrane properly and indeed remains in the water due to its high hydrophilicity ¹ (highly dissolved in water, water solubility: 290 g/L at 20 °C). They affirmed that the rejection of small neutral solutes (such as NDMA) is mainly due to its molecular size and membrane pore size. NDMA (MW 74.08) is in fact can be quite small of 73 Da, which is approximately close to 100 Da (Daltons) MWCO ² (molecular weight cut off of the RO membrane such as Koch membrane) (Andrea et al. 2010). Therefore, it can be said that size exclusion is the dominant mechanism for the removal of N-nitrosamine. This can possibly explain the poor rejection of NDMA in the RO systems. It can therefore be argued that the removal

¹ A hydrophilic molecule is one whose interactions and affinity with water and other polar substances are more thermodynamically favorable than their interactions with oil or other hydrophobic solvents. They are typically charge-polarized and capable of hydrogen bonding. This makes these molecules soluble not only in water but also in other polar solvents (Merriam-Webster dictionary).

² MWCO is defined as the molar mass above which more than 90% of a given compound is rejected (Andrea et al. 2010)

of NDMA using laboratory-scale and full-scale RO wastewater treatment process has not proved so far to be entirely efficient and that there is room for improvement. In conclusion, it is evident that RO membranes showed some promise, but they were not always efficient to remove NDMA.

2.5 Experimentation of RO wastewater treatment process

This section presents the literature of experiments for the removal of phenolic and N-nitrosamine from wastewater using the RO process.

2.5.1 Phenolic compounds

2.5.1.1 Dimethylphenol

A pilot-scale cross-flow RO filtration system of one commercial thin film Perma-TFC polyamide composite RO membrane packed into a spiral wound module (Make: Permionics, Vadodara, India, 0.75 m²) was used by Srinivasan et al. (2009) in the experiments of aqueous feed solutions of dimethylphenol. The characteristics of the spiral wound module are presented in Table 2.1. The experiments of dimethylphenol were carried out for five groups of feed concentrations varies between 2.125x10⁻³ kmol/m³ to 10.6x10⁻³ kmol/m³. Also, for each group of inlet feed concentration, the experiments were carried out for a set of feed pressure varies between 4.93 atm to 14.8 atm with a range of 31.5 °C to 34.5 °C of operating temperature. The feed was pumped in a constant feed flow rate of 3.33x10⁻⁴ m³/s in the experiments of dimethylphenol removal.

Table 2.1. Membrane characteristics and geometry

Property	Value
Make	Ion Exchange, India
Membrane material	TFC Polyamide
Module configuration	Spiral wound
Feed spacer thickness (t_f)	0.85 mm
Permeate channel thickness (t_p)	0.78 mm
Effective membrane area (A)	0.75 m ²
Module length (L)	0.45 m
Module width (W)	1.6667 m
Module diameter	2.5 inches

2.5.1.2 Chlorophenol and dimethylphenol

Sundaramoorthy et al. (2011b) and Srinivasan et al. (2011) used a laboratory pilot-scale cross flow RO filtration system of a commercial thin film composite RO membrane packed into a spiral wound module (Ion Exchange, India Ltd., 7.8456 m²) in their experimental work to remove chlorophenol and dimethylphenol from aqueous solutions of different concentrations. Table 2.2 shows the characteristics of the module used. The solutes concentrations varied from 0.778x10⁻³ to 6.548x10⁻³ kmol/m³. The feed was pumped at three flow rates of 2.166x10⁻⁴, 2.33x10⁻⁴ and 2.583x10⁻⁴ m³/s with a set of pressures varying from 5.83 to 13.58 atm for each flow rate.

Fig. 2.1 shows the schematic diagram of the corresponding experimental setup used by Srinivasan et al. (2009) and Srinivasan et al. (2011) and Sundaramoorthy et al. (2011b) of an individual spiral wound RO process.

Table 2.2. Membrane characteristics and geometry

Property	Value
	Ion Exchange, India Ltd.,
Maker and configuration	TFC Polyamide, spiral
	wound
Feed (t _f) and permeate (t _p) channel thickness	0.8 (mm) and 0.5 (mm)
Module length (L) and width (W)	0.934 (m) and 8.4 (m)
Membrane volume	6.2764x10-3 m ³
Effective membrane area (A)	7.8456 m ²
Module diameter	0.0825 (m)
Maximum operating temperature (°C)	40
Maximum operating pressure (atm)	24.7717
Maximum pressure drop per element (atm)	1.3817
Maximum and minimum feed flow rate (m³/s)	1x10 ⁻⁴ – 1x10 ⁻³

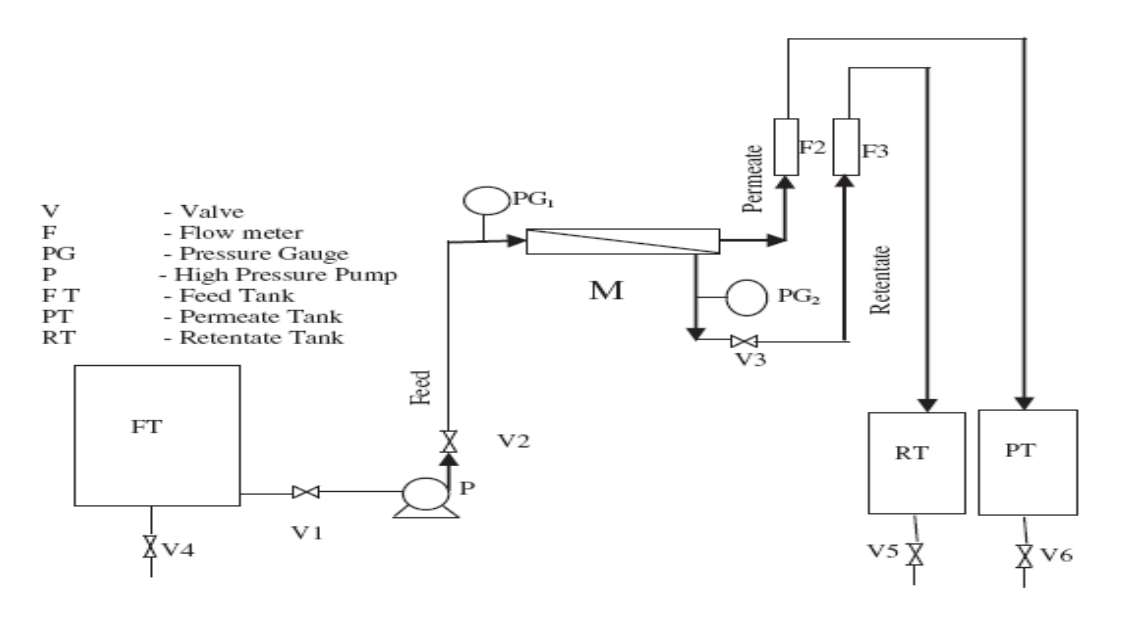


Fig. 2.1. Schematic diagram of an individual RO process (Adapted from Srinivasan et al. (2011))

2.5.2 N-nitrosamine compounds

A full-scale RO filtration system of three and seven 4-inch glass-fibre pressure vessels shown in Figs. 2.2 and 2.3, respectively were used by Fujioka (2014a) in the experiments of eight N-nitrosamine solutes rejection with a molecular weight in the range of 74 to 158 g/mol. The N-nitrosamine stock solution was prepared in pure methanol and contains 10 mg/L of each N-nitrosamine in the tested solution (pH 8.0) [N-nitrosodimethylamine-D6 (NDMA), Nnitrosomethylethylamine-D3 (NMEA), N-nitrosopyrrolidine-D8 (NPYR), Nnitrosodiethylamine-D10 (NDEA), N-nitrosopiperidine-D10 (NPIP), nitrosomorpholine-D8 (NMOR), N-nitrosodipropylamine-D14 (NDPA) and Nnitrosodi-n-butylamine-D9 (NDBA)] as summarised in Table 2.3. Also, an aqueous feed of stock solutions of NaCl, CaCl₂ and NaHCO₃ were also prepared in Milli-Q water at 2M (NaCl) and 0.1 M (CaCl2 and NaHCO3) to simulate the electrolyte composition typically found in treating wastewater. Then, the filtration experiment was carried out by introducing the stock solution of N-nitrosamine in the feed to obtain approximately 250 ng/L of each target N-nitrosamine. The feed was pumped using a high-pressure pump type (Hydra-Cell, Wanner Engineering) Inc., Minneapolis, Mn, USA), at constant volumetric flow rate of 2.43x10⁻³ m³/s, while the average permeate flux was adjusted at 2.78x10⁻⁶, 5.56x10⁻⁶, and 8.33x10⁻⁶ m/s during the experiments by increasing the operating feed pressure from 4, 6.5 and 10.1 atm. The feed solution temperature was kept along the experiments at 20±0.1 °C using a chiller/heater unit type (Neslab RTE 7, Thermo Scientific Inc., Waltham, MA, USA). Each pressure vessel holds only one spiral wound element type ESPA2-4040 (Make: Hydranautics, Oceanside, CA., USA, 7.9 m²). The pressure vessels were connected in series, where the concentrated feed solution of the first vessel was transferred to the second vessel followed by the third one. The feed tank (0.3 m³) in Figs. 2.2 and 2.3 was filled in with the model wastewater at the beginning of the process. After the process being started the collected permeate and retentate were circulated back to the feed reservoir to maintain constant feed concentration. The experimental work of Fujioka (2014a) has considered a very low concentration of N-nitrosamine. Therefore, the physical properties of diffusivity, density and viscosity have been assumed identical to water equations. The specifications of the spiral wound membrane element are given in Table 2.4.

Table 2.3. Physical and transport parameters of the eight N-nitrosamines

Name	Molecular weight (g/mol)	Inlet feed concentration, $C_{b(0)}x10^9$ (kmol/m³)	Solute permeability coefficient, Bs (m/s) at 20 °C	Reflection coefficient, σ (dimensionless)
NDMA	74.05	3.3761	5.35x10-6	0.953
NMEA	88.06	2.8389	1.14x10 ⁻⁶	0.958
NPYR	100.06	2.4985	5.12x10 ⁻⁷	0.973
NDEA	102.08	2.4490	2.26x10 ⁻⁷	0.985
NPIP	114.08	2.1914	9.25x10 ⁻⁸	0.993
NMOR	116.06	2.1540	2.06x10 ⁻⁷	0.991
NDPA	130.11	1.9214	6.02x10 ⁻⁸	0.992
NDBA	158.14	1.5808	4.33x10 ⁻⁸	0.990
Pure water permeability at 20 °C $I_{\text{m}} = 5.2 ~(\mp 0.2) \text{ L/m}^2\text{h}$ bar				

Pure water permeability at 20 °C L_p = 5.2 (\mp 0.2) L/m²h bar

Table 2.4. Specifications of the spiral wound membrane element

Property	Value
Make	Hydranautics, Oceanside, CA., USA
Membrane type and configuration	ESPA2-4040, Spiral-wound, Composite
	Polyamide
Feed and permeate spacer thickness t _f and t _p (m)	6.6x10 ⁻⁴
Membrane sheet area (m²)	7.9
Membrane sheet length L (m)	0.9
Membrane sheet width W (m)	8.7778
Characteristic length of spacer ΔL (m)	0.006
The efficiency of mixing K (dimensionless) *	0.5
Diffusion coefficient of NDMA D _b at 20 °C (m²/s)	9.7x10 ⁻¹⁰
Maximum applied pressure (atm)	41.056
Maximum operating temperature (°C)	45
Salt Rejection (dimensionless)	99.4% minimum

^{*: (}Mane et al. 2009)

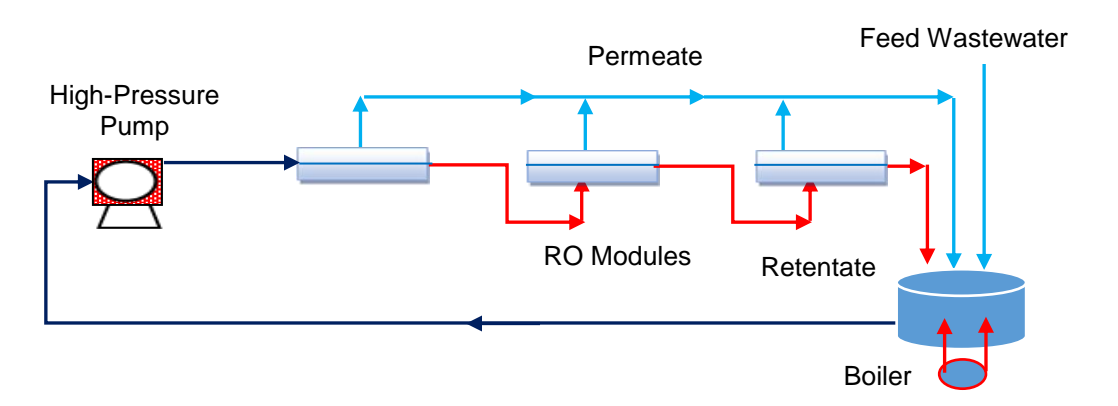


Fig. 2.2. Schematic diagram of full-scale three elements RO plant

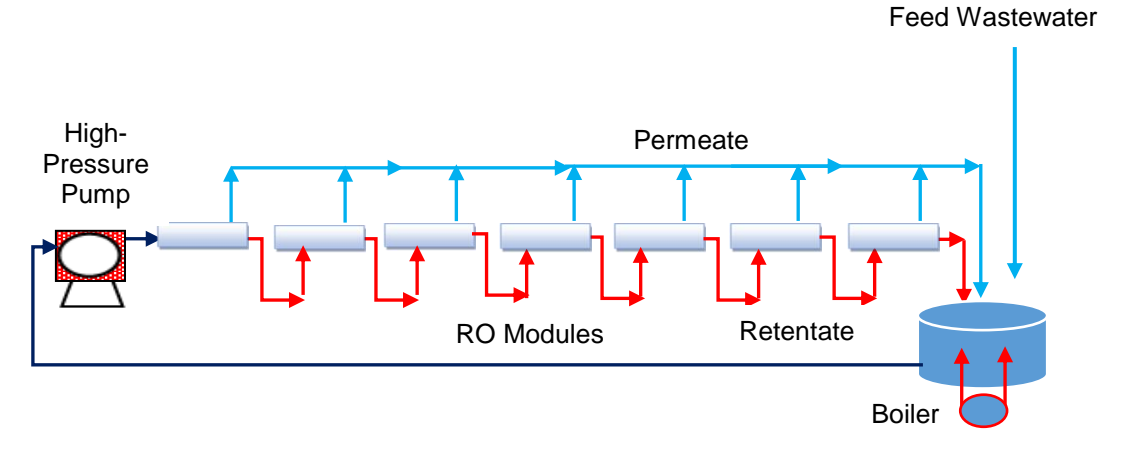


Fig. 2.3. Schematic diagram of full-scale seven elements RO plant

2.6 Feasibility of RO process in apple juice concentration

The RO process is a well-recognized technique for concentrating aqueous solutions of apple juice within a lower concentration of the yield of 25 to 30 °Brix¹. This is quite below the typical value of 45 to 60 °Brix gained by the evaporation process but it consumes higher energy (Pepper 1990). This can be attributed to the high osmotic pressure limitation of concentrated apple juices, which identifies as one of the disadvantages of using RO process. Most importantly, the RO process has affirmed its potential as the prominent process for retaining the aroma compounds (Jiao et al. 2004).

2.7 Experimentation of RO apple juice concentration

The RO system used in all of the experiments conducted by Alvarez et al. (2002) was designed in a laboratory scale experiment consisting of MSCB 2521 R99 spiral wound aromatic polyamide membrane module supplied by Sparem Spa. (Biella, Italy, 1.03 m²). The detail of the manufacturer's specification membrane module is given in Table 2.5. A' and n (dimensionless) are the spacer characteristics also given in Table 2.5 for the used spacer type. Table 2.6 shows the composition and concentration of the sugar and aroma compounds used by Alvarez et al. (2002) in all of the experiments as the feed with concentration 10.5± 0.5 °Brix. The solution was prepared from 72 °Brix concentrated apple juice by adding distilled water. Molar volume V_{bp,A} values for all sugar compounds are given in Table 2.6. Experiments are carried out using a batch operation mode where the standard flow configuration of the feed volume is plug flow (passes once time through the system) and the concentrate retentate is recycled back to the feed tank to achieve high system recovery. The permeate was recycled back to the feed tank to maintain a constant concentration and then removed from the equipment, which concentration was increased. Experiments were implemented at three different trans-membrane pressures of 14.8, 24.673 and 34.542 atm within 20 to 30 °C of temperature. The feed flow rate used are 5.5556x10⁻⁵, 1.111x10⁻⁴ and 1.6667x10⁻⁴ m³/s, respectively.

¹ Brix denotes the sugar content of an aqueous solution and traditionally used in the wine, sugar, carbonated beverage, fruit juice, maple syrup and honey industries. One-degree of °Brix means 1 gram of sucrose in 100 grams of solution and represents the strength of the solution as percentage by mass.

The next section focuses on an extensive literature review on the modelling of spiral wound RO process considering water treatment and food processing. The previous developed models of seawater desalination will be implicitly included to highlight the gap between the two sectors.

Table 2.5. Specifications of spiral wound membrane element and module constraints (Álvarez et al. 2002)

Make	Sparem Spa. (Biella, Italy)
	MSCB 2521 R99, Spiral-
Membrane type and configuration	wound,
	Polyamide membrane
Active surface area (A) (m²)	1.03
Feed and permeate spacer thickness (t _f) and (t _p) (m)	0.0007 and 0.00055
Membrane sheet length (L) and width (W) (m)	0.44 and 2.3409
Hydraulic diameter (m)	9.6x10 ⁻⁴
Max. operating pressure (atm)	41.4508
Max. operating temperature (°C)	50
Min. and Max. feed flow rate (m ³ /s)	2.5x10 ⁻⁵ – 1.6667x10 ⁻⁴
Spacer type	NALTEX-151-129
A' (dimensionless) *	7.38
n (dimensionless) *	0.34
ϵ (dimensionless) **	0.9058

^{*: (}Da Costa et al. 1994), **: (Al-Bastaki and Abbas 2003)

Table 2.6. Characteristics of the sugar and aroma compounds and inlet concentration in the model solution of 10.5 °Brix (Matsuura et al. 1976; Malaiyandi et al. 1982; Álvarez et al. 1998; Álvarez et al. 2002); (parameter estimation, Model Type_6)

Compound	Molecular weight M _{wt} , (kg/kmol)	Concentratio n C _{b(0)} , (kmol/m³)	Molar volume, V _{bp,A} (m³/kmol)	Free energy parameter $(-\frac{\Delta\Delta G}{RT})_{25 \text{ °C}}$	Steric Taft number, (δ*Es*) _{25°C}	Solute transport parameter, B _{s,25 °C} (m/s)
sucrose	342	0.035555	0.215689	-1.76	-7.42	2.329x10 ⁻¹⁰ *
glucose	180	0.138000	0.116987	1.81	-5.42	6.1146x10 ^{-8*}
malic acid	134	0.029104	0.083337			5.40x10 ⁻⁸
fructose	180	0.340722	0.106351	1.59	-5.56	4.2660x10 ^{-8*}
sorbitol	182	0.018406	0.122343	1.82	-5.57	5.3158x10 ^{-8*}
ethyl acetate	88.11	0.000566	0.097683	2.11	-0.07	4.818x10 ⁻⁶
ethyl butanoate	116.16	0.000129	0.132150	1.54	-0.43	1.739x10 ⁻⁶
ethyl-2-methyl butanoate	130.19	5.37x10 ⁻⁵	0.150508	1.47	-1.20	0.223x10 ⁻⁶
isopentyl acetate	130.19	0.000130	0.148618	1.47	-0.35	0.387x10 ⁻⁶
Hexyl acetate	144.22	6.926E-05	0.166274	1.85	-0.40	1.564x10 ⁻⁶
trans-2- hexenal	98.143	0.000712	0.116004			4.574x10 ⁻⁶
hexanal	100.2	0.000149	0.123095	2.19	-0.40	2.084x10 ⁻⁶
isobutanol	74.12	0.000269	0.092421	2.42	-0.93	0.302x10 ⁻⁶
butanol	74.12	0.000269	0.091506	2.17	-0.39	1.905x10 ⁻⁶
isopentanol	88.15	0.000169	0.108771	2.12	-0.35	0.297x10 ⁻⁶
hexanol	102.18	0.000293	0.125522	2.81	-0.40	1.556x10 ⁻⁶

^{*:} Calculated by parameter estimation, Model Type_6, Section 3.6.1.2 in Chapter 3

2.8 Modelling of RO process

Modelling of any industrial process plays a significant role in understanding of the process mechanism and aids the process design. Secondly, it helps to evaluate the impact of the operating parameters via simulation. This can lead to improve the process performance via optimisation.

2.8.1 Steady state and dynamic modelling

The performance of many industrial processes can be analysed using two simulation methods. Generally, the models are developed in two versions, steady state and dynamic. Dynamic models use variable flow and loads, whereas steady state models use constant flows and loads in respect to time. In other words, the inclusion of time variation in the dynamic one compared to zero-time derivation in steady state models is the main difference between these models. Therefore, it can be said that the dynamic simulation models are much more complex than steady state models because of their ability to predict the process response for a range of operating conditions in time. Moreover, the dynamic models are useful in examining the response of the process at any significant time of operation.

2.8.2 Membrane transport theories

Several RO theoretical transport models have been explored by various researchers to predict solute and solvent fluxes resulting in three types of models; the pore model (diffusion and convection-based), the non-porous model (diffusion-based) and the phenomenological model based on thermodynamic (Soltanieh and Gill 1981). However, a thorough literature review has been carried out by the author indicates that the solution diffusion model and irreversible thermodynamics model are the most widely used to describe the performance of membrane separation systems. The next section highlights in detail these important models developed to illustrate the separation phenomena of water and solute in RO process.

2.8.2.1 Solution diffusion model

The solution diffusion model can be considered as one of the simplest non-porous or homogeneous models related to transport mechanism criteria. Lonsdale et al. (1965) proposed the beginning stage of the solution diffusion model and insisted that the separation process can be achieved in RO units by both dissolving and

diffusing of each species in the solution (salt and solvent) independently through the membrane with dropping of the interaction between salt-solvent-membrane. In other words, this criterion is characterised by assuming that each solvent and solute are dissolved in the membrane separately on the high-pressure side and they are then diffused in individual fluxes through the membrane under the impact of pressure and concentration differences. The quality of permeate separation occurs due to the mobility of dissolved solute and the rate of its diffusion (Wijmans and Baker 1995). Thus, the fluxes of solvent and solutes are effectively concerned with the values of solubility and diffusivity of solvent and each solute in the membrane (Lonsdale et al. 1965).

In line with this model, the solvent flux J_w (m/s) is proportional to the divergence between the hydraulic pressure difference ΔP (atm) and the osmotic pressure difference $\Delta \pi$ (atm) across the membrane by the construction (Lonsdale et al. 1965)

$$J_{w} = A_{w} (\Delta P - \Delta \pi) \tag{2.1}$$

$$\Delta \pi = RT (C_w - C_p) \tag{2.2}$$

R and T (0.082 (atm m³)/(°K kmol), °K) are the Gas low constant and operating temperature, respectively. In addition, the salt flux J_s (kmol/m²s) is formulated as

$$J_{s} = B_{s} \left[C_{w} - C_{p} \right] \tag{2.3}$$

Lonsdale et al. (1965) stated that the membrane solvent water permeability constant $A_{\rm w}$ (m/s atm) depends on the structure of the membrane, while the salt permeability constant $B_{\rm s}$ (m/s) depends on salt composition and membrane structure. It is easy to see that this model assumes that the salt flux does not depend on the pressure difference. Occasionally, the solution diffusion model requires only a few parameters to be known to measure the mechanism of transport including the water and solute transport parameters. Finally, one of the imperfections of this model that it neglects the impact of pressure on solute flux, and the inclusion of pore flow and the membrane characteristics.

2.8.2.2 Irreversible thermodynamic model

The concept behind the irreversible thermodynamic model is derived from the principle theory of non-equilibrium thermodynamic systems, which are a type of thermodynamics that simulates most systems found in nature such as the transport processes (Fowler and Guggenheim 1965). Basically, the irreversible

thermodynamics model depends on non-equilibrium thermodynamic equations, which consider the membrane as a black box where slow processes are occurring near the equilibrium. Unfortunately, this implies that there is insufficient information for describing flow, transport mechanism and the structure of the membrane, one that can be accounted for as one of its imperfections. Hence, the applicability of using the irreversible thermodynamics model for accurate speculation of membrane separation is decreased.

The starting fundamental formula for the irreversible thermodynamic model was established by Kedem and Katchalsky (1958) and then by Spiegler and Kedem (1966) for a dilute two-component non-electrolyte system of water and solute as linear equations and non-linear equations, respectively relating the fluxes of these components.

The interesting aspect of this work is the idea that they found that these equations assumed in the solution diffusion model have only two permeability coefficients; the solute permeability coefficient and the water permeability coefficient, which were judged unsuitable for the irreversible thermodynamic processes. They believed that there should be a combination of three parameters rather than two parameters. Therefore, a third parameter of the reflection coefficient is added in order to express the broad criteria of a sensible interaction between the solutesolvent-membrane, which generates and enhances an acting force between them. Therefore, the interaction between the solute, solvent and membrane are included in this model for the first time, and the phenomenological relations can explain the reason of fluxes (Jonsson 1980; Sapienza et al. 1990; Van Gauwbergen and Baeyens 1998). They assumed that the variation of pressure and concentration gradients (the chemical potential) to be linear with low levels of solvent flow rates and the three membrane parameters, specific hydraulic permeability $L_{\rm p}$ (m/atm s), local solute permeability ω (kmol/m² s atm) and reflection coefficient σ (-) are constant. Moreover, the reflection coefficient can be considered as a scalar of the membrane semi-permeability by varying from zero for non-ideal membrane of non-solute selectivity to one of the ideal membrane, which passes only solvent (Spiegler and Kedem 1966). Hence, the transport models have been modified in order to include the reflection coefficient parameter σ , which describes the solute rejection. This is used as a parameter to evaluate the selectivity of solutes by the membrane (Zelman 1972; Muldowney and Punzi 1988) and measure the coupling of solute-solvent fluxes through the membrane (Marriott 2001). Therefore, the water and solute flux equations are

$$J_{w} = L_{p} \left(\Delta P - \sigma \Delta \pi \right) \tag{2.4}$$

$$J_{s} = \omega RT \left(C_{w} - C_{p}\right) + C_{s}^{\sim} (1 - \sigma) J_{w}$$

$$(2.5)$$

 C_s^{\sim} (kmol/m³) is the average solute concentration that can be defined as

$$C_{s}^{\sim} = \frac{C_{b} - C_{p}}{\ln\left(\frac{C_{b}}{C_{p}}\right)} \approx \frac{C_{b} + C_{p}}{2} \tag{2.6}$$

Eq. (2.4) shows that the reflection coefficient controls the osmotic pressure. Eq. (2.5) expresses the solute flux by incorporating of two terms, the first term illustrates the diffusive solute flux, while the second term illustrates the solute transport mechanism by convection, which is caused by the coupling between the solute and solvent through three parameters, σ , C_s^{\sim} and J_w . In the case where there is no coupling between the solvent and solute, the term of convection will be zero (solution diffusion model).

Unfortunately, the expression of average concentration (Eq. 2.6) is not exact in the event of high solvent flux or high concentration difference (Mason and Lonsdale 1990). Furthermore, the three transport parameters of this model are independent of each other and can simply represent the original phenomenological coefficients. They can be expressed as less independent of concentration (Kedem and Katchalsky 1958; Jonsson 1980; Soltanieh and Gill 1981; Van Gauwbergen and Baeyens 1998).

The main difference between the irreversible thermodynamic model and solution diffusion model is that the interaction between the solute, solvent, and membrane are specifically included in the irreversible thermodynamic model. As a result, this model is more widely used to describe the performance of the membrane separation in RO systems than any other investigated models (Mason and Lonsdale 1990; Murthy and Gupta 1998). However, Mujtaba (2012) showed that the solution diffusion model is the simplest non-porous or homogeneous model and one that is widely used in RO systems.

2.8.3 Overview of the spiral wound RO modelling

In the past two decades, many models have been reported in the literature for spiral wound RO configuration used to predict the removal of organic and non-organic compounds from aqueous solutions. These models used to speculate the membrane performance for a spiral wound module with different features and

applications based on some critical assumptions. These models have been applied to seawater and brackish water and validated against experimental data. Some comments on previous literature are made in the following.

A lumped model was developed by Gupta (1985) for a spiral wound module under laminar and turbulent flows and based on the solution diffusion model. It presumes constant mass transfer coefficient and solute concentration at the feed channel and neglects solute concentration at the permeate channel.

Avlonitis et al. (1991), Boudinar et al. (1992), Avlonitis et al. (1993) and Avlonitis et al. (2007) showed steady state two-dimensional (2D) models based on the solution diffusion theory. These models considered a full axial flow of solution, but they neglected the components of the tangential feed flow and the axial permeate flow. Also, it assumed constant physical properties and ignoring the variance of permeate concentration at constant mass transfer coefficient and ignored the concentration polarisation impact. Moreover, Boudinar et al. (1992) stated the pressure loss in the two channels being a function of feed and permeate friction parameters (Darcy's law for porous media).

Marriott and Sørensen (2003) developed a 2D dynamic model for a spiral wound RO module by using a mass, momentum, and energy balance equations. Whilst the model has relaxed several common assumptions, the variation of bulk concentration due to solvent flux through the membrane was not considered.

Geraldes et al. (2005) developed a 1D steady state model for spiral wound RO membranes based on the solution diffusion model by ignoring the pressure drop in the permeate channel and also the diffusion flow in the feed channel.

Based on the three-parameter model of Spiegler and Kedem (1966), Senthilmurugan et al. (2005) and Mane et al. (2009) developed models for turbulent flow by considering the pressure drop in both channels. Whereas, Mane et al. (2009) used the irreversible thermodynamic principles to develop two-dimensions (x and y) for the feed flow rate and stimulated the rejection of boron by using two commercially spiral wound modules in pilot-scale and full-scale RO seawater desalination processes with varying pH and pressures.

Sagne et al. (2009) investigated a one-dimensional (1D) dynamic model from the solution diffusion model to predict the performance of a spiral wound RO process on the dilute aqueous solution rejection of five volatile organic compounds (Acetic acid, Butyric acid, 2-Phenylethanol, 2,3-Butanediol, and Furfural) from brackish

water serviced in the fermentation industries. The model ignored the impact of the concentration polarisation and degraded the solute flux.

Oh et al. (2009) developed a comprehensive lumped model based on the solution diffusion principles for the simulation and optimisation of spiral wound RO system for seawater desalination. They assumed constant mass transfer coefficient and constant water flux in the case of changing the inlet feed flow rate. They also assumed constant permeate pressure.

Kaghazchi et al. (2010) proposed a 1D model based on the solution diffusion model where the bulk flow rate was calculated as an average value of inlet and outlet feed flow rates.

For an industrial scale RO desalination process, Chen-Jen et al. (2010) studied the dynamic characteristics and process operation by developing a mathematical 1D dynamic model. This work has combined the model of Oh et al. (2009) with that of Marriott and Sørensen (2003) and considered the impact of solvent flux on the bulk concentration.

Patroklou et al. (2013) developed a model for boron rejection based on the irreversible thermodynamic model and validated the model using experimental data of Mane et al. (2009).

Generally, all the models were developed for a spiral wound RO process and validated against experimental data derived for sea and brackish water (Sundaramoorthy et al. 2011a). A number of observations can be made on the models developed for RO process and validated against wastewater treatment as summarised in the next section.

Ahmad et al. (2007) developed a lumped model suitable for the multiple solutes system for dynamic simulation and prediction of membrane filtration in terms of permeate flux and concentration of each solute. This model was based on the irreversible thermodynamic principles and validated against experimental data derived from pre-treated palm oil mill effluent as a feed using a PVDF hollow fibre membrane module in a pilot plant scale RO system. In this aspect, Verliefde et al. (2009) proposed a transport model based on the Spiegler and Kedem model for the rejection of organic solutes for nano-filtration membranes.

Sundaramoorthy et al. (2011a) and Sundaramoorthy et al. (2011b) suggested a 1D steady state model, which is based on the solution diffusion model and assumed constant pressure and concentration at the permeate channel. Then,

an accepted convergence is achieved when the model prediction is compared with experimental data of chlorophenol and dimethylphenol solutes separately. Fujioka et al. (2014b) developed a 1D model based on the the irreversible thermodynamic principles of Spiegler and Kedem model and considered a variety of operating parameters by assuming zero permeate pressure. The model was validated against experimental data of N-nitrosamine rejection.

2.8.4 Modelling of spiral wound RO based on phenolic and N-nitrosamine compounds

This section specifically focuses on implementing an extensive review of the all past modelling of spiral wound RO process for the removal of phenolic and N-nitrosamine compounds from wastewater.

2.8.4.1 The model of Srinivasan et al. (2009 and 2010)

Srinivasan et al. (2009) and Srinivasan et al. (2010) used a simple lumped model based on the solution diffusion model to characterise the rejection of dimethylphenol and phenol from wastewater using an individual spiral wound RO process. The experiments of dimethylphenol and phenol removal from wastewater are described in Section 2.5.1.1. The schematic diagram of the RO filtration process is given in Fig. 2.1. Table 2.1 shows the characteristics of the RO membrane used.

Assumptions

- 1. Constant permeate pressure of 1 atm at the permeate channel.
- 2. Validity of the Vant Hoff's relation to express the osmotic pressure.
- 3. Validity of the film theory model to characterise the concentration polarisation.
- 4. Constant values of water and solute transport parameters.
- 5. Constant solute concentrations at the feed and permeate channels.
- 6. The underlying process was assumed to be isothermal.

Model equations

Table A.1 in Appendix A shows the model equations.

Parameters estimation

A graphical method of Murthy and Gupta (1999) was used to estimate the model transport parameters ($A_{\rm w}$ and $B_{\rm s}$). Table 2.7 shows the estimated values of these parameters.

Table 2.7. Results of parameter estimation

Solute	Parameter	Value
Dimethylphenol	A_{w}	$8.6428 \times 10^{-7} \left(\frac{m}{a tm s}\right)$
	B _s	$1.1822 \times 10^{-7} \left(\frac{\text{m}}{\text{s}}\right)$
Phenol	A _w	$5.9393x10^{-7} \left(\frac{m}{atm s}\right)$
	B _s	$6.5367 \times 10^{-7} \left(\frac{\text{m}}{\text{s}}\right)$

2.8.4.2 The model of Sundaramoorthy et al. (2011a)

A 1D model has been developed for an individual spiral wound RO process by Sundaramoorthy et al. (2011a). The model was able to predict the spatial variation of operating parameters along the membrane length. The experiments of chlorophenol and dimethylphenol removal from wastewater are described in Section 2.5.1.2. The schematic diagram of the RO filtration process is given in Fig. 2.1. Table 2.2 shows the characteristics of the RO membrane used. The assumptions of the model of Srinivasan et al. (2009) are valid except the relaxation of constant feed concentration at the feed channel. The model equations are given in Table A.2 in Appendix A with the two mass transfer coefficient correlations of dimethylphenol and chlorophenol.

Parameters estimation

Sundaramoorthy et al. (2011a) developed a graphical method to estimate the model unknown parameters including water $A_{\rm w}$ and solute $B_{\rm s}$ transport parameters and the friction factor b. Table 2.8 shows the parameters considering the membrane type Ion Exchange, India for the experiments of chlorophenol and dimethylphenol removal from wastewater.

Table 2.8. Results of parameter estimation measured at 30 - 32 °C

Solute	Parameter	Value
	A_{w}	$9.5188 \times 10^{-7} \left(\frac{\text{m}}{\text{atm s}}\right)$
Chlorophenol	B _s	$8.468 \times 10^{-8} \left(\frac{m}{s}\right)$
	b	$8529.45 \left(\frac{\text{atm s}}{\text{m}^4}\right)$
	A_{w}	$9.7388 \times 10^{-7} \left(\frac{m}{a \text{tm s}}\right)$
Dimethylphenol	B _s	$1.5876 \times 10^{-8} \left(\frac{m}{s}\right)$
	b	$9400.9 \left(\frac{a \operatorname{tm s}}{m^4}\right)$

2.8.4.3 The model of Fujioka et al. (2014b)

A comprehensive work to investigate the performance of a full-scale spiral wound RO plant was carried out by Fujioka et al. (2014b) who developed a specific 1D model based on the irreversible thermodynamics principles and hydrodynamic calculations to investigate the total N-nitrosamine rejection from wastewater. The experiments of N-nitrosamine removal from wastewater are described in Section 2.5.2. The schematic diagram of the RO filtration process of three and seven modules connected in a series configuration were shown in Figs. 2.2 and 2.3, respectively, while Table 2.4 shows the characteristics of the RO membrane module used.

Assumptions

- The pressure drop in the feed section was identified using Schock and Miquel model.
- 2. Local permeate pressure at the permeate channel was taken as zero.
- 3. The underlying process was assumed to be isothermal.

Model equations

The model equations are given in Table A.3 in Appendix A.

Parameter estimation

Fujioka et al. (2014b) used an iteration procedure to minimise the difference between the model prediction and the observed feed pressure to characterise the unknown friction parameter of the model. This method yielded the values of feed friction parameters of 3.9, 4.3 and 5.5 (-) at permeate flow rate of 2.78x10⁻⁶,

5.56x10⁻⁶ and 8.33x10⁻⁶ m/s, respectively. However, the water and solute permeability constants and the reflection coefficient of each solute are calculated experimentally and given in Table 2.3.

2.8.5 Overview of the spiral wound RO modelling of phenolic and N-nitrosamine compounds

The following are some critique regarding the model developed for the removal of phenolic and N-nitrosamine compounds from wastewater using the spiral wound RO process.

- A limited number of published models describing spiral wound RO process and especially for wastewater treatment is available in the public domain.
 Also, there are only a few validation studies of mathematical models with wastewater experimental data.
- Most of the suggested models have assumed constant pressure in the permeate channel. See for example the model of Srinivasan et al. (2009 and 2010).
- It is proved that the available literature includes a few attempts which explored the distributed modeling of spiral wound RO process used especially for wastewater treatment, which comprises the investigation of operating parameters and their impact along the membrane length and width.
- In most existing spiral wound published models, the feed flow rate is in the axial direction, while the permeate flow rate is in the spiral direction. See for example the model of Fujioka et al. (2014b). However, it is supposed to account the impact of tangential feed flow rate and axial permeate flow rate within the mathematical model due to the promotion of turbulence caused by the existence of turbulence promoting net (feed spacer). Also, using high pressures will make a substantial variation in the fluid mixing, mass transfer coefficient and pressure drop.
- Fujioka et al. (2014b) have only developed a distributed model for spiral wound RO process for wastewater treatment relying on the Spiegler and Kedem model. The model assumed zero pressure at the permeate channel. There is therefore a clear need to develop a new distributed model for a spiral wound module applicable to wastewater treatment data

based on using the principles of the irreversible thermodynamic equations albeit with relaxing the assumption of zero pressure on the permeate side.

2.8.6 Modelling of spiral wound RO based apple juice concentration

Several attempts can be found in the literature based on the RO process to improve the concentration of apple juice. Therefore, many models are developed in order to measure permeate flux and to elucidate the rejection of one component and multi-component fruit solutions. A critique on the current literature is discussed in the following section.

Nabetani et al. (1992a) proposed a new correlation to estimate the osmotic pressure of sucrose and glucose solution using thermodynamic definition of the osmotic pressure. The proposed equations assume that the osmotic pressure can be expressed in terms of solute concentration. Accordingly, Nabetani et al. (1992b) developed a lumped model using the combination of sucrose and glucose osmotic pressure developed in Nabetani et al. (1992a) with the solution diffusion model equations. The model can predict the permeation of apple juice solution considering the solution physical properties of both one component and a binary solute solution. The model has been validated for a tubular RO module type (ZF 99) supplied by PCI (Paterson Candy International, England) and shows a good agreement between experimental RO data and those calculated on the basis of the solution diffusion model. However, this particular model considered only sucrose and glucose solute concentration in the bulk retentate with ignoring the permeate concentration.

Alvarez et al. (1997) used the solution diffusion model and the film theory with the proposed osmotic pressure of Nabetani et al. (1992b) to predict the permeate flux in apple juice concentration. This was done by using a tubular polyamide RO membrane type (AFC 99) supplied by PCI (Paterson Candy International, England). The model incorporated the physico-chemical correlations to evaluate the characteristics of concentrated apple juice. However, the model ignored the solute concentration at the permeate side and degraded the osmotic pressure caused by fructose and sorbitol despite considering the contribution of sucrose, glucose, and malic acid to the osmotic pressure. Furthermore, Álvarez et al. (1998) used the procedure developed by Matsuura et al. (1974) to calculate the solute transport parameter for each aroma compound for a spiral wound RO aromatic polyamide membrane type (MSCB 2521 R99) supplied by Separem

Spa. (Biella, Italy). Table 2.6 reports the values of free energy parameter, steric Taft number and solute transport parameter for each aroma compound. Then, the solution diffusion model is used to estimate the rejection of hydrophilic aroma compounds by considering the average value of inlet feed and retentate as the concentration of bulk solution but overlooked the osmotic pressure. After that, Álvarez et al. (2001) studied the rejection of aroma compounds using experimental data of solute transport parameter for each aroma compounds calculated for the same above module of RO membrane in the solution diffusion model. Similarly, this work shows the influence of temperature and feed flow rate on pure water permeability coefficient. The model studied was used to predict the impact of operating conditions such as feed flow rate and concentration on the permeate flux and aroma rejections. However, feed osmotic pressure is referred only to glucose.

Álvarez et al. (2002) used the same procedure developed in the work shown above to predict the aroma compounds rejection and the permeate flux during the RO concentration of apple juice at laboratory and pilot-scales of MSCB 2521 R99 and MSCE 4040 R99 spiral wound membrane supplied by Separem Spa. (Biella, Italy), respectively. The model can predict the influence of operating conditions on permeate flux and aroma compounds rejection. However, this work not only ignored the contribution of fructose and sorbitol in feed osmotic pressure, but also neglected the concentration at the permeate side. Considerably, Table A.4 in Appendix A shows the model equations of the model developed by Álvarez et al. (2002) in apple juice concentration.

2.8.7 Overview of the spiral wound RO modelling of apple juice concentration

The following are some specific critique regarding the models developed for apple juice concentration based a spiral wound RO process:

• It is evident from the above statement that all the published RO process modelling for the concentration of apple juice have been carried out using the entire arrangement as a black box and simply taking average inputs and outputs parameter values. In this aspect, the finite difference approach needs to be used instead as it gives more accurate results because it considers the variation of the operating parameters along the entire system. The above studies have been proposed to describe flux behaviour and compounds retention by relying on the assumption that the osmotic pressure of sugar is only caused by glucose, sucrose, and malic acid, and thus ignoring fructose and sorbitol. Pereira et al. (1976) confirmed that glucose and fructose have greater mass transfer and solute transport characteristics than that of sucrose.

2.9 RO performance enhancements

Significant research from academic and industrial societies are made towards the enhancement of the RO process by optimising the operating conditions, superstructure and modules configuration, multi-stage, implementing an energy recovery device, membrane type and integrated process. The next sections categorise several methods of the RO enhancement and also highlights the gap between seawater desalination and wastewater treatment processes.

2.9.1 Operating parameters

Generally, as the water is removed, and the solute is rejected and accumulated at the membrane surface, the water flux drops due to an increase in the osmotic pressure of the feed and concentration polarisation impact. They are considered as the main factors causing flux deterioration. These impediments can be fixed by altering the operating condition such as, feed pressure, concentration, temperature, and cross-flow velocity and also by turbulence promotion, back flushing/washing and pulsed flow. Therefore, the operating conditions of inlet feed has significant effect on the performance of RO process and it is important to speculate the output rejection against the variation of feed parameters. This in turn will lead to find the optimum conditions of optimum performance of solute rejection.

Analysing the effects of operating parameters on the performance of wastewater RO treatment process is addressed in several studies. For example, Madaeni and Koocheki (2006) studied the operating parameters of trans-membrane pressure, temperature, and concentration, which influence the total flux and rejection of a solution containing nitrate, nitrite, sulphite, and phosphate using spiral wound RO pilot-plant. The results showed that trans-membrane pressure and temperature cause the highest impact on water flux compared to feed concentration, while the solute rejection is extremely affected by feed

concentration with a minor contribution for both the feed pressure and temperature.

Mohammadi et al. (2009) showed a steadily increase of chromium rejection due to an increase in operating pressure and flow rate for a pilot plant scale of a spiral wound RO module type 2521 TE made by a Korean CSM company. Also, the results showed insignificant impact of chromium feed concentration on its removal. However, the impact of temperature shows an optimum value, which attends maximum rejection.

2.9.1.1 Simulation of phenolic compounds removal by spiral wound RO process Li et al. (2010) studied the influence of feed flow rate, temperature, pressure, and concentration, on the performance of several NF and RO membranes (plate and frame module) to remove phenol in phenolics-containing synthetic wastewater. The results show small influence of feed flow rate and concentration on phenol rejection. However, the phenol rejection declines remarkably with temperature. Specifically, the phenol rejection clearly increases at low and medium pressures with insignificant incline at higher pressures. Tabassi et al. (2014) used a laboratory scale spiral wound RO thin film composite membrane type SG 2514TF of 0.6 m² area from GE Osmonics Company to study the influence of operating parameters on phenol rejection from aqueous solutions based on the Spiegler-Kedem model. The results depicted the increasing of phenol rejection with increasing operating pressure and feed concentration.

Khazaali et al. (2014) studied the influence of feed pressure, flow rate, and concentration on the rejection of aqueous solutions of bisphenol A (BPA) using a low-pressure polyamide RO membrane type TW30-1812-100 (Dow FilmTec Company) of 0.446 m² area. The bisphenol rejection increases due to an increase in feed pressure and flow rate. However, the results showed critical values of feed pressure and flow rate at which the rejection is maximised. In this respect, the rejection of bisphenol decreases due to an increase in feed concentration. However, low feed concentration can achieve low bisphenol rejection.

Srinivasan et al. (2009) and Srinivasan et al. (2010) have experimentally investigated the impact of operating parameters of an individual spiral wound RO process on the removal of dimethylphenol and phenol from wastewater, respectively. It is evident that increasing the operating pressure enhances the

removal of dimethylphenol and phenol. However, the permeate concentration increases due to increasing feed concentration.

2.9.1.2 Simulation of N-nitrosamine compounds removal by spiral wound RO process

Fujioka et al. (2014b) have experimentally investigated the impact of operating parameters of a pilot-scale of three spiral wound modules connected in a series configuration on the removal of N-nitrosamine from wastewater. The results showed a positive impact of operating pressure on the permeate flux and the removal of pollutants in addition to a negligible impact on solute flux. An increase of feed temperature resulted in a significant decrease of N-nitrosamine removal. This is because of enlarging the pore size within an active skin layer as a result to an increase of operating temperature (Sharma et al. 2003).

2.9.1.3 Overview of simulation phenolic and N-nitrosamine compounds

A critical review of the literature elucidates the following issues regarding the simulation of phenolic and N-nitrosamine compounds removal from wastewater:

- No study can be found in the literature to analyse the dynamic simulation of the removal of phenolic compounds from wastewater.
- Obviously, the impact of operating conditions on the removal of phenolic compounds rejection of multi-stage spiral wound RO process is not achieved yet.
- The detailed simulation of the removal of N-nitrosamine compounds of multi-stage RO process including energy recovery device has not been investigated yet.
- The removal of phenolic and N-nitrosamine compounds from wastewater using individual or multi-stage spiral wound RO processes has not been yet optimised by manipulating the operating conditions, where no study can be found for this purpose.

2.9.2 RO energy consumption

Significant research from academic and industrial societies are made towards the reduction of energy consumption of the RO process by optimising the operating conditions, investigating the number of stages, modules configuration, implementing an energy recovery device (ERD) and membrane type (Villafafila

and Mujtaba 2003; Zhu et al. 2009; Li 2011). Turbines and pressure exchangers options are used in the optimisation solution of Villafafila and Mujtaba (2003) who have reduced energy consumption by up to 50%.

However, the following reflects the issue regarding the RO wastewater treatment process:

 The efficacy and the analysis of the energy consumption of multi-stage spiral wound RO process with the existence of the turbine or ERD in the process of phenolic and N-nitrosamine compounds removal from wastewater has not been explored yet.

2.9.3 Multi-stage and multi-pass RO design

Several major adjustments in multi-stage seawater RO plant configurations had been examined in the literature. However, one of the best methods for RO superstructure optimisation has been developed by El-halwagi (1992) based on the state space approach, which considered the membrane module type and feed specification. It is experimentally proved that a single-pass RO system could not meet the requirements of low concentration of some impurities. Also, Du et al. (2016) confirmed the increasing strict constraints of the boron concentration in drinking water regulations, which holds a real challenge of the RO desalination system design. Therefore, the permeate reprocessing design (multi-pass) has been experienced as a compulsory choice due to the stringent limits of permeate concentration of some impurities such as boron. This in turn has enhanced the seawater RO process when very high permeate quality is required. Interestingly, Magara et al. (1998), Redondo et al. (2003) and Farhat et al. (2013) used this design and alleviated the boron concentration in drinking water with promising results through the RO desalination process.

In the aspect of the wastewater treatment, Hafez and El-Mariharawy (2004) used a full-scale plant using several technologies such as pH-adjustment, addition of the polymer coagulant, chlorination, dechlorination, filtration including RO membrane separation of two-stage/two-pass design of medium pressure RO membrane (maximum 16 bar) process to remove chromium from tannery effluent. The results showed that the plant can remove 99.9% of chromium based on the combined technologies used.

A critical review of the literature confirms the following issues:

- The assessment of multi-stage and multi-pass RO process design for the removal of phenolic compounds from wastewater has not been achieved yet.
- The research community has not addressed the performance of different configurations of multi-stage RO wastewater process for removing Nnitrosamine from wastewater.

2.9.4 Simulation of apple juice concentration by spiral wound RO process

The concentration of apple juice using the RO process is mainly affected by the sequence of operating parameters of feed pressure, temperature, and flow rate as reported in many studies (Sheu and Wiley 1983; Alvarez et al. 1997; Álvarez et al. 1998; Alvarez et al. 2001). In this line, Matsuura et al. (1974) affirmed that low operating temperature of the RO process can increase the retention of aroma components. Sheu and Wiley (1983) confirmed that the processing capacity of apple juice concentration is increased due to an increase in the operating temperature between 20 to 60 °C. Chou et al. (1991) deduced that lowering operating temperature and maximising the operating pressure (within the permitted limits of operation) can help to provide a concentrate stream of highflavour components content and an acceptable flux. Álvarez et al. (1998) studied the impact of operating pressure and flow rate on the permeation of apple juice through an individual spiral wound RO aromatic polyamide membrane type MSCB 2521 R99. The rejection of aroma compounds was observed to increase with the pressure and flow rate in the range of considered operating conditions. Álvarez et al. (2001) concluded that the permeate flux and aroma rejection are increased because of increased feed flow rate in a single spiral-wound RO process.

2.9.5 Enhancement of apple juice concentration process

The inclusion of the RO process as a first step of different processes in fruit juice concentration is considered in a commercial plant coupled with freeze concentration and/or evaporation. This technology can effectively double the operating capacity and improve both color and flavour characteristics (Girard et al. 2000b). For example, Matsuura et al. (1975a) used a two stage RO process in apple juice concentration process to increase flavour components recovery. In the first stage, the concentration of fruit juice sugars is chosen, while in the

second stage aroma compounds are recovered by filtering the permeate of the first stage. In this study, it is concluded that increasing pressure and lowering the processing temperature during the second stage can enhance the recovery of aroma compounds. Matsuura et al. (1975a) used the procedure developed by Matsuura et al. (1974) to calculate the solute transport parameter for each aroma compound, then the performance of RO has been investigated utilising their earlier proposed model (Matsuura and Sourirajan 1973). Some combinations of different types of membranes have been suggested for juice concentration and aroma recovery. Walker (1990) used a two-stage RO configuration to concentrate orange juice to 60 °Brix, while retaining the fresh juice flavour. The method comprises of three elements in series of high rejection aromatic polyamide hollow fiber membranes (Stage 1) and two low-rejection membranes in series (Stage 2). The raw orange juice is fed to Stage 1, while the retentate is fed to Stage 2. Moreover, the permeates of the two stages are blended and recycled to the feed of Stage 1. This configuration has lowered the cost of orange juice production in comparison to freeze concentration processes. Nabetani (1996) tested an integrated series of RO-NF membrane system for concentrating fruit juice. The feed juice of 10 °Brix is firstly concentrated with RO membranes to 30 °Brix and the retentate is then concentrated to 45 °Brix in NF membranes.

Alvarez et al. (2000) developed an integrated membrane process for producing apple juice and apple juice aroma concentrates, which involves clarification by microfiltration, pre-concentration by RO to 25 °Brix, and pervaporation to recover the aroma compounds and thermal evaporation to concentrate the clarified product from 25 to 72 °Brix. A series configuration of two spiral-wound RO modules is used in the experiments of Araujo and Maciel (2009) for assessing the performance of two types of commercial polyamide membranes for concentrating orange juice. The results show that the second module improves the productivity of orange juice measured in °Brix.

An optimisation based model has been achieved by Kiss et al. (2004) using a series of different types of membranes including; microfiltration (MF) and RO followed by nanofiltration (NF). The sugar content in the retentate measured in 'Brix and permeate flux were modelled using the linear regression of experimental data with time, and the model parameters are estimated using the Stat-graphics 5.1 program. The optimum independent variables of feed flow rate, trans-membrane pressure and temperature were investigated for optimum 'Brix.

Souza et al. (2013) tested the integration of the two membrane processes of RO and osmotic evaporation in order to concentrate clarified camu—camu juice with focusing on the phenolic compounds, vitamin C, and antioxidant activity of the final product. It is concluded that total solids content increased from 75 to 288 g kg⁻¹ and from 288 to 566 g kg⁻¹ using the RO process and osmotic evaporation, respectively. This confirmed the potential of the proposed membrane integration for camu—camu juice. To the best of the author's knowledge, there appears to be a gab in the use of an optimisation of the spiral wound RO network model for apple juice concentration. There also appears that the impact of different RO network configurations for concentrating apple juice has neither been explored nor yet achieved.

2.10 Conclusions

This chapter reviewed and discussed the feasibility of the RO process towards the removal of phenolic and N-nitrosamine compounds from wastewater and for the concentration of fruit juices in particular apple juices as an example of food processing. In this aspect, the associated experimental research of phenolic and N-nitrosamine compounds removal from wastewater and apple juice concentration were presented. The criterion of the chapter is focused on proving the maturity or otherwise of these models ranging from organic to non-organic compounds removal from water and wastewater including phenolic and Nnitrosamine compounds. The review has been designed to yield a one stop-shop critical appraisal and evolution of all the underlying models and associated concepts as well as considerations for improvement. It is clear from the research described in this chapter that RO remains as the most promising and economically viable separation process for removing harmful contents from wastewater at levels commensurate with environmental legislation. The state-ofthe-art provided in this chapter indicates that significant progress has been made for removing N-nitrosamine and phenolic compounds from wastewater, but there is still room for improvement for achieving a better and cheaper solution. Finally, a critical review of further improvement in the RO process is addressed, which showed the gap between the seawater desalination and wastewater treatment. This in turn elucidates the interest of this thesis. Finally, the performance of RO process was critically analysed for apple juice concentration.

Chapter 3

Spiral Wound Reverse Osmosis Process Modelling and Validation

3.1 Introduction

The implication of the RO process in different industrial applications demonstrate the effective economic process of separation and readily explain the large rise of RO markets. This in turn has motivated further interest in developing and optimising the associated mathematical models. Investigation and development of such transport models for RO operation have directed the attention to researching a specific pattern of RO with the perfect conditions for the separation process. These models also enable the evaluation of the performance properties of the membrane with regard to its quality of separation.

The spiral wound concept is the most commonly used model in RO as, it can readily be applied in a variety of different applications. However, there remains the challenge of having a reliable design for high process performance of the process. It is therefore important to develop rigorous and accurate mathematical modelling methodology requiring less experimental and pilot studies. This usually consists of a set of ordinary algebraic and differential equations, which are used to predict the process behaviour and thus facilitate the implementation of an effective optimisation process for minimising technical risks and costs.

Several mathematical models can be found in the literature for the RO membrane module transport phenomena. In contrast, few models are developed to explore the variation of operating parameters in one and two dimensions of the membrane especially for wastewater treatment. Specifically, the merit of distributed modelling is the considerations of the variance of all the operating parameters along the axial and tangential axes of the feed and permeate sides. This will offer a more accurate prediction of the performance of the process in comparison to lumped modelling. In this respect, it is important to note that the 2D modelling has the advantage of providing a facility for predicting the process performance more accurately than the 1D modelling. This is because the pattern of feed flow rate along the tangential direction for both the retentate and permeate sides are taken into consideration.

One of the requirements for designing control systems of RO is the development of a dynamic model, which can predict the transient characteristics of the plant.

It is therefore highly advantages to have a dynamical model capable of yielding a more efficient process control strategy and be used later to maintain the separation cost at an acceptable level.

This chapter focuses on presenting all the models developed in this research and associated performances of the most recent wastewater treatment methods based on the spiral wound RO process for the removal of high toxicological organic compounds from wastewater. In this respect, this chapter presents the models developed for the spiral wound RO process considering the apple juice concentration as an example of food processing. It provides a comprehensive explanation on various lumped and distributed models with illustrating a detailed validation studies against experimental results gathered from the literature.

The models developed are basically divided into two sections based on the solution diffusion model and irreversible thermodynamic model. The mathematical modelling of the membrane facilitates simulation and optimisation studies required for identifying the most effective design of the system. Finally, the methodology of gPROMS software used for modelling, simulation and optimisation is explained in detail.

3.2 Solution diffusion model

This section outlines all the models developed based on the validity of solution diffusion model. Moreover, the models developed are divided into distributed and lumped models.

3.2.1 Distributed models

3.2.1.1 Model Type_1

A mathematical 1D steady and dynamic model applicable for dilute binary aqueous solution in a spiral wound RO process has been developed. The model can predict the flow rate, concentration, pressure, and temperature in each point along the two sides of the membrane length regarding operating time. Besides, this model can predict the dynamic behavior of water flux, solute flux, and solute concentration on the wall of the membrane. This model is able to consider any organic compound in case of providing the proper mass transfer coefficient model.

Assumptions

- 1. A flat membrane sheet with negligible channel curvature.
- 2. Validity of the Darcy's law for the feed channel where the friction parameter is applied to characterise the pressure drop.
- 3. Validity of the film model theory to estimate the concentration polarisation impact.
- 4. Constant 1 atm pressure at the permeate side.
- 5. The permeate concentration will be varied along the membrane length, but the mean value will be considered as the fresh water output concentration for the calculation of the whole unit solute rejection. This is attributed to the direction of the accumulated permeate flow rate, which is in the spiral direction.
- 6. Solvent and solute transport parameters are constant.
- 7. The model is relaxed the assumptions of constant physical properties and concentration of the fresh water on the permeate side.
- 8. The bulk concentration varies along the membrane length due to the impact of both plug-flow and diffusion flow.
- 9. Negligible impact of feed spacer on the fluid patterns at the feed channel.
- 10. Constant friction factor of feed channel is assumed due to laminar flow.

Note, these assumptions are considered based on the extensive literature review on RO process models considered by others (as referenced in Section 2.8.3 in Chapter 2) for desalination. The wound membrane is basically treated as unwound, which has a similar configuration of the plate-and-frame module. This assumption was made by several researchers such as Senthilmurugan et al. (2005) and Sundaramoorthy et al. (2011a). This assumption is used to simplify the complex configuration of a spiral wound RO module. Also note, Gu et al. (2017) developed a successful one-dimensional model despite neglecting the presence of feed spacer and this model was validated against experimental data of seawater desalination (although not for wastewater treatment).

Model equations

The solution diffusion model assumes no interaction between the solute and solvent fluxes. The solvent flux is proportional to the divergence between the hydraulic pressure difference and the osmotic pressure difference across the

membrane. The solute flux is calculated from the concentration difference across the two sides of the membrane. Therefore, the solvent and solute molar fluxes $(J_w \text{ and } J_s)$ (m/s and kmol/m² s) are (Lonsdale et al. 1965)

$$J_{w(x)} = A_w \left(\Delta P_{b(x)} - \Delta \pi_{(x)} \right) \tag{M.1.1}$$

$$J_{s(x)} = B_s (C_{w(x)} - C_{p(x)})$$
 (M.1.2)

 $A_{\rm w}$ (m/atm s) and $B_{\rm s}$ (m/s) are the pure water and solute permeability constants of the membrane, respectively. $\Delta P_{\rm b}$ is the trans-membrane pressure and $\Delta \pi$ is the osmotic pressure difference along the length of the membrane L (m) defined by Eqs. (M.1.3) and (M.1.4). Likewise, $(\Delta P_{\rm b} - \Delta \pi)$ (atm) is the quantity of force per unit area required to cope with the osmotic pressure and to release pure water from the feed solution. $C_{\rm w}$ and $C_{\rm p}$ (kmol/m³) are the solute concentration at the membrane wall and permeate side, respectively.

$$\Delta P_{b(x)} = (P_{b(x)} - P_p) \tag{M.1.3}$$

$$\Delta \pi_{(x)} = RT_{b(x)} (C_{w(x)} - C_{p(x)})$$
(M.1.4)

R, T_b , P_b and P_p (atm m³/kmol K, K and atm) are the gas constant, temperature, pressure at the feed channel, and permeate pressure, respectively. The accumulated impermeable solute on the membrane surface causes the concentration polarisation layer and can be determined by using the stagnant film model proposed by Taniguchi (1978). Therefore, J_w is linked to concentration polarisation and k (m/s) (Assumption 3) by the following equation

$$\frac{(C_{w(x)} - C_{p(x)})}{(C_{b(x)} - C_{p(x)})} = \exp\left(\frac{J_{w(x)}}{k_{(x)}}\right)$$
(M.1.5)

 $C_{b(x)}$ (kmol/m³) is the solute concentration at the feed channel. $k_{(x)}$ is the mass transfer coefficient for the back diffusion of the solute from the membrane to the bulk solution on high pressure side of the membrane along the membrane length. Substituting Eqs. (M.1.3) and (M.1.4) in Eq. (M.1.1) and Eq. (M.1.5) in Eq. (M.1.2) gives

$$J_{w(x)} = A_w \left((P_{b(x)} - P_p) - RT_{b(x)} (C_{w(x)} - C_{p(x)}) \right)$$
(M.1.6)

$$J_{s(x)} = B_s \exp\left(\frac{J_{w(x)}}{k_{(x)}}\right) \left(C_{b(x)} - C_{p(x)}\right)$$
(M.1.7)

The solute flux through the membrane can be written as

$$J_{s(x)} = J_{w(x)} C_{p(x)}$$
 (M.1.8)

The total (whole module) mass and solute balance can be presented as

$$\frac{F_{b(0)} \rho_{b(0)}}{M_{wb(0)}} = \frac{F_{b(x)} \rho_{b(x)}}{M_{wb(x)}} + \frac{F_{p(x)} \rho_{p(x)}}{M_{wp(x)}}$$
(M.1.9)

 $F_{b(0)}$, $\rho_{b(0)}$, $F_{b(x)}$, $\rho_{b(x)}$, $F_{p(x)}$, $\rho_{p(x)}$ and $M_{wb(x)}$ (m³/s, kg/m³, g/gmol) are the feed flow rate and density at (x = 0) and at any point along the feed and permeate channels and molecular weight of solution, respectively. By assuming constant density and molecular weight (due to small quantity of contaminant), Eq. (M.1.9) can be written as

$$F_{b(0)} = F_{b(x)} + F_{p(x)}$$
 (M.1.10)

$$F_{b(0)} C_{b(0)} = F_{b(x)} C_{b(x)} + F_{p(x)} C_{p(x)}$$
(M.1.11)

The solution flow rate in x-axis can be estimated with the water flux through the membrane as

$$\frac{dF_{b(x)}}{dx} = -\frac{dF_{p(x)}}{dx} = -W J_{w(x)}$$
 (M.1.12)

W (m) is the width of membrane. Similarly, the permeate flow rate for each subsection is

$$F_{p(x)} = J_{w(x)} W \Delta x \tag{M.1.13}$$

 Δx (m) is the length of the sub-section. The pressure drop along the length of the membrane can be accounted from the momentum balance equation, which is based on the Darcy's law (Assumption 2) where the pressure loss is caused by the wall friction along the membrane.

$$\frac{dP_{b(x)}}{dx} = -b F_{b(x)}$$
 (M.1.14)

b (atm s/m⁴) is the friction factor along the feed and permeate channels.

The conservation equations of the dynamic model

The solution concentration varies along the membrane length due to the impact of the plug-flow and diffusion terms. According to solute balance along (x-axis) of membrane length and for sub-section of (Δx) , the change of solute hold-up can be written as

$$\frac{d(C_{b(x)}W t_f \Delta x)}{dt} = (F_s W t_f)_{x=0} - (F_s W t_f)_{x=\Delta x} - J_{s(x)} W \Delta x$$
(M.1.15)

 F_s (kmol/m² s) is the solute molar flux in the x-direction. Dividing the two sides of the above equation by the volume of sub-section with an arrangement, it reduces to

$$\frac{d(C_{b(x)})}{dt} = -\left[\frac{(F_s)_{x=\Delta x} - (F_s)_{x=0}}{\Delta x}\right] - \frac{J_{s(x)}}{t_f}$$
(M.1.16)

$$\frac{d(C_{b(x)})}{dt} = -\left[\frac{dF_{s(x)}}{\Delta x}\right] - \frac{J_{s(x)}}{t_{f}} \tag{M.1.17}$$

The solute molar flux can be defined as

$$F_{s(x)} = \frac{C_{b(x)} F_{b(x)}}{W t_f} - D_{b(x)} \frac{dC_{b(x)}}{dx}$$
(M.1.18)

 $D_{b(x)}(m^2/s)$ is the diffusivity coefficient of solute in water. The second term of Eq. (M.1.18) explains the effect of dispersion flux in the bulk fluid. Finally, the set of dynamic model equations for the solution and permeate concentrations can be written as

$$\frac{dC_{b(x)}}{dt} = -\frac{C_{b(x)}}{t_f W} \frac{dF_{b(x)}}{dx} - \frac{F_{b(x)}}{t_f W} \frac{dC_{b(x)}}{dx} + \frac{d}{dx} \left[D_{b(x)} \frac{dC_{b(x)}}{dx} \right] - \frac{J_{w(x)} C_{p(x)}}{t_f} \tag{M.1.19} \label{eq:master}$$

Similarly, for the permeate concentration

$$\frac{dC_{p(x)}}{dt} = -\frac{C_{p(x)}}{t_p W} \frac{dF_{p(x)}}{dx} - \frac{F_{p(x)}}{t_p W} \frac{dC_{p(x)}}{dx} + \frac{d}{dx} \left[D_{p(x)} \frac{dC_{p(x)}}{dx} \right] + \frac{J_{w(x)} C_{p(x)}}{t_f}$$
(M.1.20)

 D_p , t_f (m²/s, m) are the diffusivity coefficient of permeate along the length of the membrane, which varies with temperature and concentration, respectively. As can be seen from the above two equations, the dynamic behaviour of both feed and permeate concentrations is controlled by the flux of solute penetrate the membrane. Also, the dynamic behaviour of feed flow rate, feed pressure can be estimated from Eqs. (M.1.12) and (M.1.14) as

$$\frac{dF_{b(x)}}{dt} = \left[\left\{ -W \left(A_w \left((P_{b(x)} - P_p) - R T_{b(x)} \exp \left(\frac{J_{w(x)}}{k_{(x)}} \right) \left(C_{b(x)} - C_{p(x)} \right) \right) \right\} - \frac{dF_{b(x)}}{dx} \right] \left(\frac{F_{b(x)}}{t_f W} \right) \quad (M.1.21)$$

$$\frac{dP_{b(x)}}{dt} = \left[\left\{ \left(-b F_{b(x)} \right) \right\} - \frac{dP_{b(x)}}{dx} \right] \left(\frac{F_{b(x)}}{t_f W} \right) \tag{M.1.22}$$

Furthermore, the water and solute fluxes through the membrane and wall concentration are

$$\frac{\mathrm{d}J_{w(x)}}{\mathrm{d}t} = \left\{ \left(A_w \left((P_{b(x)} - P_p) - RT_{b(x)} \left(C_{w(x)} - C_{p(x)} \right) \right) \right) - J_{w(x)} \right\} \left(\frac{F_{b(x)}}{t_\varepsilon W \Lambda x} \right) \tag{M.1.23}$$

$$\frac{\mathrm{d}J_{\mathrm{s}(\mathrm{x})}}{\mathrm{d}t} = \left\{ \left(B_{\mathrm{s}} \exp\left(\frac{J_{\mathrm{w}(\mathrm{x})}}{k_{(\mathrm{x})}}\right) \left(C_{\mathrm{b}(\mathrm{x})} - C_{\mathrm{p}(\mathrm{x})} \right) \right) - J_{\mathrm{s}(\mathrm{x})} \right\} \left(\frac{F_{\mathrm{b}(\mathrm{x})}}{t_{\mathrm{f}} \, \mathrm{W} \, \Delta \mathrm{x}} \right) \tag{M.1.24}$$

$$\frac{dC_{w(x)}}{dt} = \left\{ \left(C_{p(x)} + \exp\left(\frac{J_{w(x)}}{k_{(x)}}\right) \left(C_{b(x)} - C_{p(x)} \right) \right) - C_{w(x)} \right\} \left(\frac{F_{b(x)}}{t_f \, W \, \Delta x} \right)$$
 (M.1.25)

The last set of equations contains the energy balance dynamic equations of feed and permeate temperatures along the length of the membrane. By assuming well insulated system

$$\frac{dT_{b(x)}}{dt} = \left[\frac{F_{b(x)} \left(T_{b(x-1)} - T_{b(x)} \right)}{t_f W \Delta x} \right] - \left[\frac{J_{w(x)} \left(T_{b(x)} - T_{p(x)} \right)}{t_f} \right]$$
(M.1.26)

$$\frac{dT_{p(x)}}{dt} = \left[\frac{J_{w(x)} (T_{b(x)} - T_{p(x)})}{t_f} \right]$$
 (M.1.27)

 T_b and T_p (°C) are the temperature at feed and permeate channels, respectively. The values of average solute rejection, total recovery, and permeate flow rate at each point and overall permeate flow rate values are calculated as follows

$$Rej_{(av)} = \frac{C_{b(x=L)} - C_{p(av)}}{C_{b(x=L)}} x100$$
 (M.1.28)

 $C_{b(x=L)} \ \text{and} \ C_{p(av)}$ are the retentate and average permeate concentrations, respectively.

$$C_{p(av)} = \frac{\sum C_{p(x)}}{\text{n.sub-divisions}} \dots (x = 0 \text{ to } x = L)$$
 (M.1.29)

$$Rec_{(Total)} = \frac{F_{p(Total)}}{F_{b(0)}} \times 100 \tag{M.1.30}$$

$$F_{p(x)} = J_{w(x)} W \Delta x \tag{M.1.31}$$

$$F_{p(Total)} = \sum F_{p(x)} \dots \dots (x = 0 \text{ to } x = L)$$
 (M.1.32)

 $Rec_{(Total)}$ is the total recovery rate of the whole unit. $F_{p(x)}$ and $F_{b(0)}$ are the permeate flow rate at each point on the membrane and the inlet feed flow rate, respectively.

The conservation equations of steady state model

The feed and permeate concentration can be estimated by eliminating the holdup term in the dynamic model Eqs. (M.1.19) and (M.1.20) and re-arrangement yields

$$0 = -\frac{c_{b(x)}}{t_f \ W} \frac{dF_{b(x)}}{dx} - \frac{F_{b(x)}}{t_f \ W} \frac{dC_{b(x)}}{dx} + \frac{d}{dx} \left[D_{b(x)} \frac{dC_{b(x)}}{dx} \right] - \frac{J_{w(x)} \ C_{p(x)}}{t_f} \tag{M.1.33}$$

$$0 = -\frac{c_{p(x)}}{t_p \ W} \frac{dF_{p(x)}}{dx} - \frac{F_{p(x)}}{t_p \ W} \frac{dC_{p(x)}}{dx} + \frac{d}{dx} \left[D_{p(x)} \frac{dC_{p(x)}}{dx} \right] + \frac{J_{w(x)} \ C_{p(x)}}{t_f} \tag{M.1.34}$$

Eqs. (M.1.33) and (M.1.34) can be re-written as

$$\frac{d\frac{(C_{b(x)}F_{b(x)})}{dx}}{dx} = -\frac{J_{s(x)}}{t_f} + \frac{d}{dx} \left(D_{b(x)} \frac{dC_{b(x)}}{dx} \right)$$
(M.1.35)

$$\frac{d\frac{\left(C_{p(x)}F_{p(x)}\right)}{t_{p}W}}{dx} = \frac{J_{s(x)}}{t_{f}} + \frac{d}{dx}\left(D_{p(x)}\frac{dC_{p(x)}}{dx}\right) \tag{M.1.36}$$

Also, the energy balance equations (assuming a constant heat capacity for feed and permeate) for the feed channel can be written as

$$F_{b(x)} (T_{b(x-1)} - T_{b(x)}) = J_{w(x)} (T_{b(x)} - T_{p(x)}) W \Delta x$$
(M.1.37)

$$(T_{b(x)} - T_{p(x)}) = 0$$
 (M.1.38)

The degree of freedom analysis of Model Type_1 is presented in Table A.5 in Appendix A and the specification of variables and input data are given in Tables A.6 and A.7 in Appendix A, respectively.

Model validation

This is carried out using experimental data of Sundaramoorthy et al. (2011b) from a laboratory scale spiral wound RO based wastewater treatment process removing chlorophenol (Section 2.5.1.2 in Chapter 2). The characteristics of the spiral wound module are presented in Table 2.2. The transport parameters of this model ($A_{\rm w}$, $B_{\rm s}$ and b) are predicted by Sundaramoorthy et al. (2011b) also shown in Table 2.8. Tables 3.1 – 3.3 compare the experimental results of chlorophenol removal and the model prediction for several operating parameters and process performance with different inlet feed flow rates, pressures, and concentrations. As can be seen, the predicted values of the theoretical model are in a good agreement with experimental ones over the ranges of pressure and concentration.

Table 3.1. Model Type_1 validation with experimental results for inlet feed flow rate of ($F_{b(0)} = 2.166 \times 10^{-4} \text{ m}^3\text{/s}$)

)x10 ³ ol/m³)	%Error) x10 ³ ol/m³)	%Error	%	Rej _{av}	%Error	F _{b(L)} x10) ⁴ (m³/s)	%Error
No	P _{b(0)} , atm	T _{b(0)} , °C	C _{b(0)} x10 ³ (kmol/m³)	Ехр.	Model	70L1101	Exp.	Model	70L1101	Ехр.	Model	7001101	Exp.	Model	70L1101
1	5.83	30	0.778	0.854	0.8502	0.50	0.37	0.393	-6.21	56.7	53.76	5.18	1.80	1.888	-4.88
2	7.77	30	0.778	0.9042	0.901	0.35	0.368	0.375	-2.14	59.3	57.8	2.52	1.67	1.754	-5.02
3	9.71	30	0.778	0.948	0.935	1.33	0.366	0.375	-2.45	61.4	59.89	2.45	1.59	1.620	-1.88
4	11.64	30	0.778	1.002	0.983	1.96	0.363	0.381	-5.04	63.8	61.24	4.01	1.50	1.489	0.73
5	13.58	30	0.778	1.065	1.036	2.73	0.36	0.391	-8.61	66.2	62.27	5.93	1.37	1.357	0.94
6	5.83	32	1.556	1.711	1.723	-0.68	0.652	0.696	-6.74	61.9	59.57	3.76	1.906	1.896	0.52
7	7.77	32	1.556	1.778	1.823	-2.50	0.642	0.635	1.09	63.9	65.18	-2.00	1.736	1.764	-1.61
8	9.71	32	1.556	1.850	1.936	-4.62	0.631	0.613	2.85	65.9	68.34	-3.70	1.63	1.632	-0.14
9	11.64	32	1.556	1.943	2.064	-6.17	0.624	0.608	2.46	67.9	70.51	-3.84	1.523	1.502	1.33
10	13.58	32	1.556	2.05	2.209	-7.75	0.615	0.613	0.22	70.0	72.22	-3.17	1.416	1.373	2.98
11	5.83	32	2.335	2.575	2.58	-0.17	0.886	0.94	-6.09	65.6	63.25	3.58	1.868	1.906	-2.03
12	7.77	32	2.335	2.662	2.73	-2.53	0.884	0.852	3.619	66.8	68.81	-3.00	1.761	1.777	-0.90
13	9.71	32	2.335	2.791	2.9	-3.90	0.882	0.814	7.70	68.4	71.95	-5.19	1.666	1.649	1.02
14	11.64	32	2.335	2.894	3.09	-6.74	0.88	0.801	8.97	69.6	74.11	-6.47	1.566	1.523	2.74
15	13.58	32	2.335	3.044	3.31	-8.70	0.88	0.802	8.86	71.1	75.78	-6.58	1.478	1.398	5.41
16	5.83	32	3.891	4.245	4.268	-0.54	1.244	1.18	5.14	70.7	72.35	-2.33	1.898	1.925	-1.42
17	7.77	32	3.891	4.444	4.525	-1.82	1.231	1.24	-0.73	72.3	72.59	-0.40	1.808	1.800	0.44
18	9.71	32	3.891	4.590	4.801	-4.59	1.299	1.17	9.93	71.7	75.68	-5.55	1.681	1.677	0.23
19	11.64	32	3.891	4.753	5.111	-7.51	1.198	1.14	4.84	74.8	77.78	-3.98	1.65	1.557	5.63
20	13.58	32	3.891	5.029	5.46	-8.55	1.187	1.126	5.13	76.4	79.38	-3.90	1.536	1.437	6.44
21	5.83	31	6.226	6.80	6.75	0.85	1.668	1.82	-9.11	75.5	73.08	3.20	1.923	1.951	-1.47
22	7.77	31	6.226	7.111	7.105	0.09	1.657	1.59	4.04	76.7	77.55	-1.10	1.828	1.838	-0.54
23	9.71	31	6.226	7.381	7.495	-1.54	1.491	1.495	-0.26	79.8	80.05	-0.31	1.75	1.726	1.37
24	11.64	31	6.226	7.763	7.928	-2.12	1.475	1.451	1.62	81.0	81.69	-0.85	1.641	1.615	1.58
25	13.58	31	6.226	8.049	8.411	-4.48	1.457	1.436	1.44	81.9	82.92	-1.24	1.575	1.506	4.38

Table 3.2. Model Type_1 validation with experimental results for inlet feed flow rate of ($F_{b(0)} = 2.33 \times 10^{-4} \text{ m}^3\text{/s}$)

					x10 ³ ol/m³)	%Error	1 ()	x10 ³ ol/m³)	%Error	%	Rej _{av}	%Error	F _{b(L)} 10	⁴ (m³/s)	- %Error
No	P _{b(0)} , atm	Т _{b(0)} , °С	$C_{b(0) x}10^3$ (kmol/m³)	Ехр.	Model	70L1101	Ехр.	Model	/0L1101	Ехр.	Model	70L1101	Ехр.	Model	70L1101
1	5.83	30	0.778	0.856	0.844	1.42	0.375	0.393	-4.80	56.2	53.4	4.98	1.957	2.057	-5.10
2	7.77	30	0.778	0.890	0.882	0.92	0.373	0.371	0.32	58.1	57.83	0.46	1.86	1.922	-3.33
3	9.71	30	0.778	0.937	0.923	1.49	0.372	0.368	0.88	60.3	60.04	0.43	1.742	1.788	-2.64
4	11.64	30	0.778	0.984	0.967	1.73	0.37	0.373	-0.81	62.4	61.41	1.58	1.639	1.655	-0.97
5	13.58	30	0.778	1.033	1.014	1.91	0.367	0.381	-3.89	64.5	62.42	3.22	1.542	1.524	1.16
6	5.83	32	1.556	1.703	1.708	-0.26	0.632	0.698	-10.44	62.9	59.11	6.02	2.01	2.063	-2.63
7	7.77	32	1.556	1.765	1.8	-1.95	0.625	0.628	-0.48	64.6	65.11	-0.78	1.894	1.93	-1.90
8	9.71	32	1.556	1.839	1.903	-3.46	0.618	0.601	2.63	66.4	68.39	-2.99	1.794	1.799	-0.27
9	11.64	32	1.556	1.926	2.018	-4.73	0.605	0.593	1.85	68.6	70.58	-2.88	1.684	1.668	0.95
10	13.58	32	1.556	2.023	2.148	-6.14	0.599	0.595	0.66	70.4	72.26	-2.64	1.594	1.538	3.51
11	5.83	31	2.335	2.568	2.54	1.11	0.804	0.853	-6.09	68.7	66.45	3.27	2.022	2.078	-2.81
12	7.77	31	2.335	2.673	2.67	0.12	0.802	0.76	5.23	70	71.35	-1.92	1.907	1.952	-2.35
13	9.71	31	2.335	2.783	2.815	-1.14	0.796	0.732	8.04	71.4	73.98	-3.61	1.815	1.826	-0.60
14	11.64	31	2.335	2.900	2.973	-2.50	0.786	0.722	8.14	72.9	75.7	-3.84	1.707	1.702	0.29
15	13.58	31	2.335	3.035	3.15	-3.78	0.777	0.725	6.69	74.4	76.97	-3.45	1.591	1.579	0.75
16	5.83	31	6.226	6.768	6.71	0.86	1.726	1.82	-5.44	74.5	72.76	2.33	2.082	2.117	-1.68
17	7.77	31	6.226	7.029	7.03	0.00	1.645	1.582	3.82	76.6	77.24	-0.84	1.987	2.004	-0.85
18	9.71	31	6.226	7.287	7.392	-1.43	1.472	1.471	0.06	79.8	80.1	-0.37	1.902	1.89	0.63
19	11.64	31	6.226	7.622	7.787	-2.16	1.433	1.418	1.04	81.2	81.79	-0.72	1.815	1.778	2.03
20	13.58	31	6.226	7.971	8.225	-3.17	1.419	1.395	1.69	82.2	83.02	-0.99	1.734	1.667	3.86

Table 3.3. Model Type_1 validation with experimental results for inlet feed flow rate of ($F_{b(0)}$ 2.583x10⁻⁴ m³/s)

				. ,	x10 ³ ol/m³)	%Error	1 (₎ x10 ³ ol/m³)	%Error	%	Rej _{av}	%Error	F _{b(L)} x10) ⁴ (m³/s)	%Error
No	P _{b(0)} , atm	Т _{ь(0)} , °С	C _{b(0)} x10 ³ (kmol/m ³)	Ехр.	Model	70L1101	Ехр.	Model	70L1101	Ехр.	Model	70L1101	Ехр.	Model	7021101
1	5.83	29.5	0.778	0.850	0.835	1.84	0.359	0.407	-13.37	57.8	51.21	11.40	2.2	2.317	-5.31
2	7.77	29.5	0.778	0.893	0.867	2.95	0.352	0.380	-8.12	60.6	56.14	7.35	2.075	2.182	-5.15
3	9.71	29.5	0.778	0.932	0.902	3.21	0.347	0.375	-8.06	62.8	58.44	6.94	1.953	2.048	-4.86
4	11.64	29.5	0.778	0.960	0.939	2.17	0.343	0.377	-10.11	64.3	59.8	6.99	1.838	1.915	-4.18
5	13.58	29.5	0.778	1.008	0.979	2.91	0.34	0.384	-12.94	66.3	60.74	8.38	1.72	1.783	-3.66
6	5.83	31	1.556	1.698	1.68	1.07	0.591	0.634	-7.27	65.2	62.25	4.52	2.262	2.327	-2.87
7	7.77	31	1.556	1.76	1.756	0.22	0.572	0.564	1.39	67.5	66.86	0.94	2.148	2.196	-2.23
8	9.71	31	1.556	1.825	1.839	-0.76	0.553	0.539	2.53	69.7	70.67	-1.39	2.042	2.065	-1.14
9	11.64	31	1.556	1.909	1.93	-1.06	0.55	0.532	3.25	71.2	72.43	-1.72	1.947	1.936	0.56
10	13.58	31	1.556	1.996	2.031	-1.73	0.549	0.534	2.73	72.5	73.7	-1.65	1.85	1.807	2.32
11	5.83	31	2.335	2.548	2.518	1.18	0.767	0.863	-12.51	69.9	65.73	5.96	2.29	2.337	-2.052
12	7.77	31	2.335	2.657	2.633	0.91	0.752	0.757	-0.69	71.7	71.24	0.64	2.173	2.209	-1.69
13	9.71	31	2.335	2.735	2.759	-0.87	0.744	0.715	3.83	72.8	74.07	-1.74	2.08	2.083	-0.14
14	11.64	31	2.335	2.841	2.898	-2.00	0.733	0.699	4.54	74.2	75.85	-2.22	1.97	1.957	0.65
15	13.58	31	2.335	2.987	3.051	-2.12	0.726	0.697	3.99	75.7	77.15	-1.91	1.868	1.833	1.87
16	5.83	32	3.891	XX	4.204	XX	XX	1.43	XX	XX	65.98	XX	XX	2.347	XX
17	7.77	32	3.891	XX	4.403	XX	XX	1.218	XX	XX	72.33	XX	XX	2.223	XX
18	9.71	32	3.891	4.504	4.625	-2.68	1.126	1.123	0.26	75	75.71	-0.94	2.113	2.099	0.66
19	11.64	32	3.891	4.635	4.869	-5.02	1.108	1.076	2.88	76.1	77.9	-2.36	2.07	1.976	4.54
20	13.58	32	3.891	4.831	5.141	-6.39	1.092	1.054	3.47	77.4	79.5	-2.71	1.972	1.854	5.98
21	5.83	31	6.226	6.733	6.655	1.16	1.845	1.854	-0.48	72.6	72.15	0.61	2.337	2.374	-1.60
22	7.77	31	6.226	6.977	6.943	0.49	1.549	1.57	-1.35	77.8	77.38	0.53	2.253	2.26	-0.31
23	9.71	31	6.226	7.213	7.261	-0.65	1.486	1.441	3.02	79.4	80.14	-0.93	2.17	2.145	1.15
24	11.64	31	6.226	7.497	7.608	-1.47	1.387	1.377	0.72	81.5	81.9	-0.49	2.09	2.031	2.78
25	13.58	31	6.226	7.794	7.991	-2.52	1.325	1.345	-1.50	83	83.17	-0.20	2.012	1.918	4.67

Note: (xx) means the experimental data have not been reported

3.2.1.2 Model Type_2

The literature shows that the models previously developed are restricted to 1D of a spiral wound RO process used especially for wastewater treatment and clearly neglect the tangential direction impact. Therefore, a 2D mathematical (steady state and dynamic) model applicable for dilute aqueous solution in a spiral wound RO system has been developed. Specifically, this model is considered as an extension of Model Type_1 by considering the variation of operating parameters along the two axes of the membrane.

Assumptions

The assumptions were made for the Model Type_1 are valid for Model Type_2 except the relaxation of a constant permeate pressure at the permeate channel (1 atm). However, reasonable assumptions were used to develop this model.

 The average value of the permeate concentration for all the increments in two dimensions will be taken as the total permeate concentration.

Model equations

Dynamic axial and vertical water flux and solute flux are represented as

$$\frac{dJ_{w(x,y)}}{dt} = \left\{ \left(A_w \left((P_{b(x,y)} - P_{p(x,y)}) - RT_{b(x,y)} \left(C_{w(x,y)} - C_{p(x,y)} \right) \right) \right) - J_{w(x,y)} \right\} \left(\frac{F_{b(x,y)}}{t_f \Delta x \Delta y} \right)$$
(M.2.1)

$$\frac{\mathrm{d}J_{\mathrm{s}(\mathrm{x},\mathrm{y})}}{\mathrm{d}t} = \left\{ \left(B_{\mathrm{s}} \exp\left(\frac{J_{\mathrm{w}(\mathrm{x},\mathrm{y})}}{k_{(\mathrm{x},\mathrm{y})}}\right) \left(C_{\mathrm{b}(\mathrm{x},\mathrm{y})} - C_{\mathrm{p}(\mathrm{x},\mathrm{y})} \right) \right) - J_{\mathrm{s}(\mathrm{x},\mathrm{y})} \right\} \left(\frac{F_{\mathrm{b}(\mathrm{x},\mathrm{y})}}{t_{\mathrm{f}} \Delta \mathrm{x} \Delta \mathrm{y}}\right) \tag{M.2.2}$$

Dynamic axial and vertical membrane wall concentration is

$$\frac{dC_{w(x,y)}}{dt} = \left\{ \left(C_{p(x,y)} + exp\left(\frac{J_{w(x,y)}}{k_{(x,y)}} \right) \left(C_{b(x,y)} - C_{p(x,y)} \right) \right) - C_{w(x,y)} \right\} \left(\frac{F_{b(x,y)}}{t_f \Delta x \Delta y} \right)$$
 (M.2.3)

Pressure difference and dynamic axial and vertical feed pressure and permeate pressure in both axes are given as

$$\Delta P_{b(x,y)} = (P_{b(x,y)} - P_{p(x,y)})$$
 (M.2.4)

$$\frac{dP_{b(x,y)}}{dt} = \left[\left[\left(\left(-b \; F_{b(x,y)} \right) \right) \left(\frac{F_{b(x,y)}}{\Delta x \; t_f} \right) \right] - \left[\left(\frac{dP_{b(x)}}{dx} \right) \left(\frac{F_{b(x,y)}}{\Delta y \; t_f} \right) \right] - \left[\left(\frac{dP_{b(y)}}{dy} \right) \left(\frac{F_{b(x,y)}}{\Delta x \; t_f} \right) \right] \right] \quad (\text{M.2.5})$$

$$\frac{\mathrm{d}P_{p(x,y)}}{\mathrm{d}t} = \left[\left[\left(\left(-b \; F_{p(x,y)} \right) \right) \left(\frac{F_{p(x,y)}}{\Delta y \; t_p} + \frac{F_{p(x,y)}}{\Delta x \; t_p} \right) \right] - \left[\left(\frac{\mathrm{d}P_{p(x,y)}}{\Delta y} \right) \left(\frac{F_{p(x,y)}}{\Delta y \; t_p} \right) \right] - \left[\left(\frac{\mathrm{d}P_{p(x,y)}}{\Delta y \; t_p} \right) \left(\frac{F_{p(x,y)}}{\Delta y \; t_p} \right) \right] \right] \tag{M.2.6}$$

Dynamic axial and vertical feed flow rate and permeate flow rate are calculated by

$$\frac{dF_{b(x,y)}}{dt} = \left\{ \left[-(\Delta y) \left(J_{w(x,y)} \right) \right] - (\frac{dF_{b(x,y)}}{dx}) \right\} \left\{ \frac{F_{b(x,y)}}{t_f \Delta y} \right\} + \left\{ \left[-(\Delta x) \left(J_{w(x,y)} \right) \right] - (\frac{dF_{b(x,y)}}{dy}) \right\} \left\{ \frac{F_{b(x,y)}}{t_f \Delta x} \right\}$$
 (M.2.7)

$$F_{p(x,y)} = J_{w(x,y)} \Delta x \Delta y \tag{M.2.8}$$

The dynamic variation of axial and vertical feed and permeate concentrations are

$$\begin{split} \frac{dC_{b(x,y)}}{dt} &= -\frac{C_{b(x,y)}}{t_f \Delta y} \, \frac{dF_{b(x,y)}}{dx} - \frac{F_{b(x,y)}}{t_f \Delta y} \frac{dC_{b(x,y)}}{dx} + \frac{d}{dx} \left[D_{b(x,y)} \frac{dC_{b(x,y)}}{dx} \right] - \frac{C_{b(x,y)}}{t_f \Delta x} \, \frac{dF_{b(x,y)}}{dy} - \\ & \qquad \qquad \frac{F_{b(x,y)}}{t_f \Delta x} \frac{dC_{b(x,y)}}{dy} + \frac{d}{dy} \left[D_{b(x,y)} \frac{dC_{b(x,y)}}{dy} \right] - \frac{J_{s(x,y)}}{t_f} \\ \frac{dC_{p(x,y)}}{dt} &= -\frac{C_{p(x,y)}}{t_f \Delta y} \, \frac{dF_{p(x,y)}}{dx} - \frac{F_{p(x,y)}}{t_f \Delta y} \frac{dC_{p(x,y)}}{dx} + \frac{d}{dx} \left[D_{p(x,y)} \frac{dC_{p(x,y)}}{dx} \right] - \frac{C_{p(x,y)}}{t_f \Delta x} \, \frac{dF_{p(x,y)}}{dy} - \\ & \qquad \qquad \frac{F_{p(x,y)}}{t_f \Delta x} \frac{dC_{p(x,y)}}{dy} + \frac{d}{dy} \left[D_{p(x,y)} \frac{dC_{p(x,y)}}{dy} \right] + \frac{J_{s(x,y)}}{t_f} \end{split} \tag{M.2.10}$$

Eq. (M.2.11) is used to calculate the average value of permeate concentration. This in turn used to calculate the average solute rejection

$$C_{p(av)} = \frac{\sum C_{p(x,y)}}{\text{n.sub-divisions}}$$
 (M.2.11)

$$Rej_{(av)} = \frac{C_{b(x=L,y)} - C_{p(av)}}{C_{b(x=L,y)}} x100$$
 (M.2.12)

Dynamic axial and vertical feed and permeate temperatures are

$$\frac{dT_{b(x,y)}}{dt} = \left[\frac{F_{b(x,y)} \left(T_{b(x-1,y)} - T_{b(x,y)} \right)}{t_f \Delta x \Delta y} \right] - \left[\frac{J_{w(x,y)} \left(T_{b(x,y)} - T_{p(x,y)} \right)}{t_f} \right]$$
(M.2.13)

$$\frac{dT_{p(x,y)}}{dt} = \left[\frac{J_{w(x,y)} \left(T_{b(x,y)} - T_{p(x,y)} \right)}{t_f} \right]$$
 (M.2.14)

The total permeate flow rate in the permeate channel is calculated as the summation of permeate flux of all the dimensions of axes. This is used to calculate the total recovery

$$F_{p(Total)} = \sum F_{p(x,y)}$$
 (M.2.15)

$$Rec_{(Total)} = \frac{F_{p(Total)}}{F_{b(0,y)}} \times 100$$
 (M.2.16)

Table A.8 in Appendix A presents the set of 2D dynamic model equation of Model Type_2, which are used to estimate the degree of freedom in Tables A.9 and A.10 in Appendix A.

Parameter estimation

The determination of the unknown parameters of the proposed model in addition to the operating parameters are key when solving the model equations. The parameters of the model are estimated by using the proposed graphical method of linear fit of Sundaramoorthy et al. (2011a). This model includes the solvent transport coefficient A_w , dimethylphenol transport coefficient B_s and the feed

channel friction parameter b. The results of parameter estimation are based on the experimental data of Srinivasan et al. (2011) and given in Table 3.4. The estimated values of $A_{\rm w}$ and $B_{\rm s}$ parameters showed some convergence than the values suggested by Srinivasan et al. (2011).

Table 3.4. Results of parameter estimation

Parameter	Estimated value	(Srinivasan et al. 2011) values
b	$9400.9 \left(\frac{atm s}{m^4}\right)$	$9400.9 \left(\frac{\text{atm s}}{\text{m}^4}\right)$
A _w	$9.42009x10^{-7} \left(\frac{m}{atm s}\right)$	$9.7388 \times 10^{-7} \left(\frac{m}{atm s}\right)$
B _s (dimethylphenol)	$2.22577x10^{-8} \left(\frac{m}{s}\right)$	$1.5876 \times 10^{-8} \left(\frac{m}{s}\right)$

Model validation

The steady state version of Model Type_2 is validated using experimental data of Srinivasan et al. (2011) for the rejection of dimethylphenol as solute in aqueous solutions. Tables 3.5 - 3.7 depict the comparison between experimental results of Srinivasan et al. (2011) and the model predictions for three groups of feed flow rates; (each group holding five different feed concentrations under five different feed pressures). This is carried out by estimating percentage of error between the experimental and the model predictions. Generally, the predicted values of the theoretical model are in a good agreement with the experimental ones. Also, Tables 3.5 – 3.7 show the agreement between the experimental and predicted values of outlet feed concentration and dimethylphenol rejection for the whole data within 5% error and 2.1% error, respectively. However, the model is able to predict the permeate concentration within a maximum of 15% error and less than 4% error for about 76% of retentate flow rate readings. Finally, 79% of retentate pressure readings are within 4% error as well. Therefore, it can be said that the permeate concentration represents the particular parameter that causes the biggest error.

Table 3.5. Model Type_2 validation with experimental results for inlet feed flow rate of ($F_{b(0,y)} = 2.166 \times 10^{-4} \text{ m}^3\text{/s}$)

				,	utlet), tm)		Cb(out	let)x10³ ol/m³)		C _{p(av)}) x10³ ol/m³)		Re	ej _(av)		Fb(outlet)	x10 ⁴ (m ³ /s)	
No	Pb (inlet) (atm)	Tb (inlet) (°C)	Cb(inlet) x10 ³ (kmol/m ³)	Exp.	The.	%Error	Exp.	The.	%Error	Exp.	The.	%Error	Exp.	The.	%Error	Ехр.	The.	%Error
1	5.83	32.5	0.819	4.46	4.06	8.96	0.9500	0.9230	2.84	0.0931	0.0885	4.84	0.902	0.904	-0.22	1.8	1.916	-6.44
2	7.77	32.5	0.819	6.31	6.06	3.96	1.0164	0.9909	2.51	0.0864	0.0734	15.0	0.915	0.9259	-1.19	1.67	1.786	-6.94
3	9.71	32.5	0.819	8.14	8.06	0.98	1.0821	1.0710	1.03	0.0790	0.0662	16.2	0.927	0.9382	-1.20	1.59	1.656	-4.15
4	11.64	32.5	0.819	9.98	10.05	-0.70	1.1562	1.1650	-0.75	0.0740	0.0623	15.8	0.936	0.9466	-1.13	1.5	1.528	-1.86
5	13.58	32.5	0.819	11.8	12.05	-2.11	1.2568	1.2800	-1.83	0.0729	0.0600	17.6	0.942	0.9531	-1.17	1.37	1.399	-2.11
6	5.83	31	1.637	4.41	4.05	8.16	1.8839	1.8300	2.86	0.1526	0.1730	-13.3	0.919	0.9051	1.51	1.851	1.932	-4.37
7	7.77	31	1.637	6.27	6.05	3.50	2.0227	1.9580	3.20	0.1335	0.1405	-5.24	0.934	0.9276	0.68	1.736	1.807	-4.08
8	9.71	31	1.637	8.09	8.05	0.49	2.1210	2.1100	0.52	0.1209	0.1272	-5.21	0.943	0.9397	0.34	1.63	1.681	-3.12
9	11.64	31	1.637	9.93	10.03	-1.00	2.2882	2.2830	0.22	0.1167	0.1189	-1.88	0.949	0.9479	0.11	1.523	1.557	-2.23
10	13.58	31	1.637	11.76	12.03	-2.29	2.4255	2.4940	-2.82	0.1140	0.1140	0.00	0.953	0.9543	-0.13	1.416	1.433	-1.20
11	5.83	31	2.455	4.37	4.042	7.50	2.7989	2.7310	2.42	0.2575	0.2367	8.07	0.908	0.9133	-0.58	1.868	1.942	-3.96
12	7.77	31	2.455	6.22	6.038	2.92	2.9783	2.9170	2.06	0.2204	0.1900	13.7	0.926	0.9348	-0.95	1.761	1.819	-3.29
13	9.71	31	2.455	8.05	8.034	0.19	3.1192	3.1350	-0.50	0.1778	0.1680	5.51	0.943	0.9464	-0.36	1.666	1.696	-1.80
14	11.64	31	2.455	9.89	10.02	-1.31	3.3529	3.3880	-1.04	0.1710	0.1557	8.94	0.949	0.954	-0.52	1.566	1.576	-0.63
15	13.58	31	2.455	11.72	12.016	-2.52	3.5062	3.6900	-5.24	0.1683	0.1482	11.9	0.952	0.9598	-0.81	1.478	1.453	1.69
16	5.83	30	4.092	4.32	4.03	6.71	4.6600	4.5070	3.28	0.3029	0.2730	9.87	0.935	0.9393	-0.45	1.898	1.962	-3.37
17	7.77	30	4.092	6.17	6.024	2.36	4.8066	4.7870	0.40	0.2884	0.3130	-8.52	0.94	0.9344	0.59	1.808	1.848	-2.21
18	9.71	30	4.092	8	8.017	-0.21	5.1470	5.1160	0.60	0.2625	0.2740	-4.38	0.949	0.9467	0.24	1.681	1.731	-2.97
19	11.64	30	4.092	9.84	10	-1.62	5.2933	5.4950	-3.80	0.2382	0.2525	-6.00	0.955	0.954	0.10	1.65	1.617	2.00
20	13.58	30	4.092	11.67	11.99	-2.74	5.6648	5.9410	-4.87	0.2096	0.2380	-13.5	0.963	0.9597	0.34	1.536	1.502	2.21
21	5.83	31.5	6.548	XX	4.025	XX	XX	7.1620	XX	XX	0.5141	XX	XX	0.9282	XX	XX	1.978	XX
22	7.77	31.5	6.548	6.13	6.017	1.84	7.7583	7.6060	1.96	0.3724	0.3878	-4.13	0.952	0.949	0.31	1.828	1.863	-1.91
23	9.71	31.5	6.548	7.96	8.01	-0.62	8.1052	8.1220	-0.20	0.3080	0.3299	-7.11	0.962	0.9593	0.28	1.75	1.747	0.17
24	11.64	31.5	6.548	9.79	9.993	-2.07	8.6566	8.7160	-0.68	0.2597	0.2970	-14.3	0.97	0.9659	0.42	1.641	1.633	0.48
25	13.58	31.5	6.548	11.62	11.98	-3.09	8.9111	9.4110	-5.60	0.2406	0.2760	-14.7	0.973	0.9706	0.24	1.575	1.517	3.68

Note: (xx) means the experimental data have not been reported.

Table 3.6. Model Type_2 validation with experimental results for inlet feed flow rate of ($F_{b(0,y)} = 2.33 \times 10^{-4} \text{ m}^3\text{/s}$)

				Pb(out	let), (atm)		Cb(outle (kmo	,		C _{p(av)} (kmo			Rej	j _(av)		,	let)x10 ⁴ ³ /s)	
No	Pb(inlet), (atm)	Tb(inlet), (°C)	Cb(inlet) ×10³ (kmol/m³)	Ехр.	The.	%Error	Ехр.	The.	%Error	Exp.	The.	%Error	Ехр.	The.	%Error	Exp.	The.	%Error
1	5.83	32.5	0.819	4.39	3.92	10.7	0.9432	0.912	3.24	0.091	0.088	3.06	0.903	0.902	0.02	1.957	2.085	-6.54
2	7.77	32.5	0.819	6.23	5.916	5.04	1.0058	0.974	3.16	0.085	0.072	15.4	0.915	0.925	-1.16	1.86	1.955	-5.10
3	9.71	32.5	0.819	8.06	7.916	1.78	1.0600	1.045	1.41	0.074	0.064	12.8	0.93	0.938	-0.87	1.742	1.825	-4.76
4	11.64	32.5	0.819	9.9	9.907	-0.07	1.1246	1.130	-0.47	0.0731	0.060	17.2	0.935	0.946	-1.22	1.639	1.694	-3.35
5	13.58	32.5	0.819	11.73	11.908	-1.51	1.196	1.228	-2.66	0.062	0.058	6.75	0.948	0.952	-0.49	1.542	1.566	-1.55
6	5.83	31	1.637	4.34	3.91	9.90	1.875	1.811	3.41	0.151	0.173	-13.8	0.919	0.904	1.63	2.01	2.1	-4.47
7	7.77	31	1.637	6.19	5.899	4.70	1.983	1.928	2.77	0.128	0.139	-7.83	0.935	0.927	0.81	1.894	1.9758	-4.31
8	9.71	31	1.637	8.02	7.905	1.43	2.092	2.062	1.48	0.119	0.124	-3.93	0.943	0.939	0.34	1.794	1.848	-3.01
9	11.64	31	1.637	9.86	9.89	-0.30	2.201	2.217	-0.68	0.112	0.115	-2.40	0.949	0.947	0.12	1.684	1.723	-2.31
10	13.58	31	1.637	11.68	11.88	-1.71	2.361	2.400	-1.62	0.111	0.110	0.63	0.953	0.954	-0.10	1.594	1.5988	-0.30
11	5.83	31	2.455	4.29	3.898	9.13	2.773	2.706	2.43	0.230	0.237	-2.95	0.917	0.912	0.51	2.022	2.109	-4.30
12	7.77	31	2.455	6.14	5.894	4.00	2.951	2.875	2.58	0.212	0.187	11.8	0.928	0.934	-0.73	1.907	1.986	-4.14
13	9.71	31	2.455	7.97	7.89	1.00	3.100	3.070	0.96	0.173	0.164	5.24	0.944	0.946	-0.25	1.815	1.863	-2.64
14	11.64	31	2.455	9.81	9.876	-0.67	3.280	3.294	-0.42	0.164	0.151	7.62	0.95	0.954	-0.42	1.707	1.74	-1.93
15	13.58	31	2.455	11.64	11.88	-2.06	3.502	3.558	-1.59	0.154	0.143	6.87	0.956	0.959	-0.37	1.591	1.618	-1.69
16	5.83	30	4.092	4.25	3.887	8.54	4.554	4.468	1.90	0.291	0.277	4.97	0.936	0.938	-0.21	2.072	2.129	-2.75
17	7.77	30	4.092	6.1	5.88	3.60	4.796	4.724	1.51	0.273	0.310	-13.3	0.943	0.934	0.92	1.974	2.015	-2.07
18	9.71	30	4.092	7.92	7.87	0.63	4.993	5.022	-0.56	0.244	0.269	-9.93	0.951	0.946	0.48	1.887	1.897	-0.52
19	11.64	30	4.092	9.76	9.85	-0.92	5.179	5.361	-3.51	0.222	0.246	-10.4	0.957	0.954	0.30	1.805	1.783	1.21
20	13.58	30	4.092	11.59	11.85	-2.24	5.436	5.755	-5.86	0.195	0.231	-18.0	0.964	0.959	0.44	1.722	1.664	3.36
21	5.83	31.5	6.548	XX	3.88	XX	XX	7.104	XX	XX	0.519	XX	XX	0.926	XX	XX	2.144	XX
22	7.77	31.5	6.548	6.05	5.873	2.92	7.555	7.510	0.59	0.355	0.384	-8.25	0.953	0.948	0.44	1.987	2.029	-2.11
23	9.71	31.5	6.548	7.88	7.87	0.12	7.813	7.997	-2.36	0.296	0.324	-9.12	0.962	0.959	0.28	1.902	1.913	-0.57
24	11.64	31.5	6.548	9.72	9.85	-1.33	8.180	8.510	-4.02	0.253	0.290	-14.3	0.969	0.965	0.31	1.815	1.798	0.93
25	13.58	31.5	6.548	11.54	11.84	-2.59	8.674	9.126	-5.21	0.234	0.268	-14.4	0.973	0.970	0.25	1.734	1.681	3.05

Note: (xx) means the experimental data have not been reported

Table 3.7. Model Type_2 validation with experimental results for inlet feed flow rate of ($F_{b(0,y)} = 2.583 \times 10^{-4} \text{ m}^3/\text{s}$)

				,	utlet), tm)		,	let)x10³ ol/m³)			_{v)} x10 ³ nol/m³)		Re	j _(av)		Fb(outle	,	
o _N	Pb(inlet) (atm)	Tb(inlet) (°C)	Cb(inlet)x10 3 (kmol/m³)	Ехр.	The.	%Error	Ехр.	The.	%Error	Exp.	The.	%Error	Ехр.	The.	%Error	Exp.	The.	%Error
1	5.83	32.5	0.819	4.27	3.69	13.5	0.9290	0.8997	3.15	0.0864	0.08958	-3.68	0.907	0.9004	0.72	2.199	2.345	-6.63
2	7.77	32.5	0.819	6.11	5.69	6.87	0.9975	0.9533	4.43	0.0798	0.07102	11.0	0.92	0.9255	-0.59	2.075	2.21	-6.50
3	9.71	32.5	0.819	7.94	7.69	3.14	1.0610	1.0160	4.24	0.0626	0.06267	-0.11	0.941	0.9383	0.28	1.953	2.08	-6.50
4	11.64	32.5	0.819	9.78	9.67	1.12	1.1160	1.0840	2.86	0.0558	0.0582	-4.30	0.95	0.9462	0.40	1.838	1.955	-6.36
5	13.58	32.5	0.819	11.61	11.68	-0.60	1.2073	1.1783	2.40	0.0495	0.0551	-11.3	0.959	0.9531	0.61	1.72	1.807	-5.05
6	5.83	31	1.637	4.22	3.68	12.7	1.8481	1.7880	3.25	0.1460	0.1750	-19.8	0.921	0.9016	2.10	2.261	2.359	-4.33
7	7.77	31	1.637	6.07	5.68	6.42	1.9523	1.8890	3.24	0.1230	0.1370	-11.3	0.937	0.9271	1.05	2.148	2.23	-3.81
8	9.71	31	1.637	7.89	7.67	2.78	2.0456	2.0050	1.98	0.1166	0.1210	-3.77	0.943	0.9396	0.36	2.042	2.107	-3.18
9	11.64	31	1.637	9.73	9.67	0.61	2.1461	2.1360	0.47	0.1116	0.1149	-2.95	0.948	0.9478	0.02	1.947	1.982	-1.79
10	13.58	31	1.637	11.56	11.66	-0.86	2.2204	2.2880	-3.04	0.1088	0.1056	2.94	0.951	0.9538	-0.29	1.85	1.855	-0.27
11	5.83	31	2.455	4.17	3.675	11.8	2.7457	2.6720	2.68	0.2279	0.2400	-5.30	0.917	0.91	0.76	2.29	2.368	-3.40
12	7.77	31	2.455	6.02	5.671	5.79	2.8985	2.8200	2.71	0.2000	0.1847	7.65	0.931	0.9345	-0.37	2.173	2.245	-3.31
13	9.71	31	2.455	7.85	7.668	2.31	2.9821	2.9880	-0.19	0.1670	0.1602	4.07	0.944	0.9464	-0.25	2.08	2.121	-1.97
14	11.64	31	2.455	9.66	9.654	0.06	3.1659	3.1790	-0.41	0.1488	0.1463	1.68	0.953	0.9539	-0.09	1.97	1.997	-1.37
15	13.58	31	2.455	11.51	11.65	-1.21	3.3142	3.3990	-2.55	0.1392	0.1376	1.14	0.958	0.9595	-0.15	1.868	1.874	-0.32
16	5.83	29	4.092	XX	3.66	XX	XX	4.4080	XX	XX	0.3163	XX	XX	0.9282	XX	XXX	2.393	XX
17	7.77	29	4.092	XX	5.65	XX	XX	4.6300	XX	XX	0.2320	XX	XX	0.9498	XX	XX	2.278	XX
18	9.71	29	4.092	7.8	7.65	1.92	4.9000	4.8820	0.36	0.2303	0.1981	13.9	0.953	0.9594	-0.67	2.113	2.162	-2.31
19	11.64	29	4.092	9.61	9.63	-0.20	5.0476	5.1640	-2.30	0.2120	0.1803	14.9	0.958	0.965	-0.73	2.07	2.047	1.11
20	13.58	29	4.092	11.47	11.62	-1.30	5.3657	5.4860	-2.24	0.1878	0.1698	9.58	0.965	0.969	-0.41	1.972	1.93	2.12
21	5.83	31.5	6.548	4.08	3.66	10.2	7.1666	7.0360	1.82	0.3870	0.3810	1.55	0.946	0.9458	0.02	2.337	2.401	-2.73
22	7.77	31.5	6.548	5.93	5.65	4.72	7.5021	7.3880	1.52	0.3451	0.3812	-10.4	0.954	0.9483	0.59	2.253	2.287	-1.50
23	9.71	31.5	6.548	7.75	7.64	1.41	7.8270	7.7960	0.39	0.2896	0.3172	-9.53	0.963	0.9593	0.38	2.17	2.170	-0.01
24	11.64	31.5	6.548	9.57	9.637	-0.70	8.0064	8.2550	-3.10	0.2482	0.2810	-13.2	0.969	0.9658	0.33	2.09	2.053	1.77
25	13.58	31.5	6.548	11.42	11.62	-1.75	8.5037	8.7780	-3.22	0.2296	0.2589	-12.7	0.973	0.9705	0.25	2.011	1.936	3.72

Note: (xx) means the experimental data have not been reported

3.2.1.3 Comparison of performance using 1D and 2D models

The Model Type_1 developed (1D dynamic and steady state model) has been incorporated thermophysical properties of the dimethylphenol and the prediction of several key parameters (Rej_(av) and Rec_(Total)) of the process is outlined in Table 3.8 together with the prediction of the same parameters obtained using the 2D model of the Model Type_2 (under steady state condition). As can be seen from Table 3.8, the accuracy of prediction using 2D model has significantly improved compared to experimental results thus justifying further investigation of the process using 2D model.

Table 3.8. Comparison of 1D and 2D models predictions against experimental data of (Srinivasan et al. 2011) for dimethylphenol removal from wastewater

Exp. Nu.	C _{b(inlet)} (kmol/m³)	P _{b(inlet)} (atm)	F _{b(inlet)} (m³/s)	Tb (°C)	Parameter	Exp. value (Srinivasan et al. 2011)	1D Model	Error%	2D Model	Error%
					Rej _(av)	97.3	96.5373	0.783	98.0197	-0.739
_	0.55,40-3	40.50	0.50,40-4	24.5	$C_{b(outlet)}$	0.00850	0.0088	-3.853	0.00878	-3.326
1	6.55x10 ⁻³	13.58	2.58x10 ⁻⁴	31.5	Rec _(Total)	22.1447	27.0909	-22.33	25.6416	-15.79
					F _{b(outlet)}	2.01x10 ⁻⁴	1.90x10 ⁻⁴	5.700	1.93x10 ⁻⁴	3.787
					Rej _(av)	96.9	95.9413	0.989	97.7175	-0.843
2	6.55x10 ⁻³	11.64	2.58x10 ⁻⁴	31.5	$C_{b(outlet)}$	0.00800	0.0083	-3.682	0.00826	-3.202
	0.55810	11.04	2.30010	31.3	$Rec_{(Total)}$	19.0863	22.1123	-15.854	20.8074	-9.017
					F _{b(outlet)}	2.09x10 ⁻⁴	2.02x10 ⁻⁴	3.311	2.05x10 ⁻⁴	1.81
					Rej _(av)	96.3	95.0446	1.303	97.2688	-1.006
3	6.55x10 ⁻³	9.71	2.58x10 ⁻⁴	31.5	$C_{b(outlet)}$	0.00782	0.0078	-0.080	0.00780	0.311
3	0.55810	9.71	2.30010	31.3	Rec _(Total)	15.9891	17.1569	-7.303	15.9702	0.118
					F _{b(outlet)}	2.17x10 ⁻⁴	2.14x10 ⁻⁴	1.178	2.17x10 ⁻⁴	0.037
					Rej _(av)	97.3	96.5654	0.754	98.0130	-0.732
4	6.55x10 ⁻³	13.58	2.33x10 ⁻⁴	31.5	$C_{b(outlet)}$	0.00867	0.0091	-5.821	0.00913	-5.326
4	6.55810	13.36	2.33810	31.3	Rec _(Total)	25.5793	30.1017	-17.679	28.5398	-11.573
					F _{b(outlet)}	1.73x10 ⁻⁴	1.64x10 ⁻⁴	5.273	1.68x10 ⁻⁴	3.058
					Rej _(av)	96.9	95.9834	0.945	97.7124	-0.838
5	6.55x10 ⁻³	11.64	2.33x10 ⁻⁴	31.5	$C_{b(outlet)}$	0.00818	0.0085	-4.606	0.00851	-4.118
3	0.55810	11.04	2.33810	31.3	$Rec_{(Total)}$	22.1030	24.6555	-11.548	23.2545	-5.209
					F _{b(outlet)}	1.82x10 ⁻⁴	1.77x10 ⁻⁴	2.720	1.8x10 ⁻⁴	0.981
					Rej _(av)	96.2	95.1263	1.116	97.2753	-1.117
6	6.55x10 ⁻³	9.71	2.33x10 ⁻⁴	31.5	$C_{b(outlet)}$	0.00781	0.0080	-2.597	0.00798	-2.180
0	0.00010	9.71			Rec _(Total)	18.3690	19.2215	-4.640	17.9640	2.204
					$F_{b(outlet)}$	1.90x10 ⁻⁴	1.89x10 ⁻⁴	0.730	1.91x10 ⁻⁴	-0.580

3.2.1.4 Model Type_3

The main concern of any industrial wastewater is the existence of several organic and non-organic compounds, which are harmful to human beings and marine life. Several previous studies modelled the spiral wound RO process considering the removal of a single organic contaminant from wastewater. However, only a few attempted the modelling of the spiral wound RO process for the removal of several organic and non-organic compounds from waste water. Al-Bastaki (2004) developed a lumped model to study the performance of a spiral wound RO process for removing Na₂SO₄ and methyl orange dye from wastewater. However, the development of a distributed model for the spiral wound RO process for the removal of multi-compounds simultaneously from wastewater has not been considered yet and is the main focus of this work. Therefore, a 1D steady state model based on a wastewater treatment spiral wound RO system is developed to simulate the transport phenomena of multi-compounds and water through the membrane.

Assumptions

The new following assumptions were considered to build this model.

- 1. A flat membrane sheet with negligible channel curvature.
- 2. Validity of the Darcy's law for the feed channel where the friction parameter is applied to characterise the pressure drop.
- 3. The contribution of all the compounds to the osmotic pressure is considered.
- 4. Validity of the film model theory to estimate the concentration polarisation impact.
- 5. Constant 1 atm pressure at the permeate side.
- A constant solute concentration is assumed in the permeate channel and the average value will be calculated from the inlet and outlet permeate solute concentrations.
- 7. The underlying process is isothermal. Therefore, the temperatures of the feed, retentate, and permeate are equal.
- 8. Negligible impact of feed spacer on the fluid patterns at the feed channel.
- 9. Constant membrane transport parameters.
- Constant friction factor of feed channel is assumed due to laminar flow.

Model equations

Permeate flux (m/s) at any point along the x-axis is calculated in Eq. (M.3.1). The second term of this equation represents the total osmotic pressure (atm)

$$J_{v(x)} = A_w \left\{ \Delta P_{b(x)} - \left[\sum_{i}^{n} \left(R(T_b + 273.15) \left(\frac{J_{v(x)} C_{p(i)(x)}}{B_{s(i)}} \right) \right] \right\}$$
 (M.3.1)

The solute flux of each component is

$$J_{s(i)(x)} = B_{s(i)} (C_{w(i)(x)} - C_{p(i)(av)})$$
(M.3.2)

i,n are the solute under consideration and the total number of solutes, respectively. Feed flow rate (m³/s), velocity (m/s), feed pressure (atm) and permeate flow rate (m³/s) are estimated as

$$\frac{dF_{b(x)}}{dx} = -W J_{v(x)}, \qquad U_{b(x)} = \frac{F_{b(x)}}{t_f W}, \qquad \frac{dP_{b(x)}}{dx} = -b F_{b(x)}, \qquad \frac{dF_{b(x)}}{dx} = -\frac{dF_{p(x)}}{dx}$$
(M.3.3)

Operating pressure and pressure loss (atm) along the feed channel are given as

$$\Delta P_{b(x)} = P_{b(x)} - P_{p}$$
 $P_{loss} = P_{b(0)} - P_{b(L)}$ (M.3.4)

Feed solute concentration (kmol/m³) is

$$\frac{c_{b(i)(x)}}{t_f W} \frac{dF_{b(x)}}{dx} + \frac{F_{b(x)}}{t_f W} \frac{dC_{b(i)(x)}}{dx} = \frac{d}{dx} \left[D_{b(i)(x)} \frac{dC_{b(i)(x)}}{dx} \right] - \frac{\left(J_{w(x)} \, C_{p(i)(x)} \right)}{t_f} + \frac{\left(J_{w(x)} \, C_{b(i)(x)} \right)}{t_f} \tag{M.3.5}$$

Permeate solute concentration (kmol/m³) of each solute at x=0 and x=L are calculated in the counter of Eqs. (M.3.6), which then used to calculate average permeate concentration (kmol/m³) of each solute in Eq. (M.3.7). The last term of Eq. (M.3.5) represents the change of bulk concentration due to solvent through the membrane.

$$C_{p(i)(0)} = \frac{B_{s(i)} C_{b(i)(0)} e^{\frac{J_{w(0)}}{k(i)(0)}}}{J_{w(0)} + B_{s(i)} e^{\frac{J_{w(0)}}{k(i)(0)}}} \qquad C_{p(i)(L)} = \frac{B_{s(i)} C_{b(i,L)} e^{\frac{J_{w(L)}}{k(i)(L)}}}{J_{w(L)} + B_{s(i)} e^{\frac{J_{w(L)}}{k(i)(L)}}}$$
(M.3.6)

$$C_{p(i)(av)} = \frac{C_{p(i)(0)} + C_{p(i)(L)}}{2}$$
(M.3.7)

Wall solute concentration (kmol/m³) of each solute is given as

$$\frac{(C_{w(i)(x)} - C_{p(i)(av)})}{(C_{b(i)(x)} - C_{p(i)(av)})} = \exp\left(\frac{J_{w(x)}}{k_{(i)(x)}}\right) \tag{M.3.8}$$

Total permeate recovery (-) and rejection (-) of each component (Sundaramoorthy et al. 2011a)

$$Rec = \frac{F_{p(L)}}{F_{b(0)}} x \ 100 \qquad \qquad Rej_{(i)} = \frac{C_{b(i)(L)} - C_{p(i)(av)}}{C_{b(i)(L)}} x 100 \qquad \qquad (M.3.9)$$

Eq. (M.3.10) is used to calculate the mass transfer coefficient (m/s) of each considered solute except chlorophenol and dimethylphenol (Wankat 1990)

$$k_{(i)(x)} = 1.177 \, \left(\frac{U_{b(x)} \, D_{b(i)(x)}^2}{t_f \, L} \right)^{0.333} \tag{M.3.10}$$

Model validation

The RO filtration system of Sundaramoorthy et al. (2011b) shown in Fig. 2.1 in Chapter 2 is used to investigate the simultaneous removal of multi-compounds from wastewater. Also note, in the absence of experimental data in the literature for multi-compounds removal from wastewater, the model developed in this work has been validated against experimental data of Sundaramoorthy et al. (2011b) for the removal of a single compound (chlorophenol) from wastewater. Therefore, the characteristics of the membranes used are given in Table 2.2 in Chapter 2. The water permeability constant and friction factor are given in Table 2.8 in Chapter 2. However, the solute transport parameters (B_s) of the selected compounds were gathered from the literature and given in Table 3.9. The model shows a very good agreement in terms of rejection and recovery of water (Fig. 3.1).

Table 3.9. Physical and transport parameters of the eight selected organic compounds

Compound	Membrane	B _s (m/s)	Reference
Dimethylphenol	Ion Exchange, India	1.5876x10 ⁻⁸	(Srinivasan et al. 2011)
Chlorophenol	Ion Exchange, India	8.4680x10 ⁻⁸	(Sundaramoorthy et al. 2011b)
Phenol	Permionics, India	6.5367x10 ⁻⁷	(Srinivasan et al. 2010)
Methyl orange dye	FilmTec SW30	3.2000x10 ⁻⁹	(Al-Bastaki 2004)
Aniline	DESAL-3B	4.1900x10 ⁻⁶	(Hidalgo et al. 2014)
Ammonium	SEPA-SSIC	1.1696x10 ⁻⁷	(Bodalo et al. 2005)
Cyanide	DESAL-3	2.1861x10 ⁻⁶	(Bódalo et al. 2004a)
Sulphate	SEPA-SSIC	3.9869x10 ⁻⁸	(Bódalo et al. 2004c)

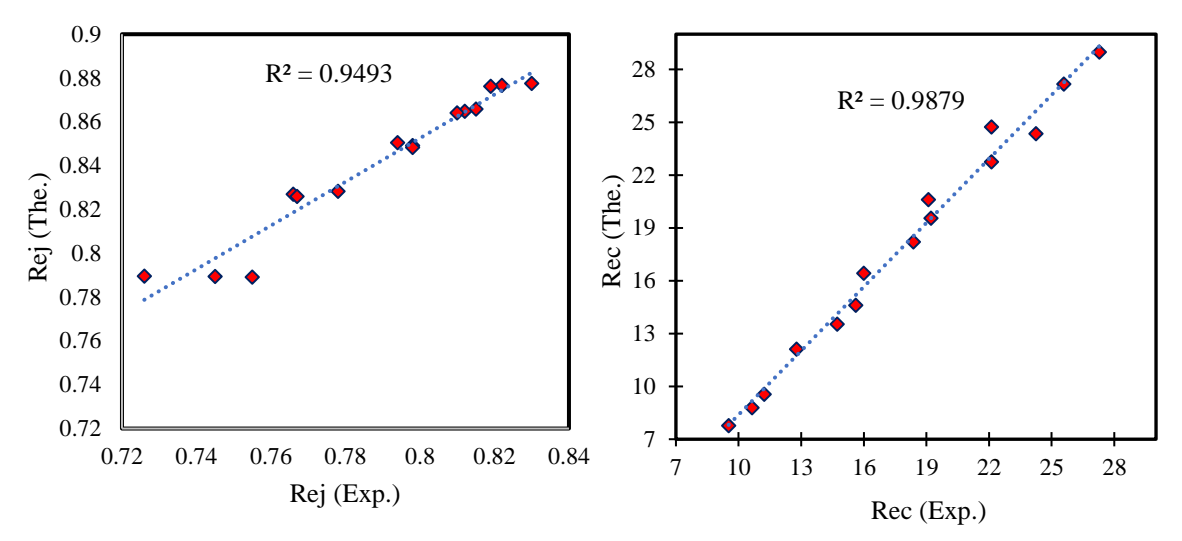


Fig. 3.1. The model validation results

3.2.2 Lumped models

3.2.2.1 Model Type_4

This section shows the development of a simple steady state lumped model that can be used to simulate the phenomenon of solvent and solute transport through the membrane, and one that incorporates the fluid physical properties to predict the rejection of organic compounds for a spiral wound RO process and multistage RO process. The development of this model is readily based on the same assumption were taken to develop Model Type_1. However, the assumption of constant solvent and solute transport parameters is relaxed by considering the impact of operating temperature on the membrane transport parameters.

Assumptions

- 1. A flat membrane sheet with negligible channel curvature.
- 2. Validity of the Darcy's law for the feed channel where the friction parameter is applied to characterise the pressure drop.
- 3. Validity of the film model theory to estimate the concentration polarisation impact.
- 4. Constant 1 atm pressure at the permeate side.
- 5. The impact of operating temperature on the membrane transport parameters is considered.
- 6. Negligible impact of feed spacer on the fluid patterns at the feed channel.
- 7. Constant friction factor of feed channel is assumed due to laminar flow.

Model equations

$$J_{w} = A_{w(T_{b})} \left[\Delta P_{b} - \Delta \pi_{Total} \right]$$
 (M.4.1)

$$\Delta P_{b} = \frac{(P_{b(in)} + P_{b(out)})}{2} - P_{p}$$
(M.4.2)

$$J_s = B_{s(T_h)} (C_w - C_p)$$
 (M.4.3)

 $P_{b(in)}$, $P_{b(out)}$ (atm) are inlet feed pressure and retentate pressure, respectively. The total osmotic pressure difference $\Delta\pi_{Total}$ (atm) is

$$\Delta \pi_{\text{Total}} = (\pi_{\text{w}} - \pi_{\text{p}}) \tag{M.4.4}$$

 $\pi_{\rm w}$, $\pi_{\rm p}$ (atm) are the osmotic pressure of solute at the membrane wall concentration $C_{\rm w}$ (kmol/m³) and the osmotic pressure at permeate channel regarding the permeate concentration $C_{\rm p}$ (kmol/m³).

$$\pi_{\rm w} = R \left(T_{\rm h} + 273.15 \right) C_{\rm w}$$
 (M.4.5)

$$\pi_{\rm p} = R \left(T_{\rm b} + 273.15 \right) C_{\rm p}$$
 (M.4.6)

$$\frac{(C_{w} - C_{p})}{(C_{b} - C_{p})} = \exp\left(\frac{J_{w}}{k}\right) \tag{M.4.7}$$

 C_b (kmol/m³) is the bulk concentration in the feed side, taken as the average value of feed C_f (kmol/m³) and retentate concentrations C_r (kmol/m³) using Eq. (M.4.8)

$$C_{b} = \frac{C_{f} + C_{r}}{2} \tag{M.4.8}$$

The bulk feed velocity U_b is calculated as

$$U_b = \frac{Q_b}{W t_f} \tag{M.4.9}$$

Q_b (m³/s) is the bulk feed flow rate

$$Q_{\rm b} = \frac{Q_{\rm f} + Q_{\rm r}}{2} \tag{M.4.10}$$

 $Q_{\rm f}$ and $Q_{\rm r}$ (m³/s) are the feed and retentate flow rates. The process of organic compound rejection is followed by a pressure drop along the membrane edges. Therefore, the retentate pressure $P_{\rm b(out)}$ (atm) is calculated using the correlation of Sundaramoorthy et al. (2011a).

$$P_{b(out)} = P_{b(in)} - \frac{bL}{\phi \sinh \phi} \{ (Q_f + Q_r)(\cosh \phi - 1) \}$$
(M.4.11)

Ø is a dimensionless term defined as

$$\emptyset = L \sqrt{\frac{W b A_{w(T_b)}}{\left[1 + \left(\frac{A_{w(T_b)} R C_p (T_b + 273.15)}{B_{S(T_b)}}\right)\right]}}$$
(M.4.12)

The pressure loss P_{h(lose)} (atm) along the feed channel is calculated as

$$P_{b(lose)} = P_{b(in)} - P_{b(out)}$$
(M.4.13)

Substituting Eq. (M.4.13) in Eq. (M.4.2) yields

$$\Delta P_b = P_{b(in)} - \frac{P_{b(lose)}}{2} - P_p \tag{M.4.14}$$

The overall solute and mass balance equations are, respectively

$$Q_f = Q_r + Q_p \tag{M.4.15}$$

$$Q_f C_f = Q_r C_r + Q_p C_p \tag{M.4.16}$$

 Q_p (m³/s) is the total permeate flow rate. The concentration at the permeate channel can also be calculated by Eq. (M.4.17).

$$C_{p} = \frac{C_{f} B_{s(T_{b})}}{B_{s}(T_{b}) + \frac{J_{w}}{\exp(\frac{J_{w}}{U})}}$$
(M.4.17)

$$Rej = \frac{C_f - C_p}{C_f} x100 \tag{M.4.18}$$

$$Rec = \frac{Q_p}{Q_e} \times 100$$
 (M.4.19)

$$Q_{p} = J_{w} A \tag{M.4.20}$$

A (m²) is the effective membrane area. In this model, the specific energy consumption is considered

$$E = \frac{\frac{((P_{b(in)} \times 101325) Q_f)}{Q_p \varepsilon_{pump}}}{36E5}$$
 (M.4.21)

 $\epsilon_{\rm pump}$ (dimensionless) is the pump efficiency. The impact of operating temperature on water and solute transport parameters is shown in the equations of Sarkar et al. (2008).

$$A_{w(T+273.15)} = A_{w(T_{ref}+273.15)} \frac{\mu_{b(T_{ref}+273.15)}}{\mu_{b(T+273.15)}}$$
 (M.4.22)

$$B_{s(T_b+273.15)} = B_{s(T_{ref}+273.15)} \frac{T_b + 273.15}{T_{ref} + 273.15} \frac{\mu_{b(T_{ref}+273.15)}}{\mu_{b(T_b+273.15)}}$$
 (M.4.23)

 T_{ref} (°C) is the reference temperature.

Model validation

The transport parameters A_w and B_s and the friction parameter b of this model were taken from the experimental work of Srinivasan et al. (2011) and Sundaramoorthy et al. (2011b) for the removal of dimethylphenol and chlorophenol, respectively from wastewater. The experiments were described in Section 2.5.1.2 in Chapter 2. Table 2.2 lists the membrane and module properties used in the calculations. Also, the transport parameters are given in Table 2.8. Fig. 3.2 and Table 3.10 compare the experimental results of Srinivasan et al.

(2011) and Sundaramoorthy et al. (2011b), respectively against the model prediction of several operating parameters for the removal of dimethylphenol and chlorophenol from wastewater, respectively. The validation results show a good match between the model prediction and the experimental data. This is due to high regression coefficient (R²) presented in Fig. 3.2.

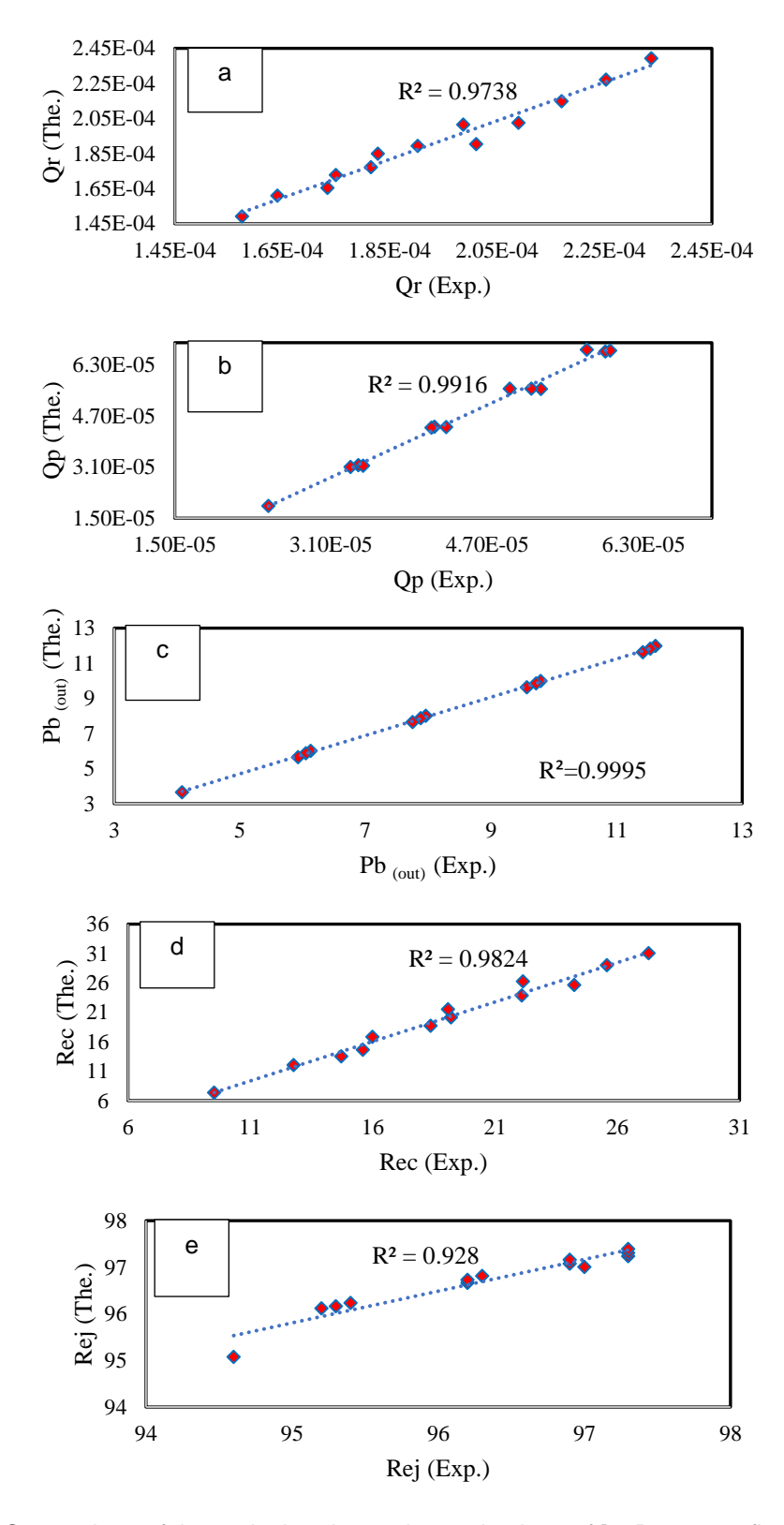


Fig. 3.2. Comparison of theoretical and experimental values of [a: Retentate flow rate, b: Permeate flow rate, c: Retentate pressure, d: Total permeate recovery and e: Dimethylphenol rejection]

Table 3.10. Model validation results against chlorophenol removal

				1						1	_	4.00				
No	$P_{b(in)}$	Т	C _f x10 ³	$Q_{\rm f}$ $\times 10^4$	$P_{b(out)}$	(<i>at</i> m)	%Error	Q _r x10 ⁴	1 (m³/s)	%Error	C _p >		%Error	R	ej	%Error
110	(atm)	(°C)	(kmol /m³)	(m³/s)	Ехр.	The.	3% E	Ехр.	The.	%E	Ехр.	The.	3%	Ехр.	The.	%E
1	9.71	30	0.778	2.166	8.3	8.16	1.6	1.59	1.63	-2.2	0.366	0.345	5.5	61.4	62.48	-1.7
2	11.64	30	0.778	2.166	10.08	10.14	-0.6	1.5	1.50	0.3	0.363	0.362	0.2	63.8	62.45	2.1
3	13.58	30	0.778	2.166	12.04	12.14	-0.8	1.37	1.37	0.3	0.36	0.381	-6.0	66.2	62.21	6.0
4	7.77	31	6.226	2.166	6.24	6.145	1.5	1.828	1.84	-0.8	1.657	1.353	18.3	76.7	80.87	-5.4
5	9.71	31	6.226	2.166	8.11	8.129	-0.2	1.75	1.73	0.9	1.491	1.301	12.6	79.8	82.54	-3.4
6	11.64	31	6.226	2.166	9.98	10.10	-1.2	1.641	1.62	0.9	1.475	1.289	12.5	81	83.62	-3.2
7	13.58	31	6.226	2.166	11.85	12.08	-1.9	1.575	1.52	3.5	1.457	1.299	10.7	81.9	84.38	-3.0
8	5.83	30	0.778	2.33	4.46	4.043	9.3	1.957	2.06	-5.2	0.375	0.321	14.2	56.2	61.59	-9.5
9	7.77	30	0.778	2.33	6.35	6.038	4.9	1.86	1.93	-3.5	0.373	0.324	13.0	58.1	62.86	-8.2
10	9.71	30	0.778	2.33	8.22	8.031	2.2	1.742	1.79	-2.8	0.372	0.334	10.0	60.3	63.26	-4.9
11	11.64	30	0.778	2.33	10.09	10.01	0.7	1.639	1.66	-1.3	0.37	0.349	5.6	62.4	63.26	-1.3
12	13.58	30	0.778	2.33	11.96	12.00	-0.3	1.542	1.53	0.7	0.367	0.367	0.0	64.5	63.05	2.2
13	5.83	31	6.226	2.33	4.27	4.027	5.6	2.082	2.12	-1.9	1.726	1.46	15.2	74.5	78.15	-4.9
14	7.77	31	2.455	2.33	6.16	6.011	2.4	1.987	2.01	-1.1	1.645	1.321	19.6	76.6	81.15	-5.9
15	9.71	31	2.455	2.33	8.03	7.996	0.4	1.902	1.90	0.2	1.472	1.263	14.1	79.8	82.83	-3.8
16	11.64	31	2.455	2.33	9.9	9.970	-0.7	1.815	1.79	1.5	1.433	1.244	13.1	81.2	83.91	-3.3
17	13.58	31	2.455	2.33	11.77	11.95	-1.5	1.734	1.68	3.1	1.419	1.248	12.0	82.2	84.68	-3.0
18	7.77	31	1.556	2.583	6.17	5.825	5.5	2.148	2.20	-2.3	0.572	0.46	19.5	67.5	73.65	-9.1
19	9.71	31	1.556	2.583	7.79	7.817	-0.3	2.042	2.07	-1.3	0.553	0.46	16.8	69.7	74.83	-7.3
20	11.64	31	1.556	2.583	9.92	9.799	1.2	1.947	1.94	0.2	0.55	0.469	14.7	71.2	75.51	-6.0
21	13.58	31	1.556	2.583	11.79	11.79	-0.0	1.85	1.81	1.9	0.549	0.484	11.8	72.5	75.93	-4.7
22	9.71	31	2.335	2.583	8.03	7.811	2.7	2.08	2.09	-0.3	0.744	0.606	18.5	72.8	77.91	-7.0
23	11.64	31	2.335	2.583	9.84	9.791	0.4	1.97	1.96	0.3	0.733	0.612	16.5	74.2	78.75	-6.1
24	13.58	31	2.335	2.583	11.74	11.78	-0.3	1.868	1.84	1.4	0.726	0.626	13.8	75.7	79.30	-4.7
25	7.77	31	6.226	2.583	6.03	5.805	3.7	2.253	2.26	-0.5	1.549	1.278	17.4	77.8	81.52	-4.7
26	9.71	31	6.226	2.583	7.9	7.790	1.3	2.17	2.15	0.8	1.486	1.212	18.4	79.4	83.23	-4.8
27	11.64	31	6.226	2.583	9.75	9.765	-0.1	2.09	2.04	2.4	1.387	1.186	14.4	81.5	84.33	-3.4
28	13.58	31	6.226	2.583	11.65	11.74	-0.8	2.012	1.93	4.1	1.325	1.182	10.7	83	85.10	-2.5

3.3 Irreversible thermodynamic model

This section presents all the model developed based on the validity of the irreversible thermodynamic model to express the transport of the solvent and solute through the membrane. Specifically, the models developed are divided into two parts; distributed and lumped models.

3.3.1 Distributed models

3.3.1.1 Model Type_5

A new explicit 1D steady state model based on the three-parameter Spiegler-Kedem methodology is developed to predict the performance of a spiral wound RO process for the rejection of organic compounds from wastewater.

Assumptions

- 1. A flat membrane sheet with negligible channel curvature.
- 2. Validity of the Darcy's law for the feed channel where the friction parameter is applied to characterise the pressure drop.
- 3. Validity of the film model theory to estimate the concentration polarisation impact.
- 4. Constant 1 atm pressure at the permeate side.
- A constant solute concentration is assumed in the permeate channel and the average value will be calculated from the inlet and outlet permeate solute concentrations.
- 6. The underlying process is isothermal.
- 7. Negligible impact of feed spacer on the fluid patterns at the feed channel.
- 8. Constant friction factor of feed channel is assumed due to laminar flow.

Model equations

$$J_{w(x)} = L_{p} \left(\Delta P_{b(x)} - \sigma \, \Delta \pi_{(x)} \right) \tag{M.5.1}$$

$$J_{s(x)} = J_{w(x)}(1 - \sigma) C_{b(av)}^{\sim} + \omega \Delta \pi_{(x)}$$
(M.5.2)

$$C_{b(av)}^{\sim} = \frac{C_{b(o)}^{\sim} + C_{b(L)}^{\sim}}{2}$$
 (M.5.3)

$$C_{b(0)}^{\sim} = \frac{C_{b(0)} - C_{p(av)}}{\ln\left(\frac{C_{b(0)}}{C_{p(av)}}\right)} \quad \text{and} \quad C_{b(L)}^{\sim} = \frac{C_{b(L)} - C_{p(av)}}{\ln\left(\frac{C_{b(L)}}{C_{p(av)}}\right)}$$
 (M.5.4)

$$\Delta \pi_{(x)} = RT_b (C_{w(x)} - C_{p(av)})$$
 (M.5.5)

Putting the osmotic pressure difference in Eq. (M.5.2), and then the solute flux is

$$J_{s(x)} = J_{w(x)} (1 - \sigma) C_{b(av)}^{\sim} + \omega R T_{b} (C_{w(x)} - C_{p(av)})$$
(M.5.6)

$$J_{s(x)} = J_{w(x)} C_{p(av)}$$
 (M.5.7)

$$\Delta P_{b(x)} = (P_{b(x)} - P_p) \tag{M.5.8}$$

By substituting Eq. (M.5.7) in Eq. (M.5.2) and with re-arrangement, yields

$$\Delta \pi_{(x)} = \frac{J_{w(x)} c_{p(av)}}{\omega} - \frac{J_{w(x)} (1 - \sigma) c_{b(av)}^{\sim}}{\omega}$$
(M.5.9)

Substituting Eq. (M.5.9) in Eq. (M.5.1) gives

$$J_{w(x)} = L_{p} \left[\Delta P_{b(x)} - \sigma \left(\frac{J_{w(x)} c_{p(av)}}{\omega} - \frac{J_{w(x)} (1 - \sigma) c_{b(av)}^{\sim}}{\omega} \right) \right]$$
 (M.5.10)

Eq. (M.5.10) can be simplified to

$$J_{w(x)} = \frac{L_{p} (\Delta P_{b(x)})}{1 + \frac{\sigma C_{p(av)} L_{p}}{\omega} - \frac{C_{b(av)}^{-1} (1 - \sigma) L_{p} \sigma}{\omega}}$$
(M.5.11)

$$\frac{dF_{b(x)}}{dx} = -W J_{w(x)}$$
 (M.5.12)

Combining Eq. (M.5.10) in Eq. (M.5.12) and take the first and second derivatives yields

$$\frac{d^{2}F_{b(x)}}{dx^{2}} = \frac{-W L_{p} \frac{dP_{b(x)}}{dx}}{1 + \frac{\sigma C_{p(av)} L_{p}}{\omega} - \frac{C_{b(av)}^{2}^{(1-\sigma)} L_{p} \sigma}{\omega}}$$
(M.5.13)

$$\frac{dP_{b(x)}}{dx} = -b F_{b(x)}$$
 (M.5.14)

Substituting Eq. (M.5.14) in Eq. (M.5.13) yields

$$\frac{d^{2}F_{b(x)}}{dx^{2}} = \frac{W L_{p b} F_{b(x)}}{1 + \frac{\sigma C_{p(av)} L_{p}}{\omega} \frac{C_{b(av)}^{\sim} (1 - \sigma) L_{p \sigma}}{\omega}}$$
(M.5.15)

Eq. (M.5.15) can be composed in the same form of Eq. (M.5.16)

$$\frac{d^2 F_{b(x)}}{dx^2} = \frac{L_p}{Z} F_{b(x)}$$
 (M.5.16)

$$Z = \frac{1 + \frac{\sigma C_{p(av)} L_p}{\omega} - \frac{C_{b(av)}^{\sim} (1 - \sigma) L_p \sigma}{\omega}}{W b}$$
 (M.5.17)

The general solution of Eq. (M.5.16) is

$$F_{b(x)} = e^{rx}$$
 where $r = \pm \sqrt{\frac{L_p}{z}}$ (M.5.18)

The boundary conditions can be used to find the final solution as follows:

At
$$x=0$$
, $F_{b(x)}=F_{b(0)}$ and at $x=L$, $F_{b(x)}=F_{b(L)}$

$$F_{b(x)} = \frac{F_{b(L)} \left(e^{\sqrt{\frac{Lp}{Z}} x} - e^{-\sqrt{\frac{Lp}{Z}} x} \right) + F_{b(0)} \left(e^{\sqrt{\frac{Lp}{Z}} (L-x)} - e^{-\sqrt{\frac{Lp}{Z}} (L-x)} \right)}{\left(e^{\sqrt{\frac{Lp}{Z}} L} - e^{-\sqrt{\frac{Lp}{Z}} L} \right)}$$
(M.5.19)

Substituting Eq. (M.5.19) in Eq. (M.5.14) and take the integration yields

$$\begin{split} P_{b(x)} &= P_{b(0)} - \frac{b}{\sqrt{\frac{Lp}{Z}}(e^{\sqrt{\frac{Lp}{Z}}L} - e^{-\sqrt{\frac{Lp}{Z}}L})} \Biggl\{ \Biggl[F_{b(L)} \left[e^{\sqrt{\frac{Lp}{Z}}x} + e^{-\sqrt{\frac{Lp}{Z}}x} - 2 \right] - F_{b(0)} \left[\left(e^{\sqrt{\frac{Lp}{Z}}(L-x)} + e^{-\sqrt{\frac{Lp}{Z}}(L-x)} \right) - \left(e^{\sqrt{\frac{Lp}{Z}}L} - e^{-\sqrt{\frac{Lp}{Z}}L} \right) \right] \Biggr\} \end{split} \tag{M.5.20}$$

Then, by taking the first derivative of Eq. (M.5.19) and combine it in Eq. (M.5.12), yields

$$J_{w(x)} = \frac{\sqrt{\frac{L_p}{z}}}{w(e^{\sqrt{\frac{L_p}{z}}}L_{-e} - \sqrt{\frac{L_p}{z}}L_{)}} \left\{ \left[F_{b(0)} \left(e^{\sqrt{\frac{L_p}{z}}(L-x)} + e^{-\sqrt{\frac{L_p}{z}}(L-x)} \right) \right] - \left[F_{b(L)} \left(e^{\sqrt{\frac{L_p}{z}}x} + e^{-\sqrt{\frac{L_p}{z}}x} \right) \right] \right\} \quad \text{(M.5.21)}$$

Equating Eq. (M.5.21) to Eq. (M.5.11), the pressure drop along the x-axis is written as

$$\Delta P_{b(x)} = \frac{\sqrt{\frac{\overline{Lp}}{Z}} Zb \left\{ \left[F_{b(0)} \left(e^{\sqrt{\frac{\overline{Lp}}{Z}} (L-x)} + e^{-\sqrt{\frac{\overline{Lp}}{Z}} (L-x)} \right) \right] - \left[F_{b(L)} \left(e^{\sqrt{\frac{\overline{Lp}}{Z}} x} + e^{-\sqrt{\frac{\overline{Lp}}{Z}} x} \right) \right] \right\}}{L_p \left(e^{\sqrt{\frac{\overline{Lp}}{Z}} L} - e^{-\sqrt{\frac{\overline{Lp}}{Z}} L} \right)}$$
 (M.5.22)

Simply at $(x = 0, \Delta P_{b(x)} = \Delta P_{b(0)} = P_{b(0)} - P_p)$, Eq. (M.5.22) can be re-arranged to find an expression for the retentate flow rate

$$F_{b(L)} = \frac{F_{b(0)} \left(e^{\sqrt{\frac{L_p}{Z}} L} + e^{-\sqrt{\frac{L_p}{Z}} L} \right)}{2} - \frac{\Delta P_{b(0)} \sqrt{\frac{L_p}{Z}} \left(e^{\sqrt{\frac{L_p}{Z}} L} + e^{-\sqrt{\frac{L_p}{Z}} L} \right)}{2b}$$
(M.5.23)

$$\frac{d\frac{\left(C_{b(x)}F_{b(x)}\right)}{t_{f}W}}{dx} = -\frac{J_{w(x)}C_{p(av)}}{t_{f}} + \frac{J_{w(x)}C_{b(x)}}{t_{f}} + \frac{d}{dx}\left(D_{b(x)}\frac{dC_{b(x)}}{dx}\right) \tag{M.5.24}$$

$$\frac{(C_{w(x)} - C_{p(av)})}{(C_{b(x)} - C_{p(av)})} = \exp\left(\frac{J_{w(x)}}{k_{(x)}}\right)$$
(M.5.25)

The combination of Eq. (M.5.25) and Eq. (M.5.7) in Eq. (M.5.2), yields

$$J_{w(x)} C_{p(av)} = C_{b(av)}^{\sim} (1 - \sigma) J_{w(x)} + \omega R T_b (C_{b(x)} - C_{p(av)}) e^{\frac{J_{w(x)}}{k_{(x)}}}$$
(M.5.26)

Re-arranging Eq. (M.5.26) for the average permeate solute concentration gives

$$C_{p(av)} = \frac{C_{b(av)}^{\sim} (1-\sigma) J_{w(x)} + \omega R T_b C_{b(x)} e^{\frac{J_{w(x)}}{k_{(x)}}}}{J_{w(x)} + \omega R T_b e^{\frac{J_{w(x)}}{k_{(x)}}}}$$
(M.5.27)

To simplify Eq. (M.5.27), the reflection coefficient will be assumed as ($\sigma = 1$), then

$$C_{p(av)} = \frac{\omega R T_b C_{b(x)} e^{\frac{J_{w(x)}}{k_{(x)}}}}{J_{w(x)} + \omega R T_b e^{\frac{J_{w(x)}}{k_{(x)}}}}$$
(M.5.28)

Eq. (M.5.28) can be re-written in the form of Eq. (M.5.29) and to be compatible with the calculating the average permeate solute concentration by considering the solution diffusion model.

$$C_{p(av)} = \frac{B_s C_{b(x)} e^{\frac{J_{w(x)}}{k_{(x)}}}}{J_{w(x)} + B_s e^{\frac{J_{w(x)}}{k_{(x)}}}}$$
(M.5.29)

Eq. (M.5.29) is used in both (x = 0 and x = L) and then take the average value as the average solute concentration in the permeate channel.

$$Rej_{(av)} = \frac{C_{b(L)} - C_{p(av)}}{C_{b(L)}} x100$$
 (M.5.30)

$$F_{p(Total)} = \sum F_{p(x)} \qquad (from x = 0 \text{ to } x = L)$$
 (M.5.31)

$$F_{p(x)} = J_{w(x)} W \Delta x \tag{M.5.32}$$

Parameter estimation

Experimental data of Fujioka et al. (2014b) is used to estimate unknown transport parameters of the process model. The membrane transport parameters B_s and the reflection coefficients σ of the eight selected N-nitrosamine solutes are assumed to be constants (Table 2.3 in Chapter 2) and taken from Fujioka et al. (2014b) who considered a constant feed flow rate. Fujioka et al. (2014b) considered variable operating pressures in their experiments for the removal of eight N-nitrosamine. For this purpose, the water permeability coefficient $L_{\mbox{\scriptsize p}}$ and the friction parameter b will be estimated for each run from these experiments using the gEST parameter estimation tool available in the gPROMS software. The results of the parameter estimation are given in Table 3.11, which clearly show the variation of transport parameters with the operating conditions for eight N-nitrosamine experiments. For the convenience of the reader, few experimental and predicted values of retentate flow rate and retentate pressure are included in Table 3.12 with the calculation of relative error and sum of the squared errors. The results of parameter estimation show that permeability constants vary with the operating pressure enhancing (although slightly) the permeability constant of water with increasing pressure except for 10.1 atm that associated with higher values of friction. The registered values of friction parameters vary between 58 to 353 atm s/m⁴ for the operating pressures 4, 6.51 and 10.1 atm, respectively. This in turn can confirm the relation between the operating pressure and friction factor. Also, the parameter estimation method shows that the water permeability

coefficients L_p for the set of used pressures varies between 1.0×10^{-6} to 1.30×10^{-6} m/s atm for the membrane type ESPA2-4040 Hydranautics, Oceanside, CA., USA at 2.43×10^{-3} m³/s and 20 °C of feed flow rate and temperature, respectively. Table 2.4 in Chapter 2 includes the design and operating parameters of the spiral wound membrane element.

Table 3.11. Results of parameter estimation

			ı						
N-nitrosamine	$C_{b(0)} x 10^9$	$P_{b(0)}$	b	$L_p x 10^6$					
- Tritiocarrino	(kmol/m ³)	(atm)	(atm s/m ⁴)	(m/s atm)					
NDMA	3.3761	4.0	58.89	1.1000					
NDMA	3.3761	6.51	177.23	1.1293					
NDMA	3.3761	10.1	352.74	1.1770					
NMEA	2.8389	4.0	58.81	1.0878					
NMEA	2.8389	6.51	177.76	1.1283					
NMEA	2.8389	10.1	353.34	1.0730					
NPYR	2.4985	4.0	59.46	1.0994					
NPYR	2.4985	6.51	177.42	1.1349					
NPYR	2.4985	10.1	351.14	1.0431					
NDEA	2.4490	4.0	59.02	1.0000					
NDEA	2.4490	6.51	176.24	1.3060					
NDEA	2.4490	10.1	351.03	1.0053					
NPIP	2.1914	4.0	58.96	1.0000					
NPIP	2.1914	6.51	175.01	1.0565					
NPIP	2.1914	10.1	352.53	1.0282					
NMOR	2.1540	4.0	58.94	1.000					
NMOR	2.1540	6.51	177.34	1.1724					
NMOR	2.1540	10.1	353.15	1.0867					
NDPA	1.9214	4.0	58.98	1.0000					
NDPA	1.9214	6.51	177.64	1.0897					
NDPA	1.9214	10.1	350.79	1.0568					
NDBA	1.5808	4.0	58.96	1.0000					
NDBA	1.5808	6.51	175.33	1.2104					
NDBA	1.5808	10.1	351.86	1.0301					
$F_{b(0)} = 2.43x10^{-3} \text{ m}^3\text{/s and } T_b = 20 \text{ °C}$									

Table 3.12. Results of relative errors and sum of square errors

N- nitrosamine	C _{b(0)} x10 ⁹ (kmol /m ³)	P _{b(0)} (atm)	F _{b(L)} x10 ³	$F_{b(L)}^{Cal.}$ x10 ³	Relative Errors	P _{b(L)} ^{Exp.}	$P_{b(L)}^{\text{Cal.}}$	Relative Errors	Sun of square errors SSE (-) x10 ⁴
NDMA	3.3761	10.1	2.23	2.225	4.31x10 ⁻⁶	7.890	7.895	-5.28x10 ⁻³	5.16
NMEA	2.8389	10.1	2.23	2.234	3.18x10 ⁻⁵	7.890	7.887	1.09x10 ⁻²	9.44
NPYR	2.4985	10.1	2.23	2.233	-3.35x10 ⁻⁶	7.890	7.893	-3.71x10 ⁻³	3.69

Model validation

The Model Type_5 has been validated by comparing the model predictions results with those obtained from actual experimentation of Fujioka et al. (2014b).

Fig. 3.3 compares the observed and modeled feed pressure along the x-axis for three different overall permeate fluxes. Fig. 3.4 compares the observed and modeled average permeate flux and retentate flow rate as a function to inlet feed pressure. Fig. 3.5 compares the model rejections of eight N-nitrosamines solutes at three different overall permeate fluxes against experimental results, which shows high value of R^2 (regression coefficient). Furthermore, Fig. 3.4 shows that the model can be used to simulate the observed data of retentate flow rate at high operating pressure albeit with a minor deviation (1%). It is expected that the inaccurate estimation of $L_{\rm p}$ of such pressure might causes this deviation.

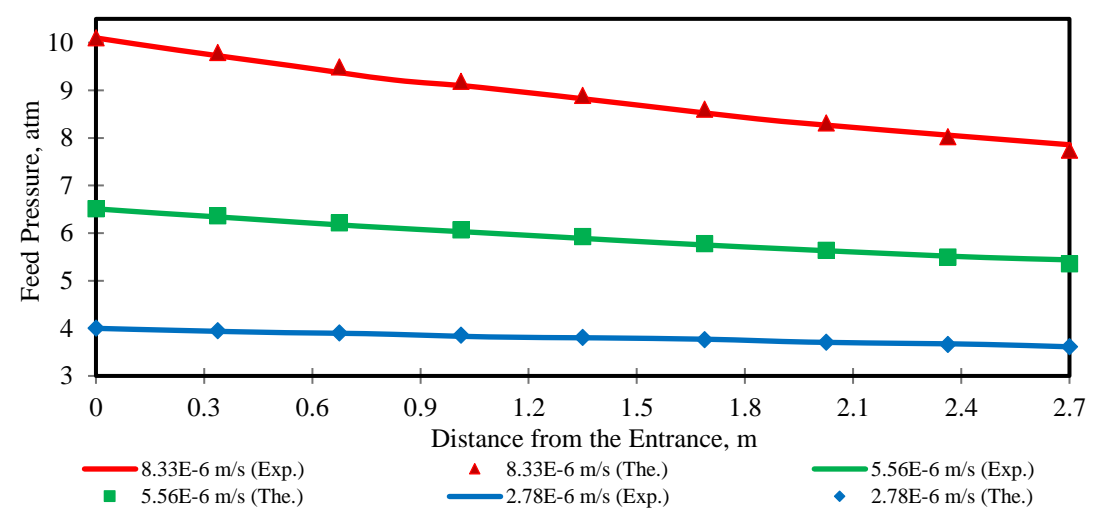


Fig. 3.3. Observed and modeled feed pressure versus the membrane length for three different average permeate fluxes (initial conditions of NDMA, 3.3761x10⁻⁹ kmol/m³, 2.43x10⁻³ m³/s, and 20 °C)

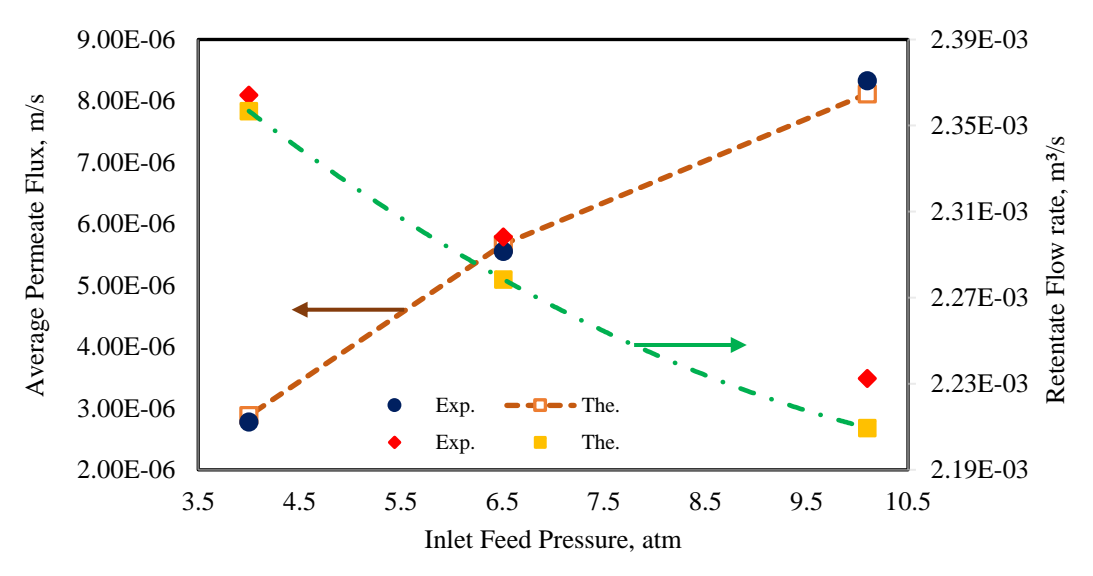


Fig. 3.4. Observed and modeled average permeate flux and retentate flow rate versus inlet feed pressure (initial conditions, 3.3761x10⁻⁹ kmol/m³, 2.43x10⁻³ m³/s, and 20 °C)

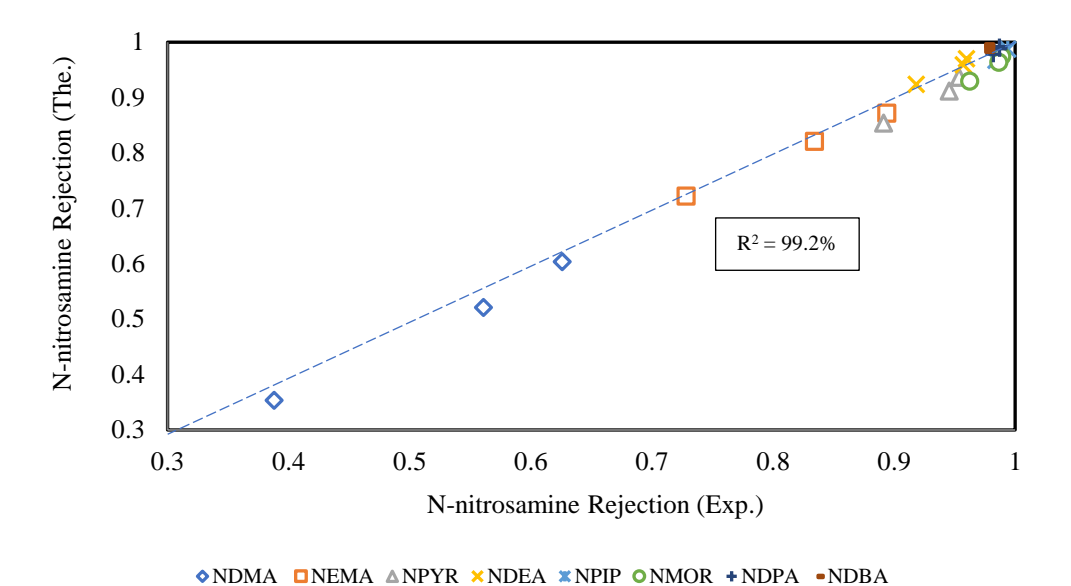


Fig. 3.5. Experimental and modelled rejections of eight N-nitrosamine solutes at three average permeate fluxes of (2.78x10⁻⁶, 5.56x10⁻⁶ and 8.33x10⁻⁶ m/s) (initial conditions, 2.43x10⁻³ m³/s and 20 °C)

3.4 Mass transfer equations of organic compounds

The mass transfer equations used in the developed models of the selected organic compounds are described in the next section.

3.4.1 Chlorophenol and dimethylphenol

The mass transfer coefficient k (m/s) in the high-pressure channel of the module depends on the solution properties, such as viscosity, solute diffusivity, and the hydrodynamic conditions in the channel, which is a function of pressure, concentration, flow rate, and temperature. It means that k will vary with the membrane length and width.

The mass transfer coefficient of chlorophenol at the feed channel can be calculated from Sundaramoorthy et al. (2011b)

$$k_{(x)} de_b = 147.4 \ D_{b(x)} \ Re_{b(x)}^{0.13} \ Re_{p(x)}^{0.739} \ C_{m(x)}^{0.135} \eqno(3.1)$$

The mass transfer coefficient of dimethylphenol at the feed channel can be calculated from Srinivasan et al. (2011)

$$k_{(x)} de_b = 246.9 D_{b(x)} Re_{b(x)}^{0.101} Re_{p(x)}^{0.803} C_{m(x)}^{0.129}$$
 (3.2)

The exponents in the above two equations have been experimentally predicted by Sundaramoorthy et al. (2011b) and Srinivasan et al. (2011) for chlorophenol and dimethylphenol aqueous solutions, respectively and showed a fit about 0.99 as a regression coefficient in the method of least squares. Also, $C_{\rm m}$ is a dimensionless solute concentration.

$$C_{m(x,y)} = \frac{C_{b(x,y)}}{\rho_w}$$
 (3.3)

 $\rho_{\rm w}$ is the molal density of water (55.56 kmol/m³).

The Reynolds number on the feed and permeate channels can be calculated from

$$Re_{b(x)} = \frac{\rho_{b(x)} \, de_b \, F_{b(x)}}{t_f \, W \, \mu_{b(x)}} \tag{3.4}$$

$$Re_{p(x)} = \frac{\rho_{p(x)} de_p J_{w(x)}}{\mu_{p(x)}}$$
 (3.5)

 de_b and de_p (m) are the equivalent diameters of the feed and permeate channels, respectively.

$$de_b = 2t_f (3.6)$$

$$de_{p} = 2t_{p} \tag{3.7}$$

 $t_{\rm f}$, $t_{\rm p}$ (m) are the height of feed channel and permeate channel, respectively.

3.4.2 N-nitrosamine

The mass transfer coefficient $k_{(x)}$ (m/s) of N-nitrosamine at any point along the x-axis of membrane length was estimated using the empirical correlation of Senthilmurugan et al. (2005) and Mane et al. (2009) as given below

$$k_{(x)} = 0.753 \left(\frac{K}{2-K}\right)^{0.5} \left(\frac{D_{b(x)}}{t_f}\right) \left(\frac{\mu_{b(x)} \rho_{b(x)}}{D_{b(x)}}\right)^{0.1666} \left(\frac{2 t_f^2 U_{b(x)}}{D_{b(x)} \Delta L}\right)^{0.5} \tag{3.8}$$

 $K, D_b, \mu_b, \rho_b, t_f, \Delta L$ and U_b are the efficiency of mixing net (i.e. spacer) (K = 0.5) (dimensionless), diffusion coefficient (m^2/s), dynamic viscosity (kg/m s), density (kg/m^3), feed channel height (m), characteristic length of mixing net (m) and feed velocity (m/s), respectively.

3.5 The physical properties equations

This research highlights the experimental work of dilute chlorophenol, dimethylphenol, and N-nitrosamine aqueous solutions of wastewater gathered from the literature. For modelling purpose, the physical properties equations of the solutions have been conceived as identical to water equations. The proposed correlations of Koroneos et al. (2007) to calculate the physical properties of seawater (diffusion coefficient, viscosity, and density) are being considered. The Solute diffusivity of the feed solution and permeate (m²/s) are

$$D_{b(x)} = 6.725 \times 10^{-6} \exp \left\{ 0.1546 \times 10^{-3} \left(C_{b(x)} \times 18.0125 \right) - \frac{2513}{T_{b(x)} + 273.15} \right\} \tag{3.9}$$

$$D_{p(x)} = 6.725 \times 10^{-6} \exp \left\{ 0.1546 \times 10^{-3} \left(C_{p(x)} \times 18.0125 \right) - \frac{2513}{T_{p(x)} + 273.15} \right\} \tag{3.10}$$

The viscosity of feed and permeate (kg/m s) are

$$\mu_{b(x)} = 1.234x10^{-6} \exp\left\{ (0.0212 C_{b(x)} x18.0153) + \frac{1965}{T_{b(x)} + 273.15} \right\}$$
 (3.11)

$$\mu_{p(x)} = 1.234x10^{-6} \exp\left\{ (0.0212 C_{p(x)} x18.0153) + \frac{1965}{T_{p(x)} + 273.15} \right\}$$
(3.12)

The density of feed and permeate (kg/m³) are

$$\rho_{b(x)} = 498.4 \text{ m}_{f(x)} + \sqrt{\left[248400 \text{ m}_{f(x)}^2 + 752.4 \text{ m}_{f(x)} \text{ C}_{b(x)} \text{ x} 18.0153\right]}$$
(3.13)

$$\rho_{p(x)} = 498.4 \ m_{p(x)} + \sqrt{\left[248400 \ m_{p(x)}^2 + 752.4 \ m_{p(x)} \ C_{p(x)} \ x18.0153\right]} \eqno(3.14)$$

$$m_{f(x)} = 1.0069 - 2.757x10^{-4} T_{b(x)}$$
 (3.15)

$$m_{p(x)} = 1.0069 - 2.757x10^{-4} T_{p(x)}$$
 (3.16)

3.6 RO models for apple juice concentration process

This section presents the models developed for the apple juice concentration using a spiral wound RO process. Specifically, the following sections will exhibit distributed and lumped models developed based on the solution diffusion model.

3.6.1 Distributed model

Several models have been published on RO process that predict the permeate flux and aroma compounds rejections for aqueous solutions apple juice. These models were described in Section 2.8.6 in Chapter 2. The solution diffusion model in its lumped version has been applied for the previous models. However, no distributed modeling can be found in the literature for apple juice concentration RO process. The aim of this section is to present the development of a new distributed steady state model (1D) that will relax several earlier assumptions.

3.6.1.1 Model Type_6

Specifically, a number of differential equations have been developed based on the solution diffusion model. As well as this, the contribution of all sugar species in the feed osmotic pressure will be taken into consideration. Besides, the model estimates the physical properties of apple juice using the empirical equations that shows the impact of concentration and temperature derived from the literature. Also, the solute transport parameters of sugar species were determined based on the concept of free energy parameter.

Assumptions

- The module is made up of porous flat sheet with no feed spacers and negligible leaf curvature.
- 2. Validity of the Darcy's law for the feed channel, which assumes that the pressure drop is proportional to the feed flow rate and the friction parameter is applied to characterise the pressure drop.
- Validity of the film model theory to estimate the concentration polarisation impact.
- 4. The feed osmotic pressure is caused by the impact of all the species found in sugar and not restricted to only sucrose, glucose, and malic acid.
- 5. Constant pressure of 1 atm on the permeate side.
- 6. Constant solute transport parameters of sugar and aroma compounds.
- 7. The underlying process is isothermal.
- 8. Constant friction factor of feed channel is assumed due to laminar flow.

Model equations

$$J_{w(x)} = A_{w(T_b)} \left(\Delta P_{b(x)} - \Delta \pi_{\text{Total }(x)} \right) \tag{M.6.1}$$

 $A_{w(T_b)}$ was experimentally determined for the spiral wound module type (MSCB 2521 R99) using pure water and accounts for the pore distribution of the membrane, porosity, and membrane thickness. Álvarez et al. (2001) introduced the following correlation to show the impact of feed flow rate and operating temperature on $A_{w(T_b)}$

$$A_{w(T_b)} = 9.059 \text{x} 10^{-7} \, \left(\frac{T_b}{25}\right)^{0.62} \left(\frac{36.0 \text{x} 10^5 \, F_{b(0)}}{400}\right)^{-0.1447} \tag{M.6.2}$$

The above equation confirms that the water permeability coefficient slightly decreased with inlet feed flow rate and increased with temperature.

$$\Delta P_{b(x)} = (P_{b(x)} - P_p) \tag{M.6.3}$$

The overall trans-membrane pressure (TMP) (atm) for each run is calculated as

$$TMP = \frac{P_{b(0)} + P_{b(L)}}{2} - P_{p}$$
 (M.6.4)

Because the aroma compounds concentration is very small compared to the sugar compounds in apple juice, $\Delta \pi_{Total(x)}$ can only refer to the summation of the

osmotic pressure difference of sugar compounds along the length of the membrane. The osmotic pressure difference of each sugar species can be defined as

$$\Delta \pi_{(i)(x)} = \pi_{(i)Cw(x)} - \pi_{(i)Cp(av)}$$
(M.6.5)

i represents the particular sugar species under consideration. $\pi_{(i)Cw(x)}$, $\pi_{Cp(i)(av)}$ (atm) are the osmotic pressure of any sugar compound at the membrane wall and permeate channel, respectively. Eq. (M.6.5) can be written as

$$\Delta \pi_{(i)(x)} = R T_b \left(C_{w(i)(x)} - C_{p(i)(av)} \right)$$
(M.6.6)

The solute flux $J_{s(i)(x)}$ (kmol/m² s) of any sugar or aroma compounds.

$$J_{s(i)(x)} = B_{s(i)} \left(C_{w(i)(x)} - C_{p(i)(av)} \right)$$
(M.6.7)

 $B_{s(i)}$ (m/s) is the solute transport parameter of the determined species (sugar or aroma), which is assumed as a constant along the length of the membrane (Assumption 6).

$$J_{s(i)(x)} = J_{w(x)} C_{p(i)(av)}$$
(M.6.8)

Eq. (M.6.6) can be written as

$$\Delta \pi_{(i)(x)} = R T_b \frac{J_{s(i)(x)}}{B_{s(i)}}$$
 (M.6.9)

Substituting Eq. (M.6.8) in Eq. (M.6.9) and combining the result in Eq. (M.6.1) with re-arrangements yields to Eq. (M.6.10).

$$J_{w(x)} = \frac{A_{w(T_b)} B_{s(i)} \Delta P_{b(x)}}{B_{s(i)} A_{w(T_b)} R T_b C_{p(i)(av)}}$$
(M.6.10)

Based on Assumption 5, Eq. (M.6.11) can readily be derived as

$$\frac{\mathrm{d}\,\Delta P_{\mathrm{b}(\mathrm{x})}}{\mathrm{d}\mathrm{x}} = \frac{\mathrm{d}\,P_{\mathrm{b}(\mathrm{x})}}{\mathrm{d}\mathrm{x}} \tag{M.6.11}$$

Darcy's law can be used to express the feed pressure drop along the x-axis (Assumption 2)

$$\frac{dP_{b(x)}}{dx} = -b F_{b(x)}$$
 (M.6.12)

$$F_{b(0)} = F_{b(x)} + F_{p(x)} \tag{M.6.13}$$

Taking the total mass balance across a small section in the feed channel of the unit, gives

$$\frac{dF_{b(x)}}{dx} = -W J_{w(x)}$$
 (M.6.14)

Furthermore, taking the derivative of Eq. (M.6.13) yields Eq. (M.6.15) to express the variation of permeated flow rate along the x-axis as

$$\frac{dF_{b(x)}}{dx} = -\frac{dF_{p(x)}}{dx} = -W J_{w(x)}$$
(M.6.15)

Dividing Eq. (M.6.12) and Eq. (M.6.14), yields

$$\frac{d \, \Delta P_{b(x)}}{d F_{b(x)}} = \frac{b \, F_{b(x)}}{W \, J_{w(x)}} \tag{M.6.16}$$

The above equation can be written in the form of Eq. (M.6.17) by putting the value of solvent flux from Eq. (M.6.10).

$$F_{b(x)} dF_{b(x)} = \frac{W A_{w(T_b)} B_{s(i)} \Delta P_{b(x)}}{b \left(B_{s(i)} + A_{w(T_b)} R T_b C_{p(i)(av)}\right)} d\Delta P_{b(x)}$$
(M.6.17)

Further simplification yields the following expression

$$F_{b(x)} dF_{b(x)} = \vartheta_{(i)} \Delta P_{b(x)} d\Delta P_{b(x)}$$
 (M.6.18)

$$\vartheta_{(i)} = \frac{W A_{w(T_b)} B_{s(i)}}{b \left(B_{s(i)} + A_{w(T_b)} R T_b C_{p(i)(av)}\right)}$$
(M.6.19)

 $\vartheta_{(i)}$ is a parameter that can be calculated for all the sugar and aroma compounds and then the average value will be considered as $\vartheta_{(mix)}$ for the rest of calculations.

$$\vartheta_{(\text{mix})} = \frac{\sum_{i=1}^{n} \frac{W A_{w(T_b)} B_{s(i)}}{b \left(B_{s(i)} + A_{w(T_b)} R T_b C_{p(i)(av)}\right)}}{n}$$
(M.6.20)

n is the total number of sugar and aroma compounds. Re-arrangement with integration of Eq. (M.6.18) gives a correlation to calculate the feed flow rate at any point along the x-axis

$$F_{b(x)} = F_{b(0)} + \vartheta_{(mix)}^{0.5} \left(\Delta P_{b(x)} - \Delta P_{b(0)} \right)$$
(M.6.21)

Substituting Eq. (M.6.21) into Eq. (M.6.12) and taking the integration facilitates the calculation of the trans-membrane pressure in any point along the x-axis

$$\Delta P_{b(x)} = \Delta P_{b(0)} - b \, x \, F_{b(0)} - b \, x \, \Delta P_{b(x)} \left(\vartheta_{(mix)} \right)^{0.5} + b \, x \, \Delta P_{b(0)} \left(\vartheta_{(mix)} \right)^{0.5} \quad (M.6.22)$$

Substituting Eqs. (M.6.20) and (M.6.22) into Eq. (M.6.10) with re-arrangement gives

$$J_{w(x)} = \frac{\vartheta_{(mix)} b}{W} \left(\Delta P_{b(0)} - b x F_{b(0)} - b x \Delta P_{b(x)} \left(\vartheta_{(mix)} \right)^{0.5} + b x \Delta P_{b(0)} \left(\vartheta_{(mix)} \right)^{0.5} \right)$$
(M.6.23)

Also, another equation for solvent flux can be derived by taking the derivative of Eq. (M.6.11) with respect to the x-axis as follows

$$\frac{\mathrm{d}J_{w(x)}}{\mathrm{d}x} = \frac{\vartheta_{(\mathrm{mix})} \, \mathrm{b}}{\mathrm{W}} \left(\frac{\mathrm{d}\Delta P_{b(x)}}{\mathrm{d}x} \right) \tag{M.6.24}$$

Substituting Eq. (M.6.12) into Eq. (M.6.24), gives

$$\frac{\mathrm{d}J_{w(x)}}{\mathrm{d}x} = \frac{\vartheta_{(\mathrm{mix})} b}{W} \left(-b F_{b(x)}\right) \tag{M.6.25}$$

The variation of solvent flux in the x-axis can be calculated by the following equation

$$\begin{split} J_{w(x)} &= J_{w(0)} - \left(\frac{\vartheta_{(mix)}}{W} \ b^2 \ x \ F_{b(0)}\right) + \left(\frac{\vartheta_{(mix)}^2 \ b^3}{W} \ \Delta P_{b(0)} \ \left(\frac{x^2}{2}\right)\right) - \\ &\left(\frac{\vartheta_{(mix)}^2 \ b^4}{W} \ F_{b(0)} \ \left(\frac{x^3}{6}\right)\right) - \left(\frac{\vartheta_{(mix)}^{2.5} \ b^4}{W} \ \Delta P_{b(x)} \ \left(\frac{x^3}{6}\right)\right) + \left(\frac{\vartheta_{(mix)}^{2.5} \ b^4}{W} \ \Delta P_{b(0)} \ \left(\frac{x^3}{6}\right)\right) \end{split} \tag{M.6.26}$$

Moreover, it is assumed that the osmotic pressure is caused by the impact of all the species found in sugar (Assumption 4) in contrary to the statement of Álvarez et al. (2001) who neglects both fructose and sorbitol. Therefore, the solvent flux at x = 0 is calculated using Eq. (M.6.27) regarding the osmotic pressure, which is caused by sugar compounds (sucrose, glucose, malic acid, fructose, and sorbitol).

$$J_{w(0)} = A_w \left(\Delta P_{b(0)} - \left(\pi_{su(0)} + \pi_{g(0)} + \pi_{m(0)} + \pi_{f(0)} + \pi_{so(0)} \right) \right)$$
 (M.6.27)

 $\pi_{su(0)}$, $\pi_{g(0)}$, $\pi_{m(0)}$, $\pi_{f(0)}$ and $\pi_{so(0)}$ are the osmotic pressure (atm) of sucrose, glucose, malic acid, fructose and sorbitol, respectively. The estimation of the osmotic pressure caused by sucrose, glucose, and malic acid at any point along the x-axis is carried out using the empirical equation of Nabetani et al. (1992b) as can be seen in Eq. (M.6.28)

$$\pi_{su(x)} + \pi_{g(x)} + \pi_{m(x)} = -\frac{R \, T_b}{V_w} \, \ln \left\{ \frac{\left[\frac{\left(1000 - C_{w(su)(x)} - C_{w(g)(x)}\right)}{M_{ww}}\right] - \left[\frac{\left(4 \, C_{w(su)(x)}\right)}{M_{su}}\right] - \left[\frac{\left(2 \, C_{w(g)(x)}\right)}{M_g}\right]}{\left[\frac{\left(1000 - C_{w(su)(x)} - C_{w(g)(x)}\right)}{M_{ww}}\right] - \left[\frac{\left(4 \, C_{w(su)(x)}\right)}{M_{su}}\right] - \left[\frac{\left(2 \, C_{w(g)(x)}\right)}{M_g}\right]} \right\} + \frac{R \, T_b \, C_{w(m)(x)}}{M_{max}}$$

$$\frac{R \, T_b \, C_{w(m)(x)}}{M_{max}} \qquad (M.6.28)$$

R, V_w and M_{ww} (kpa m³/ K kmol, m³/kmol, kg/kmol) are the gas constant, the molar volume of water and the molecular weight of water, respectively. M_{su} , M_g and M_{ma} (kg/kmol) are the molecular weights of sucrose, glucose, and malic acid, respectively are reported in Table 2.6 in Chapter 2. Note, all the concentrations expressed in Eq. (M.6.28) are referred to the concentration of the species at the wall membrane and expressed in (kg/m³). However, the contribution of fructose and sorbitol to osmotic pressure is calculated by Eqs. (M.6.29) and (M.6.30), respectively.

$$\pi_{f(x)} = \frac{R T_b C_{w(f)(x)}}{M_f}$$
 (M.6.29)

$$\pi_{so(x)} = \frac{R T_b C_{w(so)(x)}}{M_{so}}$$
 (M.6.30)

 $\rm M_{\rm f}, M_{\rm so}$ are the molecular weight of fructose and sorbitol, respectively. The concentration of the sugar and aroma compounds at the wall membrane was

estimated based on Assumption 3, which in turn is based on the validity of the film model theory where the solvent flux is linked to concentration polarisation and mass transfer coefficient k (m/s) by the following equation

$$\frac{(C_{w(i)(x)} - C_{p(i)(av)})}{(C_{b(i)(x)} - C_{p(i)(av)})} = \exp\left(\frac{J_{w(x)}}{k_{(i)(x)}}\right) \tag{M.6.31}$$

$$U_{b(x)} = \frac{F_{b(x)}}{W t_f}$$
 (M.6.32)

Integration of Eq. (M.6.12) yields

$$\begin{split} P_{b(x)} &= P_{b(0)} - \left[b \; F_{b(0)} \, x \right] + \left[\vartheta_{(mix)} \; b^2 \; \left(\frac{x^2}{2} \right) \; \Delta P_{b(0)} \right] - \left[\vartheta_{(mix)} \; b^3 \; F_{b(0)} \left(\frac{x^3}{6} \right) \right] - \\ & \left[\vartheta_{(mix)} ^{1.5} \; b^3 \; \Delta P_{b(x)} \left(\frac{x^3}{6} \right) \right] + \left[\vartheta_{(mix)} ^{1.5} \; b^3 \; \Delta P_{b(0)} \left(\frac{x^3}{6} \right) \right] \end{split} \tag{M.6.33}$$

The sugar or aroma compounds concentration at the feed channel and at any point along the x-axis is calculated using Eq. (M.6.34) as proposed by Lee et al. (2010).

$$\frac{d\frac{C_{b(i)(x)}F_{b(x)}}{t_fW}}{dx} = -\frac{J_{w(x)}C_{p(i)(av)}}{t_f} + \frac{J_{w(x)}C_{b(i)(x)}}{t_f} + \frac{d}{dx}\left(D_{b(i)(x)}\frac{dC_{b(i)(x)}}{dx}\right)$$
(M.6.34)

Then, substituting Eq. (M.6.31) and Eq. (M.6.8) into Eq. (M.6.7) with rearrangement gives a correlation to calculate the concentration of any sugar or aroma compound at the permeate side. This equation will be used twice at x=0 and x=L as can be shown in Eqs. (M.6.35) and (M.6.36), respectively, and the average solute permeate concentration $C_{p(i)(av)}$ (kmol/m³) is calculated using Eq. (M.6.37) as follows

$$C_{p(i)(0)} = \frac{B_{s(i)} C_{b(i)(0)}}{J_{w(0)} + B_{s(i)}} \frac{e^{\frac{J_{w(0)}}{k_{(i)(0)}}}}{e^{\frac{J_{w(0)}}{k_{(i)(0)}}}}$$
(M.6.35)

$$C_{p(i)(L)} = \frac{B_{s(i)} C_{b(i)(L)}}{J_{w(L)} + B_{s(i)}} \frac{e^{\frac{J_{w(L)}}{k_{(i)(L)}}}}{e^{\frac{J_{w(L)}}{k_{(i)(L)}}}}$$
(M.6.36)

$$C_{p(i)(av)} = \frac{C_{p(i)(0)} + C_{p(i)(L)}}{2}$$
(M.6.37)

The volumetric permeated flow rate along the x-axis in the permeate channel is

$$F_{p(x)} = W \int_{x=0}^{x=L} J_{w(x)} dx$$
 (M.6.38)

$$Rej_{(i)} = \frac{C_{b(i)(L)} - C_{p(i)(av)}}{C_{b(i)(L)}} x100$$
(M.6.39)

$$Rec_{\text{(Total)}} = \frac{F_{p(\text{Total})}}{F_{b(0)}} \times 100 \tag{M.6.40}$$

3.6.1.2 The physical properties equations

The mass transfer coefficient of each species is a function of pressure, concentration, flow rate and temperature, which means that k_i (m/s) varies with the membrane length. Schock and Miquel (1987) correlation is used to estimate the mass transfer coefficient along the x-axis for any species of sugar or aroma compounds as given in Eq. (M.6.41)

$$k_{(i)(x)} = 0.065 \, \left(\frac{D_{b(i)(x)}}{d_b}\right) \, Re_{b(x)}^{0.875} \, \, Sc_{(i)(x)}^{0.25} \eqno(M.6.41)$$

 $D_{b(i)(x)}$, $Re_{b(x)}$, $Sc_{(i)(x)}$ (m²/s, dimensionless) are the diffusion coefficient of any sugar or aroma compound, the Reynolds number and the Schmidt number of any sugar or aroma compound at any point along the x-axis, respectively. The terms can be calculated as follows:

$$Re_{b(x)} = \frac{\rho_{b(x)} d_h U_{b(x)}}{\mu_{b(x)}}$$
 (M.6.42)

$$Sc_{(i)(x)} = \frac{\mu_{b(x)}}{\rho_{b(x)} D_{b(i)(x)}}$$
 (M.6.43)

 $\rho_{b(x)}$, $\mu_{b(x)}$ and d_h (kg/m³, kg/m s, m) are the apple juice density, viscosity, and the hydraulic diameter, respectively.

The apple juice viscosity can be calculated as a function of concentration in °Brix and temperature using Eq. (M.6.44) (Constenla et al. 1989).

$$\frac{\mu_{b(x)}}{\mu_w} = \exp\left(\frac{A^* \, {}^{\circ}Brix_{(x)}}{100 - B^* \, {}^{\circ}Brix_{(x)}}\right) \tag{M.6.44}$$

 $\mu_{\rm w}$ and °Brix_(x) are the viscosity of water (8.94x10⁻⁴ kg/m s) and the concentration of apple juice in °Brix. A^* and B^* are parameters related to the temperature and can be estimated using Eqs. (M.6.45) and (M.6.46).

$$A^* = -0.25801 + \frac{817.11}{T_b} \tag{M.6.45}$$

$$B^* = 1.8909 - 3.0212 \times 10^{-3} T_b \tag{M.6.46}$$

Eq. (M.6.47) can be used to calculate the variation of apple juice concentration in °Brix along the length of membrane regarding the concentration of the mixture in kg/m³.

°Brix_(x) = 0.099198
$$\left(\sum_{i=1}^{n} C_{(x,n)}\right)$$
 (M.6.47)

 $C_{(i)(x)}$ (kg/m³) is the concentration of any sugar or aroma compounds at any point along the x-axis and calculated using Eq. (M.6.48)

$$C_{(i)(x)} = C_{b(i)(x)} M_{wt(i)}$$
 (M.6.48)

i represents the particular species of any sugar or aroma compounds. $M_{wt\,(i)}$ (kg/kmol) is the molecular weight of any species under consideration.

The apple juice density is calculated using Eq. (M.6.49) as a function of concentration in °Brix and temperature (Constenla et al. 1989).

$$\rho_{b(x)} = 0.8272 + 0.34708 \exp(0.01 \, {}^{\circ}\text{Brix}_{(x)}) - 5.479 \, x10^{-4} \, T_b \tag{M.6.49}$$

Then, the diffusion coefficient for any sugar species $D_{SU(x)}$ (m²/s) and aroma compounds $D_{AR(x)}$ (m²/s) along the x-axis can be calculated using the empirical equation proposed by Gladdon and Dole (1953) as can be seen in Eqs. (M.6.50) and (M.6.51), respectively

$$D_{SU(x)} = D_s \left(\frac{\mu_W}{\mu_{h(x)}}\right)^{0.45}$$
 (M.6.50)

$$D_{AR(x)} = D_a \left(\frac{\mu_w}{\mu_{b(x)}}\right)^{0.45}$$
 (M.6.51)

D_s, D_a (m²/s) are referred to the diffusion coefficient of any species of sugar and aroma compounds, respectively in a very dilute solution. These coefficients have been calculated using the proposed correlation of Wilke and Chang (1955).

$$D_{a} = \left(\frac{7.4 \times 10^{-8} (2.6 \,\mathrm{M_{w}})^{0.5} (\mathrm{T_{b}} + 273.15)}{(1000 \,\mu_{\mathrm{b(x)}}) (1000 \,\mathrm{V_{bp,A}})^{0.6}}\right) \times 10^{-4} \tag{M.6.52}$$

The above equation is correlated to be compatible with the units used. $M_{\rm w}$ and $V_{\rm bp,A}$ (kg/kmol, m³/kmol) are the molecular weight of water (18.01528 kg/kmol) and the molar volume of the solute, respectively at its normal boiling point.

Parameter estimation

Friction parameter

In this work, the friction parameter has been estimated using an optimization methodology of the gEST parameter estimation tool developed in gPROMS. This method has been used on the experimental data of Álvarez et al. (2002) in order to optimise the value of friction parameter. The registered value of friction parameters for the membrane type MSCB 2521 R99 of effective area 1.03 m² is 90 (atm s/m⁴).

Solute transport parameters

The solute flux of sugar and aroma compounds through the membrane is given by the product of solute transport parameter and the solute concentration difference at the two channels of the unit as expressed in Eq. (M.6.7). Thus, for calculation purposes, a separate value of the solute transport parameter is required for each species for multiple solutes feed.

Solute parameters of aroma compounds

The solute parameters of aroma compounds B_s (m/s) for the RO module consisting of a spiral wound aromatic polyamide membrane type (MSCB 2521 R99) were calculated using the equation of Álvarez et al. (2001).

$$B_{s(i)} = B_{s(i) Ref.} \exp^{0.098(T_b - T_{Ref})}$$
 (M.6.53)

i represents the particular species under consideration. $B_{s(i)}$, $B_{s(i)}$ Ref and T_{Ref} are the solute parameter of any aroma compounds at temperature (T_b) and the reference temperature of 25 °C (T_{Ref}) , respectively. Eq. (M.6.53) was obtained for a temperature range of 15 °C to 30 °C. The estimated values of solute parameter for each aroma compounds at 25 °C are shown in Table 2.6 in Chapter 2.

Solute parameters of sugar compounds

The solute transport parameters B_s (m/s) of sugar compounds were calculated using the correlation of Matsuura et al. (1976), which assumed the concept of free energy parameter ($-\Delta\Delta G/RT$) governing non-ionized polar organic solutes in aqueous solution RO separation. Eq. (M.6.54) shows the general form of this correlation

$$\ln B_{s(i)} = \ln C_{NaCl}^* + \left(-\frac{\Delta \Delta G}{RT_b} \right)_i + \delta^* E s^* \tag{M.6.54} \label{eq:macl}$$

i represents the particular species under consideration. $\ln C_{NaCl}^*$ is a constant depending on the chemical nature of the membrane and the effective pore size, where NaCl as the reference solute. However, the steric Taft number (δ^*Es^*) is characteristic of each solute in the bulk solution and represents the properties of the solute on the membrane-solution interface and relates to the membrane type. For the aromatic polyamide membrane type, Matsuura et al. (1976) found the quantity $\ln C_{NaCl}^*$ using the experimental solute transport parameter data $B_{s\,NaCl}$ for a completely ionized inorganic solute taken NaCl as a reference, and the known values of $(-\Delta\Delta G/RT)$ for both Na^+ and Cl^- ions as can be shown in Eq. (M.6.55).

$$\ln B_{s \text{ NaCl}} = \ln C_{\text{NaCl}}^* + \left[\left(-\frac{\Delta \Delta G}{RT} \right)_{\text{cation}} + \left(-\frac{\Delta \Delta G}{RT} \right)_{\text{anion}} \right]$$
 (M.6.55)

Then, the numerical value of $(-\Delta\Delta G/RT)$ for several monovalent inorganic cations and anions in aqueous solutions used in conjunction with aromatic polyamide membrane in RO has been obtained using Eq. (M.6.56) (Dickson et al. 1975; Matsuura et al. 1975b).

$$\ln B_{s \text{ NaCl}} = \ln C_{\text{NaCl}}^* + \left[\left(-\frac{\Delta \Delta G}{RT} \right)_i \right]$$
(M.6.56)

The free energy parameter of each sugar species ($-\Delta\Delta G/RT$) and the steric Taft number (δ^*Es^*) of each species of sugar are calculated by Matsuura et al. (1976) (Table 2.6 in Chapter 2). Finally, the transport parameter for each species of sugar for the aromatic polyamide membrane type (MSCB 2521 R99) at 25 °C can be calculated using Eq. (M.6.56) as reported in Table 2.6 in Chapter 2. However, the transport parameter of malic acid was taken from Malaiyandi et al. (1982).

Model validation

The Model Type_6 developed for a spiral wound RO process for the apple juice concentration process has been validated by comparing the model predictions results with those obtained from actual experimentation for a MSCB 2521 R99 spiral wound RO aromatic polyamide membrane module carried out by Álvarez et al. (2002). Fig. 3.6 shows the model rejections of two selected aroma compounds, Isopentyl acetate and trans-2-hexanal at two different inlet feed flow rates versus the operating temperature and against experimental results. Fig. 3.7 shows the variation of Isopentyl acetate rejection versus the operating transmembrane pressure at three different inlet feed flow rates with comparative data between the model and experiments results. Also, Figs. 3.8 and 3.9 show the experimental and theoretical results of outlet water flux and feed flow rate versus the operating trans-membrane pressure for different inlet feed flow rates at temperature 20 °C. The clear corroboration with experimental data readily shows the suitability of the model to measure the observed retention and water flux parameters with an accepted error over the operating ranges of transmembrane pressures and temperatures. Fig. 3.6 shows that the model tends to only underestimate the rejection of trans-2-hexanal at lower operating temperatures and inlet feed flow rate. This might attribute to the inaccurate estimation of the transport membrane parameter at such conditions.

Similarly, Fig. 3.8 shows that the model predicts the water flux within an accepted error, except at high inlet feed flow rate and operating pressure. This is due to

the use of a constant value of water permeability coefficient in all the calculations. It can be argued that this coefficient decreases exponentially with the operating trans-membrane pressure as a result to membrane compaction. At the same time, the water permeability coefficient increases due to an increase in the operating temperature that causes a reduction in water viscosity. It is expected that these reasons contribute to the slight discrepancy between the outputs of the model and experiments at these conditions.

Fig. 3.9 shows the consistence between the model prediction and experiments results for the retentate flow rate versus the operating trans-membrane pressure using three different inlet feed flow rates. Finally, a 10% maximum error agreement is obtained in a comparison between experimental and calculated rejection for all aroma compounds as presented in Fig. 3.10. The relatively small discrepancy can be attributed to two reasons. Firstly, the actual experiments of Álvarez et al. (2002) is carried out using apple juice concentration of 11 °Brix not 10.5 °Brix. Secondly, constant solute transport parameters of aroma compounds are used in the calculation of solute flux through the membrane as can be seen in Eq. (M.6.7).

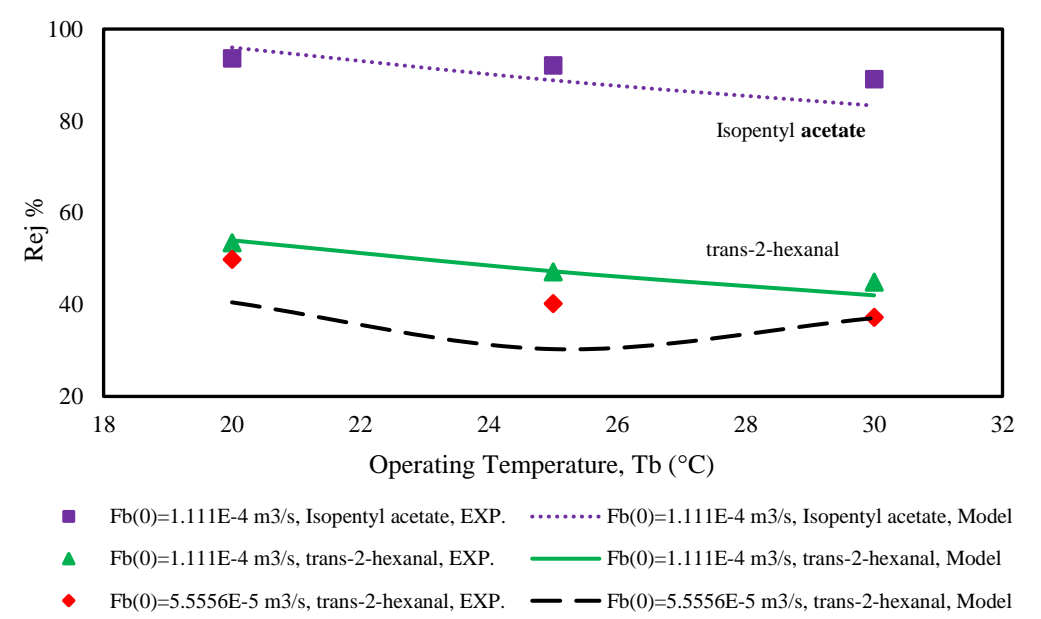


Fig. 3.6. Experimental and model rejections of the two selected aroma compounds versus average operating temperature for two different inlet feed flow rates at inlet conditions (${}^{\circ}$ Brix = 10.5, TMP = 34.542 atm)

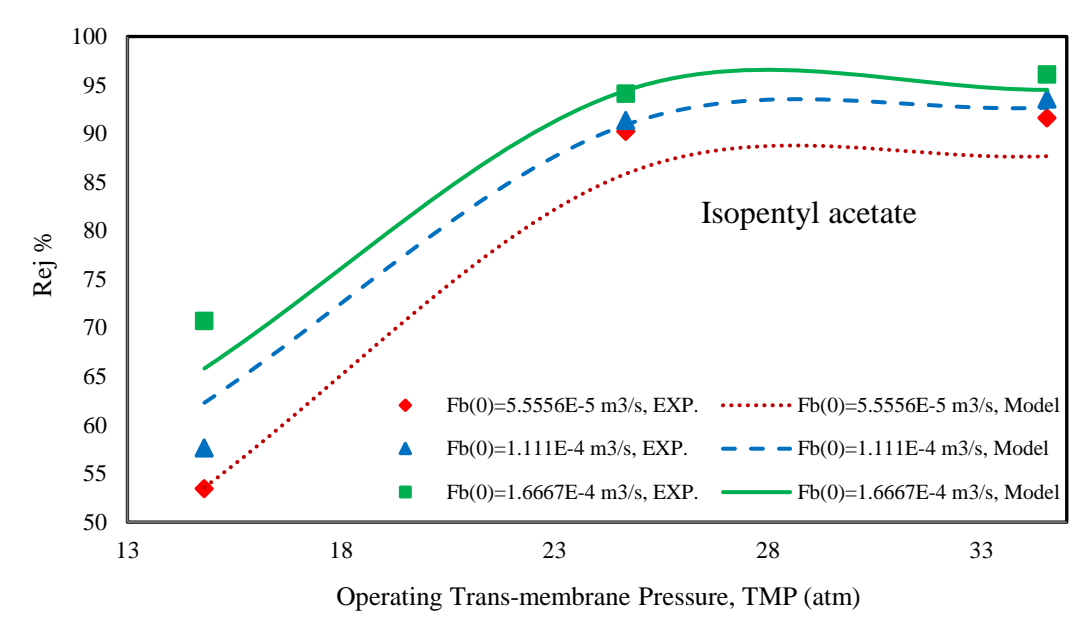


Fig. 3.7. Experimental and model Isopentyl acetate rejection versus operating trans-membrane pressure for three different inlet feed flow rates at inlet conditions (${}^{\circ}$ Brix = 10.5, T_b = 20 ${}^{\circ}$ C)

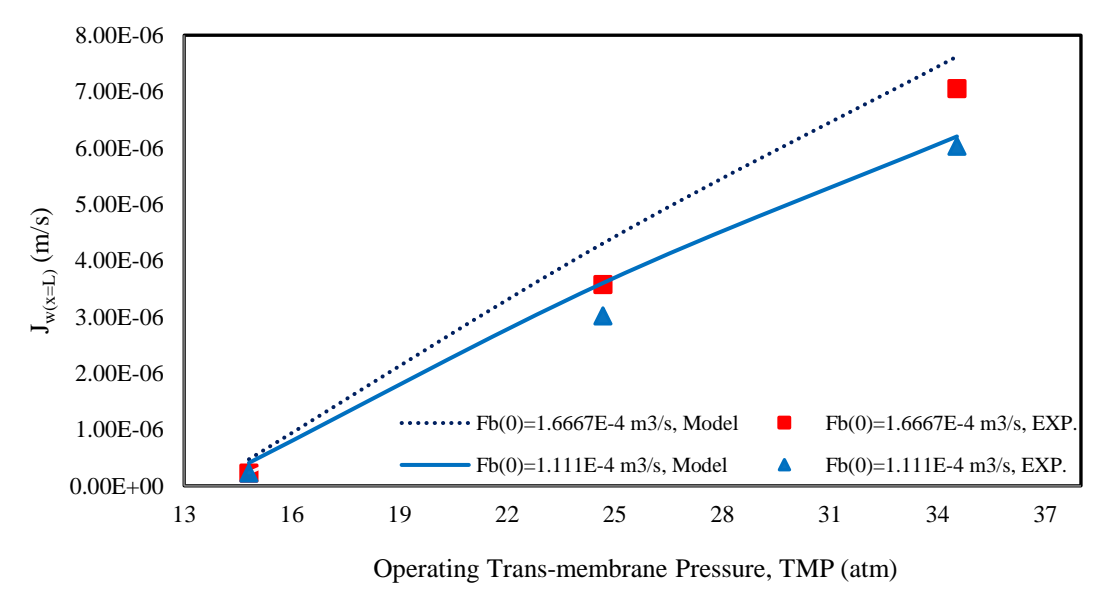


Fig. 3.8. Experimental and model outlet water flux versus operating trans-membrane pressure for two different inlet feed flow rates at inlet conditions (${}^{\circ}$ Brix = 10.5, $T_b = 20 {}^{\circ}$ C)

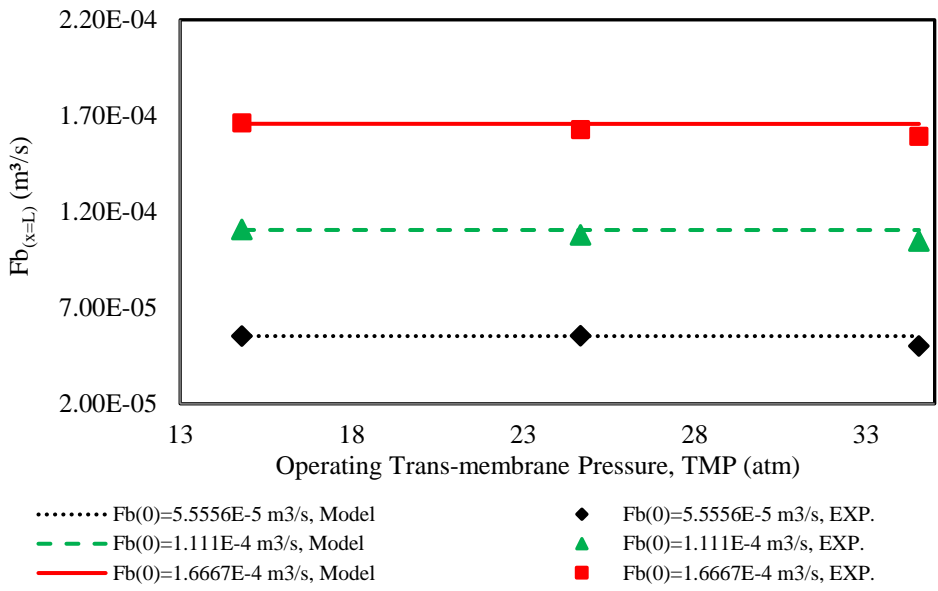


Fig. 3.9. Experimental and model retentate flow rate versus operating trans-membrane pressure for three different inlet feed flow rates at inlet conditions (${}^{\circ}$ Brix = 10.5, $T_b = 20 {}^{\circ}$ C)

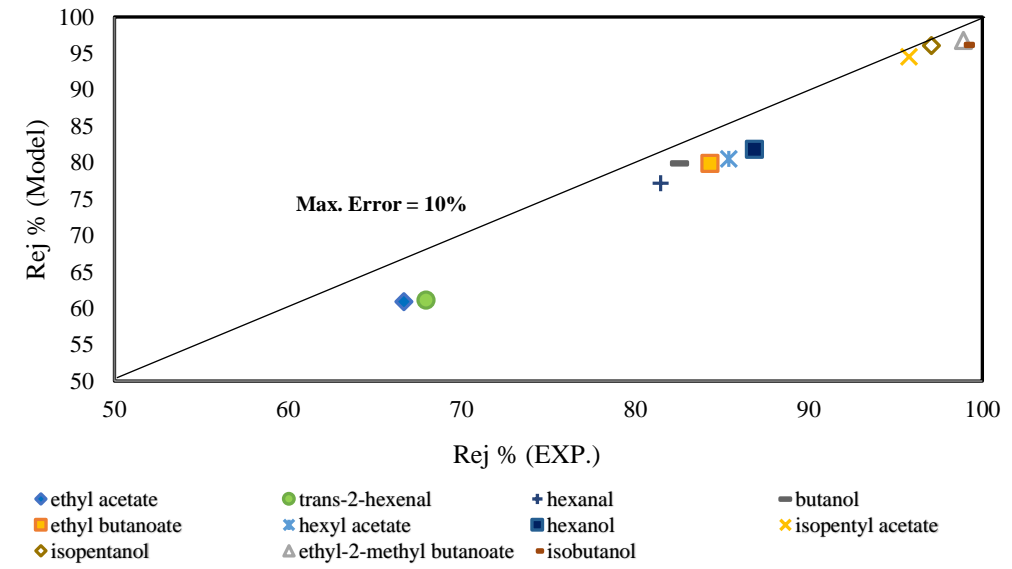


Fig. 3.10. Experimental and predicted aroma compounds rejection at inlet conditions (°Brix = 10.5, $T_b = 20$ °C, TMP = 34.542 atm, $F_{b(0)} = 1.6667 \times 10^{-4}$ m³/s)

3.6.2 Lumped model

3.6.2.1 Model Type_7

The main objective of this section is to present the development of a simple lumped parameter model based on the solution diffusion model. The model used to predict the concentration process of apple juice using a spiral wound membrane and then investigate the model equations of a full-scale plant considering the interaction between several stages of the RO system.

The assumptions made to develop the Model Type_6 are valid for the Model Type_7. However, the impact of operating temperature is considered in both the water and sugar species transport parameters. Also, the pressure drop across the membrane was predicted for the first time using the Da Costa equation that includes the characteristics of feed spacer. Also, a constant atmospheric pressure on the permeate channel of 101.325 kpa (1 atm) is considered. Moreover, the process of apple juice concentration using a multi-stage RO network based on a spiral wound module is mathematically modelled to simulate and optimise the concentration of apple juice considering the limits of operation and the constraints of both the module and RO layout.

Model equations

Water and solute fluxes are

$$J_{w} = A_{w} \left[\left(\frac{(P_{b(in)} + P_{b(out)})}{2} - P_{p} \right) - (\Delta \pi_{Total}) \right]$$
(M.7.1)

$$J_{s(i)} = B_{s(i)} \left(C_{w(i)} - C_{p(i)} \right) \tag{M.7.2}$$

Water permeability and solute transport parameters of any sugar compounds are

$$A_{w (T_b)} = 9.059 \times 10^{-7} \left(\frac{T_b}{25}\right)^{0.62} \left(\frac{36.0 \times 10^5 \text{ Q}_f}{400}\right)^{-0.1447}$$
(M.7.3)

$$B_{s(i)} = B_{s(i),Ref} \exp^{0.098(T_b - T_{Ref})}$$
 (M.7.4)

The total osmotic pressure difference of sugar is represented in the counter of Eq. (M.7.5), while feed osmotic pressure caused by sucrose, glucose, and malic acid is given in Eq. (M.7.6)

$$\Delta\pi_{Total} = (\pi_{su,w} + \pi_{g,w} + \pi_{ma,w} + \pi_{f,w} + \pi_{so,w}) - (\pi_{su,p} + \pi_{g,p} + \pi_{ma,p} + \pi_{f,p} + \pi_{so,p})$$
(M.7.5)

$$\begin{split} \pi_{su,w} + \pi_{g,w} + \pi_{ma,w} &= -\frac{R\left(T_b + 273.15\right)}{V_w} \ln \left\{ \frac{\left[\frac{\left(1000 - C_{su,w} - C_{g,w}\right)}{M_{wb}}\right] - \left[\frac{\left(4 \ C_{su,w}\right)}{M_{su}}\right] - \left[\frac{\left(2 \ C_{g,w}\right)}{M_{g}}\right]}{\left[\frac{\left(1000 - C_{su,w} - C_{g,w}\right)}{M_{wb}}\right] - \left[\frac{\left(4 \ C_{su,w}\right)}{M_{su}}\right] - \left[\frac{\left(2 \ C_{g,w}\right)}{M_{g}}\right]}} \right\} + \\ &\frac{\frac{R\left(T_b + 273.15\right) \ C_{ma,w}}{M_{ma}}}{M_{ma}} \end{split} \tag{M.7.6}$$

In this respect, osmotic pressures caused by fructose and sorbitol are

$$\pi_{f,w} = R (T + 273.15) C_{f,w}$$
 $\pi_{so,w} = R (T + 273.15) C_{so,w}$
(M.7.7)

Osmotic pressure of any sugar species at the permeate channel is

$$\pi_{i,p} = R (T + 273.15) C_{i,p}$$
 (M.7.8)

Membrane surface concentration and bulk concentration are

$$\frac{(C_{w(i)} - C_{p(i)})}{(C_{b(i)} - C_{p(i)})} = \exp\left(\frac{J_w}{k_i}\right) \qquad C_{b(i)} = \frac{C_{f(i)} + C_{r(i)}}{2}$$
(M.7.9)

Inlet and outlet apple juice density and average apple juice density are

$$\rho_{in} = \left[0.8272 + (0.3471 \exp\left(0.01 \,^{\circ} \text{Brix}_{in}\right)) - (5.479 \,^{\circ} \text{x}10^{-4} \,^{\circ} \text{(T}_b + 273.15))\right] \text{x} \, 10^3$$

(M.7.10)

$$\rho_{out} = \left[0.8272 + (0.3471 \exp \left(0.01 \, ^{\circ} \! \text{Brix}_{out} \right)) - (5.479 \, \text{x} 10^{-4} \, (T_b + 273.15)) \, \right] \! \text{x} \, 10^3 \qquad \left(\text{M.7.11}\right)$$

$$\rho_{\text{mix}} = \frac{\rho_{\text{in}} + \rho_{\text{out}}}{2} \tag{M.7.12}$$

Inlet and outlet concentrations of apple juice in Brix are

°Brix_{in} = 0.09945
$$\left(\sum_{i=1}^{n} C_{f(i)}\right)$$
 (M.7.13)

°Brix_{out} = 0.09945
$$\left(\sum_{i=1}^{n} C_{r(i)}\right)$$
 (M.7.14)

Inlet and outlet apple juice viscosity and average apple juice viscosity are

$$\frac{\mu_{\text{in}}}{\mu_{\text{w}}} = \exp\left(\frac{A^* \, {}^{\circ}\text{Brix}_{\text{in}}}{100 - B^* \, {}^{\circ}\text{Brix}_{\text{in}}}\right) \tag{M.7.15}$$

$$\frac{\mu_{\text{out}}}{\mu_{\text{w}}} = \exp\left(\frac{A^* \, {}^{\circ}\text{Brix}_{\text{out}}}{100 - B^* \, {}^{\circ}\text{Brix}_{\text{out}}}\right) \tag{M.7.16}$$

$$\mu_{\text{mix}} = \frac{\mu_{\text{in}} + \mu_{\text{out}}}{2} \tag{M.7.17}$$

A* and B* are defined in Eqs. (M.6.45) and (M.6.46). Also, Eqs. (M.6.50) and (M.6.52) are used to predict the diffusion coefficient for any sugar species and diffusion coefficient for any sugar species in a very dilute solution, respectively. The retentate pressure and the pressure drop are calculated based on Da Costa et al. (1994)

$$P_{b(out)} = P_{b(in)} - \Delta P_{drop}$$
(M.7.18)

$$\Delta P_{\text{drop}} = \left(\frac{\rho_{\text{mix}} \ U_b^2 \ L \ C_{\text{td}}}{2 \ \text{dh}}\right) x 10^{-3} \tag{M.7.19}$$

$$C_{\rm td} = \frac{A'}{Re_{\rm mix}^{\rm n}} \tag{M.7.20}$$

 $C_{\rm td}$ is the total drag coefficient. A'and n are spacer characteristics (Table 2.5 in Chapter 2). The mass transfer coefficient of each sugar species is given us

$$k_{(i)} = 0.065 \left(\frac{D_{(i)}}{d_h}\right) Re_{mix}^{0.875} Sc_{(i)}^{0.25}$$
 (M.7.21)

Bulk velocity and flow rate are

$$U_{b} = \frac{Q_{b}}{W t_{f} \epsilon}$$
 $Q_{b} = \frac{Q_{f} + Q_{r}}{2}$ (M.7.22)

Concentration at the permeate channel for all sugar compounds and rejection are

$$C_{p(i)} = \frac{C_{f(i)} B_{s(i)}}{B_{s(i)} + \frac{J_w}{\exp(\frac{J_w}{k_{(i)}})}}$$

$$Rej_{(i)} = \frac{C_{f(i)} - C_{p,i}}{C_{f(i)}} x100$$
 (M.7.23)

Permeate flow rate and total recovery are described as

$$Q_p = J_w A$$
 Rec $= \frac{Q_p}{Q_f} x100$ (M.7.24)

The model developed above is used to represent the performance of multi stage RO process of retentate reprocessing design. Therefore, the following equations for a whole RO plant are developed as follows;

Total mass balance and material balance of the whole plant are

$$Q_{f(plant)} = Q_{r(plant)} + Q_{p(plant)}$$
(M.7.25)

$$Q_{f(plant)} C_{f(i)(plant)} = Q_{r(plant)} C_{r(i)(plant)} + Q_{p(plant)} C_{p(i)(plant)}$$
(M.7.26)

Feed flow rate of stage 1 is

$$Q_{f(plant)} = Q_{f(s=1)} \tag{M.7.27}$$

Plant retentate flow rate and permeate flow rate are

$$Q_{r(plant)} = Q_{r(s=n)}$$
 $Q_{p(plant)} = \sum_{s=1}^{n} Q_{p(s)}$ (M.7.28)

Operating pressure of stage 1 and plant retentate pressure are

$$P_{f(plant)} = P_{f(in)(s=1)} \qquad P_{f(out)(plant)} = P_{f(out)(s=n)}$$
(M.7.29)

Plant feed concentration and retentate concentration are

$$C_{f(i)(plant)} = C_{f(i)(s=1)}$$
 $C_{r(i)(plant)} = C_{r(i)(s=n)}$ (M.7.30)

Feed concentration, pressure and feed flow rate of each stage are

$$C_{f(i)(s)} = C_{r(i)(s-1)}$$
 $P_{f(in)(s)} = P_{f(out)(s-1)}$ $Q_{f(s)} = Q_{r(s-1)}$ for $s \ge 2$ (M.7.31)

Total retentate and permeate of each stage are

$$Q_{r(s)} = \sum_{PV=1}^{n} Q_{r(PV)} \qquad Q_{p(s)} = \sum_{PV=1}^{n} Q_{p(PV)}$$
 (M.7.32)

Material balance of each stage

$$Q_{f(s)} C_{f(i)(s)} = Q_{r(s)} C_{r(i)(s)} + Q_{p(s)} C_{p(i)(s)}$$
(M.7.33)

Inlet and outlet apple concentrations in Brix of each stage are

°Brix
$$_{in(s)} = 0.09945 \left(\sum_{i=1}^{n} C_{f(i)(s)}\right)$$
 °Brix $_{out(s)} = 0.09945 \left(\sum_{i=1}^{n} C_{r(i)(s)}\right)$ (M.7.34)

Total rejection and recovery of each stage are

$$Rej_{(i)(s)} = \frac{c_{f(i)(s)} - c_{p(i)(s)}}{c_{f(i)(s)}} x100 \qquad Rec_{(s)} = \frac{Q_{p(s)}}{Q_{f(s)}} x100$$
 (M.7.35)

Plant inlet and outlet apple concentrations measured in Brix are

$$^{\circ}\text{Brix}_{\text{in(plant)}} = 0.09945 \left(\sum_{i=1}^{n} C_{f(i)(\text{plant})}\right) \tag{M.7.36}$$

°Brix_{out(plant)} = 0.09945
$$\left(\sum_{i=1}^{n} C_{r(i)(plant)}\right)$$
 (M.7.37)

Total plant rejection of each sugar species and recovery rate are

$$Rej_{(i)(plant)} = \frac{c_{f(i)(plant)} - c_{p(i)(plant)}}{c_{f(i)(plant)}} \ x100 \qquad Rec_{(plant)} = \frac{Q_{p(plant)}}{Q_{f(plant)}} \ x100 \qquad (M.7.38)$$

3.7 gPROMS software for modelling, simulation and optimisation

gPROMS Model Builder is a powerful modelling platform for steady state and dynamic simulation, and optimisation. Undoubtedly, it can be successfully used for any process in case of providing an accurate mathematical model. Among all other modelling software, the gPROMS suits has several key advantages include ease to use interface, handling both steady state and dynamic operation, experiments representation and design, drag and drop flowsheets to MS Excel to examine the results, and sensitivity analysis. Moreover, it provides the model validation scheme, which enable the user to fit the model prediction to match the experimental data (parameter optimisation). Also, it provides the degree of freedom, which is useful to examine the model structure and investigate the problem specification. Most importantly, the model equations can be built in any hierarchy compared to Matlab. In other words, the order in which the equations are declared is of no importance. Also, it can handle many algebraic, differential, and partial differential equations with a fast posing for accurate models.

3.7.1 gPROMS model builder platform

For the advantages mentioned above, the gPROMS suite (Process System Enterprise Ltd 2001) has been used to simulate the spiral wound RO process by implementing several mathematical models developed. The model developed is a set of algebraic and differential equations written in model entity. However, the model variables are set in lower and upper bounds and default values specified in variable types entity. Whereas, the process entity includes the setting of process parameters (module specifications) and assigned variables. Once the model built in gPROMS, several activates can be carried out such as experimental design, parameter estimation, and process optimisation. The optimisation entity enables the user to carry out a non-linear optimisation (NLP) problem and Mixed-Integer non-linear (MINLP) optimisation problems. The gPROMS project tree with the provided entities are shown in screenshot picture of Fig. 3.11. The model platform contains several information required to build the model as follows:

 PARAMETER: This is used to declare the real, integer constants where cannot be the result of simulation. The parameters are declared in the PROCESS entity.

- VARIABLE: This is used to declare the model variables that already set at lower and upper limits and default values in the Variable Type entity. The specified variables are assigned in the PROCESS entity.
- EQUATION: This section used to specify the model equations.
 Fig. 3.12 shows the screenshot of the model entity sections.

The process platform contains several sections as follows:

- UNIT: This is used to identify the process name.
- SET: This is used to declare the model parameters.
- ASSIGN: This is used to declare the specified variables. Basically, the
 degree of freedom is associated with the number of variables that should
 be assigned to pose the model successfully.
- INITIAL: This is used to declare the initial values of the differential variables at t = 0, which are required to commence a dynamic simulation.
- SOLUTIONPARAMETER: This is used to control various aspects of model-based activities include solver setting and drop and drag flowsheets etc.
- SCHEDUALE: This is used to implement a variable disturbance for a specified period of time.

The well posed models enable the user to plot the simulation results using gRMS plotting channel in 2D and 3D graphs. Also, the Microsoft Excel output channel can be used to generate an Excel file of the simulation results.

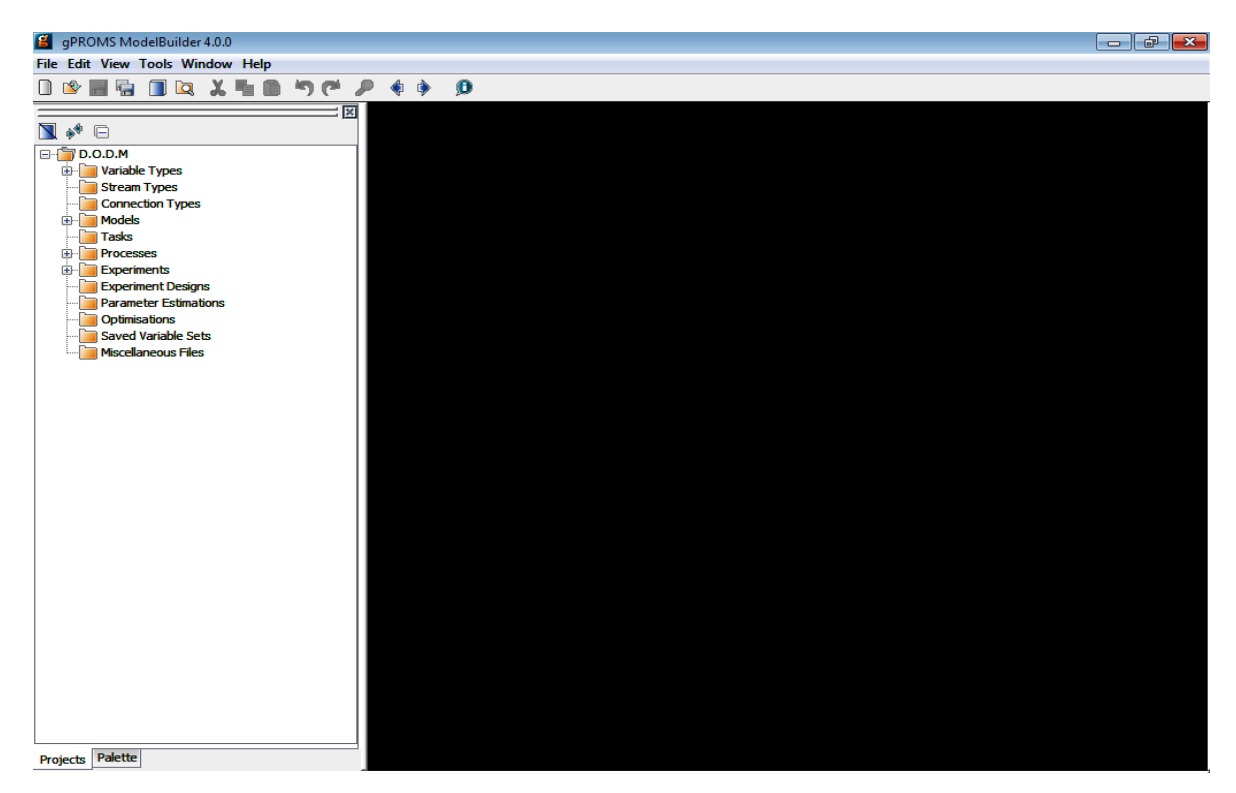


Fig. 3.11. Screenshot of the project entities for the gPROMS

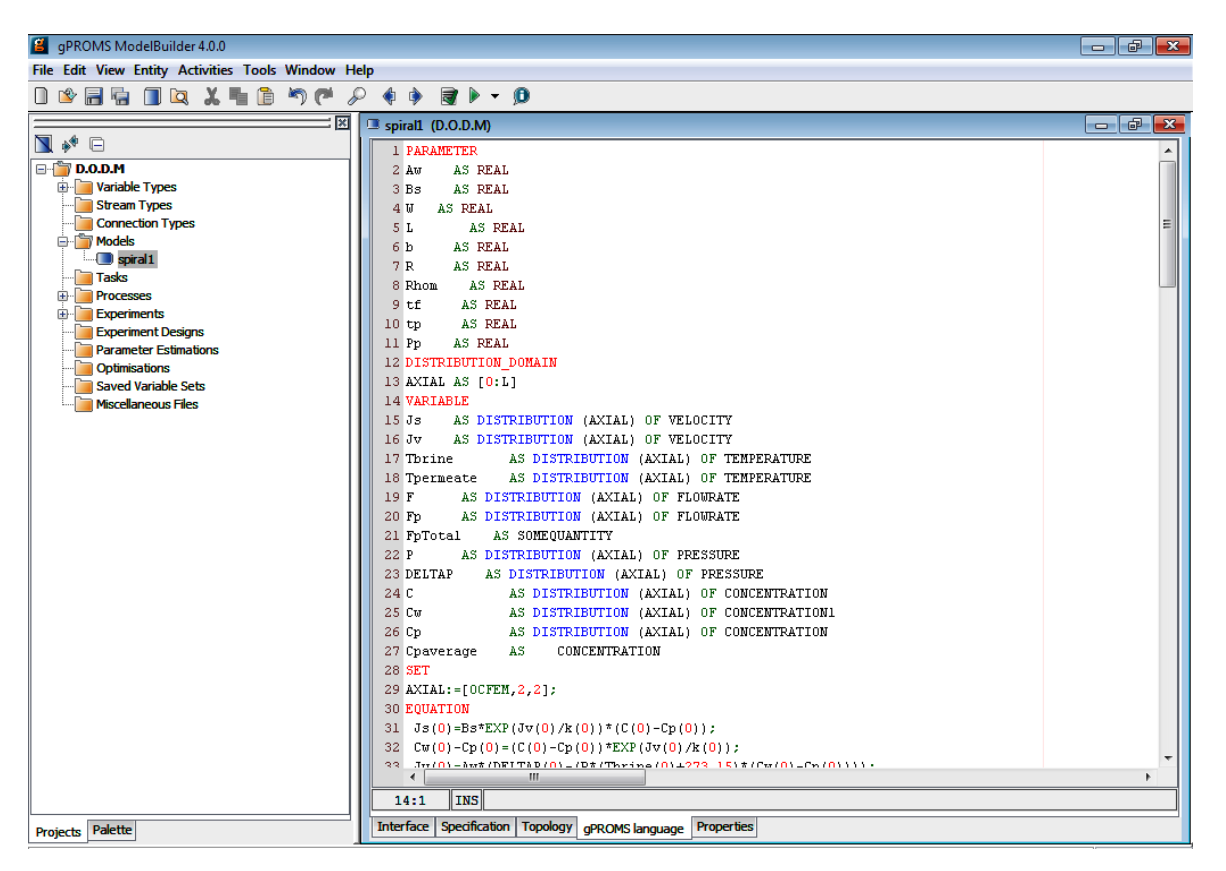


Fig. 3.12. Screenshot of the model entity

The optimisation entity contains three essential sections of General, Controls and Constraints. The objective function (maximise or minimise) is declared in the

General section. The bounds on the optimisation decision variables will often be declared in the Controls section, while the Constraints section is used to declare other constraints type as follows:

End-point constraints: These are certain conditions of operating variables
that the system must satisfy at the end of operation. These constraints
include equality and inequality constraints type. The inequality constraints
are within lower and upper limits. Fig. 3.13 shows a screenshot of
optimisation entity.

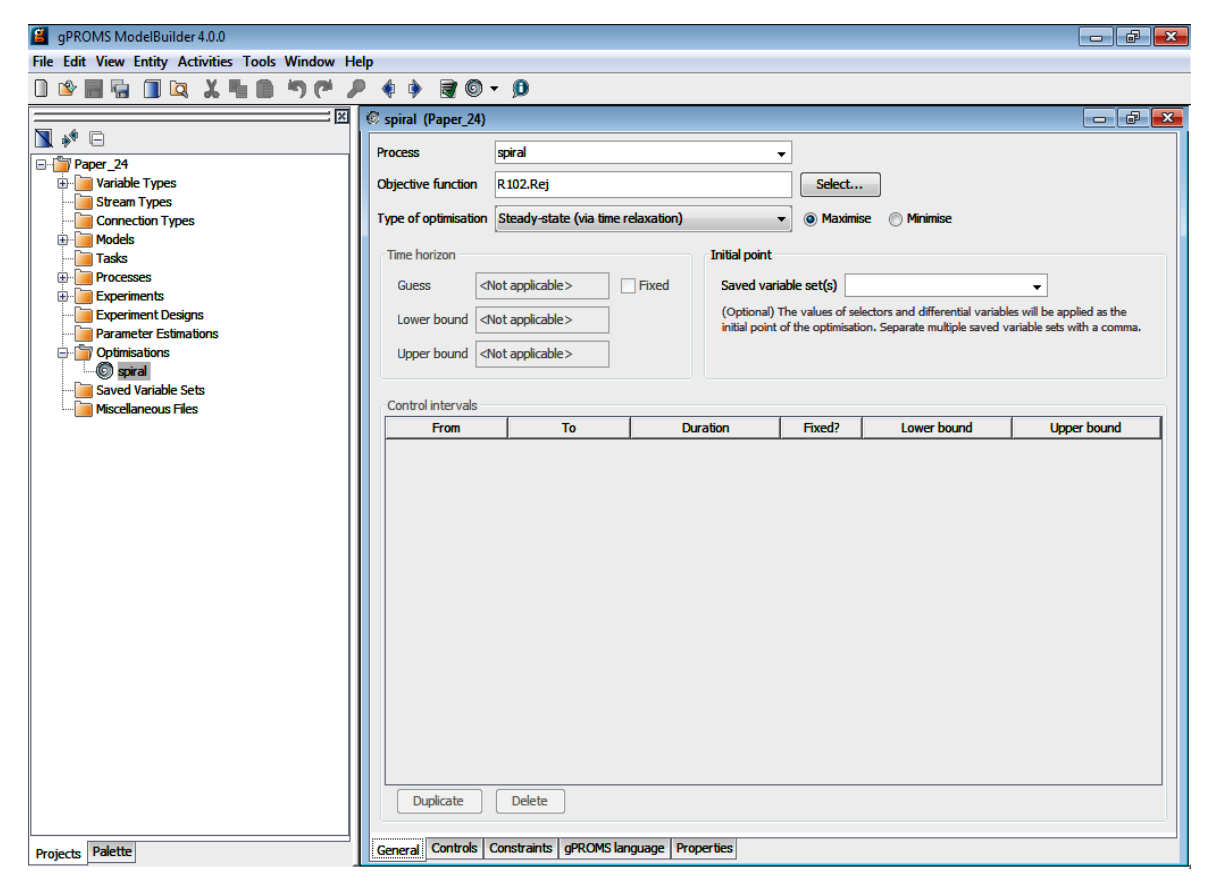


Fig. 3.13. Screenshot of the optimisation entity

3.8 Simulation solver

Several types of simulation solvers are provided by gPROMS. These solvers are in the PARAMETERESTIMATION section of the PROCESS entity. The simulation solver type DASOLV has been used in this research where it is able to solve mixed sets of non-linear algebraic and differential equations.

3.9 Parameter estimation

Any mathematical model of industrial process contains one or several unidentifiable parameters. In other words, these parameters cannot be determined from the available observational data. Mathematical parameter estimation can be used as a computational engine to attain the best solution of the model parameters for a given process in a systematic and efficient way. Consequently, the unknown parameters of any developed model and the operating conditions should be determined before solving the model equations. Murthy and Gupta (1998) have used the non-linear parameter estimation method of the Box-Kanemasu to find the model parameters. Senthilmurugan et al. (2005) adopted the simplex search method. In this research, another way has been used in order to estimate the unknown parameters, which can be executed automatically within the gPROMS parameter estimation for each set of experiments. Therefore, the aim of the optimisation is to accurately evaluate the values of several parameters depending on the experimental information that gives the best value of the performance criterion. The criterion of the gPROMS parameter estimation is to minimise the sum of square errors (SSE) between the experimental values of several parameters and the calculated values. This can be achieved by altering the model parameters from an initial guesstimate value to optimal values based on experimental data. In other words, the optimisation of these parameters is achieved by fitting the experimental data to the model predicted values by varying certain model parameters in order to maximise the probability that the model will closely predict. The gPROMS software provides a mathematical solver tool called as MXLKHD, which is based on maximum likelihood optimisation.

Accordingly, the next section describes in detail the parameter estimation of Model Type_5 (as an example) which is quite similar for all the other developed models in this research.

The experimental data of Fujioka et al. (2014b) is used to predict the best values of unknown parameters for each run of experiments, which are then used with the known parameters to check the process performance under the specified operating conditions. Specifically, the parameter estimation tool of the gEST in the gPROMS is used to predict the unknown parameters of the developed Model Type_5 of L_p , and b.

The process model equations of any distributed model developed can be written in a compact form as follows:

$$f(z, x(z), x^{-}(z), u(z), v) = 0; [z_0, z_f]$$

z is the independent variable (length of membrane), x(z) is the set of all differential and algebraic variables, $x^-(z)$ represents the derivative of x(z) with respect to length of membrane, u(z) is the control variables and v denotes the constant parameters of the process. The membrane length under consideration $[z_0, z_f]$ and function f is assumed to be continuously differentiable with respect to all its arguments. Please note that for any lumped models developed, the nonlinear algebraic equations can be written in a compact form as:

f(x, u, v) = 0, where x is the set of all algebraic variables, u is the set of decision variables need to be optimised and v represents the constant parameters of the model.

The estimation of these parameters is achieved by minimising the sum of the square errors (SSE) between the experimental retentate flow rate $F_{b(L)}$, total permeated water $F_{p(Total)}$, retentate pressure $P_{b(L)}$ and average N-nitrosamine rejection $Rej_{(av)}$ and the predicted values from the model. The parameter estimation problem can be therefore described as follows:

Given: The time invariant parameters: Inlet feed concentration, flow rate, pressure and temperature.

The measured parameters: Retentate measured flow rate, pressure, water flux, total permeated flow rate, and average rejection.

Obtain: Water permeability coefficients and friction parameters.

Minimise: The sum of square errors (SSE).

Subject to: Process model, process constraints.

SSE is defined as:

$$SSE = \sum_{i=1}^{N_{Data}} \left[F_{b(L),i}^{Exp.} - F_{b(L),i}^{Cal.} \right]^{2}$$

 N_{Data} , $F_{b(L)}^{Exp.}$ and $F_{b(L)}^{Cal.}$ are the numbers of test runs, experimental and the calculated retentate flow rate, respectively. Also, it is important to mention that the estimation of friction factor (b) is mainly related to both the experimental and predicted value of the retentate pressure $(P_{b(L)})$ linked to the trans-membrane pressure drop along the module. The parameter estimation problem can be mathematically presented as follows:

Subject to:

Equality constraints:

Process Model: $f(z, x(z), x^{-}(z), u(z), v) = 0; [z_0, z_f]$

Inequality constraints:

$$L_p^L \le L_p \le L_p^U$$
$$b^L \le b \le b^U$$

L and U are the lower and upper bounds. The membrane lengths under consideration [0, L] and function f are assumed to be continuously differentiable with respect to all their arguments.

A simulation step of the model solver starts the parameter estimation approach by converging the equality constraints (described by f) to satisfy the bounds of inequality constraints of decision variables (L_p , and b). The problem can then be solved by renewing the decision variables in a way, which satisfies the equality and inequality constraints (Mujtaba 2004).

Basically, the parameter estimation methodology of gPROMS used in all the model developed in Chapter 3 is stated as nonlinear programming (NLP) problem subject to non-linear and differential-algebraic constraints and based on the observational data for the relevant pollutant that can be found in the literature. Broadly speaking, this methodology has frequently provided local solutions and cannot guarantee global optimality with certainty (Moles et al., 2003). In other words, there is a limitation on determining high-consistent parameters compared to stochastic global optimisation methods such as stochastic algorithm, and evolution strategies. However, the observed numerical convergence of the sum of square errors were investigated for these models has indicated confident corroboration with satisfactory solutions.

3.10 Model validation

The concept of the model validation is basically based on the experimental data collected from the literature. In this respect, the model validation has been investigated after employing the parameter estimation, which facilitates the estimation of model constants. Therefore, the model has been used the set of experimental data for training to investigate the convergence between the model predictions and observational data. This is followed by testing the same model

with another set of experimental data to be ensure that the model prediction is within the acceptable convergence. Based on this methodology, all the model developed in Chapter 3 are validated against the relevant experimental data.

3.11 Optimisation

The gPROMS software suite was used to solve the optimisation problems using Point Optimisation technique. This technique is mathematically equivalent to solve a purely algebraic problem under considering neither maximising nor minimising a nonlinear objective function subjected to general nonlinear constraints (Equality and Inequality constraints) of upper and lower limits of operation. The solving of this optimisation problem is carried out by manipulating a set of optimisation decision variables that may be either continuous or discrete. This in turn provides a prediction of the appropriate operating conditions precisely that commensurate with the objective function. There are several methods used to solve different optimisation problems. This research presents only the Nonlinear Programming problems (NLP), which have been solved using specific methods as described in the next section.

3.11.1 NLP solution technique

The Nonlinear Programming Problems are solved using different methods including, Global Optimisation Problem (GOP) (Marcovecchio et al. 2005), Successive Linear Programming (SLP) method and Sequential Quadratic Programming (SQP) method (Villafafila and Mujtaba 2003), Mixed Integer Nonlinear Programming (MINLP) (Lu et al. 2006), Genetic Algorithm (GA) method (Murthy and Vengal 2006) and multi-objective Optimisation and Genetic Algorithm (MOO+GA) (Guria et al. 2005). For the models developed in this research, the optimisation problem is posed as a Non-Linear Programming (NLP) Problem and is solved using a Successive Quadratic Programming (SQP) method.

3.11.1.1 Successive Quadratic programming (SQP) technique

The Successive Quadratic Programming (SQP) method is already included in the gPROMS software suits and used to solve steady state optimisation problems (point optimisation entities) by implementing a first-order Taylor's series approximation around as initial point specified in the process. This in turn will

convert the nonlinear functions into approximate linear functions. In other words, the process started by converging all the equality constraints (including the model equations in its compact form) and specified the inequality constraints. Secondly, the optimisation step started by updating (reinitialization) the values of decision variables (Edgar et al. 2001). Specifically, reinitialization of the decision locates a new search direction for the decision variables, which is achieved using the solution of the last successful iteration. The new values of the decision variables will be the initial point (guestimate values) for further linearization to solve the linear problem. This is continued until solving the linear problem with a specific improvement of the objective function. It is noteworthy to mention that one of the standard solvers in gPROMS software for optimisation problems is CVP_SS, which employs the DASOLV code. This solver is quite able to solve steady state and dynamic optimisation problems with both discrete and continuous optimisation decision variables (mixed integer optimisation).

3.11 Conclusions

This chapter presents the models developed for the removal of organic compounds from wastewater using a spiral wound RO process and based on the solution diffusion model and irreversible thermodynamic model. The models developed were presented in two parts of distributed and lumped models. The predictions of these models in respect of the operating conditions compare favorably to the experimental data results gathered from the literature for several organic compounds and show a good agreement with an accepted convergence for most operating parameters. Moreover, distributed and lumped models for apple juice concentration process are also presented.

This chapter also illustrates the research methodology of gPROMS Model Builder used in this research. Specifically, the full detail of the process modelling, simulation, and optimisation are presented. This also involved the parameter estimation technique that has been used to predict the unknown parameters of any mathematical model. Also, the explanation of the optimisation tool used of Successive linear programming technique is included. The process optimisation offer the determination of the process operating variables that commensurate with the maximum process operation. This in turn has yielded improved optimisation models for removing organic compounds from wastewater and to express the process of apple juice concentration.

Chapter 4

Removal of Chlorophenol from Wastewater: Steady State Simulation, and Optimisation

4.1 Introduction

Chlorophenol (C₆H₅ClO) (128.555 g/mol; water solubility: 20 g/L at 20 °C) is a toxic compound for humans and can readily be found in the water of a wide range of industries. Specifically, its low concentration can deter the usage of reused water in various industrial applications.

This chapter focuses on presenting two cases of the spiral wound RO process for the removal of chlorophenol from wastewater include the simulation and optimisation. Therefore, the objectives of this chapter can be summarised as follows:

- to analyse the impact of several operating parameters on the performance of the spiral wound RO process towards the removal of chlorophenol from wastewater.
- to explore the potential of a hypothetical two-stage/two-pass RO design process for improving low chlorophenol rejection rates via simulation and optimisation.

4.2 Case 1: Sensitivity analysis of the operating parameters

Existing literature shows that the experimental study of Sundaramoorthy et al. (2011b) is the only study that deals with the removal of chlorophenol from water using an individual spiral wound module of RO process. Therefore, this case is mainly based on the experimental data of Sundaramoorthy et al. (2011b) described in Section 2.5.1.2 in Chapter 2. The characteristics of the spiral wound module are given in Table 2.2. For this case, Model Type_1 (described in Section 3.2.1.1 in Chapter 3) is used to investigate the effect of several operating parameters on the performance of the process at steady state conditions. The transport parameters of this model (A_w , B_s and b) are also given in Table 2.8 in Chapter 2. Also, the model validation is presented in Section 3.2.1 in Chapter 3.

4.2.1 Effect of operating parameters on the spiral wound RO process performance

4.2.1.1 Inlet feed flow rate

Particularly, Fig. 4.1 shows the reduction of the feed flow rate along the membrane channel and this is due to the permeated water passing through the membrane, which reduces the velocity of feed and increases the fluid concentration along the membrane length (Fig. 4.2). It seems that the concentration of feed progresses in the subsequent sub-sections of feed channel since the solute is retained in the wall with the diffusion of water through the membrane. Additionally, increasing feed flow rate results in increasing the mass transfer coefficient and decreasing the concentration polarisation. This will decrease the solute concentration gradient along the membrane length (Fig. 4.2).

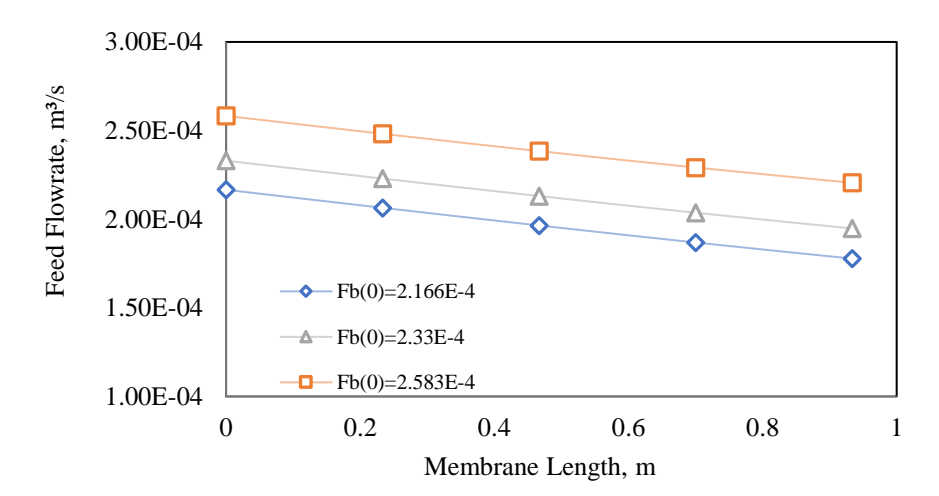


Fig. 4.1. Steady state feed flow rate along the membrane length of different inlet feed flow rates (inlet feed conditions, 2.335x10⁻³ kmol/m³, 7.77 atm, and 32 °C)

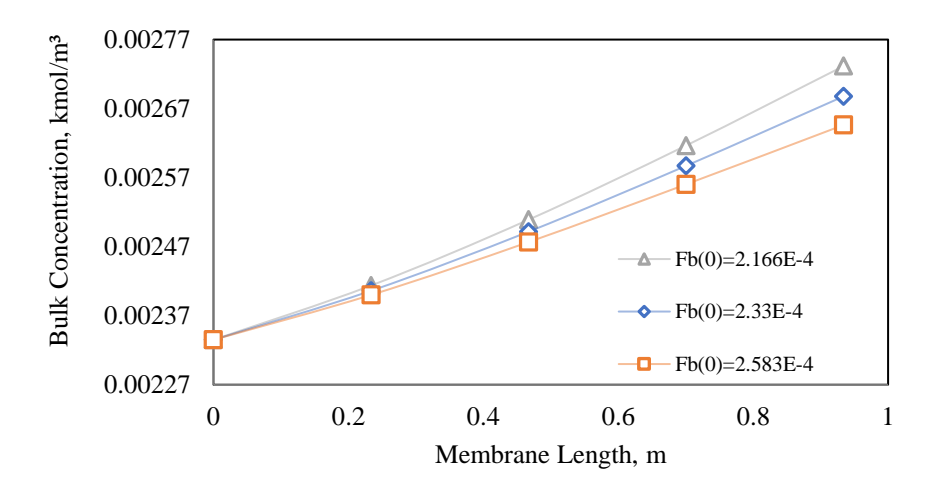


Fig. 4.2: Steady state feed concentration along the membrane length of different inlet feed flow rates (inlet feed conditions, 2.335x10⁻³ kmol/m³, 7.77 atm, and 32 °C)

The total water recovery along the membrane length decreases as the level of inlet feed flow rates increases (Fig. 4.3). This event can be attributed to high frictional pressure drop, which outweighed the gain of osmotic pressure reduction in each point along the membrane length. Thus, it will create a low driving force and decrease the residence time of feed inside the module for the flow of fresh water. Therefore, total water recovery will slightly decrease with increasing feed flow rate under approximately constant permeated flow rate. Similar results were confirmed by Lee et al. (2010).

Increasing inlet feed flow rate reduces the permeate concentration in spite of a slight change in the permeated water. The reason for this phenomenon is that increasing feed flow rate results in increasing the mass transfer coefficient and decreasing the concentration polarisation, which is followed by decreasing fluid concentration along the membrane. This will lead to a reduction in solute flux, reduction in permeate concentration and a slight increase in solute rejection (Fig. 4.4). Furthermore, increasing applied pressure reduces the concentration of the permeated water by increasing water flux.

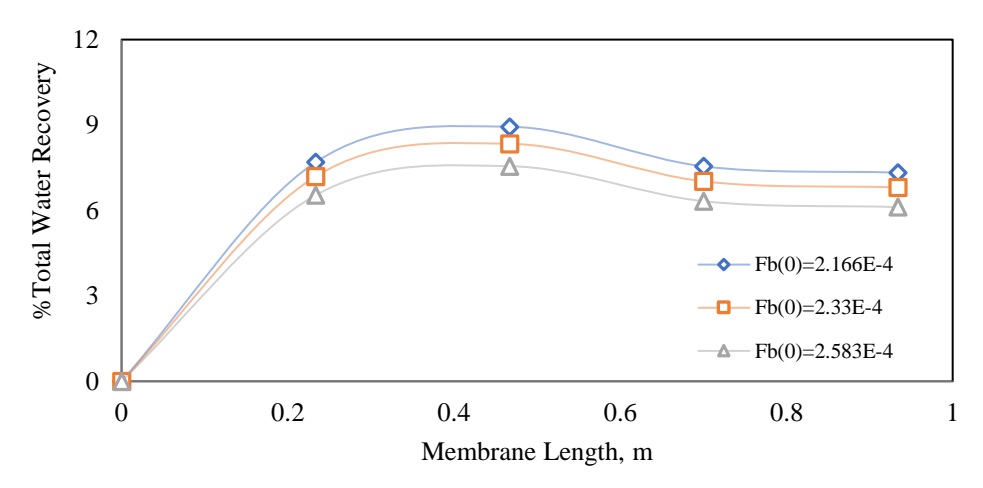


Fig. 4.3. Steady state total water recovery along the membrane length of different inlet feed flow rates (inlet feed conditions, 6.226x10⁻³ kmol/m3, 13.58 atm, and 31 °C)

It can be stated that the trend of incline for solute rejection at high velocities and high pressures conditions is slightly more obvious than at low velocities and low pressures (Fig. 4.4). This is because at high velocities, it appears that there is a dispute between the operating variables. Firstly, the mass transfer coefficient increases and the impact of concentration polarisation decreases. The greater feed flow rate reduces the wall membrane concentration and causes a decrease of osmotic pressure. However, at the same time, water flux is somewhat

decreasing with increasing friction, which reduces the quantity of water flux. Consequently, solute rejection slightly increases as a result of increasing of inlet feed flow rate in the tested range.

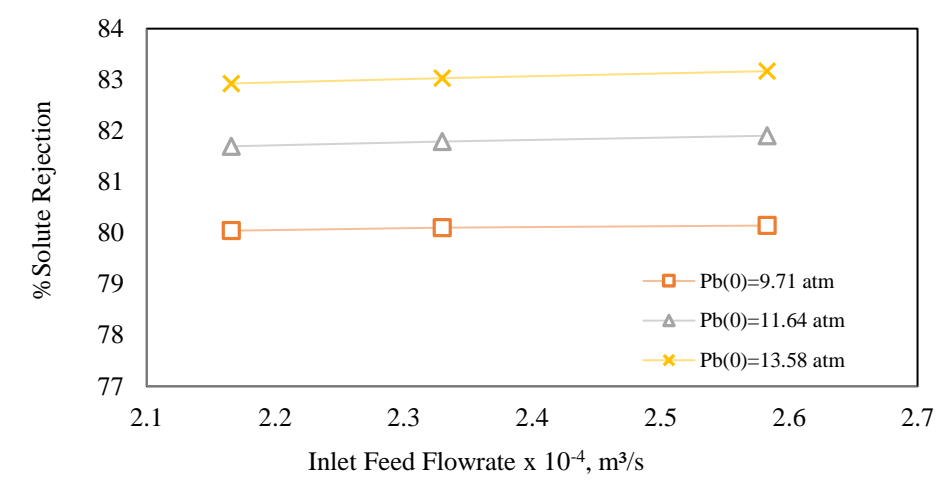


Fig. 4.4. Steady state solute rejection versus inlet feed flow rates of different inlet feed pressures (inlet feed conditions, 6.226x10⁻³ kmol/m³, and 31 °C)

4.2.1.2 Inlet feed pressure

In steady state mode, the pressure declines along the membrane channel due to pressure drop caused by the friction. Also, the water flux and total water recovery increases due to increase in operating pressure (Fig. 4.5). Basically, the operating pressure has a substantial impact on solute rejection (Fig. 4.4) by enhancing the quality of permeate and reducing the solute permeate concentration (Fig. 4.6). On the other hand, increasing inlet feed concentration for any inlet feed flow rate can cause a reduction in total water recovery (Fig. 4.5). This can be attributed to increase in the osmotic pressure that decreases the driving force of water flux and reduces the total water flux.

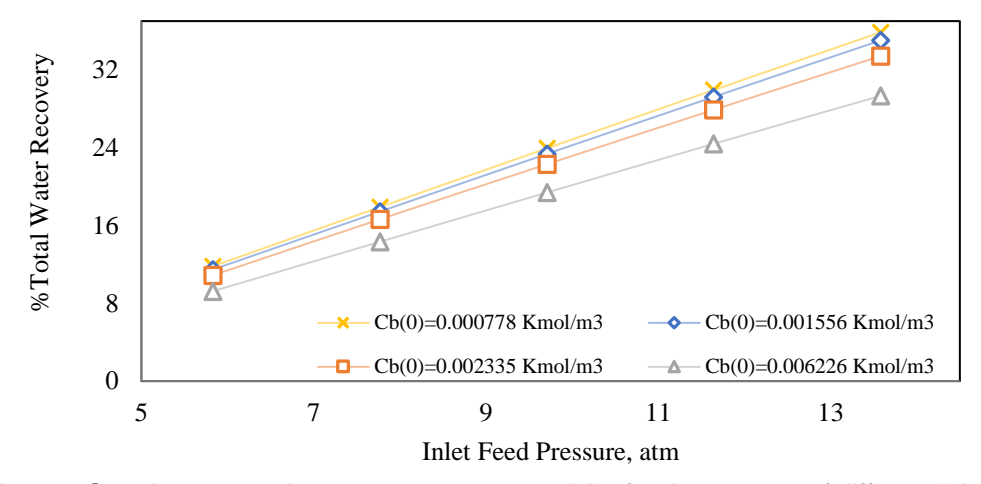


Fig. 4.5. Steady state total water recovery versus inlet feed pressures of different inlet feed concentrations (inlet feed conditions, 2.583x10⁻⁴ m³/s, and 32 °C)

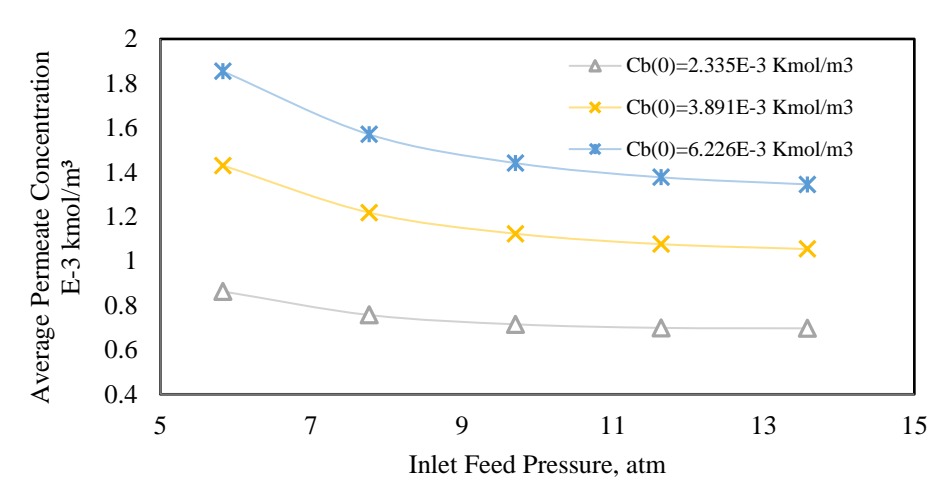


Fig. 4.6. Steady state average permeate concentration versus inlet feed pressures of different inlet feed concentrations (inlet feed conditions 2.583x10⁻⁴ m³/s and 32 °C)

4.2.1.3 Inlet feed temperature

The operating temperature has a significant role in RO process performance. Increasing inlet feed temperature decreases the viscosity and density of fluid, which accelerates the flux of water through the membrane that in turn increases total water recovery and solute rejection. Another explanation for this trend is that increasing feed temperature causes an increase of water flux due to the variation of pore size of the polymeric membrane in addition to increase in water diffusivity through the membrane. This fact is pictured in Fig. 4.7 for three different feed pressures. A similar trend of results has been observed by Goosen et al. (2002).

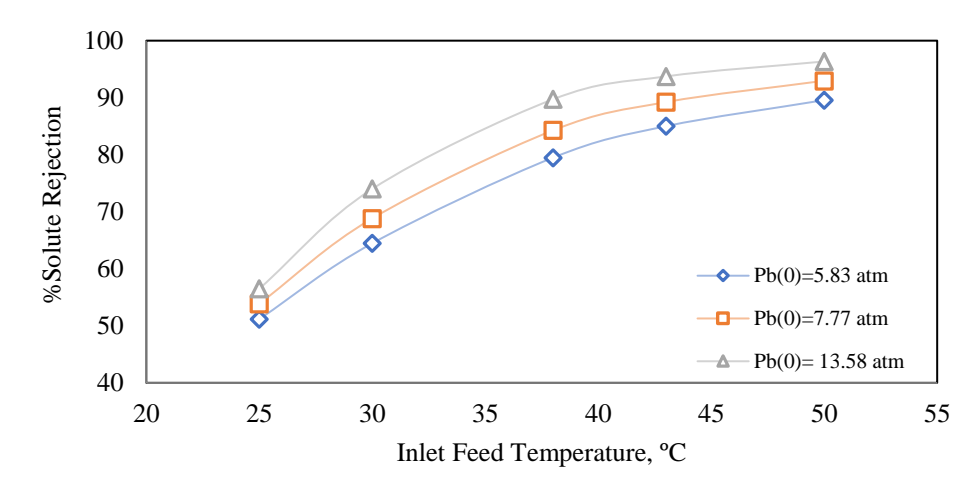


Fig. 4.7. Steady state solute rejection versus inlet feed temperatures of different inlet feed pressures (inlet feed conditions, 2.335x10⁻³ kmol/m³ and 2.166x10⁻⁴ m³/s)

4.2.1.4 Inlet feed concentration

Solute rejection increases due to an increase in inlet feed concentration and this may be due to an increase in the membrane solute isolation intensity. The membrane solute rejection intensity defined in Eq. (4.1) along the membrane channel shows this fact (Fig. 4.8).

%Solute Rejection Intensity =
$$\frac{C_{b(x)} - C_{p(x)}}{C_{b(x)}} \times 100$$
 (4.1)

The solute isolation intensity is at its maximum value at the beginning of the membrane and at its minimum at the end of the membrane. Likewise, the simulation results indicate a drop of wall membrane concentration along the membrane, which can reinforce this phenomenon. Another reason of this case can be stated by recognizing that increasing feed concentration in the feed channel is not comparable with the increase of permeate concentration at the permeate channel. Consequently, all these reasons may explain the effect of feed concentration on solute rejection (Fig. 4.9). The same findings are already confirmed by Avlonitis et al. (1993).

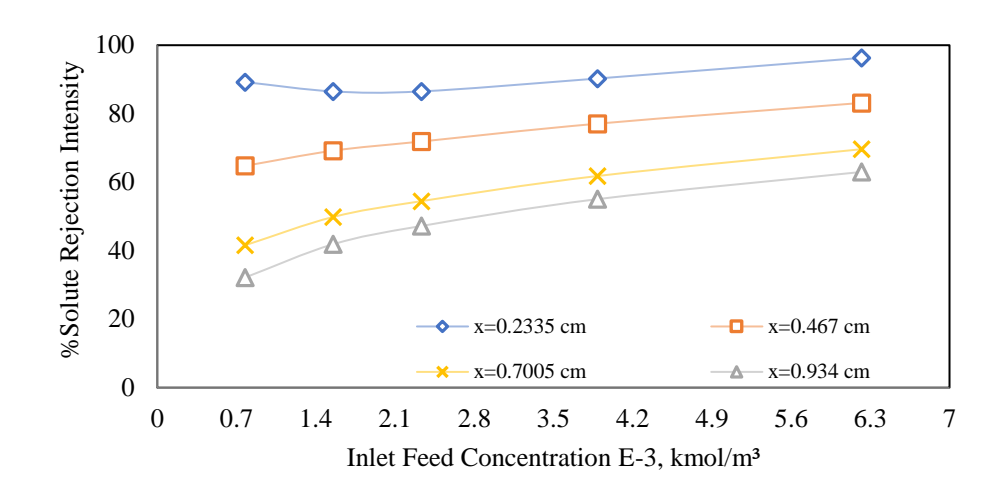


Fig. 4.8. Steady state membrane solute rejection intensity versus inlet feed concentrations of different points along the membrane length (inlet feed conditions, 2.166x10⁻⁴ m³/s, 11.64 atm, and 32 °C)

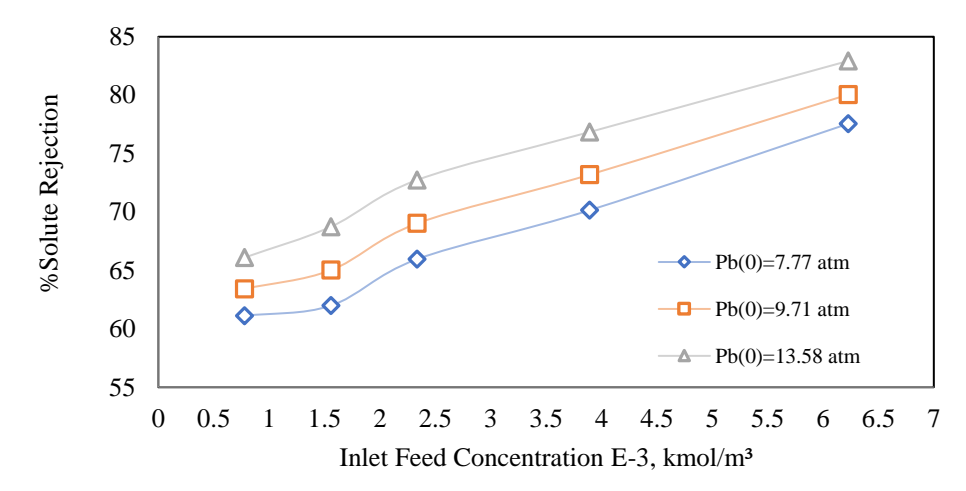


Fig. 4.9. Steady state solute rejection versus inlet feed concentrations of different inlet feed pressures (inlet feed conditions, 2.166x10⁻⁴ m³/s, and 31 °C)

For the convenience of the reader, Table 4.1 summarises the impact of operating parameters of the spiral wound RO process on the process performance indicators for the removal of phenolic compounds from wastewater.

Table 4.1. Summary of the impact of operating parameters on the performance of RO process

Operating	Permeate	Retentate	Permeate	Retentate	Solute	Recovery	Energy
parameters	conc.	conc.	flow rate	flow rate	rejection	rate	consumption
Pressure	1		1	1			1
Flow rate	1	1	1	1	1	1	1
Conc.	1		-	1	1	1	1
Temperature	1			1			₽

4.3 Case 2: Simulation and optimisation of a two-stage/two-pass spiral wound RO process

Sundaramoorthy et al. (2011b) confirmed that the maximum efficiency of eliminating chlorophenol from wastewater using an individual spiral wound RO process is around 83% at 22% water recovery and 2.034 kWh/m³ of energy consumption. Therefore, it seems that there is a necessity to investigate other RO network configurations in the hope that they will yield a higher chlorophenol removal from wastewater. The aim of this case is therefore to explore the efficiency of a hypothetical two-stage/two-pass RO design process for the removal of chlorophenol from wastewater considering model-based techniques. For this respect, Model Type_4 (described in Section 3.2.2.1 in Chapter 3) has been calibrated for use in the two-stage/two-pass multi-stage RO process for the removal of chlorophenol. Furthermore, the operational optimisation carried out is enhanced by constraining the total recovery rate to a realistic value by varying the system operating parameters according to the allowable limits of the process.

4.3.1 Description of the two stage/two pass RO process

Fig. 4.10 shows a schematic diagram of the proposed full-scale two-stage/twopass design RO process to treat wastewater containing chlorophenol. The multistage RO process contains seven pressure vessels connected in two stages, where each pressure vessel holds only one spiral wound module of a commercial thin film composite membrane element type (Ion Exchange, India). The membrane selected is identical to the one used by Sundaramoorthy et al. (2011b). Therefore, the membrane transport parameters of water $A_{\rm w}$ and chlorophenol B_s and membrane friction factor b are assumed to be the same as what investigated by Sundaramoorthy et al. (2011b) (Table 2.8 in Chapter 2). The specifications of the selected membrane are given in Table 2.1 in Chapter 2. The first stage comes with a series configuration of 3:2 pressure vessels where the wastewater is directly fed to the first section of three parallel pressure vessels and then the blended high concentration stream is forwarded to the second section of two parallel pressure vessels for further concentration. The combined low concentration permeate stream of the first stage is forwarded to stage 2 for further processing in two parallel pressure vessels. Specifically, there are two high-pressure pumps at the entrance of stages 1 and 2, while a booster pump is connected to compensate the pressure drop of first section of stage 1 to keep the

identical feed plant pressure at the second section of stage 1. The two pumps deliver a maximum of 20 atm, i.e. the same values used by Sundaramoorthy et al. (2011b). The augmentation of the two permeate streams of stage 1 has the advantage of keeping the product of stage 2 at low concentration. Also, the concentrated two streams of stages 1 and 2 are blended to form the outlet plant disposed stream.

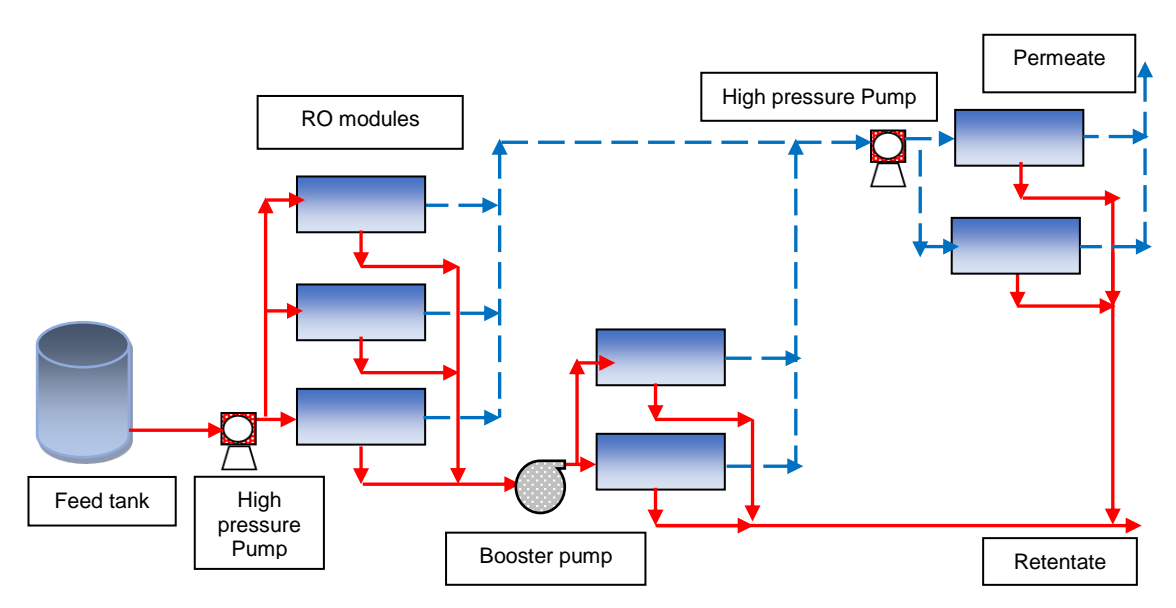


Fig. 4.10. Schematic diagram of the proposed two-stage/two-pass RO process

4.3.2 Simulation of the two Stage/two pass spiral wound RO process

A detailed simulation of the process is carried out to facilitate deeper insight of the impact of different operating conditions on the performance of the process. The simulation is carried out with chlorophenol concentration $C_{f(plant)}$ of 6.226×10^{-3} kmol/m³, which is equivalent to 800.66 ppm. Four cases were studied with different operating conditions of the plant feed flow rate $Q_{f(plant)}$, pressure $P_{f(plant)}$ and temperature $T_{(plant)}$ as shown below:

- 1.50x10⁻³ m³/s, 18 atm and 33 °C
- 7.749x10⁻⁴ m³/s, 15 atm and 32 °C
- 6.498x10⁻⁴ m³/s, 13 atm and 31 °C
- 5.40x10⁻⁴ m³/s, 12 atm and 30 °C

These operating conditions are within the upper and lower limits of the manufacturer's membrane specification (given in Table 2.2 in Chapter 2 for each membrane module) to ensure the safe working of the process. Note, the simulation is carried out within temperature range of 30 to 33° C as considered

by Sundaramoorthy et al. (2011b), although the maximum allowed temperature is 40 °C. This is due to the fact that the temperature has significant impact on the model transport parameters (A_w and B_s) at higher temperatures (say 40 °C).

The simulation results of this process are given in Table 4.2. This shows a noticeable increase in chlorophenol rejection despite low recovery rate and variable energy consumption. The low recovery rate can be attributed to the use of arbitrary values (non-optimised values) of feed flow rate, pressure, and temperature. Table 4.2 shows that the simultaneous reduction of the operating feed flow rate can support the water recovery rate despite lower product flow rate and rejection parameter. This can be attributed to increased rate of concentration polarisation as a result to the increase of the residence time of the fluid inside the module, which occurred due to reduced operating feed flow rate. The net effect of this is a reduction of the permeate flow rate and an increase in the quantity of chlorophenol penetrating the membrane, which finally retards the rejection parameter (Table 4.2). The same results of Table 4.2 essentially highlight the advantages of the proposed configuration for the removal of chlorophenol. The next section will deal with the process optimisation to achieve a higher rejection, while maintaining higher recovery but with an acceptable energy consumption.

Table 4.2. Simulation results at initial chlorophenol concentration of 6.226E-3 kmol/m³

Simulation case	Total permeate concentration, kmol/m³	Product flow rate, m³/s	Total retentate concentration, kmol/m³	Retentate flow rate, m³/s	%Rejection	%Recovery rate	Energy consumption, kWh/m³
1	2.154x10 ⁻⁴	2.326x10 ⁻⁴	7.329E-3	1.267x10 ⁻³	96.539	15.512	5.712
2	3.389x10 ⁻⁴	1.798x10 ⁻⁴	8.005E-3	5.950x10 ⁻⁴	94.556	23.208	3.349
3	4.508x10 ⁻⁴	1.454x10 ⁻⁴	7.890E-3	5.043x10 ⁻⁴	92.759	22.376	2.970
4	5.865x10 ⁻⁴	1.248x10 ⁻⁴	7.922E-3	4.151x10 ⁻⁴	90.578	23.125	2.658

4.3.3 Optimisation of the two-stage/two-pass spiral wound RO process

The optimisation methodology is based on maximising the chlorophenol rejection $Rej_{(Total)}$ (objective function) within the manufacturer's specification of membrane module (shown in Table 2.2 in Chapter 2). This includes the upper and lower limits of plant flow rate $Q_{f(plant)}$ and pressure drop per each module. However, the range of 30 to 33 °C and 5 atm to 20 atm as the operating temperature $T_{(plant)}$ and plant feed pressure $P_{f(plant)}$, respectively were selected to be within the

transport parameters investigated and in line with the capacity of the pump used in the experimental work of Sundaramoorthy et al. (2011b). Also, the optimisation considers the number of pressure vessels at the first section of stage 1 as well as the promising total water recovery of 40% at maximum chlorophenol rejection. A restricted constrain range of 1 to 2 kWh/m³ of total energy consumption $E_{(Total)}$ is held to secure the required low total energy consumption compared with the simulation results of Table 4.2. Finally, the overall pressure drop per each membrane module ΔP_{drop} is restricted at a maximum value of equal or less than the allowed value of 1.38 atm (membrane specification).

The optimisation problem can be mathematically written as follows:

$$\begin{aligned} & \text{Max} & \text{Rej}_{(Total)} \\ & Q_{f(plant)} \text{ , } P_{f(plant)} \text{ , } T_{(plant)} \end{aligned}$$

Subject to: Equality constraints:

Process Model:
$$f(x,\,u,\,v)=0$$
 Inequality constraints of the plant: 5 atm $P_{f(plant)}^{\ \ \ \ \ } \leq P_{f(plant)}^{\ \ \ \ \ \ } \leq P_{f(plant)}^{\ \ \ \ \ \ } = 0$ atm
$$3.0x10^{-4} \text{ m}^3\text{/s} \qquad Q_{f(plant)}^{\ \ \ \ \ } \leq Q_{f(plant)} \leq Q_{f(plant)}^{\ \ \ \ \ \ \ } \leq Q_{f(plant)}^{\ \ \ \ \ \ \ } = 0$$
 3.0x10⁻³ m³/s
$$30 \text{ °C} \qquad T_{(plant)}^{\ \ \ \ \ \ \ \ } \leq T_{(plant)} \leq T_{(plant)}^{\ \ \ \ \ \ \ \ \ \ \ } = 0$$

1 kWh/m³
$$\leq E_{\text{(Total)}} \leq 2 \text{ kWh/m}^3$$

 $Rec \geq 40\%$

Inequality constraints of the element:

Optimisation results

The optimisation results of chlorophenol rejection, total water recovery and total energy consumption in addition to the optimised operating parameters of feed pressure, feed flow rate and operating temperature of three optimisation cases are given in Table 4.3. The results of case 1 confirm the ability of the proposed configuration to elevate the chlorophenol experimental rejection of Sundaramoorthy et al. (2011b) by about 12.4% (from 83% to 93.325%) with 81% increase in total water recovery (from 22% to 40%), with a reduction in total

energy consumption of about 4% (from 2.034 to 1.95 kWh/m³). Generally, the optimised parameter values have a positive impact on the total energy consumption compared to simulation results shown in Table 4.2. The allowed constraint of total energy consumption is increased to the range of 2 to 3 kWh/m³ in cases 2 and 3 to investigate the process performance at higher energy consumption. Table 4.3 shows that highest energy consumption of 2.50 and 2.874 kWh/m³ required the use of higher pressure compared to case 1 that commensurate with insignificant increase of chlorophenol rejection. Therefore, case 1 yields the best optimisation results.

Table 4.3. Optimisation results at inlet chlorophenol concentration of 6.226x10⁻³ kmol/m³

	Th	ne operating con	nditions	The optimised parameters			
Case	$\begin{array}{c} \text{Pressure} \\ \text{, } P_{f(plant)} \\ \text{atm} \end{array}$	Flow rate, Q _{f(plant)} x10 ⁴ m ³ /s	$\begin{array}{c} \text{Temperature,} \\ \text{T}_{b(plant)} \ ^{\circ}\text{C} \end{array}$	%Rejection , Rej _(Total)	%Recovery , Rec _(Total)	Energy consumption, E _(Total) kWh/m³	
1	13.245	3.890	33.0	93.325	40.001	1.949	
2	16.860	5.176	33.0	94.487	40.000	2.500	
3	19.307	6.049	33.0	95.019	40.000	2.874	

4.4 Conclusions

This chapter elucidates the sensitivity analysis of the spiral wound RO process performance towards the variation of operating parameters. It is concluded that increasing applied pressure would increase the water flux through the membrane. Also, it is usual expectation that increasing inlet feed concentration would increase the diffusivity, density, and viscosity parameters, which reduces the flux of water. However, this would also increase the concentration polarisation impact that causes an increase in wall membrane concentration and increases of osmotic pressure. Moreover, increasing inlet feed temperature will decrease the viscosity and density parameters and increases the diffusivity parameter that increases the mass transfer coefficient and lifts up the water flux. Moreover, it is concluded that increasing feed flow rate has little effect on the total water flux at any pressure. Also, the membrane isolation intensity increases with increasing applied concentration. Accordingly, one of the main aims of this chapter is to improve the total product chlorophenol concentration due to increasing strict constraints of the existence of such undesirable compounds in wastewater that affect the whole living organism. Therefore, the design of two-stage/two-pass RO

configuration has been tested for the removal of chlorophenol from wastewater. A mathematical model-based simulation and optimisation methodology has been successfully applied to validate the higher performance of the proposed configuration of multi-stage RO process. The simulation results indicate a noticeably higher rejection of chlorophenol as one of the high toxic compounds found in water. The requirements of reducing the total energy consumption and at the same time elevating the rejection parameter has been achieved using an optimisation study manipulating the process parameters within allowed operational limits. A maximum of 93.3% chlorophenol rejection has been obtained for the proposed configuration. The results also show that a significantly higher recovery rate of 40% at a lower energy consumption of 1.949 kWh/m³ is possible to the proposed RO network. The optimisation results shown above confirm the necessity of two stage/two pass RO network for the possibility of high removal of chlorophenol from water with an acceptable levels of water recovery and energy consumption despite the fact that chlorophenol has high hydrophobicity properties in water (slightly dissolved in water) (20 g/L at 20 °C).

Chapter 5

Removal of Dimethylphenol from Wastewater: Dynamic Simulation

5.1 Introduction

Dimethylphenol (C₈H₁₀O) (122.167 g/mol, water solubility: 10 g/L at 20 °C) is a very toxic pollutant found in wastewater of several industrial applications. Therefore, the removal of this compound from industrial effluents is critical for the safe discharge into surface water. This chapter focuses on presenting the dynamic simulation of the spiral wound RO process for the removal of dimethylphenol from wastewater. A number of operating parameters must be controlled within the process constraints to achieve an efficient removal of pollutants from wastewater. Understanding the process dynamics is absolutely essential and is a pre-step for designing any effective controllers. To aid future development of controllers for such process, this case therefore focuses on the use of distributed two-dimensional dynamic (x and y dimensions and time) of Model Type_2 presented in Chapter 3. The model is used to capture the dynamics of the RO process for the removal of dimethylphenol from wastewater and therefore to simulate the separation mechanism of dimethylphenol aqueous solutions using a spiral wound membrane module in the RO process. The performance of the 2D model is more accurate than 1D dynamic as described in Section 3.2.1.3 in Chapter 3. Therefore, the model is used to study the dynamic behavior and the sensitivity of the unit performance to a variety of operating parameters.

5.2 Dynamic simulation

One characteristic of any industrial process is the possibility of sudden and sustained step change in input parameters, which causes a corresponding change in the process performance. This section deals with the using of the dynamic version of Model Type_2 (described in Section 3.2.1.2 in Chapter 3) to reproduce the process and analyse the sensitivity of the RO performance process under various operating parameters. The dynamic model is simulated by using changing several parameters (one at a time). The effects of processing parameters on the RO module performance are labelled in the following sections.

5.2.1 The inlet feed pressure

The impact of a step change for the operating pressures on the average retentate concentration, average permeate concentration and solute rejection for various inlet feed concentrations at fixed temperature and inlet feed flow rate are shown in Figs. 5.1 to 5.3. Figs. A.1 and A.2 in Appendix A represent the case of water recovery, and average retentate flow rate, respectively.

Up to t = 600 s, the inlet feed pressure was 9.71 atm and at t = 600 s, the operating pressure is increased by 40% to 13.58 atm.

It is clearly noted that increasing the inlet feed pressure actually raises the average retentate concentration Fig. 5.1, decreases the average permeate concentration (Fig. 5.2), increases the solute rejection Fig. 5.3, increases the total water recovery (Fig. A.1 in Appendix A) and decreases the retentate flow rate (Fig. A.2 in Appendix A) for all the tested inlet feed concentrations. This phenomenon could be described as an increase of the water flux traveling through the membrane because of a rise of the inlet feed pressure. Since the domino effect, the increase of the pressure results in a higher permeate flux due to a reduction of concentration polarisation impact, which in turn causes a rise of the retentate concentration and a reduction of the permeate concentration due to a high level of dilution. Consequently, the solute rejection is improved due to an improvement of the water flux. Also, the quantity of permeated water increases and causes higher levels of water recovery. Therefore, the retentate flow rate decreases due to an increase in the operating pressure.

Figs. 5.1 and 5.2 show that the impact of a step change in the operating pressure is slightly more visible at higher concentration solution than the lower ones. This is mainly because of the concentration polarisation in higher concentration solutions is larger than the lower concentrations. Thus, any increase in the feed pressure will have a significant influence on the concentration polarisation and solute concentration both in the feed and permeate channels compared to other solutions of lower solute concentration. Consequently, this will lead to a higher overshoot in the retentate concentration (Fig. 5.1) and a lower overshoot in the mean permeate concentration (shown as in Fig. 5.2) in response to an increase in the inlet feed pressure. Fig. 5.2 shows that the average permeate concentration has shown a unique underdamped response, where it exhibits no overshoots before getting a steady state condition. This is quite interesting when compared to other tested operating parameters where it shows slight and sharp overshoots.

This is quite reasonable due to recognizing that the step change of pressure is directly subjected to the feed channel, where the feed flow rate and retentate concentrations are directly affected compared to the permeate concentration at the permeate channel. Therefore, there is no sharp response with overshoot at the permeate concentration.

Fig. 5.3 shows the influence of the solute rejection progresses with an increase of the inlet feed concentration and this was attributed to a rise of the membrane solute isolation strength. Another reason is that rising the inlet feed concentration causes an increase in the osmotic pressure and the permeate concentration. However, the increase of permeate concentration is insignificant with the increase of bulk concentration in the feed channel, which itself results in an increase in the solute rejection commensurate with Eq. (M.2.12) in Chapter 2. A similar trend of results was confirmed for all the three types of membranes tested by Gómez et al. (2009). However, the solute rejection is mainly dependent on both the retentate concentration and permeate concentration, which relatively showed a response with overshoot (Fig. 5.3).

Fig. A.1 in Appendix A shows that the total water recovery decreases with an increase of the inlet feed concentration. It can be ascribed as a rise of the osmotic pressure, which declines the motivation of water flux and hence diminishes the quantity of permeated water in the permeate channel. For the same reason, the retentate flow rate increases because of an increase of the operating concentration (Fig. A.2 in Appendix A).

Fig. 5.2 shows that the setting time for an average permeate concentration at the permeate channel for the higher inlet feed concentration is a bit longer compared with the lower feed concentration. This is mainly because a higher solute concentration medium requires more time to settle than the lower ones (for a given volume) and vice versa. Also, Fig. 5.3 readily confirms a number of key observations:

- that the steady state solute rejection was reached between 200 and 250 s
 for the tested inlet feed concentrations, albeit with a little bit of a difference.
- that the solute rejection transient response of the lower feed concentration
 to feed pressure is irrelevant compare with a higher feed concentration.
 This is owing to a higher water flux occurring when using a lower feed
 concentration medium compared to a higher feed concentration medium
 with the impact of concentration polarisation.

that the solute rejection begins at t = 0 at its maximum because there is
no concentration polarisation in that time. Basically, the solute rejection is
gradually retarded as the solute starts to be retained along the membrane
wall until settled at a constant value.

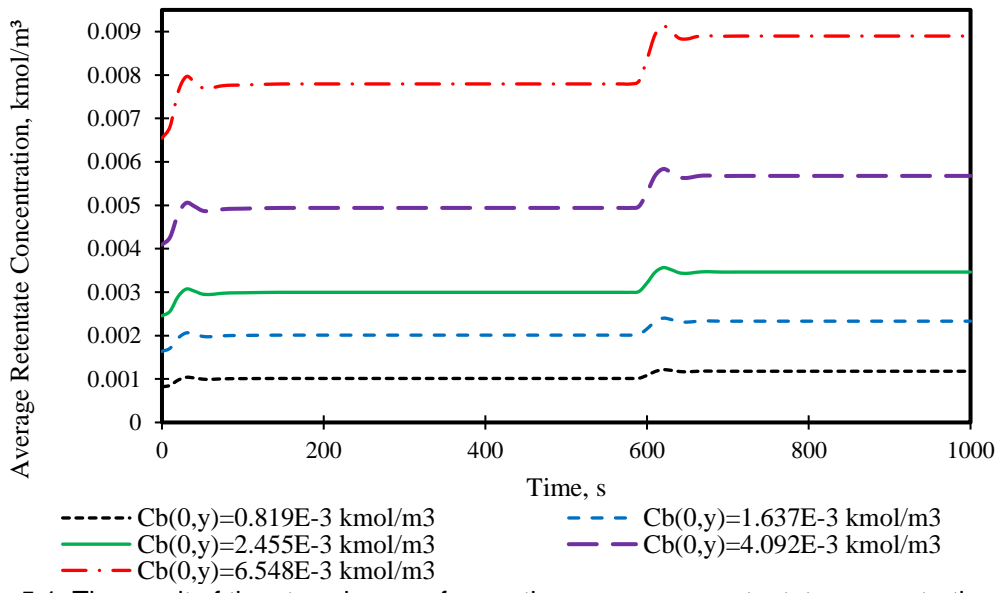


Fig. 5.1. The result of the step change of operating pressure on retentate concentration for several operating concentrations at operating conditions of 2.583x10⁻⁴ m³/s, and 31.5 °C

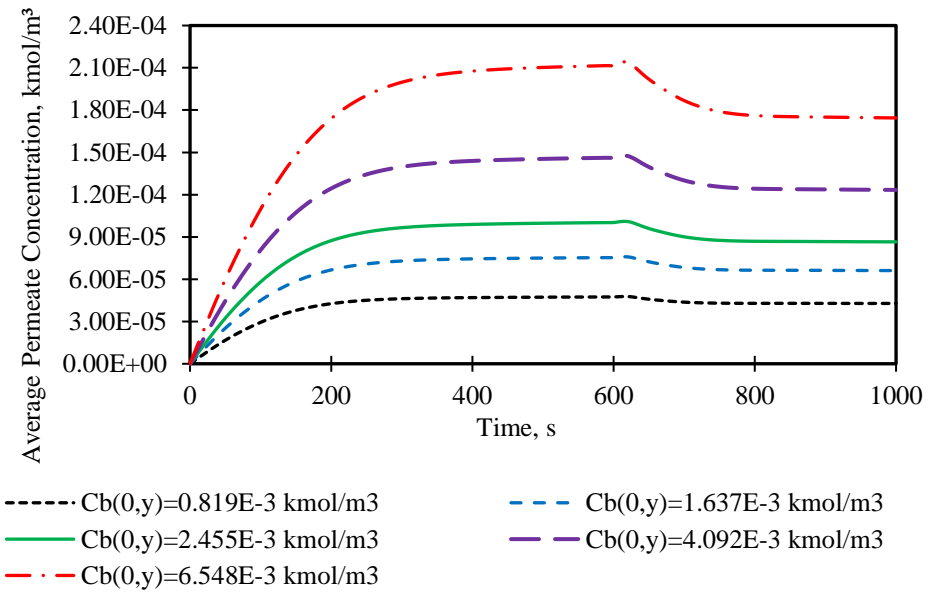


Fig. 5.2. The result of the step change of operating pressure on mean permeate concentration for several operating concentrations at operating conditions of 2.583x10⁻⁴ m³/s, and 31.5 °C

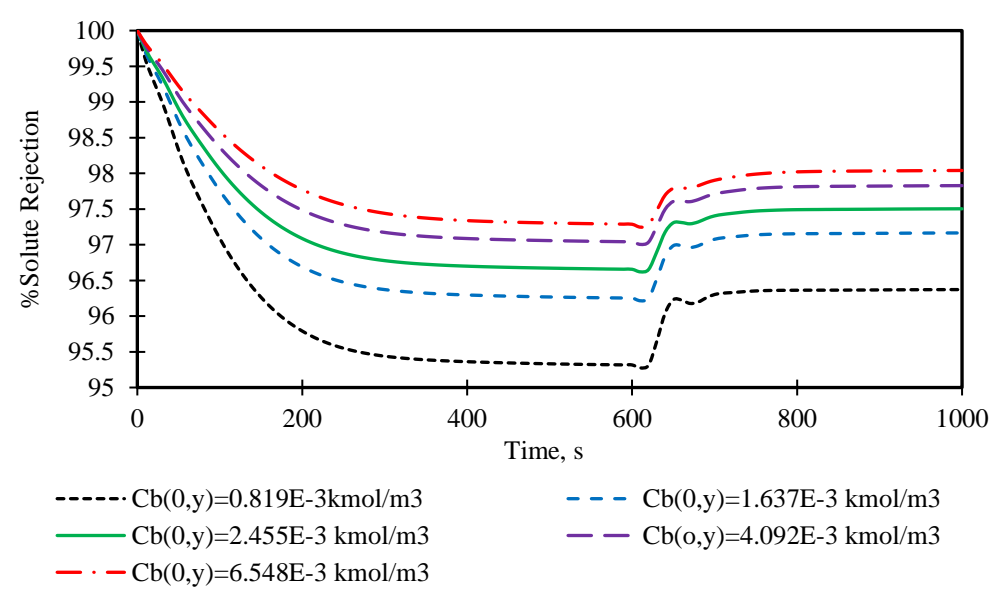


Fig. 5.3. The result of the step change of operating pressure on solute rejection for several operating concentrations at operating conditions of 2.583x10⁻⁴ m³/s, and 31.5 °C

Moreover, it is possible that any industrial process may be subjected to a multiple change of operating conditions, which is basically carried out in a gradual upward or downward change for a period of time with constant slop. Fig. 5.4 shows the impact of a multiple change in the operating pressure on the solute rejection at fixed operating concentration, flow rate, and temperature. Up to $t = 600 \, \text{s}$, the inlet feed pressure was 10 atm and is increased to 12, 14 and 16 atm at 600, 900 and 1200 s, respectively.

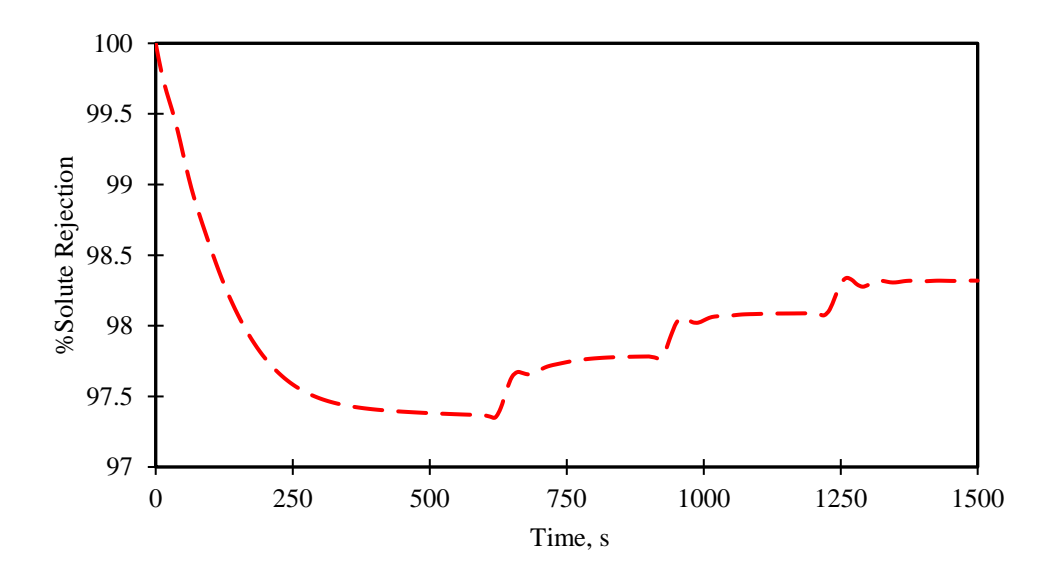


Fig. 5.4. The result of the multiple change of operating pressure on solute rejection for operating conditions of 6.548x10⁻³ kmol/m³, 2.166x10⁻⁴ m³/s, and 31.5 °C

As it is expected, the progress of operating pressure at fixed other operating parameters causes an increase in the solute rejection. Also, it can be noticed that

the multiple change of 2 atm increase has relatively different settling time, where the process can quickly be settled at higher pressures. This can be attributed to increasing the permeated water as a response to increasing the operating pressure that reduces the settling time of permeate concentration (Fig. 5.5).

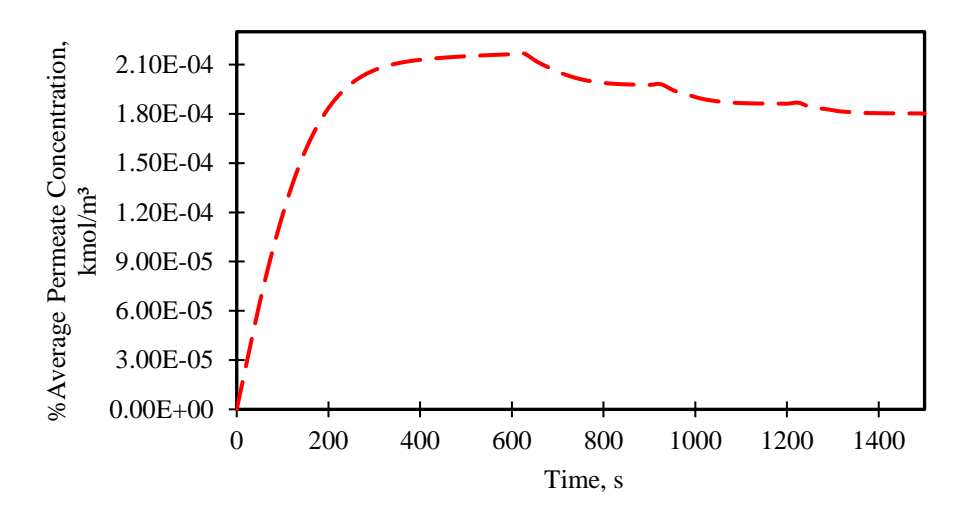


Fig. 5.5. The result of the multiple change of operating pressure on average permeate concentration for operating conditions of 6.548x10⁻³ kmol/m³, 2.166x10⁻⁴ m³/s, and 31.5 °C

5.2.2 The inlet feed flow rate

The relation of the step change of the operating feed flow rate and the average retentate concentration, rejection and average permeate concentration for several operating pressures under constant operating concentration and temperature are depicted in Figs. 5.6 to 5.8. Up to t=1000~s the operating feed flow rate is $2.33\times10^{-4}~m^3/s$, while at t=1000~s, the operating feed flow rate is increased to $2.583\times10^{-4}~m^3/s$. The system has settled within 200-250~s during the step change of the feed flow rate. Interestingly, this is quite similar to the case of a step change of inlet feed pressure. Increasing the feed flow rate causes a reduction in the concentration polarisation along the membrane, which leads to the increase of mass transfer coefficient and the reduce of the solute concentration at the feed channel and average permeate concentration at the permeate channel.

Fig. 5.6 shows that the retentate concentration endures a quick increase tracked by an instant high-pitched reduction before reaching a new fixed state after about 150 s as a reply to a step change in the inlet feed flow rate. The retentate concentration seems to decrease more when using higher pressure conditions. Moreover, it is not difficult to see that the transient response of the average

permeate concentration (Fig. 5.7) is much slower than the response of the retentate concentration for the same step change in the operating feed flow rate (Fig. 5.6). Fig. 5.6 shows that the transient effects of the retentate concentration at higher pressure conditions on step change in the feed flow rate is larger than the lower feed pressure conditions. In other words, a higher degree of oscillation and overshoot (inverse response) is exhibited at higher operating pressure as a response to the step change of operating flow rate, while a lower operating pressure has yielded a slower response. This is because of the combined and concurrent impact of the higher inlet feed flow rate and a higher applied pressure. Both of these factors are working together to reduce the solute concentration along the feed channel. This is compared to the use a lower feed pressure and a higher feed flow rate conditions. Therefore, it can be said that the average retentate concentration response will be faster and without overshoot in case of using very low operating pressures.

Fig. 5.6 shows an inverse response of the retentate concentration, where it firstly shows an increase followed by a significant decrease. The first increase is due to increasing the feed flow rate, which is commensurate with a higher velocity that reduces the residence time of the fluid inside the medium and raises the average retentate concentration. However, the rate of concentration polarisation is reduced with the operation time, which is related to increasing the mass transfer coefficient that readily reduces the bulk concentration inside the module.

Fig. 5.7 readily confirms that using high inlet feed pressures results in markedly noticeable reduction in the average permeate concentration than using low inlet feed pressure conditions. This might be attributed to an increase in the water flux caused by the high inlet feed pressure. Interestingly, Fig. 5.7 confirms that the average permeate concentration is inversely and slightly increased at low operating feed pressures compared to other feed pressures. This phenomenon can be attributed to the use of low operating pressure (lower water flux) in addition to an increase in the frictional pressure drop caused by increasing the operating feed flow rate. This decreases the advantage of osmotic pressure drop, which lastly reduces the extent of water flux and rises the concentration of permeate side. Thus, the rejection parameter decreases evidenced in Fig. 5.8. The use of high inlet feed flow rate and high inlet pressure causes a decrease in the average permeate concentration (Fig. 5.7) and an increase in the solute rejection (Fig. 5.8).

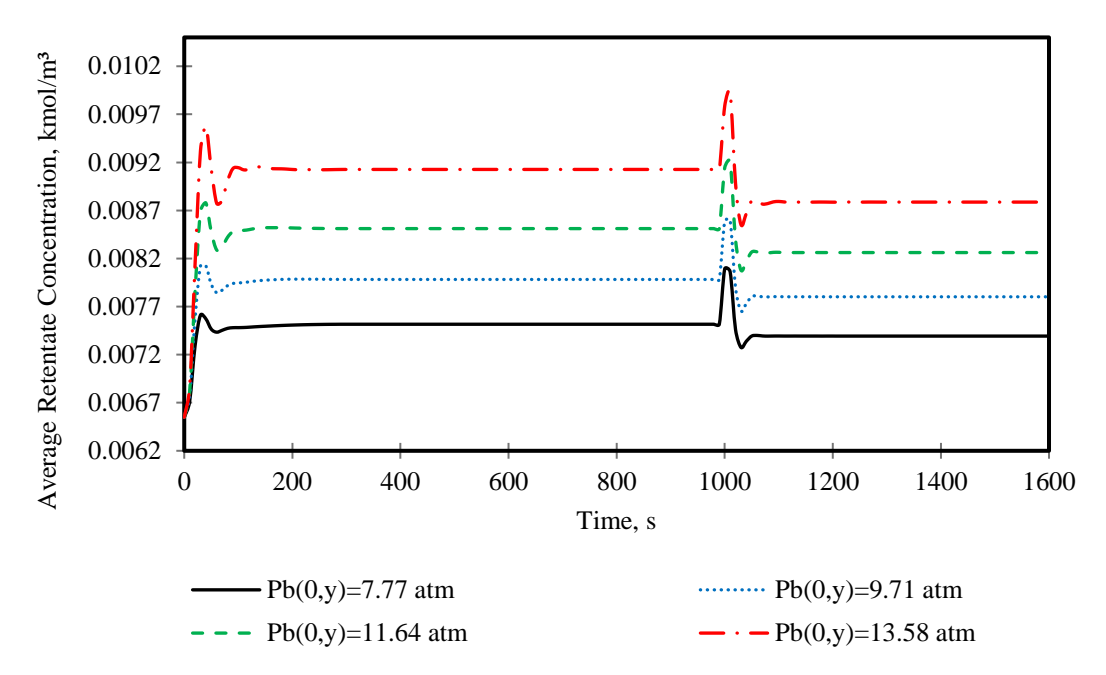


Fig. 5.6. The influence of the step change of operating feed flow rate on retentate concentration for several operating pressures at operating conditions of 6.548x10⁻³ kmol/m³, and 31.5 °C

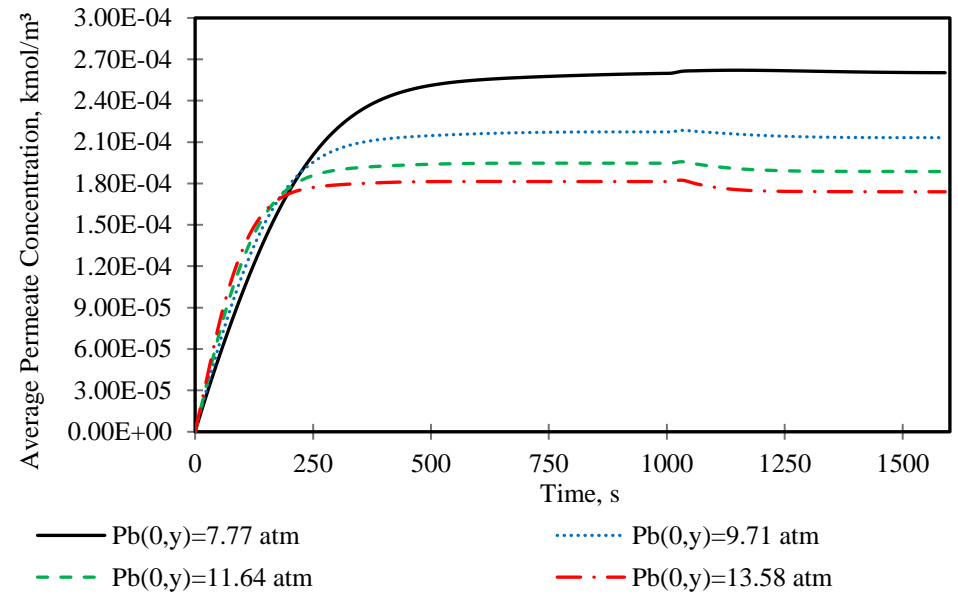


Fig. 5.7. The influence of the step change of operating feed flow rate on average permeate concentration for several operating pressures at operating conditions of 6.548x10⁻³ kmol/m³, and 31.5 °C

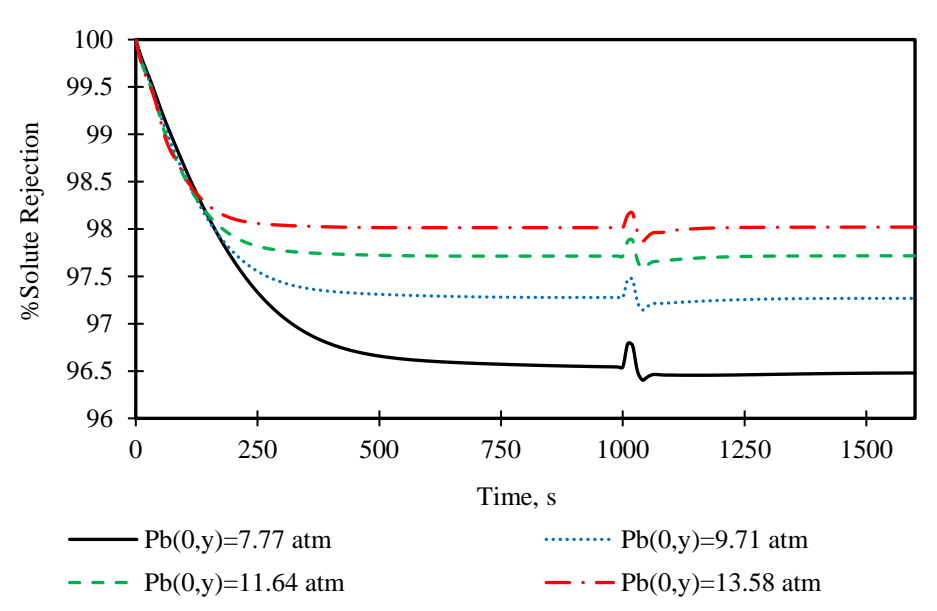


Fig. 5.8. The influence of the step change of operating feed flow rate on rejection parameter for several operating pressures at operating conditions of 6.548x10⁻³ kmol/m³, and 31.5 °C

Figs. 5.9, 5.10 and 5.11 show the response of the process for a multiple change of upward increase in the operating flow rate at constant other parameters, which is basically carried out for a period of time with different slops. Up to t = 500 s, the inlet feed flow rate was $2.166 \times 10^{-4} \text{ m}^3/\text{s}$ and is increased to $4 \times 10^{-4} \text{ m}^3/\text{s}$ and $7 \times 10^{-4} \text{ m}^3/\text{s}$ at 500 and 1000 s, respectively. In this respect, Fig. 5.9 is intentionally drawn with different time axes than in Figs. 5.10 and 5.11 to show the impact of the step change in a clearer way on the specific parameters.

Fig. 5.9 shows that a considerable overshoot followed by an inverse response occurs after increasing the operating flow rate by about 84% from 2.166x10⁻⁴ m³/s to 4x10⁻⁴ m³/s. However, the second change has shown a low degree of response after increasing the operating flow rate by 75% from 4x10⁻⁴ m³/s to 7x10⁻⁴ m³/s. This behaviour can be explained by increasing the rate of disturbance instantaneously, which observed a longer shoot response. However, increasing the feed flow rate at recent high feed flow rate is commensurate with a lower rate of disturbance that reflects a lower shoot response.

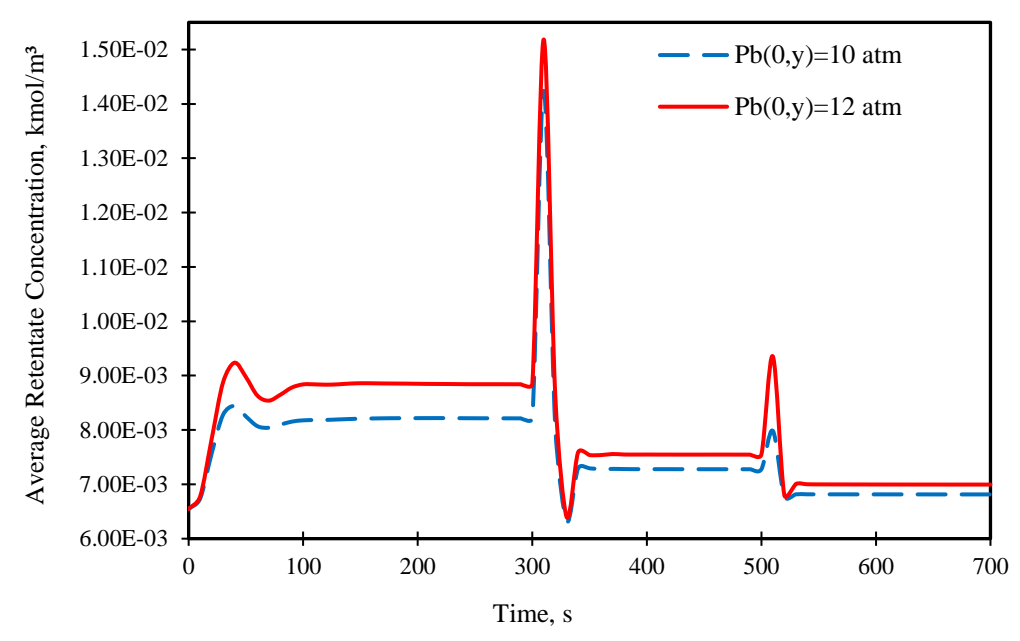


Fig. 5.9. The result of the multiple change of feed flow rate on retentate concentration for operating conditions of 6.548x10⁻³ kmol/m³, 10 atm, and 31.5 °C

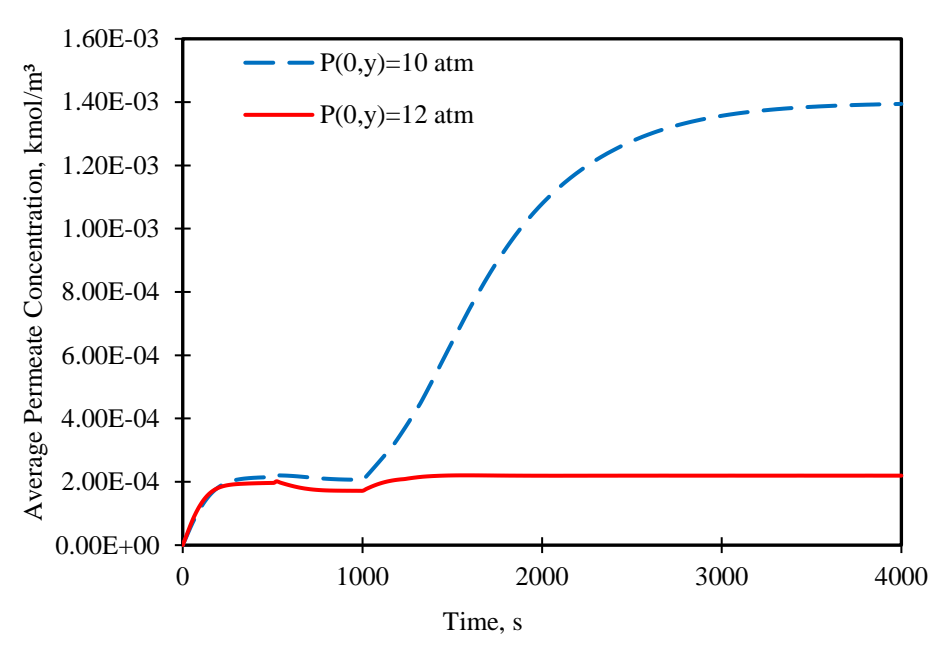


Fig. 5.10. The result of the multiple change of feed flow rate on average permeate concentration for operating conditions of 6.548x10⁻³ kmol/m³, 10 atm, and 31.5 °C

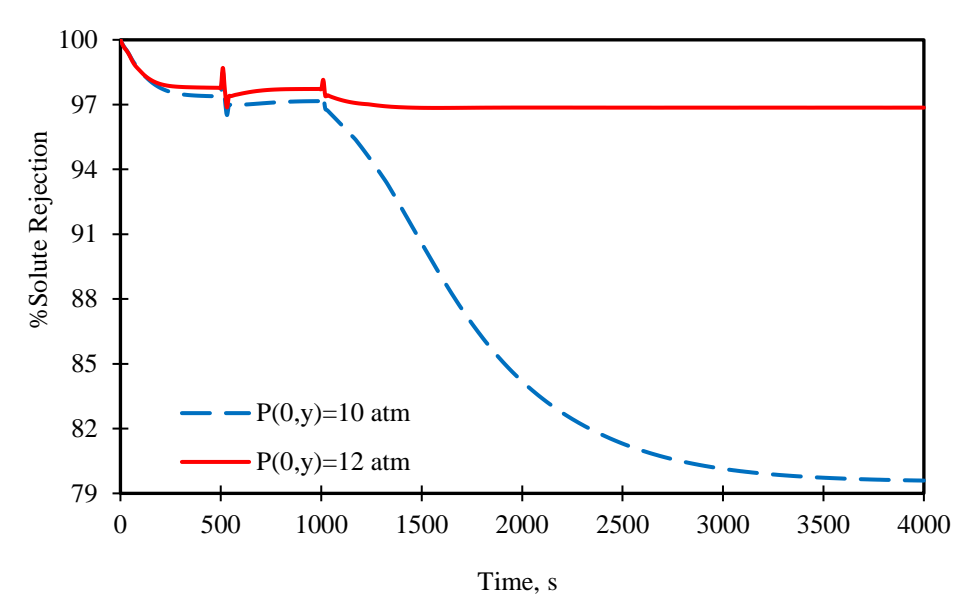


Fig. 5.11. The result of the multiple change of feed flow rate on solute rejection for operating conditions of 6.548x10⁻³ kmol/m³, 10 atm, and 31.5 °C

Fig. 5.9 confirms that increasing the operating pressure can raise the retentate concentration due to increasing the level of water penetration. Interestingly, Figs. 5.10 and 5.11 show that the process requires a longer time to be settled after imposing the second change to access the higher feed flow rate of $7x10^{-4}$ m³/s at medium operating pressure of 10 atm. This is clear in the response of both the average permeate concentration and solute rejection compared to the response of operating pressure of 12 atm. Also, the process shows a remarkable decrease in the solute rejection at operating pressure of 10 atm compared with a slight change at 12 atm. It is expected that the concurrence of high feed flow rate and medium pressure is the main reason of this fluctuation, where the 10 atm was not able to retrieve the deterioration of solute rejection caused at high feed flow rate. However, it seems that the operating pressure of 12 atm has improved the solute rejection albeit keeping the rejection at approximately constant value.

5.2.3 The inlet feed concentration

The impact of the step change of the operating concentration on the average retentate concentration, average permeate concentration and rejection parameter under several operating pressures with constant operating feed flow rate and temperature can be shown in Figs. 5.12 to 5.14. Up to t = 1000 s, the inlet feed concentration is 0.819×10^{-3} kmol/m³ and at t = 1000 s, the inlet feed concentration is increased to 6.548×10^{-3} kmol/m³.

As expected, the increase of the inlet feed concentration raises the average retentate concentration, which results in a higher osmotic pressure and permeate concentration and lower water flux.

Interestingly, the system spends more time to achieve its steady state in comparison to a step change in the inlet feed pressure and feed flow rate. This might be qualified to the growth in the degree of instability throughout the step change of the inlet feed concentration. Similarly, the system with lower feed pressure conditions needs more time to settle in comparison to higher inlet feed pressure conditions (Figs. 5.13 and 5.14). This is due to a lower water flux occurring inside the permeate channel when using lower feed pressures, which needs more time to get a constant value of solute concentration at the permeate channel in comparison to higher feed pressures. Higher feed pressure is convoyed to more permeation, which enables a steady average permeate concentration faster than applying low inlet feed pressure conditions. Indeed, Fig. 5.14 shows that the solute rejection growths because of an increase in the operating concentration as a result to a growth of the strength of membrane rejection.

Fig. 5.14 shows a strong overshoot of the relation of the rejection parameter for a step change in the operating concentration. It is probable that this is a consequence of the influence of the solute concentration on the feed side (Fig. 5.12). Fig. 5.14 shows that operating at high pressures yields better solute rejection with lower salt concentration of the permeate in comparison to that by lower pressures. This is because of a reduction in the water flux due to a reduction in the operating pressure, which hinders the rejection parameter.

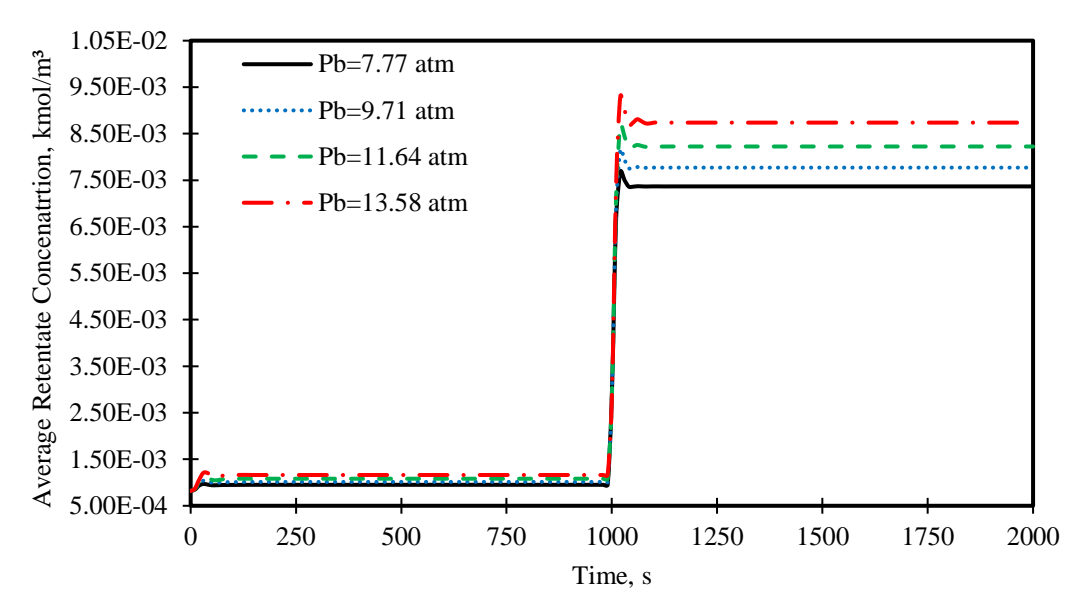


Fig. 5.12. The result of the step change of operating concentration on retentate concentration for several operating pressures at operating conditions of 2.583x10⁻⁴ m³/s, and 31.5 °C

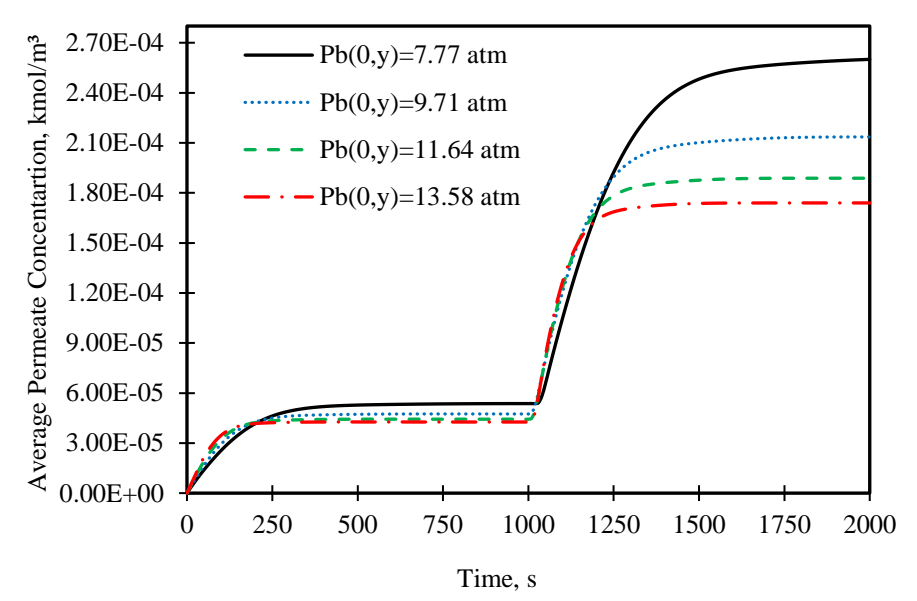


Fig. 5.13. The result of the step change of operating concentration on average permeate concentration for several operating pressures at operating conditions of 2.583×10^{-4} m³/s, and 31.5 °C

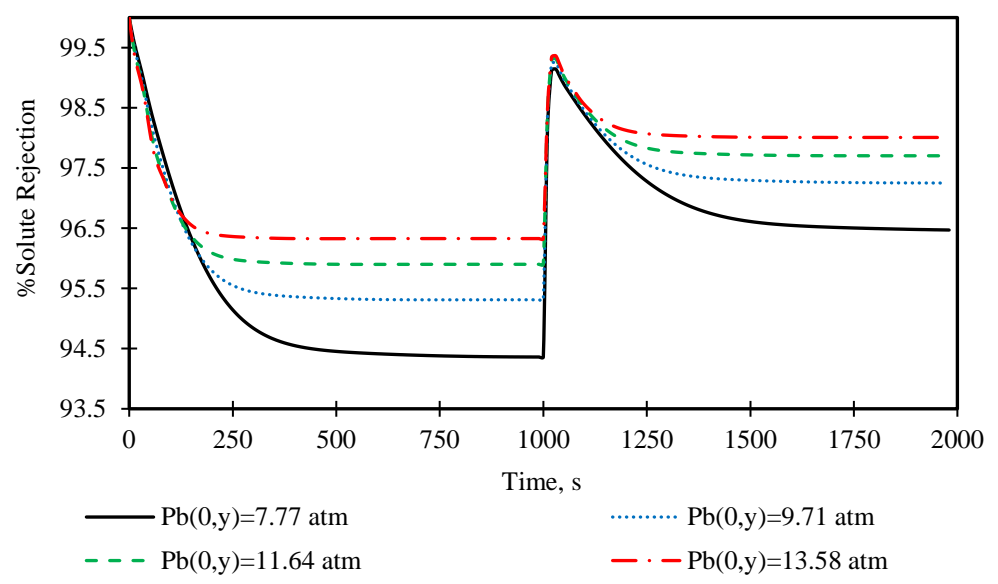


Fig. 5.14. The result of the step change of operating concentration on rejection parameter for several operating pressures at operating conditions of 2.583x10⁻⁴ m³/s, and 31.5 °C

5.2.4 The inlet feed temperature

Figs. 5.15 to 5.17 show the response of the step change of the operating temperature on the average retentate concentration, average permeate concentration and rejection for several operating pressures with constant operating feed flow rate and concentration. Up to t = 1000 s the inlet feed temperature was 31.5 °C and at t = 1000 s, the operating temperature is increased to 40 °C.

Interestingly, the process requires a longer time to settle after imposing a step change in the operating temperature. Obviously, increasing the operating temperature will lead to decrease the viscosity and density parameters, which reduces the concentration polarisation impact and causes an increase in the passage of water. That in turn leads to an increase of the retenate concentration (Fig. 5.15) and a reduction of the average permeate concentration (Fig. 5.16). In addition, increasing operating pressure will increase the average retentate concentration and reduces the average permeate concentration. Thus, the solute rejection rises because of an increase in the temperature (Fig. 5.17).

It is not complicated to see that the average retentate concentration, average permeate concentration and the solute rejection are exhibiting underdamped responses whithout clear overshoots before getting its steady state as a response to step change of operating temperature and compared with the previous tested cases. However, the same behaviour has been solely noticed for average

permeate concentration after imposing the step change of pressure, concentration and flow rate. This can be explained by the lower disturbance that can ocur after supplying a step change of temperature from 31.5 °C to 40 °C, compared with a higher degree of disturbance that is expected to occur at other step changes of operating parameters.

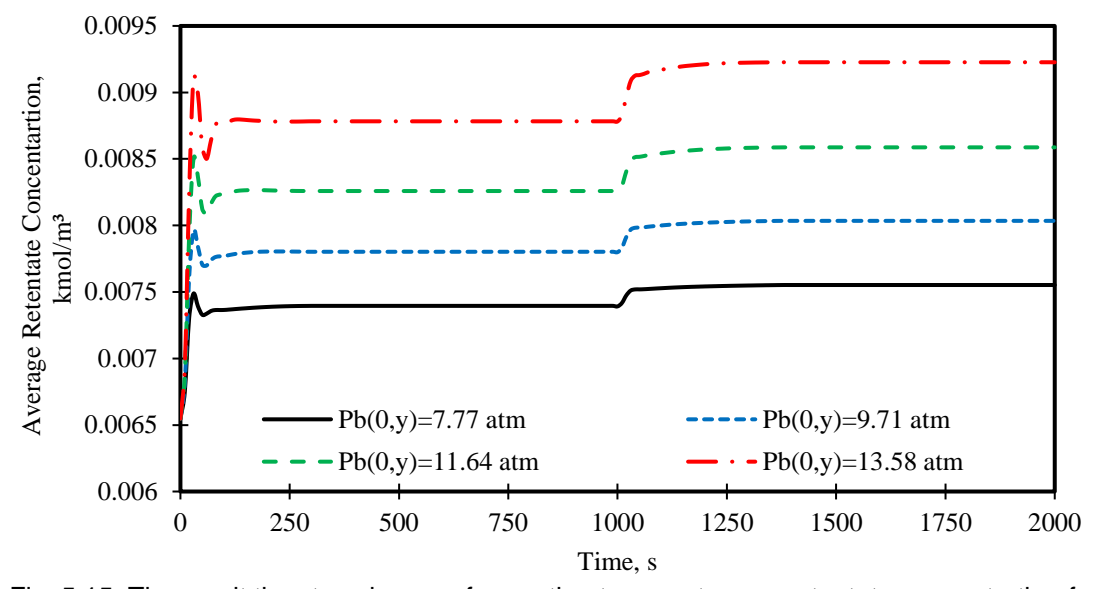


Fig. 5.15. The result the step change of operating temperature on retentate concentration for several operating pressures at operating conditions of 2.583x10⁻⁴ m³/s, and 6.548x10⁻³ kmol/m³

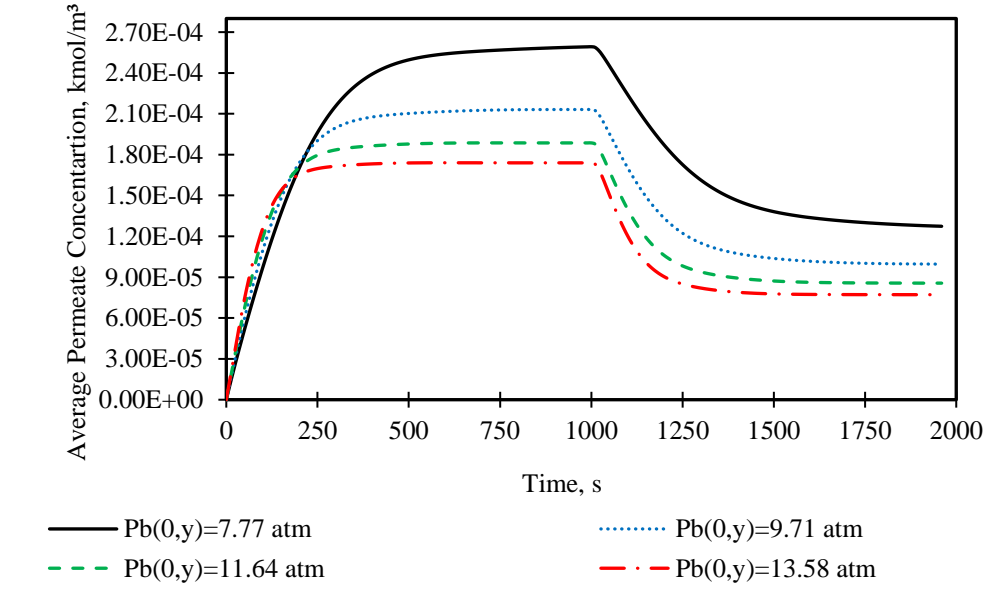


Fig. 5.16. The effects of the step change in operating temperature to mean permeate concentration for several operating pressures at operating conditions of 2.583x10⁻⁴ m³/s, and 6.548x10⁻³ kmol/m³

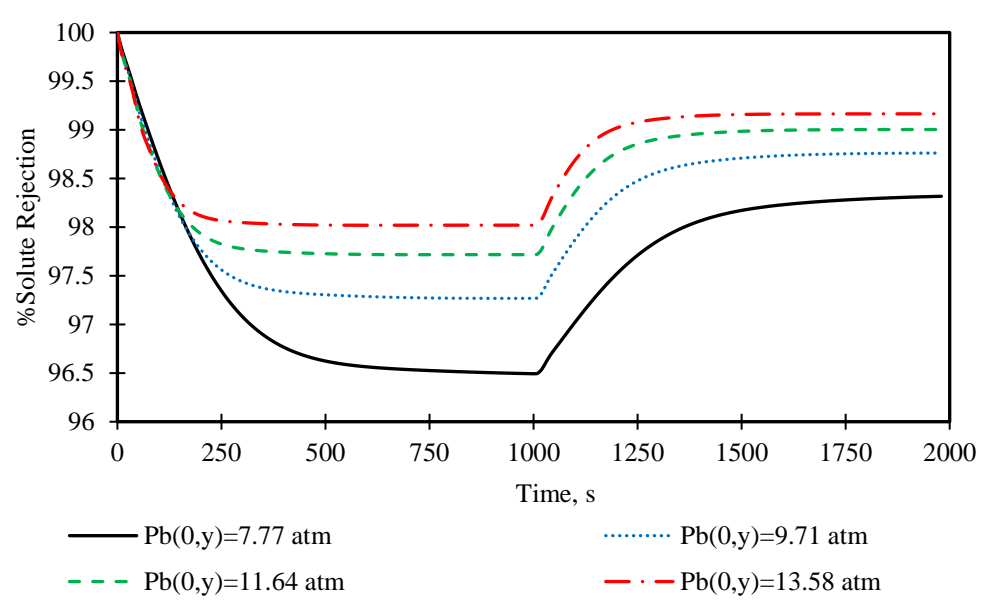


Fig. 5.17. The result of the step change of operating temperature on rejection parameter for several operating pressures at operating conditions of 2.583x10⁻⁴ m³/s, and 6.548x10⁻³ kmol/m³

It is clear from the above dynamic simulation results that the process requires a specific time to be settled after imposing a step change on the operating parameters, which is mainly dependent on the type of input parameters. The combined step change of operating concentration and temperature expenses a longer time to settle the process performance than that of the combined step change of the feed pressure and feed flow rate. From a practical aspect, it seems that such step change can occur because of a number of reasons, including an instant increase in the feed concentration, pump fault, and the season variation. As a result, the process performance is likely to be affected as a response to a step change, which might occur in the operating conditions. In other words, the process will fluctuate as a response to this change until it settles at a constant value. Specifically, the requirements of gaining a new steady state operation process is mainly associated with the measurements of the system and the weight of the stepwise.

5.3 Conclusions

RO processes are readily used for removing pollutants, such as dimethylphenol from wastewater. For a given configuration (design) of the RO process, a number of operating parameters affect the process performance. In this respect, the ultimate goal would be to design an effective and efficient controller for such process, understanding the dynamics of such process is no doubt a pre-step

which is the focus of this study. The dynamic simulation of the 2D modelling has facilitated the investigation of the impact of a step change of the operating parameters on the performance of the whole system. The dynamic simulation results show that the process requires a specific a finite time to settle after imposing a step change on several operating parameters. Most importantly, the settling time is dependent on the type of the operating parameters. Additionally, the results show that a multiple change of operating pressure yields a different process settling time, and that the process settling time is inversely related to the operating pressure. Specifically, the operating concentration and temperature step changes expense longer time to settle the process than the operating pressure and flow rate.

Chapter 6

Removal of N-Nitrosamine from Wastewater: Simulation, Network Design, and Optimisation

6.1 Introduction

Nitrosamine and specifically N-nitrosodimethylamine (NDMA) ($C_2H_6N_2O$) (74.08 g/mol, water solubility: 290 g/L at 20 °C) is an organic compound, which has been detected in chlorinated water and addressed as a probable human carcinogen. The removal of NDMA from water is becoming a real challenge due to low-molecular weight of NDMA with high hydrophilic properties (easily dissolved in water). Generally, ozone and chlorine oxidants are effectively used to abate NDMA from wastewater because of its efficiency to destroy amines. However, this high-cost process may lead to form NDMA in special cases and circumstances. For example, the existence of ammonia in wastewater can hinder the efficiency of chlorination oxidation treatment due to forming chloramine, which can easily react with other nitrogen compounds to form NDMA (Selbes et al. 2015). On the line of this research, the efficiency of the RO process to remove NDMA from wastewater was particularly in the range 40 – 70% (Krauss et al. 2010).

This chapter presents several cases for N-nitrosamine removal from wastewater as follows:

- to simulate the rejection of NDMA, NMEA, and NPYR from wastewater, total water recovery, and specific energy consumption for two configurations of with and without energy recovery device.
- to evaluate several conceptual designs of multi-stage and multi-pass designs for RO processes for NDMA rejection using model-based techniques and compute the total recovery rate and energy consumption.

6.2 Case 1: Simulation of spiral wound RO process for the removal of Nnitrosamine from wastewater

Here, the effects of operating parameters of the spiral wound RO process on the removal of N-nitrosamine, total water recovery, and energy consumption for spiral wound RO configurations are evaluated via simulation. For this purpose, the 1D distributed Model Type_5 (described in Section 3.3.1.1 in Chapter 3) developed is modified by including different mass transfer coefficient correlation,

temperature dependent water and solute permeability correlations and energy equations. The model is first validated by estimating a new set of model parameters using eight set of experimental data from the literature and is then used to simulate the process with and without energy recovery device to facilitate deeper insight of the effect of operating conditions on the process performance.

6.2.1 Proposed spiral wound RO configuration

Fig. 2.2 in Chapter 2 shows the pilot-scale cross-flow RO filtration system of three 4" glass-fiber pressure vessels used by Fujioka et al. (2014b). Fig. 6.1 shows the proposed configuration of RO configuration of this study. The main additions to this configuration compared to the configuration of Fig. 2.2 in Chapter 2 are the existence of the high-pressure pump HPP, booster pump BP, energy recovery device ERD, and the feed tank boiler (electric) as we wanted to study the impact of feed temperature on the solute rejection. The feed tank is filled with wastewater (with the same specification as considered by Fujioka et al. (2014b). The first run is carried out at a reference temperature T_{Ref} of 20 °C followed by heating the feed tank from 20 to 22 °C in one hour. Then, another treatment is carried out at the new temperature (22 °C). This is followed by a series of several runs, which are carried out in a step change of 2 °C for each run till 44 °C.

The tank feed flow rate $F_{b(Tank)}$ is split into two fractions towards ERD ($F_{b(ERD)}$) and HPP ($F_{b(HPP)}$) at atmospheric pressure P_{atm} . However, the total permeate $F_{P(Total)}$ at atmospheric pressure and the retentate are collected in the feed tank as in Fig. 2.2 in Chapter 2 to maintain a constant feed concentration. The total rejected fluid $F_{b(L)}$ discharged from the last module is 100% recycled to ERD with high pressure $P_{b(L)}$ to pressurise the feed entering ERD. More specifically, the importance of ERD is to transfer the energy from the high-pressure fluid stream by recovering the surplus pressure and delivering it directly to the incoming feed stream, which reduces the energy consumption of the RO process by recycling the fluid energy (Anderson et al. 2009). The pressure losses in the membrane module will be compensated by BP (Greenlee et al. 2009). Then, the feed flow rate of HPP ($F_{b(HPP)}$) and BP ($F_{b(ERD)}$) are collected to form the inlet feed flow rate of RO unit $F_{b(0)}$ with the inlet feed pressure $P_{b(0)}$. The performance of process rejection and recovery will be estimated by specifying the total permeate concentration and flow rate of the plant permeate stream. Moreover, the calculations of the specific

energy consumption will be carried out for both configurations of the RO pilotplant with and without ERD (Figs. 6.1 and 2.2 in Chapter 2).

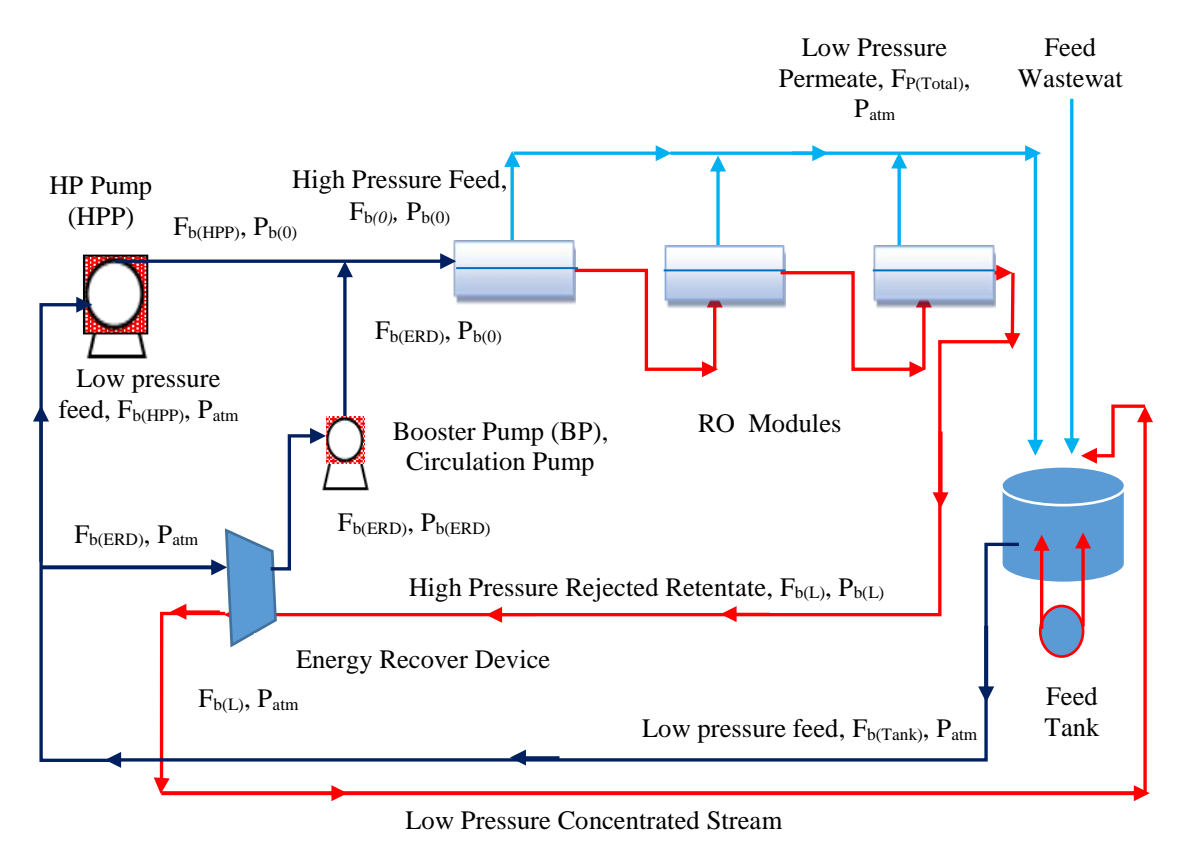


Fig. 6.1. Schematic diagram of a conventional RO pilot-scale plant

6.2.2 Model equations

In this work, following equations required are added to the original Model Type_5 thus giving the modified model. The mass transfer coefficient along the x-axis $k_{(x)}$ was estimated using the empirical correlation of Senthilmurugan et al. (2005) of Eq. (6.1).

$$k_{(x)} = 0.753 \, \left(\frac{K}{2-K}\right)^{0.5} \left(\frac{D_{b(x)}}{t_f}\right) \left(\frac{\mu_{b(x)} \, \rho_{b(x)}}{D_{b(x)}}\right)^{0.1666} \left(\frac{2 \, t_f^2 \, U_{b(x)}}{D_{b(x)} \, \Delta L}\right)^{0.5} \tag{6.1}$$

The effects of temperature variation on both water permeability L_p and solute permeability B_s coefficients are described in Eqs. (6.2) and (6.3), respectively of Sarkar et al. (2008).

$$L_{p(T_b+273.15)} = L_{p(T_0+273.15)} \frac{\mu_{b(T_0+273.15)}}{\mu_{b(T_b+273.15)}}$$
(6.2)

$$B_{s(T_b+273.15)} = B_{s(T_o+273.15)} \frac{T_b+273.15}{T_o+273.15} \frac{\mu_{b(T_o+273.15)}}{\mu_{b(T_b+273.15)}}$$
(6.3)

 T_0 is the reference temperature of 20 °C. Moreover, the specific energy consumption E1 of RO filtration system used by Fujioka et al. (2014b) is

calculated using Eq. (6.4) of Qi et al. (2012) based on the use of only a high-pressure pump. Here, $P_{b(0)}$ in atm and E1 in kWh/m³.

$$E1 = \frac{\frac{\left((P_{b(0)}^{101325}) F_{b(0)} \right)}{F_{p(Total)} \varepsilon_{pump}}}{36E5}$$
(6.4)

The calculation of the specific energy consumption for the conventional configuration of RO filtration system E2, which consists of a high-pressure pump (HPP), booster pump (BP) and energy recovery device (ERD) is carried out using Eq. (6.5). More specifically, the energy performance of the conventional pilot-plant is analysed based on the outgoing and ingoing entering energies. One of the aims of this paper is to determine the energy consumption due to its major contribution in total filtration cost, and which can reach values as high as 45% (Zhu et al. 2009).

$$E2 = \frac{\frac{(P_{b(0)} \, ^{101325)} \, F_{b(0)})}{F_{p(Total)} \, ^{\epsilon_{pump}}} - \frac{(P_{b(L)} \, ^{101325)} \, F_{b(L)} \, ^{\epsilon_{ERD}}}{F_{p(Total)}}}{36E5}$$
(6.5)

Eq. (6.6) calculates the outlet pressure of ERD $P_{b(ERD)}$ regarding the outlet pressure of membrane modules $P_{b(L)}$.

$$\varepsilon_{\rm ERD} = \frac{P_{\rm b(ERD)}}{P_{\rm b(L)}} \tag{6.6}$$

For the case where the temperature of the feed tank is raised using a boiler, the heat supplied Q (j/s) by the boiler is calculated using Eq. (6.7) with $T_{Ref} = 20$ °C. The boiler energy consumption E3 (kWh/m³ of permeate) is calculated using Eq. (6.8), while the total energy consumption E4 (kWh/ m³ of permeate) is calculated using Eq. (6.9), taking into account the energy consumption of the HPP and boiler in addition to the gain of energy using ERD.

$$\frac{d(T_{Tank}-T_{Ref})}{dt} = \frac{Q}{\rho C_D V}$$
 (6.7)

 ρ , C_p and V are the density of water (kg/m³), specific heat capacity of water (j/kg K) and volume of feed tank (m³), respectively.

$$E3 = \frac{\binom{Q}{F_{p(Total)}}}{36E5} \tag{6.8}$$

$$E4 = E2 + E3$$
 (6.9)

6.2.3 Simulation: Effect of operating parameters

To have a better insight of the impact of operating parameters on the process performance, simulations of the process configurations (Fig. 2.2 in Chapter 2 and Fig. 6.1) are carried out and results are presented.

6.2.3.1 Effect of inlet feed pressure

Table 3.11 in Chapter 3 shows that the friction parameter increases due to an increase in the operating feed pressure. Fig. 6.2 shows a linear relationship between the applied feed pressure and friction factor for a spiral wound RO module type ESPA2-4040. This relation will be used to estimate the friction parameter for each run of operating pressure.

The solute rejection, total recovery and specific energy consumption are directly affected by the operating feed pressure of the RO filtration system, which directly affects the solvent and solute fluxes through the membrane (Thomson et al. 2003). The impact of inlet feed pressure variation at constant inlet feed flow rate and temperature of 2.43x10⁻³ m³/s, and 20 °C, respectively on N-nitrosamine rejection, total recovery, and specific energy consumption for the RO configurations (shown in Fig. 2.2 in Chapter 2 and Fig. 6.1) is highlighted within the manufacturer's specification of membrane area and the maximum operating pressure.

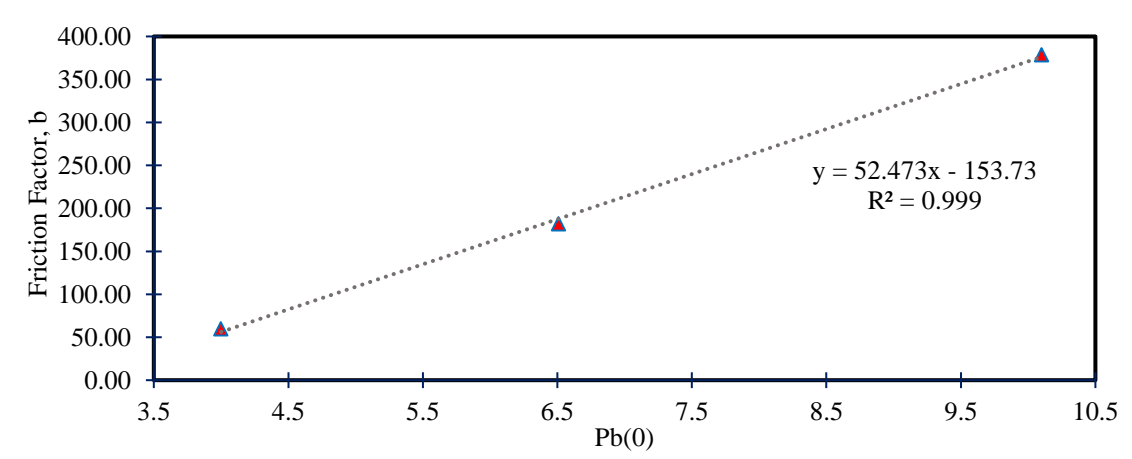


Fig. 6.2. Friction parameter versus inlet feed pressure for module type ESPA2-4040 (initial conditions 2.43x10⁻³ m³/s, and 20 °C)

Fig. 6.3 displays the relationship existing between the inlet feed pressure and N-nitrosamine rejection for three different compounds using their initial concentrations as presented in Table 3.11 in Chapter 3. It is clearly shown that

increasing the feed pressure from 10.1 to 40 atm (within the manufacturer's specification, Table 2.4 in Chapter 2) has a significant impact on N-nitrosamine rejection. It is expected that higher permeate flux increases the dilution of solute at the feed side, which passed through the membrane, and therefore results in lower permeate concentration. NDMA rejection is increased by 30% from 0.60 to 0.78 as a response to an increase in the inlet feed pressure from 10.1 to 40 atm. NMEA and NPYR rejections are increased simultaneously by 9.57% and 4.55% from 0.87 to 0.95 and from 0.936 to 0.978, respectively. These results indicate that the higher feed pressure is required to obtain higher N-nitrosamine rejection due to an increase in water flux and total water recovery.

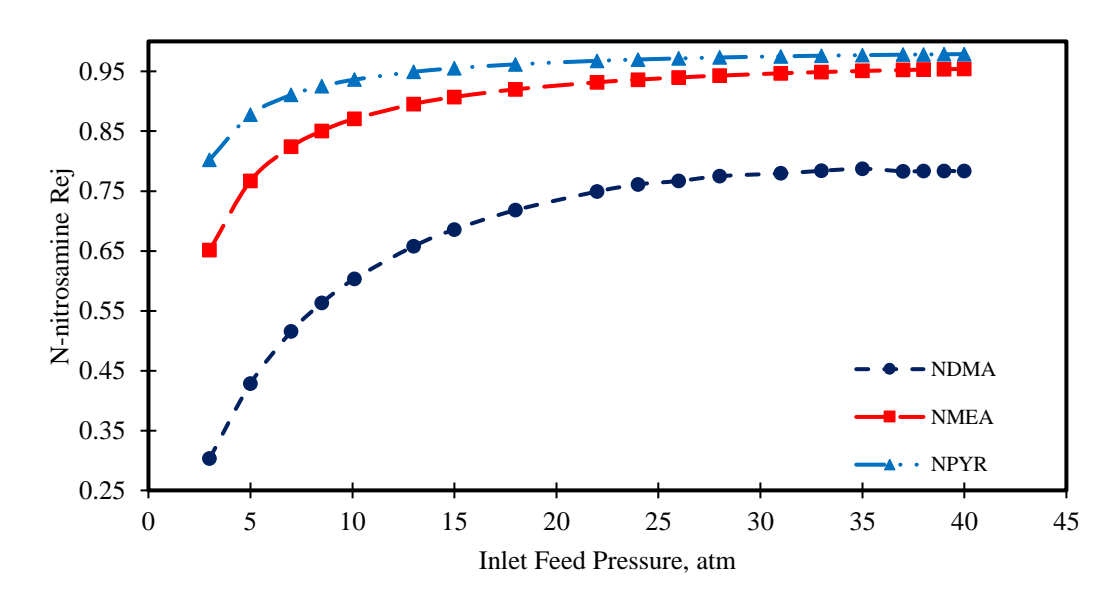


Fig. 6.3. Dependence of N-nitrosamine rejection on inlet feed pressure at inlet feed conditions of 2.43x10⁻³ m³/s, and 20 °C

Fig. 6.4 displays the relationship existing between the energy consumption and total recovery as a function of inlet feed pressure for the RO configurations (Figs. 2.2 in Chapter 2 and 6.1). This includes an investigation of the impact of both HPP and ERD efficiency for the same step change in inlet feed pressure. It is clear that the energy consumption decreases with increasing inlet feed pressure in case of using only HPP. This lower energy consumption is caused by an increase in the efficiency of pump from 80% to 85% and then to 90%. More specifically, the energy consumption is brought down by a constant value of 5.88% for all pressures by increasing the pump efficiency from 80% to 85%, while, a reduction of a constant value of 5.55% for all pressures is registered by increasing the pump efficiency from 85% to 90%. Therefore, using a higher

efficiency pump can significantly reduce the energy consumption. These results concur with Du et al. (2014).

For the RO system shown in Fig. 6.1, Fig. 6.4 shows that the addition of ERD in the RO filtration system is very important where the energy consumption can be reduced by approximately 47% at operating pressure of 10.1 atm and 31% at 40 atm than the case of only HPP mode. The reason for this is that the rejected stream flow rate is about 61 – 97% of the inlet feed flow rate and the retentate pressure is about 74 – 99% of the inlet pressure for a set of operating pressure varied between 40 to 3 atm, which results in a high amount of hydraulic energy in the rejected side. This is a substantial energy saving for the system. Also, these results indicate that increasing feed pressure will increase the total water recovery as well as an increase in the specific energy consumption. The impact of increasing the efficiency of ERD is shown by reducing the consumption of energy. However, it is clearly shown that the impact of pressure on energy consumption is more obvious at low pressures than at high pressures. The consumption of energy is slightly increased at high recovery region in comparison to a dramatic growth at low recovery region (low operating pressures). The reason of this phenomenon is that at high feed pressures and recoveries, the quantity of water to be pressurised will be less than at low recoveries and pressures. Another explanation can be drawn from Fig. 6.5, which shows a steady increase of the pressure difference between the inlet and outlet pressures due to an increase in inlet pressure. This shows that higher recovery can be achieved at higher pressures due to a higher-pressure difference along the membrane length, which reduces the energy consumption for HPP mode as illustrated in Eq. (6.5) in comparison to lower operating pressures, which are characterised by lower values of pressure difference and higher energy consumption. However, Fig. 6.4 shows that the energy consumption increases due to an increase in water recovery for the system. This test indicates that the beneficial effect of ERD addition becomes less significant in energy saving at high operating pressures in comparison to low operating pressures despite achieving higher solute rejection and lower energy consumption when compared with HPP mode.

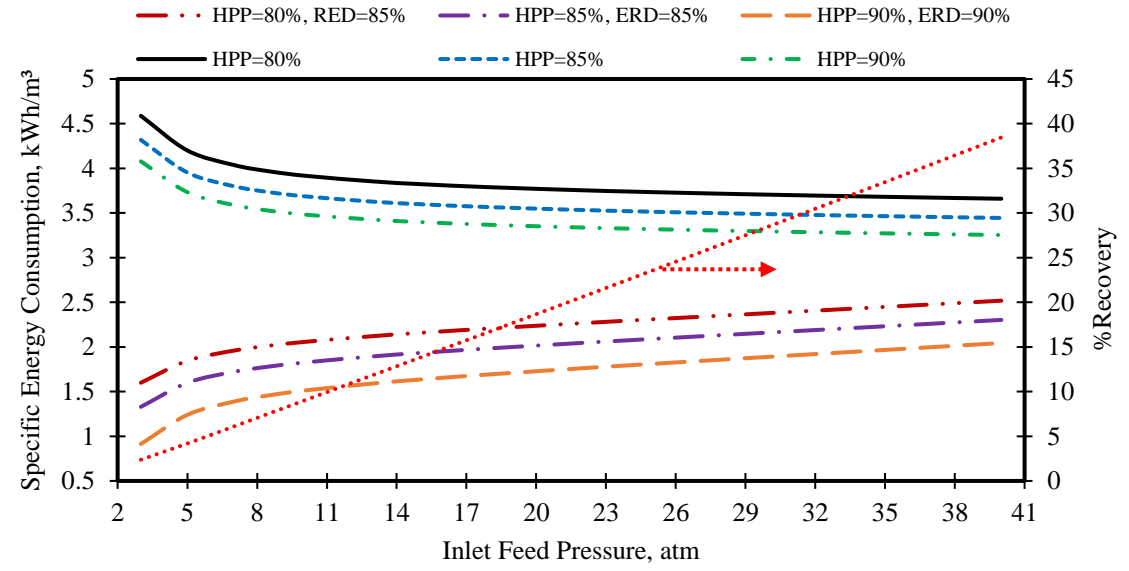


Fig. 6.4. Specific energy consumption of two types RO pilot-plants with and without ERD (Figs. 6.1 and 2.2 in Section 2.5.2 in Chapter 2) and total recovery versus inlet feed pressure at inlet feed conditions of 2.43x10⁻³ m³/s, and 20 °C

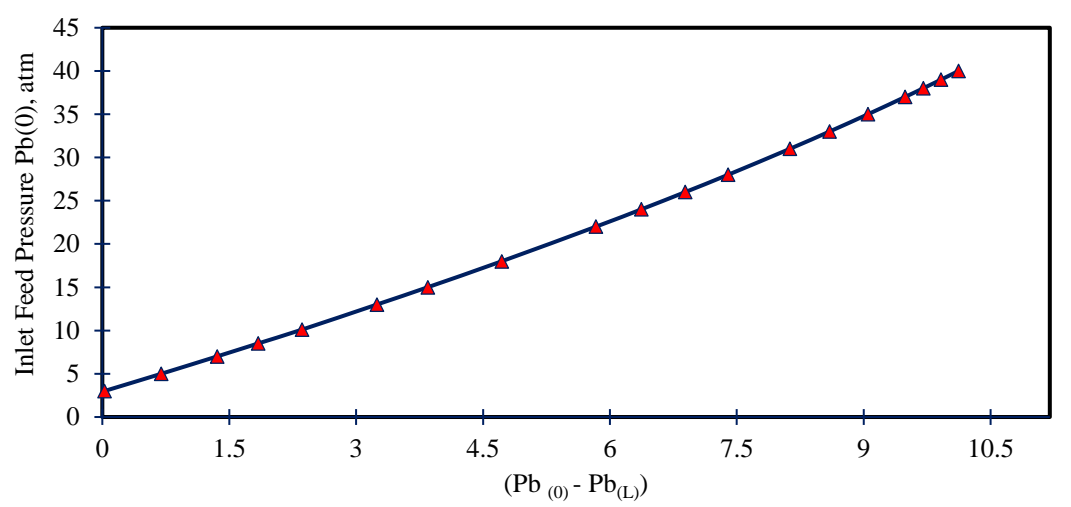


Fig. 6.5. The relation between the inlet feed pressure and the pressure difference at inlet and outlet edges at inlet conditions of 2.43x10⁻³ m³/s, and 20 °C

6.2.3.2 Effect of inlet feed flow rate

The influence of the feed flow rate at constant values of inlet feed pressure and temperature on N-nitrosamine rejection and energy consumption is considered in this section. The inlet feed flow rate is reduced by 50% from 2.43x10⁻³ m³/s to 1.215x10⁻³ m³/s by 10% step change for each run at constant inlet feed pressure and temperature of 10.1 atm and 20 °C, respectively.

It was found that a maximum recovery can be achieved at low inlet feed flow rate. This behaviour is due to the pressure drop in the high-pressure channel, which decreases when the operating feed flow rate also decreases. Similarly, an

increase in the feed flow rate will increase the loss in pressure due to higher friction along the membrane length. This reduces the advantage of having a lower average osmotic pressure and concentration polarisation; as this in turn decreases the water flux and total permeate recovery. Therefore, N-nitrosamine rejection slightly decreases due to increase in the feed flow rate as can be shown in Fig. 6.6. These results are in line with the findings of Abbas (2005). Moreover, increasing the inlet feed flow rate at constant pressure and temperature will increase the specific energy consumption due to a lower gain in total recovery, as can be shown in Fig. 6.7. Therefore, at constant operating pressure and temperature, it is recommended to work within low feed flow rates to guarantee lower energy consumption and higher rejection.

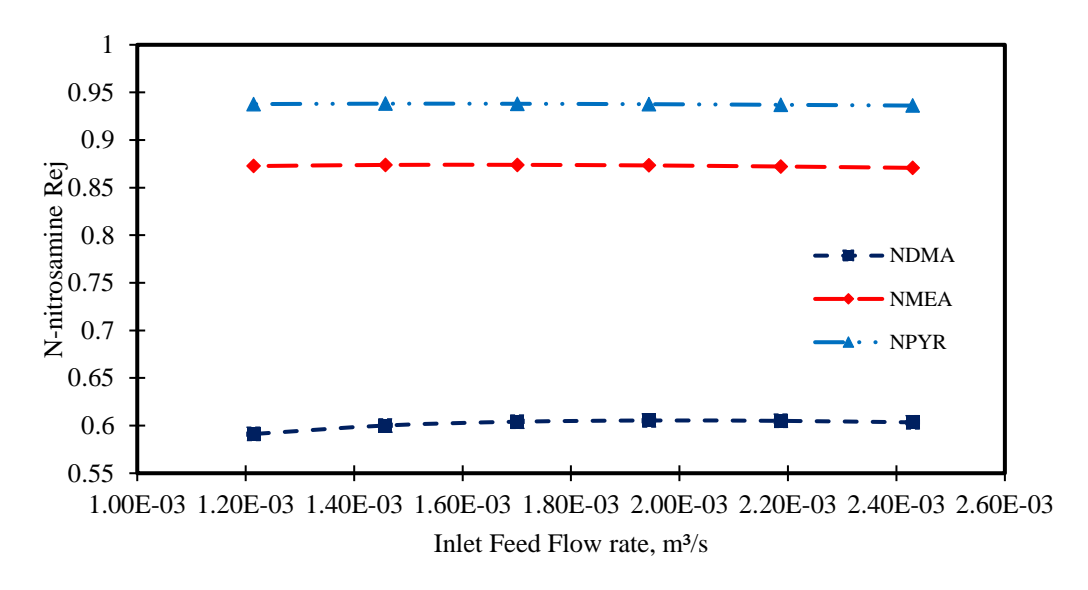


Fig. 6.6. Dependence of N-nitrosamine rejection on inlet feed flow rate at inlet feed conditions of 10.1 atm, and 20 °C

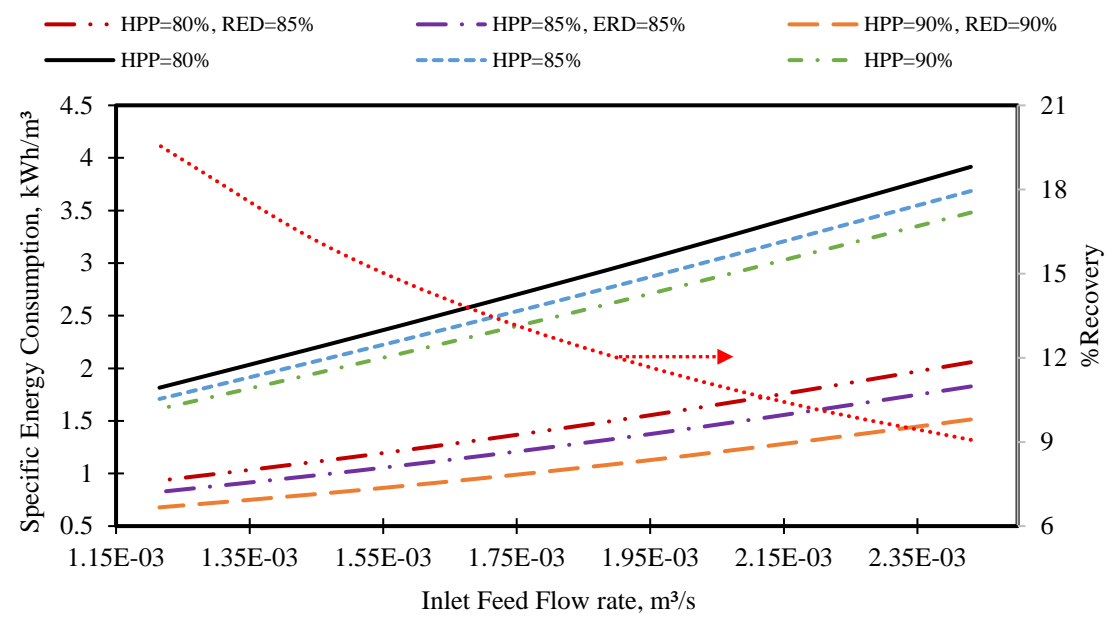


Fig. 6.7. Specific energy consumption of two types RO pilot-plants with and without ERD and total recovery versus inlet feed flow rate at inlet feed conditions of 10.1 atm, and 20 °C

6.2.3.3 Effect of inlet feed temperature

The inlet feed temperature can have a clear effect on solute rejection, water recovery and energy consumption according to Jiang et al. (2015). In this work, we evaluated and reported the performance of the RO network for every 2 °C rise in feed temperature (note the reference feed temperature is 20 °C). The total permeate recovery increase due to an increase in the feed temperature at constant inlet feed flow rate and pressure (Fig. 6.9). This is compared to a slight decrease of N-nitrosamine compounds rejection. This same trend has been reported by Fujioka (2014a), which is already attributed to increase the membrane pore size as a result to increasing operating temperature in addition to increasing the solute transport parameter. This in turn increases the solute flux and reduces the rejection parameter. The registered reduction of NDMA, NMEA and NPYR rejections are 6.5%, 1.7%, and 0.79%, respectively, compared to 67% increase in total recovery rate, when the temperature gradually increases from 20 to 44 °C. More specifically, the rejections are decreased from 0.6 to 0.56 for NDMA and from 0.87 to 0.85 for NMEA and from 0.936 to 0.926 for NPYR (Fig. 6.8). Occasionally, the gain of energy consumption is around 28% and 32% for with and without ERD configurations (Fig. 6.9). These results show the significant role of feed temperature to capture higher recovery rate in addition to lower energy consumptions.

However, the above results did not include the contribution of the boiler energy required to raise the feed temperature from 20 to 44 °C. The assumption made here is that 1 hour is enough to raise the feed temperature to the next level and the total heat supplied, Q, in Watt, is calculated using Eq. (6.7) with assuming no heat loss. To be consistent with Eqs. (6.4) and (6.5), the heat supplied is divided by the volume of produced permeate in Eq. (6.8) to calculate the boiler energy consumption. Eq. (6.9) then gives the total energy consumption for the whole system.

Fig. 6.9 also shows the cases of the total energy consumption of the system. As expected, the addition of this energy will lift the total energy consumption of the whole system. However, the interesting point here is that the consumption of energy with the boiler addition is still lower than the registered values of RO consumption without the ERD mode. Also, Fig. 6.9 shows that the total energy consumption of the process (Fig. 6.1) is reasonably increased from 20 to 22 °C due to the addition of consumed boiler power calculated by Eq. (6.8) and then continuously decreased when the tank temperature increased from 22 to 44 °C. This can be explained due to a noticeable increase of permeate flow rate as a result of increasing feed temperature. The increasing total permeate ($F_{p(Total)}$) will reduce the total energy consumptions (E1, E2, E3, E4) according to Eqs. (6.4), (6.5), (6.8) and (6.9), respectively. Note, the calculation of the boiler energy consumption is carried out when the temperature increases by an increment of 2 °C assuming no heat loss. This is done by assuming that wastewater will keep its energy before supplying any further heat.

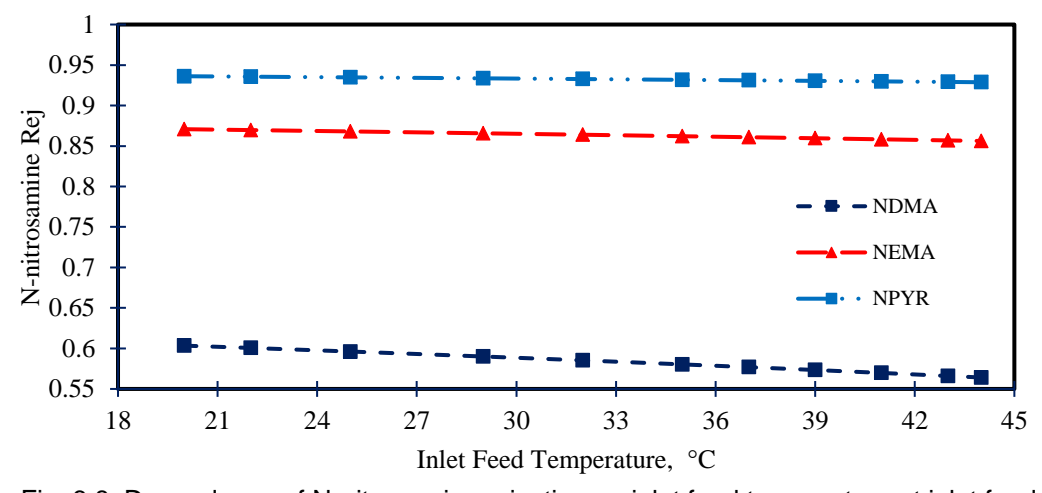


Fig. 6.8. Dependence of N-nitrosamine rejection on inlet feed temperature at inlet feed conditions of 2.43x10⁻³ m³/s, and 10.1 atm

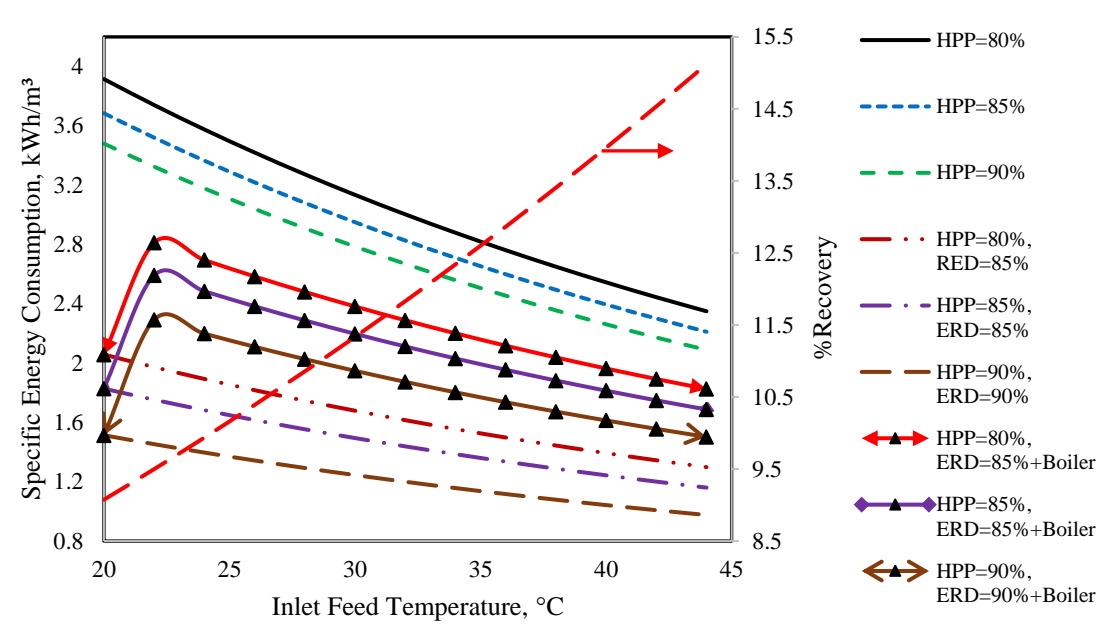


Fig. 6.9. Specific energy consumption of two types RO pilot-plants with and without ERD and ERD with Boiler and total recovery versus inlet feed temperature at inlet conditions of 2.43x10⁻³ m/s, and 10.1 atm

To sum up, it is easy to notice that an increase in the inlet feed pressure (at a constant feed flow rate and temperature) has a significant impact on N-nitrosamine rejection and total recovery. This is compared to a negative impact on N-nitrosamine rejection due to increasing the operating temperature (at constant pressure and flow rate), and flow rate (at a constant pressure and temperature). However, it is evident that the increment in the inlet feed flow rate has a negative impact total recovery. Moreover, both an increase in the inlet feed pressure (at a constant feed flow rate and temperature) and feed flow rate (at a constant feed pressure and temperature) have an adverse impact on energy consumption of ERD and HPP configurations. Also, an increase in the inlet feed temperature (at constant feed pressure and flow rate) will increase the consumption of energy within acceptable levels despite the added consumed energy of the boiler (source of heat). The combination of ERD and HPP (Fig. 6.1) can lead to a higher reduction in energy consumption compared to the RO pilot-plant used by Fujioka et al. (2014b) (Fig. 2.2 in Chapter 2).

For the convenience of the reader, Table 6.1 summarises the impact of operating parameters of the spiral wound RO process on the process performance indicators for the removal of N-nitrosamine compounds from wastewater.

Table 6.1. Summary of the impact of operating parameters on the performance of RO process

Operating	Permeate	Retentate	Permeate	Retentate	Solute	Recovery	Energy
parameters	conc.	conc.	flow rate	flow rate	rejection	rate	consumption
Pressure	1	1	1	1			1
Flow rate	1	1		1		1	
Temperature	1	1	1	1	1	1	1

6.2.4 Process optimisation

Having developed a deeper insight (in the earlier sections) of the impact of a number of operating parameters (by varying these parameters one at a time) on the rejection rates of N-nitrosamine contaminants and energy consumptions for two given RO configurations with and without energy recovery options (Figs. 6.1 and 2.2 in Chapter 2), the intention on this section is to formulate two optimisation problems, which will maximise the rejection rates and minimise the energy consumptions, while optimising the operating parameters.

The first objective is to maximise the NDMA rejection of the configuration of RO pilot-plant used by Fujioka et al. (2014b) (Fig. 2.2 in Chapter 2, without ERD) and the RO system described in Fig. 6.1 by allowing the system operating conditions to vary within the limits set in the manufacturer's specification. Any optimised operating conditions that maximise NDMA rejection would serve the rejections of NMEA and NPYR too.

The second objective is to minimise the total energy consumption of the two configurations (Figs. 2.2 in Chapter 2 and 6.1) measured in kWh per m³ of the total permeate. The results of Fujioka et al. (2014b) for solute rejections were taken as the minimum accepted values for the optimisation.

6.2.4.1 Optimisation problem 1

The optimisation problem 1 can be described as follows:

Given: Operating feed conditions, module specifications.

Optimise: Inlet feed pressure, flow rate and temperature (the optimisation variables).

Maximise: NDMA rejection.

Subject to: Equality (process model) and inequality constraints (linear bounds of optimisation variables).

As the optimisation problem can be represented mathematically as:

OP1:

Max Rej

 $F_{b(0)}$, $P_{b(0)}$, T_b Subject to:

Equality constraints:

Process Model: $f(z, x(z), x^{-}(z), u(z), v) = 0; [z_0, z_f]$

Inequality constraints:

$$\begin{array}{ll} (1 \times 10^{\text{-}3} \, \text{m}^3/\text{s}) & F_{b(0)}{}^L \leq F_{b(0)} \leq F_{b(0)}{}^U \; (2.43 \times 10^{\text{-}3} \, \text{m}^3/\text{s}) \\ \\ (3.0 \, \text{atm}) & P_{b(0)}{}^L \leq P_{b(0)} \leq P_{b(0)}{}^U \; \; (41.0 \, \text{atm}) \\ \\ (20 \, ^{\circ}\text{C}) & T_b^L \leq T_b \leq T_b^U \; \; (44 \, ^{\circ}\text{C}) \end{array}$$

The optimisation will be carried out for only NDMA, NMEA and NPYR with initial feed concentrations shown in Table 3.11 in Chapter 3.

6.2.4.2 Optimisation problem 2

The optimisation problem 2 can be described as follows:

Given: Operating feed conditions, module specifications.

Optimise: Inlet feed pressure, flow rate and temperature (the optimisation variables).

Minimise: The specific energy consumption defined in Eq. (6.9).

Subject to: Equality (process model) and inequality constraints (linear bounds of optimisation variables and solute rejection)

As the optimisation problem can be represented mathematically as:

Min E_4 (defined in Eq. 6.9)

 $F_{b(0)}, P_{b(0)}, T_b$

Subject to:

Equality constraints:

Process Model: $f(z, x(z), x^{-}(z), u(z), v) = 0; [z_0, z_f]$

Inequality constraints:

$$(1x10^{-3} \text{ m}^3/\text{s}) \quad F_{b(0)}^{\ \ L} \le F_{b(0)} \le F_{b(0)}^{\ \ U} \quad (2.43x10^{-3} \text{ m}^3/\text{s})$$

$$(3.0 \text{ atm}) \quad P_{b(0)}^{\ \ L} \le P_{b(0)} \le P_{b(0)}^{\ \ U} \quad (41.0 \text{ atm})$$

$$(20 \text{ °C}) \quad T_b^{\ \ L} \le T_b \le T_b^{\ \ U} \quad (44 \text{ °C})$$

 $Rej_{NDMA} \ge 0.6273$ $Rej_{NMEA} \ge 0.8864$ $Rej_{NPYR} \ge 0.9454$

Firstly, the results of Fujioka et al. (2014b) are given in the first row of Table 6.2 for the purpose of comparison with the optimisation results (base case). For OP1, the maximum rejections for NDMA, NMEA and NPYR are found to be 0.80, 0.951 and 0.977 with optimum feed flow rate of 2.43x10⁻³ m³/s, pressure 35.406 atm

and temperature at 20 °C with significant reduction (4.48 kWh/m³ to 3.678 kWh/m³ to 2.454 kWh/m³) in energy consumption (for all energy recovery options). For NDMA, NMEA and NPYR there is an increase of 27.5%, 7.3% and 3.34% in rejections, respectively compared to Fujioka et al. (2014b). Interestingly, the optimisation confirms that the RO process is not efficient for the removal of NDMA (compared to NMEA and NPYR) as reported by Mitch et al. (2003).

Increasing the operating temperature from 42 °C to 44 °C at the optimised conditions of OP1 showed a positive impact on the reduction in energy consumptions (all options) compared to the case at 20 °C. However, NDMA, NMMA and NPYR rejections are decreased to 0.514, 0.915 and 0.962, respectively.

The results of OP2 show that the minimum energy consumption can be significantly reduced from 4.48 kWh/m³ to 1.912 kWh/m³ to 1.046 kWh/m³ with no significant gain of N-nitrosamine rejection compared to the base case. This was possible for a much lower value of feed rate (1.30x10⁻³ m³/s), pressure (12.98 atm), and temperature at 20 °C compared to Fujioka et al. (2014b). The reduction of specific energy consumption was about 57.3% compared to Fujioka et al. (2014).

Increasing the operating temperature from 42 °C to 44 °C, OP2 results in further reduction in energy consumption (1.146 and 1.104 kWh/m³ for Figs. 2.2 in Chapter 2 and 6.1, respectively) with the same optimised conditions of OP2. For this case, the NDMA, NMEA and NPYR rejections are found to be 0.514, 0.866 and 0.936, respectively which are worse than those found at 20 °C. The reduction of specific energy consumption was about 74.4% compared to Fujioka et al. (2014). The results in Table 6.2 clearly indicate how the inlet feed pressure, temperature, and feed flow rate can potentially affect N-nitrosamine rejection and plays an important role in reducing the energy consumption.

Table 6.2. The optimisation results

	_	S						Е	nergy Co	nsumption kWI	h/m³	
No	Optimisation Problem	F _{b(0)} x 10³,m³/s	$P_{b(o)}$, atm	T _b , °C	Rej (NDMA)	<i>Rej</i> (NMEA)	Rej (NPYR)	HPP 80% (Fig. 2.2 in Chapter 2)	HPP 80%+ ERD 85%	Boiler Consumed Power	(total energy consumption) HPP 80%+ERD 85%+Boiler (Fig. 6.1)	Comments
1	Base Case	2.43	10.1	20	0.6273	0.8864	0.9454	4.48	0	0	4.48	Fujioka et al. (2014b) results
2		2.43 (opt)	35.406 (opt)	20 (opt)	0.80 (max)	0.951 (max)	0.977 (max)	3.678 (calc)	2.454 (calc)	0	2.454 (calc)	Optimised rejection at 20 °C
3	OP1	2.43 (opt)	35.406 (opt)	42-44 (Selected)	0.514	0.915	0.962	2.181 (min)	1.686 (min)	0.139	1.825	Calculated energy consumption at 44 °C
4	OP2	1.30 (opt)	12.982 (opt)	20 (opt)	0.634 (calc)	0.8941 (calc)	0.949 (calc)	1.912 (min)	1.046 (min)	0	1.046	Optimised energy consumption at 20 °C
5	OP2	1.30 (opt)	12.982 (opt)	42-44 (Selected)	0.514 (calc)	0.866 (calc)	0.936 (calc)	1.146 (min)	0.730 (min)	0.374	1.104	Calculated energy consumption at 44 °C

Inlet feed concentration $C_{b(0)}$ of each N-nitrosamine is given in Table 3.12 in Chapter 3. opt = optimised value; max = maximised value; min = minimised value

6.3 Case 2: Performance evaluation of multi-stage and multi pass RO networks for the removal of N-nitrosodimethylamine (NDMA) from wastewater

The literature confirms that the multi-stage RO process with retentate reprocessing design has not yet achieved an effective removal of Nnitrosodimethylamine-D6 (NDMA) from wastewater. This research focuses on this particular challenge and aims to evaluate several conceptual designs of multistage and multi-pass designs for RO processes for NDMA rejection using modelbased techniques and compute the total recovery rate and energy consumption for different configurations of retentate reprocessing techniques. In this research, the permeate reprocessing design methodology is used to increase the process efficiency. An extensive simulation analysis is carried out using high NDMA concentration to evaluate the performance of each configuration under similar operational conditions, thus providing a deep insight on the performance of the multi-stage RO permeate reprocessing predictive design. The second aim of this research is to assess the merits of a new proposed RO network, which has been specifically designed to include the permeate processing for high NDMA rejection and yet achieve an acceptable permeate recovery rate. Furthermore, an optimisation analysis is carried out on the final design to optimise the process with a high NDMA rejection performance and the practical recovery rate by manipulating the operating conditions of the plant within specified constraints limits. The results show a superior removal of NDMA from wastewater.

6.3.1 Modelling of a spiral wound RO process

The main objective of this section is to use the mathematical Model Type_4 after a suitable moderation to predict accurately the performance of a spiral wound RO process for the rejection of N-nitrosamine compounds from wastewater. For this to happen, the interaction between transport theories through the membrane need to be represented mathematically for building an appropriate numerical model, which will incorporate the calculations of the fluid properties. For this purpose, new assumptions were considered for the new proposed model as following:

 Validity of the Da Costa equation to predict the pressure drop across the membrane. Constant pump and energy recovery device efficiencies of 80 and 90%, respectively.

In this respect, a set of new equations is considered as described below.

• The estimation of the feed and permeate osmotic pressure can be obtained using Eqs. (6.10) and (6.11) (Fujioka et al. 2014b).

$$\pi_{\rm m} = 1.19 \, (T_{\rm b} + 273.15) \, \left(\frac{C_{\rm w}}{M_{\rm wt}}\right)$$
 (6.10)

$$\pi_{\rm p} = 1.19 \, (T_{\rm b} + 273.15) \, \left(\frac{c_{\rm p}}{M_{\rm W}t}\right)$$
 (6.11)

Mwt, T_b (kg/kmol, °C) are the molecular weight of NDMA provided in Table 2.3 in Chapter 2 and operating temperature, respectively.

The viscosity coefficient μ_b (kg/m s) is calculated using Eq. (6.12) (Fujioka et al. 2014b).

$$\mu_{b} = 2.141E - 5 \times 10^{\left(\frac{247.8}{(T_{b} + 273.15) - 140)}\right)}$$
(6.12)

• The process of NDMA rejection is accompanied by a pressure drop along the membrane edges. Therefore, the retentate pressure $P_{f(out)}$ (atm) is calculated using Eq. (6.13).

•
$$P_{f(out)} = P_{f(in)} - \Delta P_{drop}$$
 (6.13)

 ΔP_{drop} (atm) is the pressure drop of the spiral wound element, which is calculated using the proposed correlation of Da Costa et al. (1994) (Eq. 6.14) in line with Assumption 1. Da Costa et al. (1994) assumes that the pressure losses and kinetic losses are happening due to drag on feed spacer and a change in direction of flow respectively and neglecting the friction losses at the channel walls and on the spacer surface.

$$\Delta P_{\text{drop}} = \left(\frac{\rho_b U_b^2 L C_{\text{td}}}{2 d_h}\right) \times 9.8692 \times 10^{-6}$$
(6.14)

 C_{td} , d_h (dimensionless, m) are the total drag coefficient, which is calculated using Eq. (6.15) and hydraulic diameter of the feed spacer channel, respectively.

$$C_{td} = \frac{A'}{Re^n} \tag{6.15}$$

A' and n (dimensionless) are the spacer characteristics.

• The total energy consumption E1 (kWh/m³) of RO system measured in kWh per m³ of the total permeate is calculated using Eq. (6.4) based on the use of a high-pressure pump. However, in the case of using an energy recovery device ERD in the RO process network, the calculation of the total energy consumption E2 (kWh/m³) is carried out using Eq. (6.5). More

- specifically, the energy performance of the conventional pilot-plant is calculated regarding the outgoing and ingoing entering energies.
- Eq. (6.6) calculates the outlet pressure of ERD $P_{f(out)(ERD)}$, which will be going to use in next stage regarding the outlet pressure of membrane modules of the previous stage $P_{f(in)(ERD)}$.
- The feed temperature T is influencing the physical properties and the transport membrane constants, $A_{w(T)}$ and $B_{s(T)}$. Therefore, Eqs. (6.2) and (6.3) are used to investigate the impact of temperature on these parameters. Note, $A_{w(T_0)}$ and $B_{s(T_0)}$ are the permeate and NDMA transport parameters at reference temperature. These are reported in Table 6.5.

Parameters estimation

One of the main requirements of testing the proposed model in simulation studies is that the unknown parameters of the model should be estimated before solving the model equations. These parameters include; the water permeability constant $A_{w(T)}$, the NDMA transport parameter $B_{s(T)}$ and the spacer characteristics of A' and n. The model parameters were investigated using the gPROMS software and based on the same experimental data of NDMA removal from wastewater of Fujioka *et al.* (2014b). Table 6.3 shows the model parameters. The estimated dimensions of the spacer mesh (A' and n) were found to be close to the spacer type CONWED-1 as reported in the study of Da Costa *et al.* (1994) (A' = 1.29 and n = 0.24).

Table 6.3. The parameter estimation results

Parameter	Value
$A_{w(T)}$ (m/s atm)	1.1290x10 ⁻⁶
$B_{s(T)}$ (m/s)	4.0919x10 ⁻⁶
A' (-)	1.47
n (-)	0.24

Model validation

The enhanced Model Type_4 has been corroborated by comparing the model predictions results with those obtained from the actual experimentation of Fujioka et al. (2014b) of three elements of spiral wound RO process in a series configuration. This includes the removal of NDMA from wastewater at two

operating pressure of 4, and 6.51 atm. This is also carried out at $2.43x10^{-3}$ m³/s, 250 ng/L ($2.5x10^{-7}$ kg/m³), and 20 °C of feed flow rate, NDMA concentration and temperature, respectively. Table 6.4 provides a comparison of the observed and modeled values of retentate plant flow rate Q_r , total permeate flux J_w and total NDMA rejection Rej. The comparative results provided in Table 6.4 clearly show that the predicted values for the proposed model are consistent with experimental with a very low discrepancy.

Table 6.4. The model validation results

P _{f(in)}	J _w (m/	/s) x10 ⁶	Error	$Q_{\rm r}$ (m ³ /s) x10 ³		Error	Rej (-)		Error
(atm)	Ехр.	Model	%	Exp.	Model	%	Ехр.	Model	%
4	2.78	2.733	1.67	2.36	2.365	-0.22	0.388	0.3903	-0.60
6.51	5.56	5.583	-0.41	2.30	2.297	0.100	0.561	0.5555	0.96
$C_{f(NDMA)}$	$C_{f(NDMA)} = 250 \text{ ng/L}$, $Q_f = 2.43 \text{x} 10^{-3} \text{ m}^3 \text{/s}$, and $T = 20 ^{\circ}\text{C}$								

6.3.2 Multi-stage (retentate reprocessing) spiral wound RO networks description

Seawater desalination plants using RO technology are usually designed as a multi-stage process including three layouts of series, parallel and tapered design. These are usually used to control the plant, quality, and capacity (Schwinge et al. 2004).

The proposed RO industrial full-scale wastewater plant (under investigation) consists of six pressure vessels connected in different configurations of stages. Each stage holds a maximum of six pressure vessels connected in parallel, while each pressure vessel holds a maximum of three spiral wound RO membrane elements type BW30-400 of 37.2 m² produced by Dow/FilmTec and connected in series. The rationale for using three elements per pressure vessel in the proposed design, is to ensure an acceptable range of permeate recovery. This is decreased remarkably depending on the membrane location inside the pressure vessel of similar membranes connected in series. The highest flux always occurs in the first membrane due to the minimum underlying osmotic pressure. The technical specification of the high membrane area used is shown in Table 6.5. The rationale for selecting this type of membrane is its high NaCl rejection and availability of the technical characteristics, water permeability constant and restricted limits of operation in the literature (Abbas 2005).

For each proposed layout, a centrifugal high-pressure pump of 80% efficiency that can deliver the wastewater feed at a maximum of 40.463 atm is used. Fig. 6.10 shows the various configurations of the retentate reprocessing RO network (Scenario A – C) test, which will be analysed and assessed for the rejection of NDMA, total permeate recovery and energy consumption. Fig. 6.11 shows the rest of the configurations of retentate reprocessing RO network design Scenario (D – H), which have been analysed. These configurations are similar in that they use the same retentate reprocessing approach, where the concentrate stream of the first element becomes the feed to the second element and the combined retentate stream of the first stage will be the feed of the second stage. The permeate collected from all the series elements of the pressure vessel are blended with the permeate of other pressure vessels and then collected with the permeate of the second stage. The statement of working in similar operating conditions is quite applicable for any stage of pressure vessels connected in parallel. It should be noted that most of the configurations presented are similar to those found in an actual industrial plant of the RO seawater desalination process. These configurations are based on the design of slightly more elements in the first stage than the following stage. However, the author has considered the conception of upper and lower limits of operating feed flow rate for each proposed design of multi-stage RO process (6 pressure vessels).

Finally, a simulation model was developed for a spiral wound RO membrane module both in a steady state and multi-stage plant with varying operating parameters along the stages has been implemented using the gPROMS software. The model equations have been tested and solved for different operating parameters of inlet feed flow rates, pressures, NDMA concentrations and temperatures. In other words, the model is successfully simulated the process within a range of upper and lower limits of the membrane used type (BW30-400) presented in Abbas (2005). The examined simulation ranges are 5 – 40 atm, 0.001 – 0.0053 m³/s, 10 – 45 °C, and trace NDMA concentration to more than 1000 ng/L of operating pressure, feed flow rate, temperature, and concentration, respectively.

Table 6.5. Specifications of the spiral wound membrane element (Abbas 2005)

Make	Dow/FilmTec			
Membrane type and configuration	BW30-400, Spiral wound, Polyamide thin-			
Membrane type and configuration	film composite			
Hydraulic diameter of the feed spacer channel	8.126x10 ⁻⁴			
$d_{\rm h}$ (m)	0.120X1U ·			
Feed and permeate spacer thickness t_f (m)	5.93x10 ⁻⁴			
Effective membrane area A (m²)	37.2			
Membrane length L and width W (m)	1 and 37.2			
A _{w (To)} (m/ atm s) at 28.8 °C	9.5096x10 ⁻⁷			
B _{s(T_o)} (NDMA) (m/s) at 20 °C	5.35x10 ^{-6*}			
Mwt _{NDMA} (kg/kmol)	74.05			
Spacer type	(NALTEX-151-129)			
A' (dimensionless)	7.38			
n (dimensionless)	0.34			
ε (dimensionless)	0.9058			

^{*: (}Fujioka et al. 2014b)

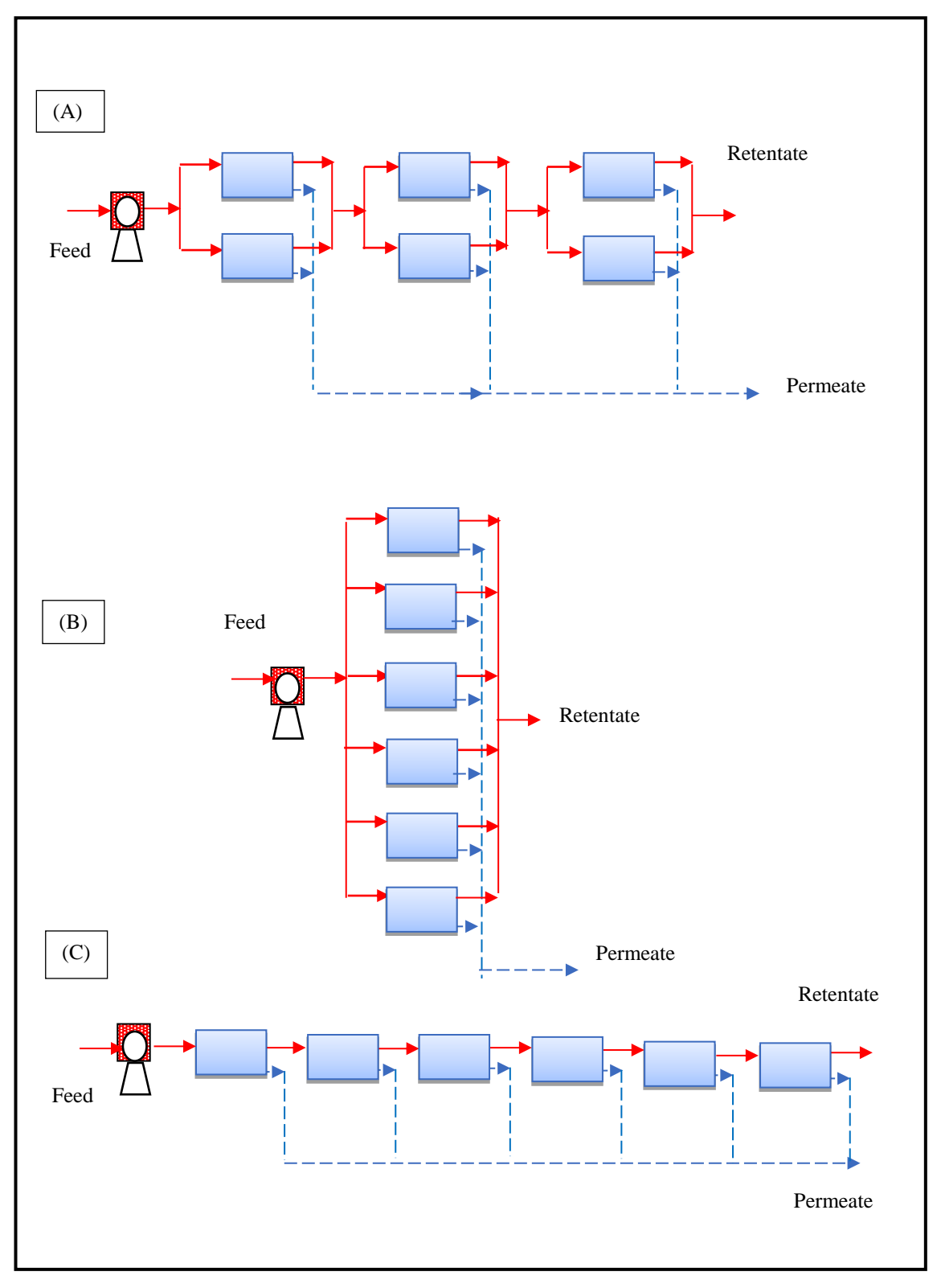


Fig. 6.10. The tested configurations of retentate reprocessing RO networks of six pressure vessels

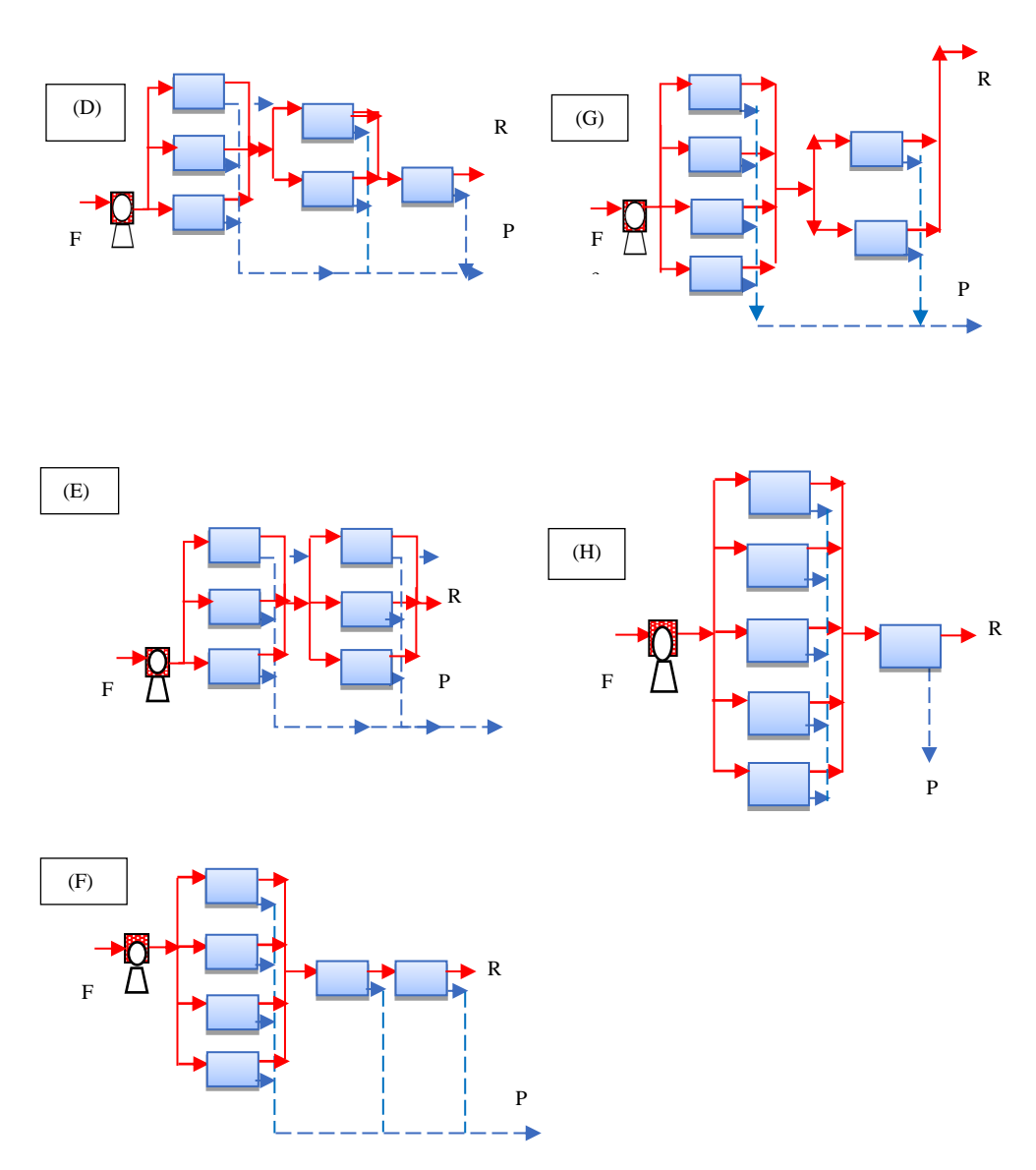


Fig. 6.11. The tested configurations of retentate reprocessing RO networks of six pressure vessels (F: Feed, P: permeate, R: Retentate)

6.3.2.1 Steady state simulation

In this section, the effect of six pressure vessel configurations shown in Figs. 6.10 and 6.11 on the NDMA rejection Rej_{plant} , total permeate recovery Rec_{plant} and total energy consumption E1 is analysed by simulation study. This is carried out

using the selected operating conditions of 1x10⁻⁶ kg/m³ (1000 ng/L), 13 atm, 8.9x10⁻³ m³/s, 25.3 °C of inlet feed concentration, pressure, flow rate, and temperature, respectively. In this respect, the Ministry of the Environment (MOE) of Ontario has regulated the allowable concentration of NDMA in drinking water at 9 ng/L (Ministry of the Environment of Ontario 2009). Najm and Trussell (2001) confirm that the NDMA formation can exceed 100 ng/L during chlorination of secondary wastewater effluent. However, wastewater and sewage water often contain significant concentrations of NDMA. The NDMA concentration of the samples collected from 20 sewage treatment plant is between non-detectable to 1000 ng/L (Krauss et al. 2009). Therefore, the author selected 1000 ng/L of NDMA concentration as it represents the maximum concentration that can be found in wastewater. Fujioka et al. (2014b) used approximately 250 ng/L as a feed concentration of NDMA in the experimental work of a pilot-scale RO plant of three stages connected in series. More recently, Fujioka et al. (2018) have used 1000 ng/L as NDMA concentration in the experiments of removal NDMA by modified three commercial RO membranes. Also, the RO process considering wastewater is usually working at the range of medium pressures between 10 to 20 atm and depending on the upper limit of the membrane module, which is already considered in this simulation. Srinivasan et al. (2009), Srinivasan et al. (2010), Srinivasan et al. (2011), Sundaramoorthy et al. (2011b) and Fujioka et al. (2014b) use the range of 5 to 15 atm for the removal of NDMA, chlorophenol, dimethylphenol and phenol from wastewater. It is noteworthy to mention that the analysis of the performance of these layouts using high membrane area of 37.2 m² has not been investigated in the literature. Table 6.6 summarises the simulation results of the selected configurations of multi-stage RO process.

Table 6.6. Simulation results of seventeen scenarios of retentate reprocessing RO networks

Scenario	Rej _{plant} (-)	Rec _{plant} (-)	E1 (kWh/m³)
Α	40.429	72.900	0.627
В	38.691	79.155	0.578
С	40.527	34.368	1.331
D	39.709	76.548	0.597
E	39.148	77.295	0.591
F	39.437	76.967	0.594
G	38.852	78.277	0.584
Н	38.743	78.698	0.581

6.3.3 Multi pass (permeate reprocessing) RO networks description

To overcome the problem of poor NDMA rejection presented in Table 6.6 of the analysed configurations shown in Figs. 6.10 and 6.11, the objective of this section is to use a permeate reprocessing technique that assumes the blending of the collected permeate of stage 1 and feed it to stage 2 and so on. The high-pressure retentate streams are blended from each stage and pass through ERD to pressurise the low-pressure permeate streams and then reject them out. This approach is pragmatic but reasonable since the flow rate of the blended permeate stream of stage 1 will be within the allowable limits of the feed flow rate of the membranes in stage 2. Fig. 6.12 shows a schematic diagram of three stages of the permeate reprocessing technique under investigation. The RO layout presented in Fig. 6.12 includes the energy recovery device ERD, which is required to transfer the pressure energy of high concentrated streams into the low-pressure permeate streams. The current model did not include any pumps, which are associated with high installation, operation, and maintenance costs. However, despite increasing the capital cost of treatment, it is expected that the power consumption of the multi-pass RO system will be reduced because of the energy recovery device ERD. To study the performance of permeate reprocessing design and to compare with other selected configurations of Figs. 6.10 and 6.11, the model of the new layout of permeate reprocessing technique has been simulated using the same operating conditions shown in Section 6.3.2.1. The final simulation results of Scenario I are shown in Table 6.7.

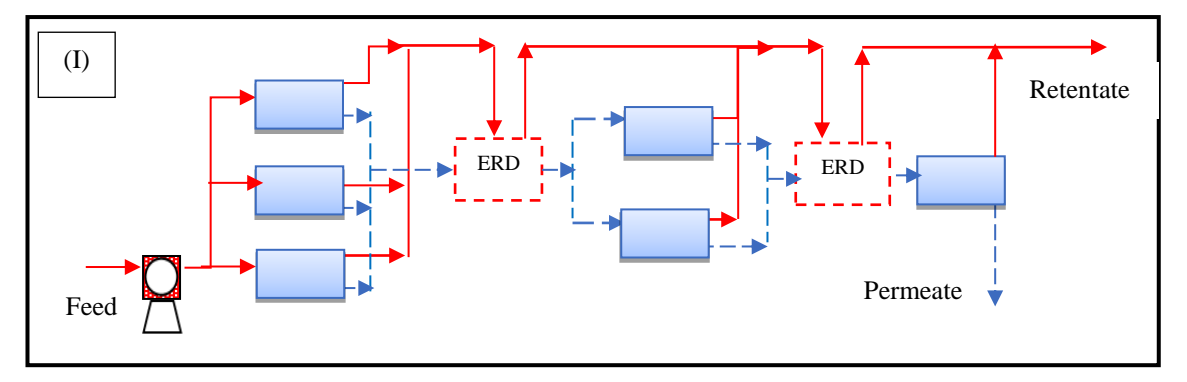


Fig. 6.12. Tested configuration of permeate reprocessing RO network of three stages

A close look at the results of Table 6.7 shows that a poor recovery rate of the proposed permeate reprocessing technique of Scenario I, and this can be considered as the main drawback of this design. The reason for this is the

disposing of the retentate streams of higher flow rate of the treatment system. It is noteworthy to mention that configuration G shown in (Fig. 6.11) has given one of the highest permeate recovery (Table 6.6), which has been selected for further validity and performance analysis of the permeate reprocessing design. The schematic diagram of permeate reprocessing of two stages of 4 and 2 parallel pressure vessels respectively can be found in Fig. 6.13 (Scenario J). Also, configurations K and L (Fig. 6.14) use both retentate and permeate reprocessing design. The three proposed configurations J, K and L are simulated using the same operating conditions mentioned in Section 6.3.2.1. The final simulation results are shown in Table 6.7.

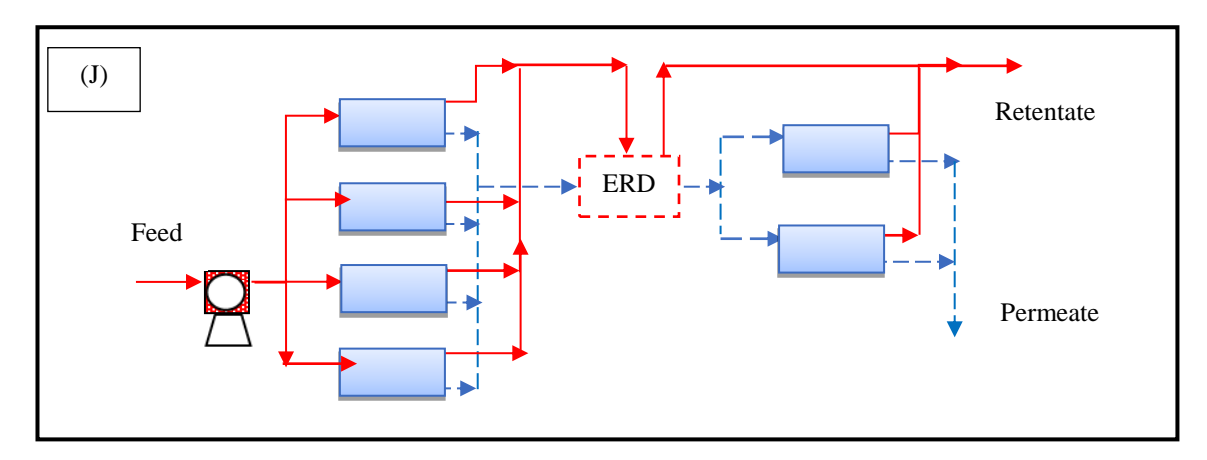


Fig. 6.13. Tested configuration of permeate reprocessing RO network of two stages

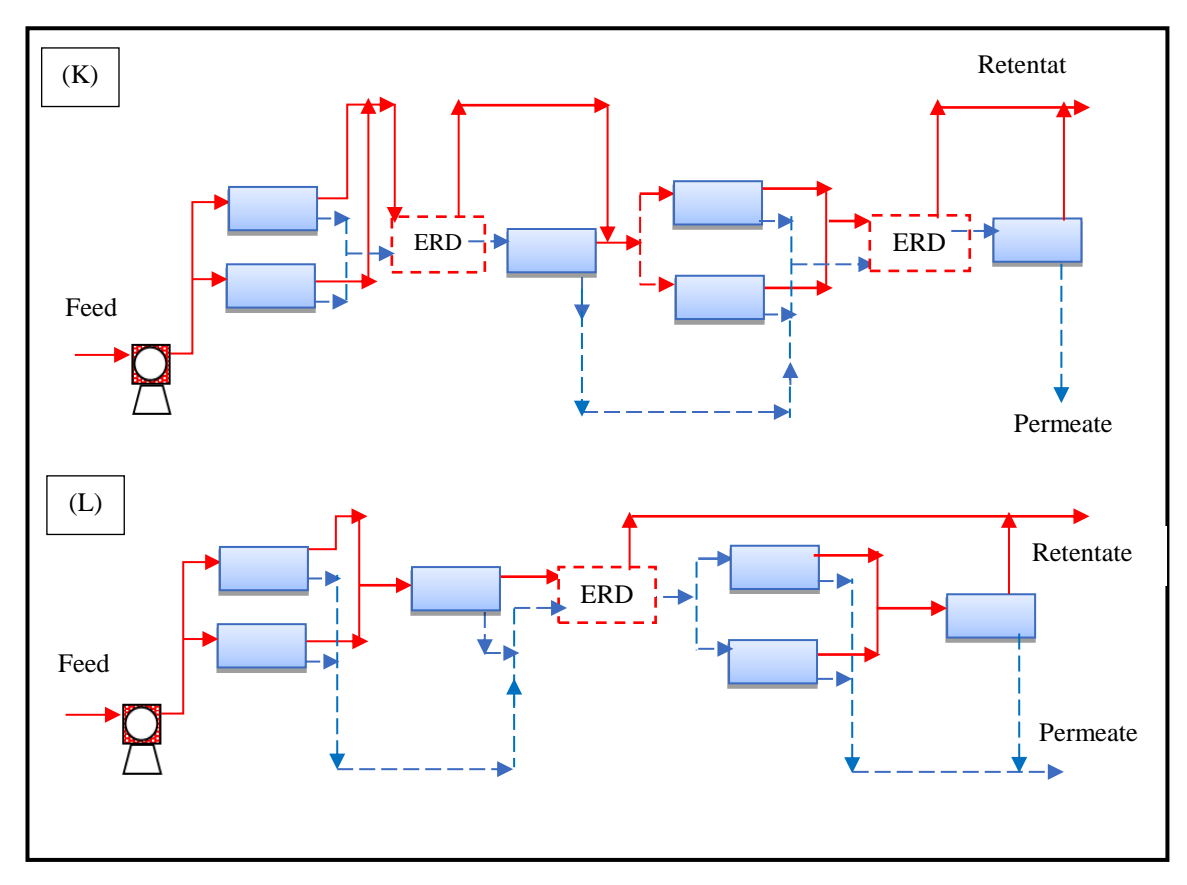


Fig. 6.14. Tested two configurations of retentate and permeate reprocessing RO network of four stages

Table 6.7. Simulation results of permeate reprocessing RO networks

Scenario	Rej _{plant} (-)	Rec _{plant} (-)	E2 (kWh/m³)
I	85.035	9.941	3.276
J	73.120	22.920	1.323
K	76.078	8.617	1.173
L	68.060	27.283	0.766

6.3.3.1 Discussion of multi-sage spiral wound RO process design performance

The evaluation of the performance of multi-stage RO process design is addressed in this section. Despite using the same operating conditions for testing the retentate reprocessing scenarios A to C, shown in Fig. 6.10 and D to H in Fig. 6.11, it is notable that the configurations tested have achieved NDMA rejection ranging between 38.69 and 40.52% (Table 6.6). The total recovery rate and energy consumption range between 34.3 and 79.15%, and 0.578 and 1.33 kWh/m³, respectively. However, configuration A is the optimal arrangement that show the best performance of NDMA rejection (Table 6.6). Configuration A has only two pressure vessels at the first stage, seemingly linked to higher performance of NDMA rejection. Nevertheless, the highest plant recovery and

lowest energy consumption result from using configurations G, H (Fig. 6.11) and B (Fig. 6.10). These configurations are designed with the high number of parallel pressure vessels at stage 1 compared to other configurations tested. This can be explained by the higher feed pressure implemented for each compartment, which lifts the water flux through the membrane and increases the total permeate recovery. It is noteworthy to mention that the recovery rate of these layouts positively increases as the number of pressure vessels of the first stage increases (Table 6.6). G, H (Fig. 6.11) and D (Fig. 6.10) configurations are based on a parallel connection of 4, 5 and 6 pressure vessels, respectively at the first stage. However, their performance of NDMA rejection yields one of the lowest scores. The main characteristic of this configuration is that the feed flow rate is immediately reduced for each compartment due to splitting it into a number of streams, which lowers the bulk velocity and the Reynold number. This is in turn reduces the mass transfer coefficient, which ultimately increases the accumulation of solute over the membrane and results in higher solute flux, which reduces the rejection parameter. Additionally, the series configuration C (Fig. 6.10) has the lowest total recovery and the highest energy consumption in comparison to other investigated layouts. This might be explained by the high feed flow rate, which is accompanied by a higher pressure drop and a lower permeate recovery, which in turn increase the total energy consumption. Fujioka et al. (2014b) tested the series superstructure of seven elements of membrane area of 7.9 m² and proved an abatement of NDMA removal. Table 6.6 shows that the design of one pressure vessel in the first stage yields a higher NDMA rejection, which is similar to those obtained for configurations C (Fig 6.10). This is because this configuration has the highest feed flow rate in the first stage, which corresponds to a higher turbulence in the feed channel and a lower concentration polarisation, which in turn increases NDMA rejection. The same findings are confirmed by Farhat et al. (2013) for the case of boron rejection. Among the evaluated configurations of Fig. 6.10, the permeate reprocessing design shown in Figs. 6.11 and 6.12 and the coupling permeate and retentate reprocessing design shown in Fig. 6.13 have undoubtedly a higher competitive design performance. However, the issue of lower permeate recovery of configuration I can be relatively solved by implementing the design of configuration J of permeate reprocessing design with four pressure vessels in stage 1, which in turn passively impacts on the rejection parameter and positively

reduces the energy consumption. Also, the results of the coupling of retentate and permeate reprocessing designs of Fig. 6.13 confirm its differentiated quality for the NDMA rejection indicators tested, in respect of, the total permeate recovery and energy consumption. Specifically, configuration K offers a higher rejection than configuration L. However, configuration L comes with higher recovery rate and lower energy consumption compared to configuration K. It is concluded therefore, that a permeate reprocessing design yields a lower permeate recovery. This implies further work to investigate a new design to resolve this issue by adjusting the removal of NDMA and lifting the total permeate

6.3.4 Predictive permeate reprocessing multi pass RO process design

recovery to the acceptable value of 40%.

The successive successful performance of the permeate reprocessing approach shown in Table 6.7 has provided a stimulus to select this technique for achieving higher NDMA rejection together with a feasible total permeate recovery. Thus, the objective of this section is to show the use of a simple predictive design of permeate reprocessing of multi-pass RO design (Scenario M) shown in Fig. 6.15, which can achieve this. A trial-and-error design method has been adopted to identify the best network and stream connections considering the permeate reprocessing. In the current work, a multi-stage superstructure of twelve pressure vessels, two pumps and three energy recovery devices were adopted as can be shown in Fig. 6.15. The restriction of lower and upper limits of operating parameters of feed flow rate and feed pressure for each membrane element has been mainly considered along the design of this network. Therefore, stages S1, S2, S5 and S6 have three membrane elements connected in series for each pressure vessel, while stages S3 and S4 contain only one element for each pressure vessel. The idea behind the second pump is to feed the collected permeate of stage 2 to stage 5 with high feed pressure for ultra-filtration purposes. However, the retentate stream of stage 2 is fed directly to stage 3 to overcome the problem of low recovery rate. Moreover, the use of an energy recovery device is to ensure the transferring of potential energy from the highpressure side to the low-pressure side considering the efficiency of the ERD. The simulation of the proposed network design shown in Fig. 6.15 is conducted

using the same operating condition given in Section 6.3.2.1. The simulation

by acquiring 11.172% and 3.19 kWh/m³ as total permeate recovery and energy consumption, respectively. It is worthy to mention that the two pumps of configuration M are working on a similar operating pressure of 13 atm along this simulation.

It is clearly recognised that the recovery rate of the new proposed configuration of permeate reprocessing is still in issue of this design, which is occurring as a result of several permeate reprocessing steps. However, the result of NDMA rejection is comparable with the findings of the previous configurations tested. Also, the effectiveness of the permeate reprocessing technique has confirmed the significance of employing this method to meet high NDMA rejection. Moreover, there is a capacity now for optimising the process to acquire the preferable permeate recovery of 40% under lower total energy consumption. This is dealt with in the next section.

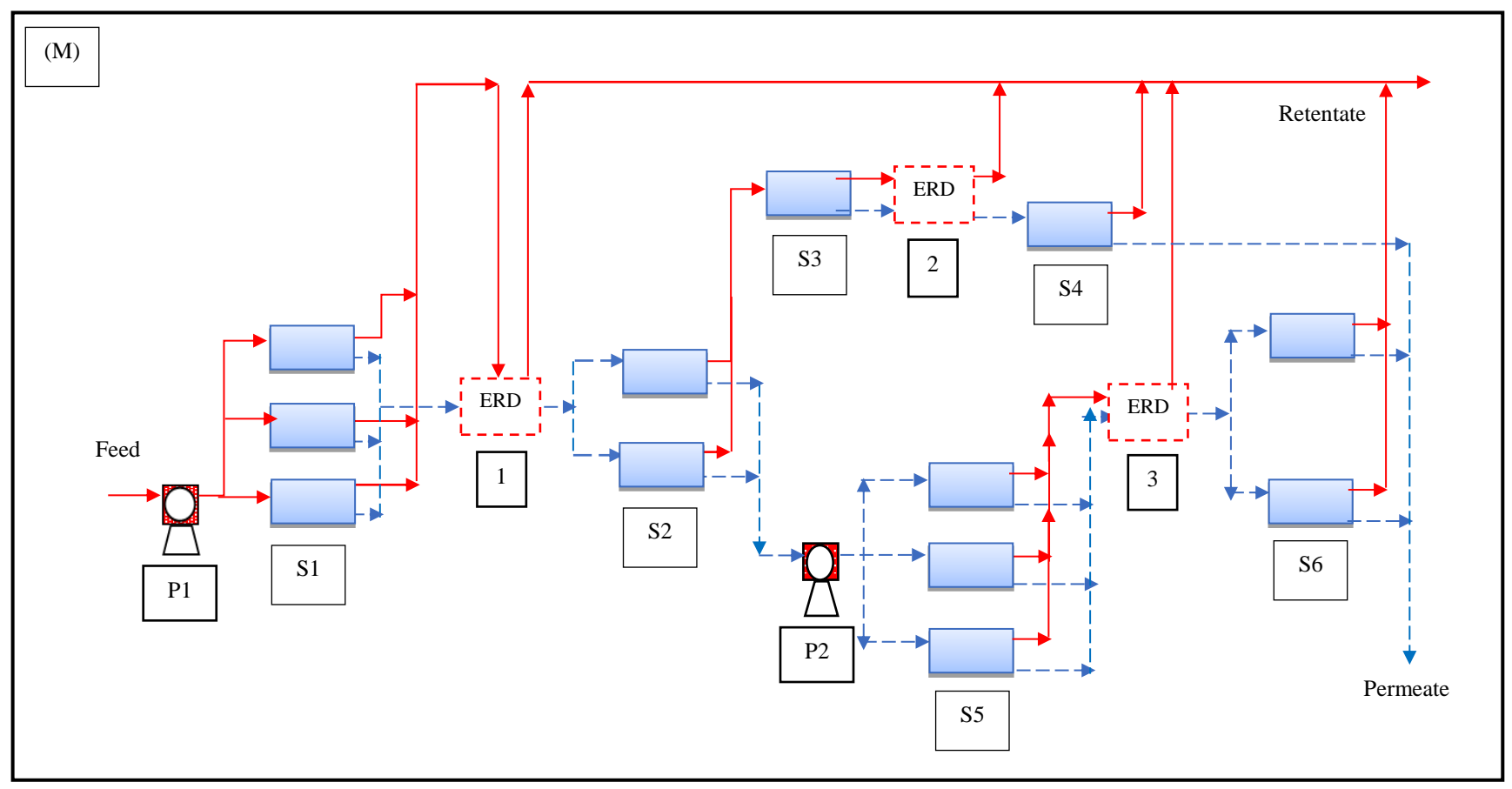


Fig. 6.15. Six stages RO network with permeate reprocessing, P: Pump, S: Stage, ERD: Energy recovery device

6.3.5 Optimisation of predictive multi pass permeate reprocessing RO process design

The optimisation of the permeate reprocessing design of multi-pass RO process shown in Fig. 6.15 is carried out using the gPROMS software.

6.3.5.1 Problem description and formulation

The objective of this section is to find optimum operating conditions of the plant shown in Fig. 6.15 for NDMA rejection, total permeate recovery and total energy consumption. Therefore, the optimisation problem is to maximise the NDMA rejection under the feasible recovery rate of 40% for the predictive design of permeate reprocessing of Fig. 6.15, by allowing the system operating conditions of the plant $(Q_{f(plant)}, P_{f(in)(plant)}, P_{f(in)(S5)})$ and $T_{b(plant)}$ to vary within the constraints of upper and lower limits. Specifically, the inlet feed flow rate of the plant $Q_{f(plant)}$ was established within the minimum and the maximum sum of three elements connected in a parallel configuration. Moreover, the optimisation problem has considered the manufacturer's specification of each single spiral wound RO membrane element in the proposed network and reported in Table 6.8, which offer the maximum and minimum practical bounds of operating conditions including; inlet feed pressure $P_{b(in)}$ and feed flow rate Q_f . These constraints provide a safe operation of the RO process. A range of 20 to 30 °C was considered as the upper and lower limits of inlet feed temperature T_{b(plant)} without considering the higher limit of 45 °C (case 1). This choice is quite acceptable for a steady-state operation of the RO system and elucidated a longlife of the membranes. Also, a constraint of 0.987 atm has been set as a maximum allowable pressure drop ΔP_{drop} (atm) along each membrane element commensurate with the supplier's specifications. The optimisation is investigated for inlet high feed concentration of 1000 ng/L, which is equivalent to 1x10⁻⁶ kg/m³ of NDMA. Also, the optimisation problem is formulated as a Non-Linear Programming (NLP) problem with process and module constraints. To examine the viability of the proposed configuration, a maximum value of 40% of total permeate recovery $\operatorname{Rec}_{(\operatorname{plant})}$ has been chosen as a stringent limit of optimisation problem to avoid increased energy consumption considering the technical specification and capacity of seawater reverse osmosis desalination plant (Peñate et al. 2011). In other words, several researchers show the feasibility of 40% of total water recovery as an effective operational strategy for the RO seawater desalination plants (Loutatidou et al. 2017). Therefore, this value has been taken to consider high quality of total recovery for such small size of wastewater RO plant, which implemented multi-pass RO design. This type of design promotes the removal of pollutants on the penalty of losing the permeate recovery. Also, it should be noted that the used membrane (BW30-400), which is already used in Brackish water desalination, can resist a total of operating pressure of 40.4 atm (Abbas 2005). This is compared to what can be seen in seawater desalination RO process where the operating pressure exceeds 79 atm (Ghobeity and Mitsos 2010). The total energy consumption E2 was constrained with a maximum of 3 kWh/m³ to ensure lower energy consumption. Occasionally, large scale seawater RO plants have an energy consumption of roughly 3.5 kWh/m³ (Wei and McGovern 2017). Therefore, the optimisation problem of the RO process with permeate reprocessing is addressed in this work as described below:

Given: Operating feed conditions, module specifications.

Optimise: Inlet feed pressure, flow rate, temperature, and inlet feed pressure of stage 5 (the optimisation variables).

Maximise: NDMA rejection.

Subject to: Equality (process model) and inequality constraints (linear bounds of optimisation variables).

Precisely, the optimisation problem is mathematically represented as follows:

 $Q_{f(plant)}$, $P_{f(in)(plant)}$, $P_{f(in)(S5)}$, $T_{b(plant)}$ Subject to:

Equality constraints:

Process Model
$$f(x, u, v) = 0$$

Inequality constraints of the plant:

$$\begin{aligned} &Q_{f(plant)}^{\ L} \leq \ Q_{f(plant)} \leq \ Q_{f(plant)}^{\ U} \\ &P_{f(in)(plant)}^{\ L} \leq \ P_{f(in)(plant)} \leq \ P_{f(in)(plant)}^{\ U} \\ &P_{f(in)(S5)}^{\ L} \leq \ P_{f(in)(S5)} \leq \ P_{f(in)(S5)}^{\ U} \\ &T_{b(plant)}^{\ L} \leq \ T_{b(plant)} \leq \ T_{b(plant)}^{\ U} \end{aligned}$$

Inequality constraints of the element:

$$\begin{aligned} Q_f^L &\leq Q_f \leq Q_f^U \\ P_{f(in)}^L &\leq P_{f(in)} \leq P_{f(in)}^U \\ T_b^L &\leq T_b^L \leq T_b^U \\ \Delta P_{drop} &\leq 0.987 \\ Rec_{(plant)} &\geq 40\% \\ E2 &< 3.0 \end{aligned}$$

The optimisation results of case 1 shows an energy consumption of 2.664 kWh/m³ (Table 6.9). Therefore, the sensitivity of optimisation technique will be subjected to the highest supplier's limit of feed temperature of 45 °C and a new constraint of energy consumption of lower than 2.664 kWh/m³ to investigate its impact on the plant performance (case 2). Therefore, the optimisation limits of operating temperature are amended, and the energy consumption constraint is added as follows:

Table 6.8. The limits of operation of the spiral-wound membrane element (Abbas 2005)

Parameter	Value
Max. feed flow rate Q _f (m³/s)	5.363x10 ⁻³
Min. feed flow rate Q _f (m³/s)	1.008x10 ⁻³
Max. operating temperature T (°C) of case 1	30
Max. operating temperature T (°C) of case 2	45
Max. operating pressure $P_{f(in)(plant)}$ (atm)	40.463
Max. pressure drop ΔP_{drop} (atm)	0.987

6.3.5.2 Optimisation results of predictive multi pass permeate reprocessing spiral wound RO design

The optimisation results of configuration M regarding the optimisation cases 1 and 2 are shown in Table 6.9. It is noticeable that the proposed configuration can offer higher NDMA rejection $\text{Rej}_{(\text{NDMA})}$ of 92.487% in case 1 together with by 40% and 2.664 kWh/m³ of total permeate recovery rate $\text{Rec}_{(\text{plant})}$ and energy consumption E2, respectively, compared to all configurations tested and shown in Figs. 6.10, 6.11, 6.12 and 6.13. Interestingly, this offers a permeate concentration of only 75 ng/L (Table 6.9), which is within the restricted limits of 100 ng/L of WHO (WHO, 2008). However, the impact of feed temperature can be shown in case 2 (A and B), which illustrated two competing options of optimum

operating conditions and shows fairly similar NDMA rejection at lower energy consumption than in case 1. This behaviour can be ascribed to the fact that the operating plant temperature has a considerable impact on both permeate $A_{w(T)}$ and NDMA $B_{s(T)}$ permeability constants of the membrane as illustrated in Egs. (6.2) and (6.3), respectively. Increasing the feed temperature to 36 and 41.633 °C will increase the water permeability constant and decrease the viscosity of water, which in turn increase the amount of water that pass through the membrane, which ultimately results in reducing the energy consumption. However, increasing the feed temperature to 36 °C causes an increase in the NDMA flux through the membrane caused by the thermodynamic increase in the NDMA osmotic pressure as a result to an increase in the NDMA permeability constant, which reduces the rejection parameter to 92.375% (permeate concentration=76 ng/L). The same findings are confirmed by Farhat et al. (2013) where the boron rejection decreases as the feed temperature increased. Also, it seems that expanding the optimisation limit of the operating temperature to 45 °C and introducing a new constraint of energy consumption of less than 2.664 kWh/m³ causes a selection of a higher feed temperature of 36 °C in case 2A, which requires an adjustment for both the operating pressures of the plant and stage 5 as well as the inlet feed flow rate to keep a constraint of 40% total recovery rate as a constraint. As a result, an increase of the feed pressure of stage 5 is mandatory to guarantee a sufficient driving force for permeate flux to maintain 40% total recovery, especially after increasing the operating feed flow rate, which causes a higher pressure drop due to a higher friction along the membrane length. Specifically, an increase in the inlet feed flow rate causes a decrease in the water flux and total permeate recovery, which negatively impacts the removal of NDMA to 92.375%.

In contrast, increasing the operating feed temperature to 41.633 °C in case 2B causes an increase in the mass transfer coefficient, which increases the rejection parameter to 93.11% (permeate concentration=69 ng/L) by reducing the concentration polarisation impact. However, the optimisation process has resulted in an increase of the inlet feed flow rate in a way to maintain the total recovery of 40% and keep the consumption of energy lower than 2.664 kWh/m³, and this has a positive impact on the rejection parameter. It can be argued therefore that the adapted design is a more effective technique for NDMA

removal, which meets both the satisfactory recovery rate and energy consumption.

More importantly, the optimised results shown in Table 6.9 is so promising especially after the experimental research that has been done by Fujioka et al. (2018). This research has improved the NDMA removal from wastewater to 92% after using a complex heat treatment method on the prototype RO membrane. However, this result is commensurate with a reduction of water permeability constant in the range between 21 to 31%, which shows very low recovery rate.

The decision variables E2 Rec_(plant) Rej_(NDMA) Case $T_{b(plant)}$ $Q_{f(plant)}$ $P_{f(in)(plant)}$ $P_{f(in)(S5)}$ (kWh/m^3) (-) (-) (m³/s) x10³ (atm) (atm) (°C) 7.9526 23.504 40.463 30.000 40.000 92.487 1 2.664 8.4510 22.201 38.109 36.000 40.000 92.375 2.500 Α 2 В 9.8887 23.390 40.033 41.633 40.001 93.110 2.612

Table 6.9. Optimisation results of configuration U

6.4 Conclusions

N-nitrosamine can contribute to several public health impacts of human carcinogens even at very low concentration. In this chapter, the removal of N-nitrosamine compounds from wastewater is considered using an experimental RO process considered in the literature. The impact of different operating parameters such as inlet feed pressure, flow rate and temperature on the rejection of N-nitrosamine compounds is investigated in detail using modelling and simulation. A number of energy recovery options have also been considered on the process and the impact of different operating parameters on the energy consumption is evaluated.

Having developed clear understandings of the impact of a number of operating parameters on the rejection of N-nitrosamine compounds and the energy consumption via sensitivity analysis (varying one parameter at a time), it was decided to simultaneously optimise these parameters to either maximise the rejections or minimise the energy consumption of the process. The optimisation results clearly show that rejection of some of the compounds can be improved by more than 27% and energy consumption can be minimised by more than 70%. Specifically, NDMA rejection is improved from 62.7% to 80%. Also, the energy

consumption is improved from 4.48 to 1.1 kWh/m³ at the optimised operating conditions.

Secondly, Different configurations multi-stage wastewater retentate reprocessing RO systems have been proposed and evaluated in terms of plant performances including; NDMA removal, total permeate recovery and energy consumption considering model-based approach. In order to further improve the performance of the initial configurations presented, a smart permeate reprocessing technique has been developed for removing NDMA from wastewater and validated. An associated simulation study has also been implemented and achieved similar operating conditions. It has enabled the assessment of the performance of both retentate and permeate reprocessing designs and confirmed the significance of lower NDMA rejection of retentate design. The research results clearly show that the proposed adaptive RO design with permeate reprocessing was able to solve this issue and with no doubt lead the way for further studies to achieve the full removal (zero discharge) of NDMA. The technique developed includes a novel design for the removal of NDMA from wastewater in a multi-stage reverse osmosis process. This design has been compared with a variety of configurations and confirmed its validity of higher performance based on three tested indicators. The results readily confirm that the proposed design is suitable for removing this carcinogenic compound for water reuse. Specifically, it has been found that the RO permeate reprocessing design process can significantly enhance the removal of NDMA from wastewater. Also, the optimisation of the proposed design yields a competitive value of 92.487% rejection and a practicable permeate recovery of 40% at an all-time low 2.664 kWh/m³ total energy consumption. Interestingly, with the inlet feed concentration of 1000 ng/L, the proposed RO configuration can reduce the permeate concentration to lower than the restricted limits of 100 ng/L of WHO. This is compared to the maximum NDMA rejection of 92% at a considerable reduction of water transport parameter of 21 to 31% for several tested membrane types as a result to the use of heat treatment method on the membrane tested (Fujioka et al., 2018).

Chapter 7

Simultaneous Removal of Organic and Non-organic Compounds from Wastewater Using RO Process: Modelling, Simulation, and Optimisation

7.1 Introduction

The modern industrialized world is generating a huge amount of wastewater containing a variety of micro-pollutants, which is discharged into rivers and oceans leading to disruption of the biological ecosystem. Therefore, the recovery of these compounds from industrial effluents is highly important. The RO process is one of the most promising technologies to produce high-quality recycling water at a reasonable cost. However, the literature has a deficiency of a computational distributed model for designing the multi-component wastewater specifically for the spiral wound RO process. This chapter uses Model Type_3 (described in Section 3.2.1.4 in Chapter 3) to predict the performance of the RO process for the removal of several organic and non-organic compounds from wastewater simultaneously. In this respect, five organic compounds and three inorganic species are assumed to be in the wastewater. The simulation of the multicomponent wastewater process is carried out for the simple design of an individual RO process. The realistic operating conditions ensuring high rejection of multi-compounds are explored via the simulation of the RO process first. This is followed by embedding the model in a multi-objective optimisation framework to simultaneously maximise the rejection and the total permeate recovery. This is carried out by optimising the operating conditions of the process, while maximising the rejection and permeate recovery. This in turn made a significant reduction of the possibility of unintentional release of the destructive compounds into the recycled water.

7.2 Specification of multi component

Five organic compounds of chlorophenol, dimethylphenol, phenol, methyl orange dye and aniline and three inorganic species of ammonium, cyanide, and sulphate in the range from 18 to 327 of molecular weight were selected to form the proposed wastewater. The transport parameters of the selected compounds were gathered from the literature and given in Table 7.1. It is noteworthy to mention that the transport parameters of the selected compounds (phenol to aniline) are

experimentally determined for different types of spiral wound membrane modules as given in Table 7.1. However, all the membranes are made as thin film composite TFC polyamide membranes.

Table 7.1. Physical and transport parameters of the eight selected organic and non-organic compounds

Compound	Chemical structure	Molecular weight (g/mol)	Membrane type, manufacturer	Reference	
Dimethylphenol	C ₈ H ₁₀ O	122.167	Ion Exchange, India	Srinivasan et al. (2011)	
Chlorophenol	C ₆ H₅CIO	128.60	Ion Exchange, India	Sundaramoorthy et al. (2011)	
Phenol	C ₆ H ₆ O	94.111	Permionics, Vadodara, India	Srinivasan et al. (2010)	
Methyl orange dye	C ₁₄ H ₁₄ N ₃ NaO ₃ S	327.34	FilmTec SW30	Al-Bastaki (2004)	
Aniline	C ₆ H ₅ NH ₂	93.19	Desalination System Inc. DESAL-3B	Hidalgo et al. (2014)	
Ammonium	NH ₄	18.04	Osmonics, SEPA- SSIC	Bódalo et al. (2005)	
Cyanide	CN-	26.02	Desalination System Inc. DESAL-3	Bódalo et al. (2004)	
Sulphate	SO ₄₋₂	96.06	Osmonics, SEPA- SSIC	Bódalo et al. (2003)	

7.3 Process simulation: Effect of operating parameters

Fig. 7.1 shows the variation of feed pressure, osmotic pressure, and water flux along the membrane length (x-axis). The feed pressure decreases along the x-axis due to pressure drop caused by the friction. This in turn reduces the water flux as a result of decreasing diving force. An increase of total osmotic pressure along the x-axis is noticed due to increasing accumulated concentration of the solutes at the membrane wall.

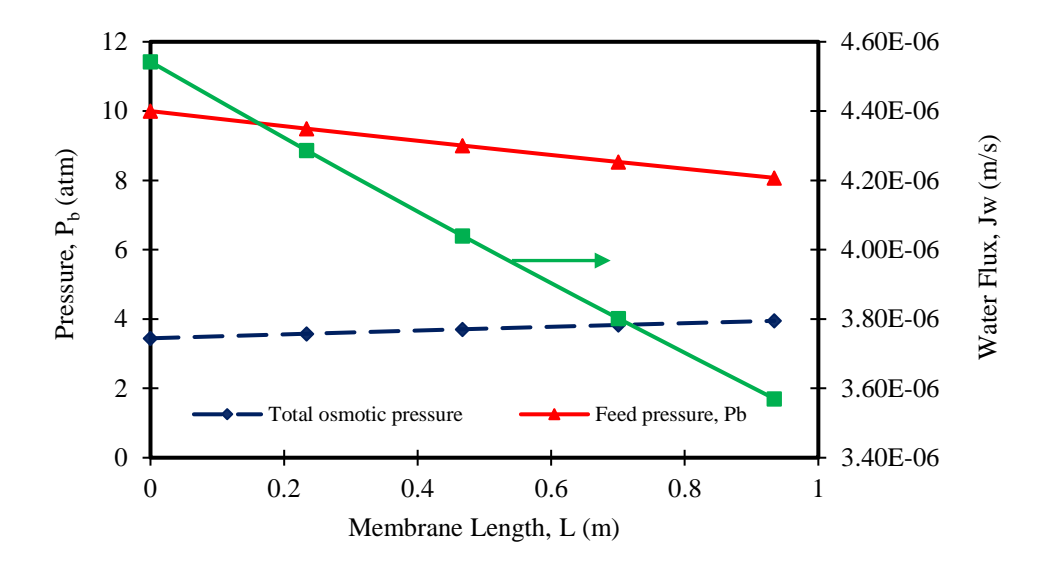


Fig. 7.1. The variation of operating parameters along the membrane length

The variation of feed concentration of the pollutants found in wastewater is expected. Therefore, the RO process performance is investigated using a range (350 to 500 ppm) of each pollutant concentration carried out at fixed feed flow rate, pressure, and temperature of 2.583x10⁻⁴ m³/s, 10 atm, and 30 °C, respectively. The selected operating parameters are within the selected membrane manufacturer specification. The considered limit of each pollutant concentration was taken regarding the highest pollutant concentration of the effluent line of copper electroplating factory in Hong Kong where it consists of 340 ppm of copper sulfate (Xijun et al. 1997). Fig. 7.2 shows the effect of increasing feed concentration of each component on the rejection and total permeate recovery. In the selected range of feed concentration, there was no considerable effect on the rejection. However, increasing the feed concentration of all the components causes a continuous reduction in permeate recovery due to increased osmotic pressure.

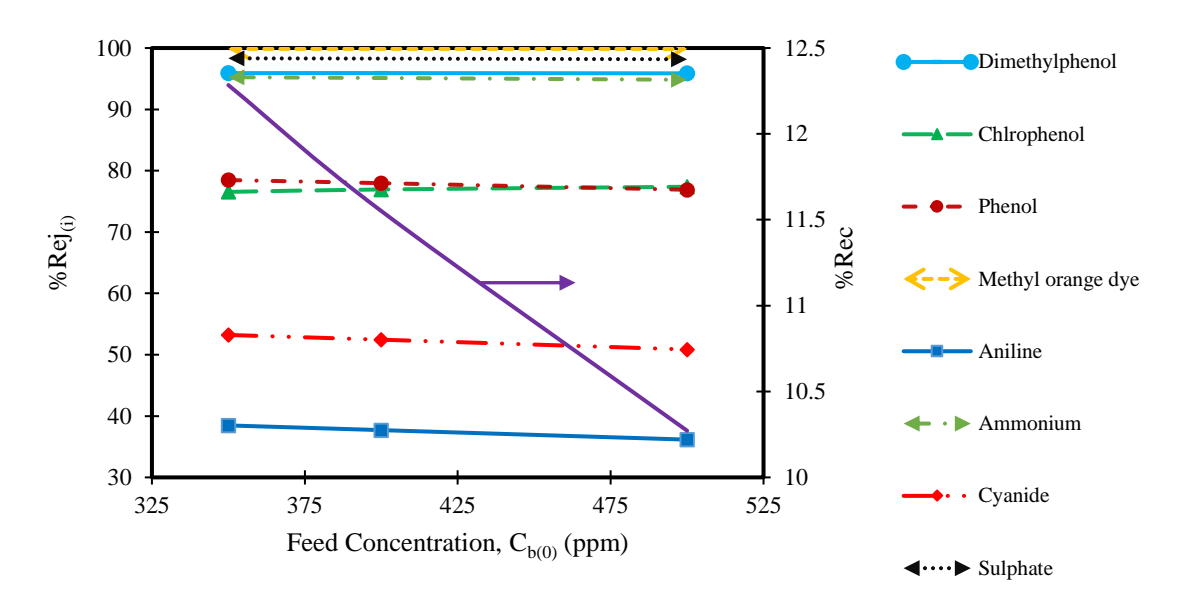


Fig. 7.2. Effect of compound concentration on rejection and recovery rate (operating conditions: 2.583x10⁻⁴ m³/s, 10 atm, and 30 °C)

Fig. 7.3 shows the impact of temperature on the removal of all compounds and permeate recovery. The simulation is carried out at fixed feed flow rate, pressure, and concentration of 2.583x10⁻⁴ m³/s, 10 atm, and 350 ppm, respectively. Specifically, Fig. 7.3 shows a positive impact of operating temperature on the removal of all compounds and permeate recovery. Increasing temperature causes more flexibility of membrane chains resulting in increasing convective transport by elevating the water flux. Also, it is noticed that diffusion transport increases due to increase in temperature, which is accompanied by a continuous reduction of average density and viscosity of the mixture.

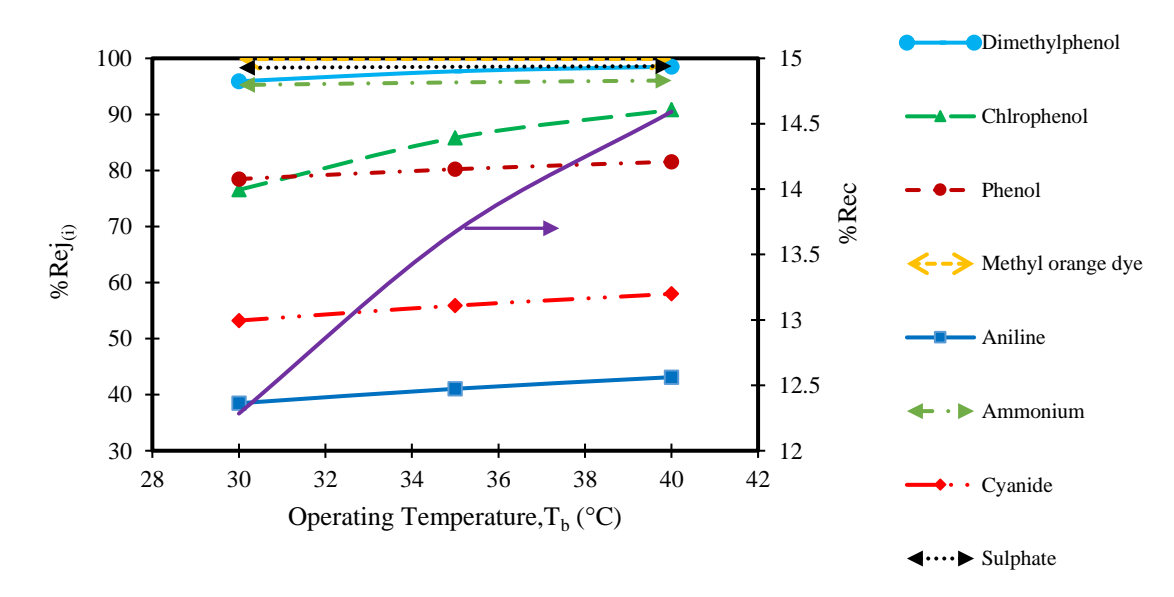


Fig. 7.3. Effect of operating temperature on rejection and recovery rate (operating conditions: 2.583x10⁻⁴ m³/s, 10 atm, and 350 ppm)

The effect of inlet feed pressure on the compounds rejection, while other variables remain constant can be distinguished through the simulation study shown in Fig. 7.4. Increasing the pressure from 10 to 20 atm causes an increase in the rejection due to increase in water flux, which dilutes the permeate. However, it seems that there is an optimum pressure, which would maximise rejection of some of compounds.

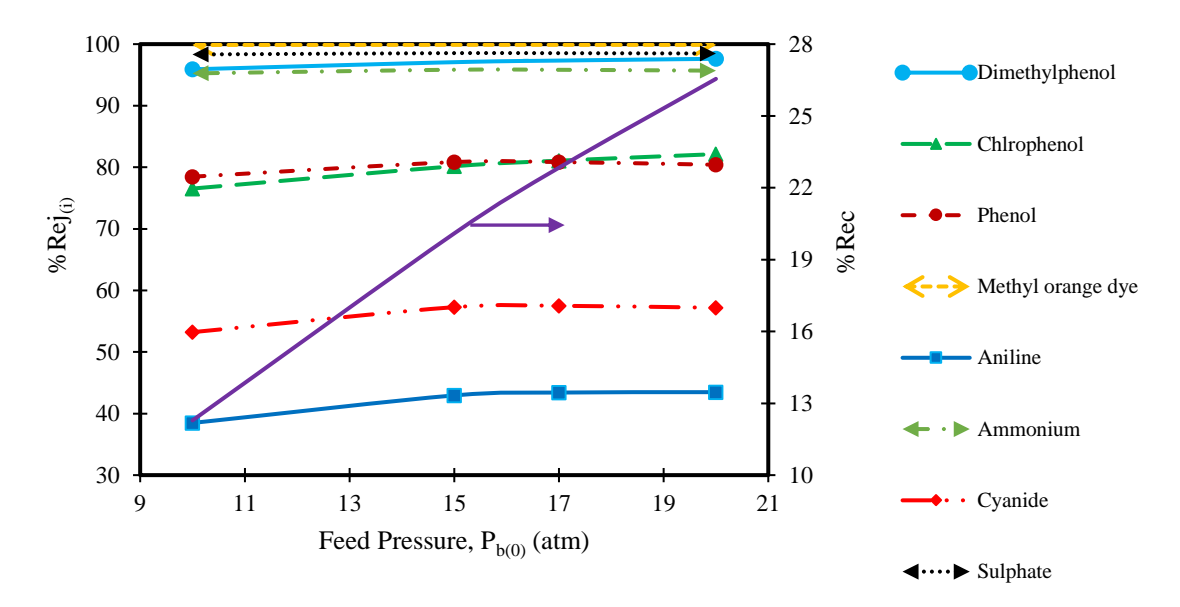


Fig. 7.4. Operating pressure verses rejection and recovery rate (operating conditions: 2.583x10⁻¹ m³/s, 30 °C, 350 ppm)

The impact of inlet feed flow rate at fixed feed pressure, concentration and temperature on the components removal and permeate recovery is shown in Fig. 7.5. The increase of feed flow rate from 2x10⁻⁴ to 2.583x10⁻⁴ m³/s causes a little increase in the rejection parameter but a remarkable decrease in permeate recovery. Increasing the feed flow rate causes a reduction in the osmotic pressure as a result of decreasing the membrane wall concentration. Increasing the feed flow rate from 2.583x10⁻⁴ to 3x10⁻⁴ m³/s causes a little decrease in rejection and steady decrease in the permeate recovery. The reduction of permeate flux is due to reduction of wastewater residence time inside the module. In this respect, it was found that a maximum recovery can be achieved at low inlet feed flow rate. This is due to decreasing the pressure drop at the feed channel as result to decreasing the operating feed flow rate.

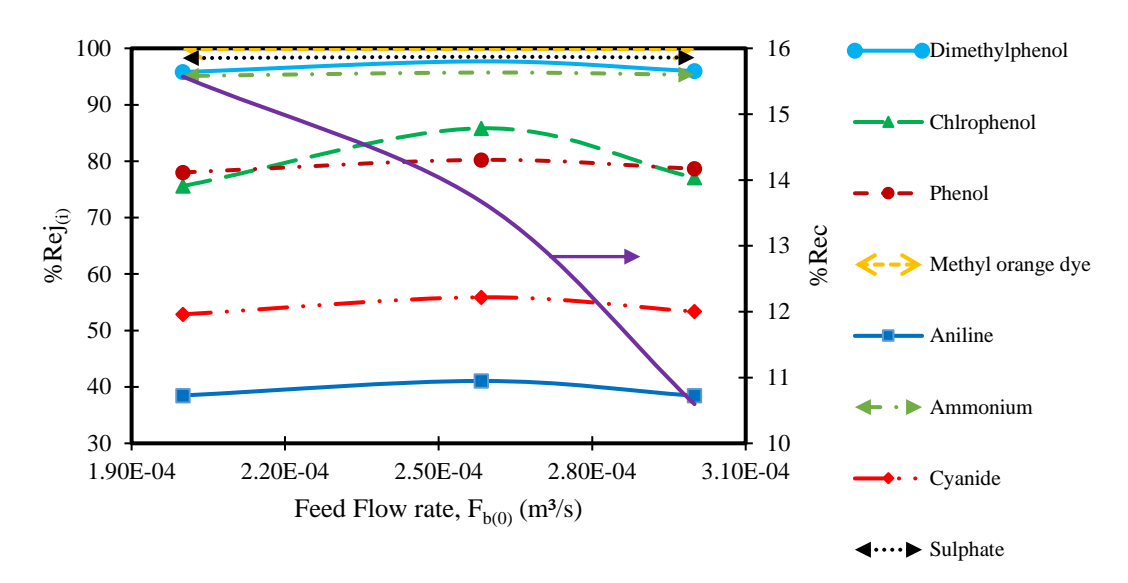


Fig. 7.5. Effect of operating feed flow rate on rejection and recovery rate (operating conditions: 10 atm, 30 °C, 350 ppm)

The simulation results show that both the operating temperature and pressure have the highest impact on the rejection and recovery parameters compared to feed flow rate and concentration. Moreover, the feed concentration and flow rate have a passive impact on recovery rate.

7.4 Process optimisation

This section deals with the multi-objective optimisation of operating conditions include the feed flow rate, pressure, and temperature at fixed feed concentration of 350 ppm for each component presented in Table 7.1. The optimisation approach will be carried out using the optimisation tool of gPROMS software to simultaneously maximise both the rejection of all components and permeate recovery based on the model equations and the upper and lower limits of the decision variables, which are reported in the mathematical optimisation expression and readily gathered from the membrane specification. The multi-objective function is presented in the following;

$$\begin{array}{ll} \text{Max} & \textit{Rej}_{(i)}, \textit{REC} \\ P_{b(0)}, F_{b(0)}, T_b \\ \text{Subject to: } \textit{Equality constraints:} \\ & \textit{Process Model:} & \textit{f(x, u, v)} = 0 \\ & \textit{Inequality constraints:} & 5 \text{ atm} \leq P_{b(0)} \leq 20 \text{ atm} \\ & 1x10^{-4} \ \frac{m^3}{s} \leq F_{b(0)} \leq 1x10^{-3} \ \frac{m^3}{s} \\ & 30 \ ^{\circ}\text{C} \leq T_b \leq 40 \ ^{\circ}\text{C} \end{array}$$

The optimal values of feed flow rate, pressure, and temperature are 7.4515×10^{-4} m³/s, 20 atm and 40 °C, respectively. The maximum permeate recovery is found to be 13.54%, while the maximum rejection of the compounds are: <Dimethylphenol, Chlorophenol, Phenol, Methyl orange dye, Aniline, Ammonium, Cyanide, Sulphate> = < 99.269, 94.922, 86.477, 99.923, 51.430, 97.253, 66.252, 99.045>. The optimisation leads to an increased rejection of all the selected components compared to what have been presented in Figs. 7.2 - 7.5. However, the low value of recovery is due to the impact of osmotic pressure of eight compounds at the same concentration of 350 ppm and accordingly reflects the performance of a single RO membrane module, which is not comparable with multi-stage RO performance.

7.5 Conclusions

The impact of operating conditions on the rejection of several organic and nonorganic compounds from wastewater and permeate recovery is evaluated using
a new one-dimensional model developed for a spiral wound RO process. The
simulation results confirmed the importance of feed pressure and temperature to
drive high performance of RO process. Finally, the multi-objective optimisation
problem finds the maximum values of the rejection of all the compounds and
permeate recovery. More importantly, the multi-objective optimisation platform
has increased the rejection of all the components at a maximum rejection of
11.865%.

The methodology presented in this research can be served as an adequate method for water treatment approaches based on the RO process in the aid to produce good quality water for several industries.

Chapter 8

Applications of Spiral Wound Reverse Osmosis for the Apple Juice Concentration: Simulation, and Optimisation

8.1 Introduction

The use of RO membrane processes for the concentration of apple juice is proposed as an alternative to the conventional concentration technique, which is based on evaporation and freezing. This is because of a significant advance in membrane technology, requirements for low energy and cost, and effective retention of aroma components. There does not appear to be a widespread agreement on the mechanisms of water and solute transport through RO membrane for aqueous solutes (Girard et al. 2000b). However, the most accepted approaches in this respect are the solution diffusion and preferential sorption theories. The first theory assumes that solvent and solute dissolve in the membrane and pass through by diffusion, while the second theory assumes that solvent and solute are adsorbed at the membrane surface and then pass through the membrane pores.

This chapter focuses on highlighting the following cases:

- to analyse the performance of membrane rejection at different concentrations, temperatures, and pressures for a laboratory scale of a spiral wound RO module based an apple juice concentration.
- to examine the capacity of different RO networks configurations for apple juice concentration and explore the best configuration that commensurate with maximising apple juice concentration using an enhanced optimisation technique.

8.2 Case 1: Analysis the apple juice concentration using a spiral wound RO process

A solution treated by RO in food industries is considered as a multi-component solution, which contains a number of solutes at different concentrations. Specifically, apple juice comprises two groups of organic compounds; sugar and aroma compounds, which are categorized as esters (the main compound), aldehydes and alcohols. Also, aroma is one of the most appreciated fresh fruit juice flavor characteristics and is of great importance by consumers. Aroma is due to many volatile organic compounds present in different concentrations,

which play a key role in customer perception and satisfaction (Cheong et al. 2010).

The 1D Model Type_6 developed (described in Section 3.6.1.1 in Chapter 3) was used to analyse the permeate flux and the performance of membrane rejection at different concentrations, temperatures, flow rate, and pressures for a laboratory scale of a spiral wound RO module.

8.2.1 Impact of operating parameters

The expectation that increasing inlet feed temperature would increase the solute rejection is validated here as it decreases the viscosity of apple juice. This accelerates the flux of water through the membrane and reduces the concentration polarisation impact. Interestingly, Fig. 3.6 in Chapter 3 shows a slight reduction of Isopentyl acetate and trans-2-hexanal rejections with operating temperature for different inlet feed flow rates. The probable explanation for this can be that by increasing the feed temperature, the solute concentration over the membrane wall will increase and causes an increase in solute flux accompanied by the penetrated water that causes an increase in the permeate solute concentration at the permeate channel. As a result, the solute rejection will decrease as expressed in Eq. (M.6.39) in Chapter 3.

To illustrate the impact of operating trans-membrane pressure and inlet feed flow rate on solute rejection, Fig. 3.7 in Chapter 3 shows the variation of Isopentyl acetate rejection versus the operating trans-membrane pressure at three different inlet feed flow rates with comparative data between the model and experiments results. It is expected that the retention of any species will increase due to the increase in operating pressure in turn due to an increase in the water flux passing the membrane. Moreover, the increase of the inlet feed flow rate causes an increase in the Isopentyl acetate rejection due to a reduction in solute flux through the membrane. The increased feed flow rate reduces the wall membrane concentration and causes a decrease of osmotic pressure along the membrane length. Therefore, an increase in the feed flow rate causes a specific impact on the solute retention by decreasing the amount of accumulated salt on the membrane wall.

Fig. 3.8 in Chapter 3 illustrates the effect of operating pressure and inlet feed flow rate in the water flux. The water flux increases due to increase in the operating pressure in line with Eq. (M.6.1) in Chapter 3, which shows that the feed pressure

has a substantial impact by bringing up the diffusion rate of water passing through the membrane. Also, it can be noticed that the impact of the inlet feed flow rate is significantly greater at higher operating pressures due to a higher reduction in concentration polarisation caused by combining the concurrent impacts of the two parameters of feed flow rate and pressure parameters.

Fig. 8.1 shows the effect of operating trans-membrane pressure in the outlet °Brix for different feed flow rates. It is expected that the concentration in °Brix will increase due to an increase in the operating pressure. This is due to the increase in water flux by increasing the pressure. The concentration in °Brix that can be obtained is limited to the range 10.55 - 11.32 of used pressure and this might be attributed to the use of small specific area of membrane module.

It is also interesting to notice that the outlet concentration in "Brix is almost the same for all three inlet feed flow rates at lower inlet operating pressure. However, there is a noted discrepancy at higher operating pressures. Overall, the concentration in "Brix decreases due to an increase in the operating feed flow rate, especially when using higher operating pressures in spite of increasing water flux with increasing inlet feed flow rate, as more specifically illustrated in Fig. 3.8 in Chapter 3. The reason for this phenomenon is that increasing feed flow rate results in increasing the mass transfer coefficient and decreasing the concentration polarisation. Also, the increased feed flow rate reduces the wall membrane concentration and causes a decrease of osmotic pressure, which is followed by decreasing sugar and aroma compounds concentration along the membrane due to a better mixing in the feed channel.

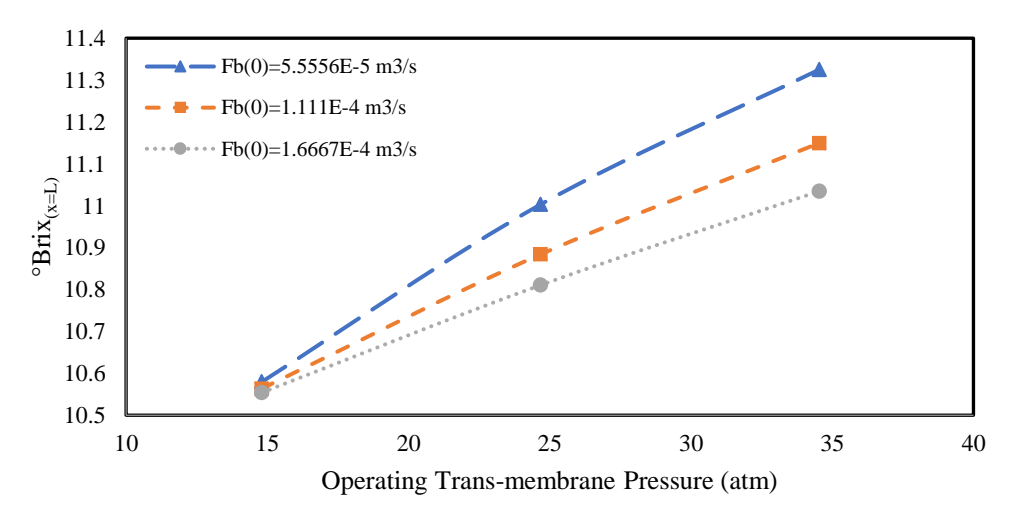


Fig. 8.1. Outlet Brix variation as a function of operating trans-membrane pressure at different inlet feed flow rates at inlet conditions ($^{\circ}$ Brix = 10.5, $T_b = 20$ $^{\circ}$ C)

Fig. 8.2 displays the variation of operating temperature within the permissible limits of the manufacturer's specifications of the module as a function of apple juice concentration measured in °Brix. It can be observed that the concentration increases as a result to increase in the operating temperature. In line with Eq. (M.6.2) in Chapter 3, the water permeability coefficient increases with increasing the operating temperature, which causes an increase in water flux that raises the apple juice concentration in the feed side.

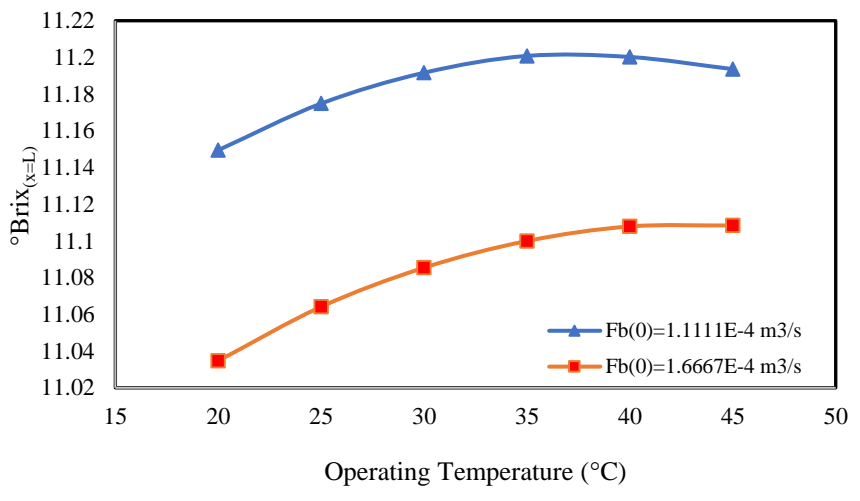


Fig. 8.2. Outlet Brix variation as a function of operating temperature at different inlet feed flow rates at inlet conditions (°Brix = 10.5, TMP = 34.542 atm)

8.3 Case 2: Optimum design of a multi-stage spiral wound RO process for the production of highly concentrated apple Juice

The main aim of this research is to maximising apple juice concentration using different spiral wound RO networks configurations using an enhanced optimisation technique. Therefore, Model Type_7 presented in Chapter 3 is designed to include a mathematical model of a spiral wound RO membrane process and a set of mathematical equations for multi-stage RO network. The optimisation problem is formulated as a Nonlinear Programming (NLP) problem with five different RO superstructures to maximise the apple juice concentration as well as the operating parameters such as feed pressure, flow rate, and temperature are optimised. Specifically, it is planned to investigate an optimal RO configuration that can achieve high apple juice concentration measured in °Brix from a set of different networks. In this case, a multi-stage RO industrial full-scale plant based on the MSCB 2521 RE99 spiral wound membrane module (Separem, SpA, Biella, Italy) of 1.03 m² area (used by Álvarez et al., 2002) is used to simulate

the process of concentrating apple juice and to identify an optimal multi-stage RO process for a specified apple juice product of high concentration measured in °Brix. Validation of the selected RO network developed is achieved by carrying out a sensitivity analysis of the operating parameters of the process on the performance of the plant.

8.3.1 Apple juice concentration plant description

The proposed RO industrial full-scale plant is consisting of four pressure vessels connected in different networks of stages. Each stage holds a maximum of two pressure vessels connected in parallel, while each pressure vessel holds a maximum of three spiral wound RO membrane elements type MSCB 2521 R99 of (1.03 m²) area supplied by Separem Spa. (Biella, Italy) connected in series. The reason for choosing this membrane is due to the availability of water and sugar compounds transport parameters in the literature in comparison to other types of membranes. The five proposed superstructures schematic diagram of the RO network can be shown in Fig. 8.3, which is similar to the specification of an actual pilot-scale RO seawater desalination process presented by Abbas (2005).

The concentrated stream of the first stage becomes the feed stream of the second stage and so on. However, the permeate streams of three elements in a pressure vessel are coupled to form the product stream of pressure vessel. Moreover, the permeate stream of all the stages are blended to form the product stream of the plant. The apple juice outlet concentration of the last stage is measured in "Brix, where it is considered as the objective function of the optimisation study.

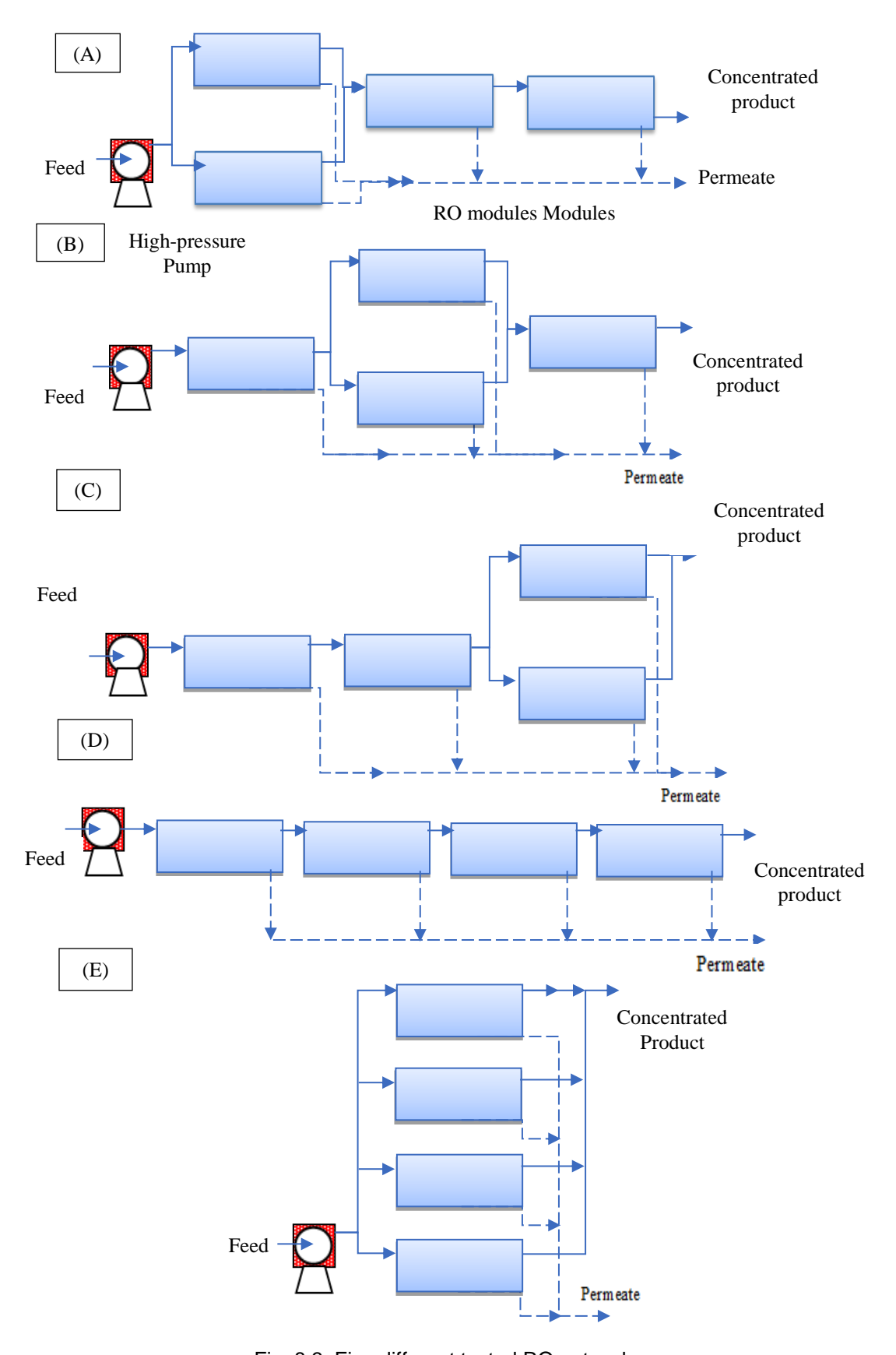


Fig. 8.3. Five different tested RO networks

8.3.2 Optimisation technique

8.3.2.1 Problem description and formulation

The objective of this section is to show the development of the RO optimisation framework based on the apple juice concentration process using multi-stage RO networks as shown in Fig. 8.3. This involves five different RO configurations and the optimisation methodology developed enables the selection of the optimal RO network configuration that can achieve a higher concentration of apple juice measured in °Brix. The optimum design of RO network is investigated for inlet apple juice feed concentration of 10.5 °Brix with equivalent concentrations of sugar compounds as given in Table 2.7 in Chapter 2. These are in turn used to analyse the influence of operating parameters of the process on the juice concentration for the selected RO network. The objective function of the optimisation algorithm developed is to maximise the apple juice concentration subjected to process and module constraints. The algorithm uses the specification and geometry of a spiral wound membrane (MSCB 2521 R99, Sparem Spa., Biella, Italy) and the module constraints of inlet pressure, flow rate and temperature as given in Table 2.6 in Chapter 2. It is noted that the feed of 10.5 °Brix has concentrated to a maximum value of 11.325 °Brix using the same above RO membrane at operating conditions of 34.54 atm, 5.5556x10⁻⁵ m³/s, and 20 °C of feed pressure, flow rate, and temperature, respectively (case 1 of Chapter 8). This will therefore raise the product concentration by using a multistage RO network.

The optimisation problem is described as follows:

Given: Operating feed conditions, module specifications.

Optimise: Inlet feed pressure, flow rate, and temperature (the optimisation variables).

Maximise: The product concentration of apple juice of the RO network under consideration.

Subject to: Equality (process model) and inequality constraints (linear bounds of optimisation variables).

Therefore, the optimisation problem is represented mathematically as follows:

 $F_{b(plant)}, P_{f(plant)}, T_{b(in)(plant)}$

Subject to:

Equality constraints:

Process Model: f(x, u, v) = 0

Inequality constraints:

$$\begin{aligned} Q_{f(plant)}^{L} &\leq Q_{f(plant)} \leq Q_{f(plant)}^{U} \\ P_{f(in)(plant)}^{L} &\leq P_{f(in)(plant)} \leq P_{f(in)(plant)}^{U} \\ T_{b(in)(plant)}^{L} &\leq T_{b(in)(plant)} \leq T_{b(in)(plant)}^{U} \end{aligned}$$

The optimisation problem entails the constraints shown below of a single spiral wound RO membrane as follows, which satisfy the maximum and minimum practical bounds of the operating conditions:

$$Q_f^{L} \leq Q_f \leq Q_f^{U}$$

$$P_{f(in)}^{L} \leq P_{f(in)} \leq P_{f(in)}^{U}$$

$$T_b^{L} \leq T_b \leq T_b^{U}$$

The limits of decision variables of inlet feed flow rate, pressure and temperature of a single RO membrane are given in Table 2.5 in Chapter2. The membrane manufacture usually specifies all these constraints.

The solute transport parameter $B_{s,i}$ for all sugar compounds (sucrose, glucose, malic acid, fructose, and sorbitol) are assumed constant at 25 °C and determined in a Model Type_6 in Chapter 6 as reported in Table 2.6 in Chapter 2. However, the transport parameter of malic acid was taken from Malaiyandi et al. (1982).

8.3.2.2 RO networks optimisation results

For the inlet feed apple juice concentration of 10.5 °Brix, the optimisation results obtained for the five scenarios of RO networks shown in Fig. 8.3 for two cases (one and three) of the number of elements per each pressure vessel are shown in Table 8.1. Also, the optimum decision variables of each RO network and its performance regarding the product concentration measured in °Brix can be shown in Table 8.1.

Table 8.1. Comparison of outlet apple juice concentration for five cases of RO networks

Scenario	Elements number	The decision variables			°Brix _{out(plant)}	
Sce	Elei	$Q_{f(plant)}$ (m ³ /s)	$P_{f(in)(plant)}(atm)$	$T_{b(in)(plant)}$ (°C)		
Α	1	5.00x10 ⁻⁵	41.45	49.22	14.84	
/	3	5.00x10 ⁻⁵	41.45	50.00	22.41	
В	1	2.50x10 ⁻⁵	41.45	42.80	15.39	
	3	2.50x10 ⁻⁵	41.45	44.66	23.67	
С	1	2.50x10 ⁻⁵	41.45	42.51	15.40	
	3	2.50x10 ⁻⁵	41.45	45.00	23.68	
D	1	2.50x10 ⁻⁵	41.45	46.92	16.76	
	3	3.68x10 ⁻⁵	41.45	45.00	25.44	
Е	1	1.00x10 ⁻⁴	41.45	35.50	12.08	
_	3	1.00x10 ⁻⁴	41.45	46.84	15.21	

It is noted that scenario D (series configuration) has achieved the optimum product concentration of 25.44 °Brix in comparison with other scenarios with a concentration percentage increase of 142%. This is in comparison to the outputs of one element of 7.85% concentration increase. Also, it is expected that the concentration of the juice is positively proportional to the number of elements for each pressure vessel. Interestingly, it is expected that the organic acids and flavour components are not changed after concentrating the apple juice to 25.44 °Brix. Miyawaki et al. (2016) confirmed that no substantial differences were observed for the apple juice before and after concentration from 13.7 to 25.5 °Brix using a progressive freeze-concentration system. In addition, the optimisation results of Table 8.1 show that both operating pressure and flow rate are the most important operational parameters, which significantly affect the performance of RO membrane in respect of the optimum values of juice concentration. However, the temperature has a lower impact where the optimum °Brix can be implemented with lower than the upper temperature bound for most scenarios. Interestingly, the optimum °Brix of all the scenarios requires high operating pressure and lower feed flow rate with a range of 35 to 50 °C of temperature, which will be explained in the next section. It can be said that the optimisation methodology has selected the upper bound of pressure due to the necessity to overcome the high osmotic pressure of apple juice. Gostoli et al. (1995) confirmed that the osmotic pressure of an orange juice is increased from 14.8 atm to 187.5 atm due to an increase in the total solids from 11% to 60%.

The feasibility of the recent work is comparable to the performance of an integrated process of Matta et al. (2004) comprising ultrafiltration UF, microfiltration MF and RO used for concentrating acerola juice. Specifically, the clarification and concentration of acerola juice processes were conducted in three tubular UF and MF membranes (0.05 m²) followed by a film composite RO membrane (0.72 m²). It was observed that juice having 7.1 °Brix is concentrated to 29.2 °Brix at operating conditions of pressure and temperature of 100 kPa (0.98 atm), 30 °C at UF/MF membranes and 6000 kPa (59.215 atm), 25 °C at RO membrane.

8.3.3 Analysing the impact of operating parameters on the product concentration

Here, the Model Type_7 developed (described in Section 3.6.2.1 in Chapter 3) is used to simulate the process, explore the sensitivity of the model to different parameters of the process, and take an overview of the outlet apple juice concentration measured in °Brix for the optimum RO network (scenario D) of four pressure vessels and twelve elements in series under the impact of varying the process parameters. Firstly, it is important to study the impact of operating pressure, flow rate and temperature on sugar species rejection due to its relationship with the bulk and retentate concentration.

Figs. 8.4, 8.5 and 8.6 illustrate the variation of sugar species rejection (sucrose, glucose, malic acid, fructose, and sorbitol) as a result to increase in operating pressure at three cases of feed flow rate at constant temperature of 40 °C.

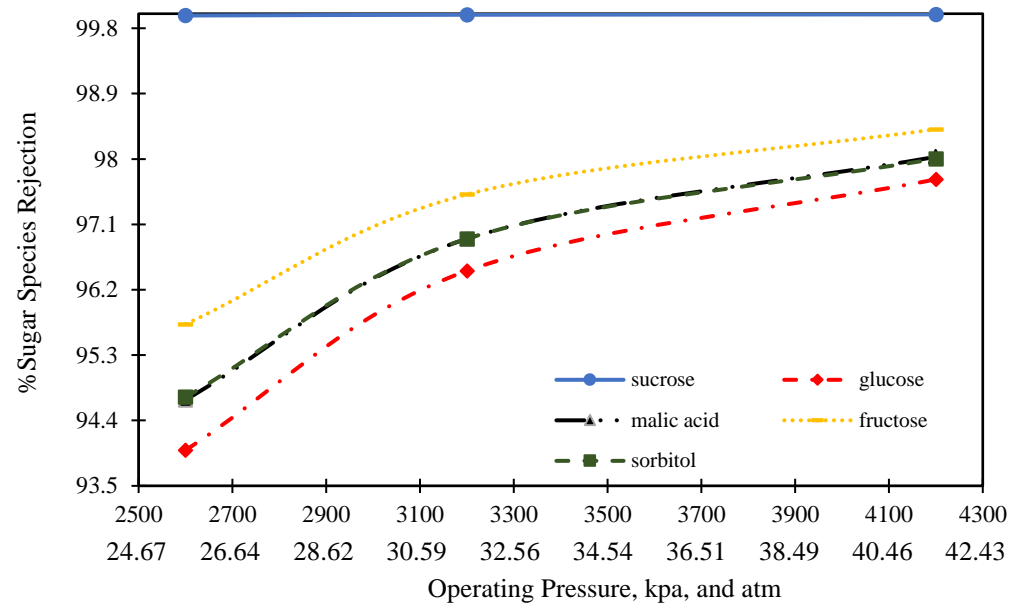


Fig. 8.4. Sugar species rejection as a function of operating pressure at inlet feed flow rate and temperature of 1x10⁻³ m³/s, and 40 °C, respectively

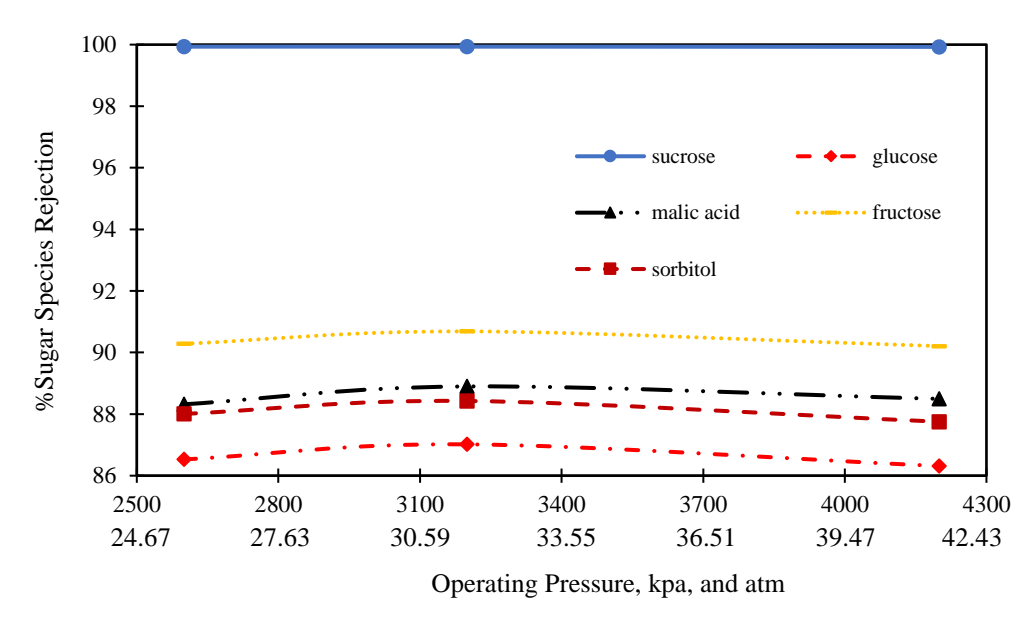


Fig. 8.5. Sugar species rejection as function of operating pressure at inlet feed flow rate and temperature of 1x10⁻⁴ m³/s, and 40 °C, respectively

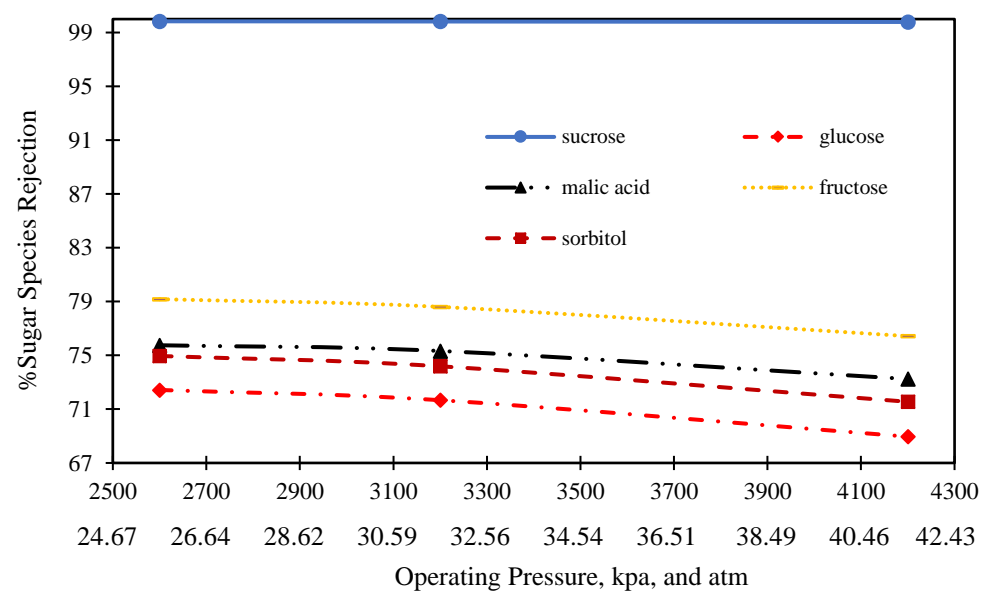


Fig. 8.6. Sugar species rejection as a function of operating pressure at inlet feed flow rate and temperature of 3.7x10⁻⁵ m³/s, and 40 °C, respectively

The expectation that increasing inlet feed pressure will increase sugar rejection due to accelerating water flux as denoted by Eq. (M.6.1) in Chapter 3. However, it seems that this phenomenon is confirmed for medium and high feed flow rates in comparison to lower ones. This is attributed to the increase in concentration and the osmotic pressure of the feed side, which in turn increases sugar flux through the membrane and permeate concentration at lower feed flow rate conditions. Therefore, sugar retention is decreased due to an increase in operating pressure as denoted by Eq. (M.6.39) in Chapter 3. In this respect, increasing inlet feed flow rate would increase water flux and sugar rejection, since this would reduce the concentration polarisation impact as shown in Figs. 8.4 and 8.5. The same impact of feed flow rate was observed by Álvarez et al. (2001) who concluded that the permeate flux and aroma rejection are increased due to an increase in feed flow rate of an individual spiral wound RO process.

The response of product concentration for the variation of both inlet feed pressure of 2200 to 4200 kpa (21.71 – 41.45 atm) and flow rate of 3.68x10⁻⁵ to 1x10⁻³ m³/s at constant operating concentration and temperature of 10.5 °Brix, and 40 °C, respectively is shown in Fig. 8.7.

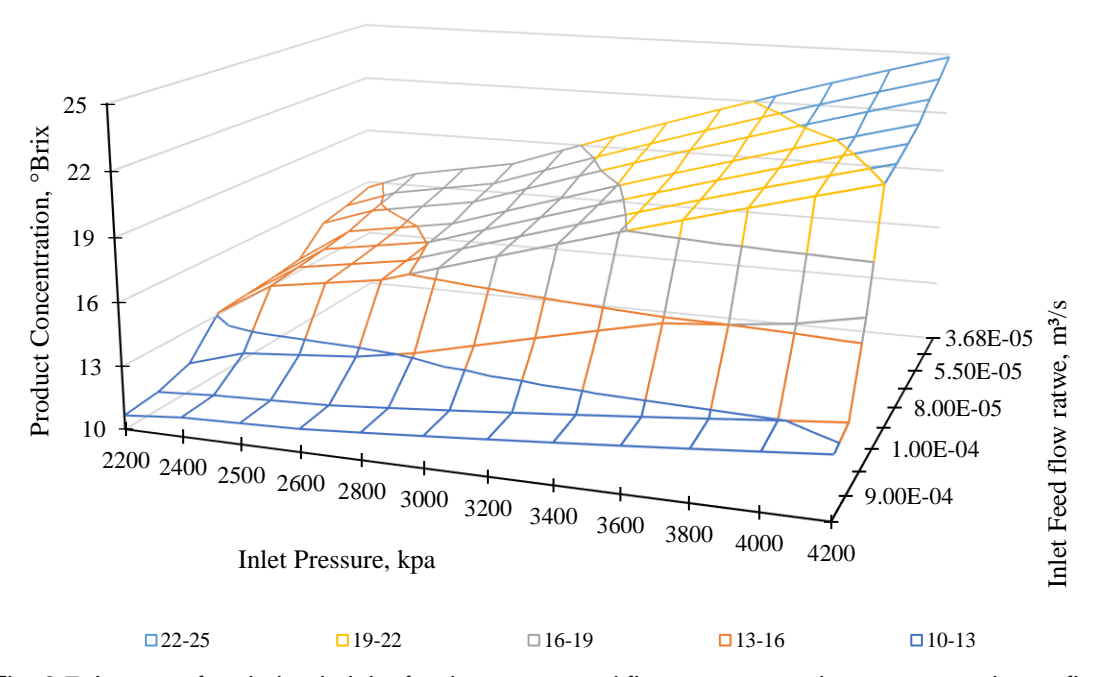


Fig. 8.7. Impact of variation in inlet feed pressure and flow rate on product concentration at fixed inlet feed concentration and temperature of 10.5 °Brix, and 40 °C, respectively

Interestingly, Fig. 8.7 shows that the product concentration increases markedly due to the increase in operating pressure at low feed flow rate, which is comparable to high feed flow rate conditions. It is concluded from Fig. 8.6 that the sugar species rejection decreases with an increase in the operating pressure at low feed flow rate in addition to a decrease in water flux and increases sugar flux. Therefore, the retentate will be concentrated due to high rates of filtration with higher feed residence time. Simply, increasing operating pressure can enhance the concentration of feed in the subsequent sub-sections of feed channel since the solute is retained in the wall with the diffusion of water through the membrane.

In contrast, using high feed flow rate conditions can cause a slight increase in product concentration. This event is caused by an increase of the water flux and retention parameter by increasing the operating pressure at high inlet feed flow rate conditions (Fig. 8.4). Simply, increasing inlet feed flow causes a reduction of osmotic pressure of feed channel and wall membrane concentration, which in turn reduces solute flux through the membrane. However, at higher operating feed flow rate, the progress of retentate concentration along the membrane channel is noticeably lower than the case of lower feed flow rate conditions, due to lower residence time of filtration. Additionally, Fig. 8.8 shows an inverse relation between the retentate sugar concentration and feed flow rate at three

operating pressures and constant temperatures. Consequently, the outlet product concentration will be increased as a function of the decreasing operating feed flow rate at any operating pressure.

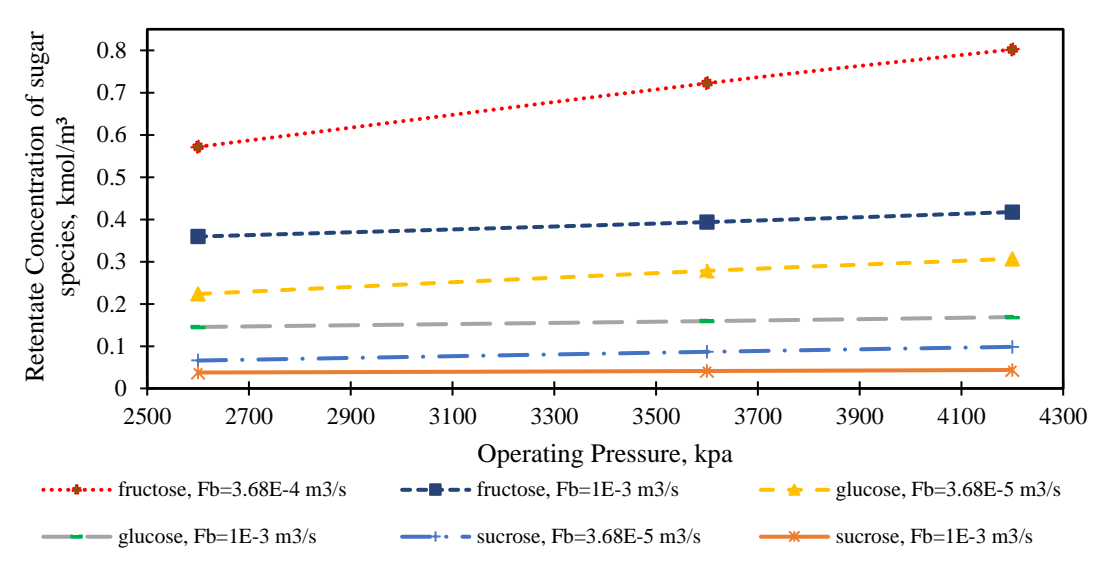


Fig. 8.8. Sugar species retention concentration verse operating pressure at two inlet feed flow rates and inlet feed concentration and temperature of 3.68x10⁻⁵ and 1x10⁻³ m³/s, 10.5 °Brix, and 40 °C

The response of product concentration for the variation of both feed pressure of 2200 to 4200 kpa (21.71 – 41.45 atm) and feed temperature of 30 to 45 °C at constant operating concentration and flow rate of 10.5 °Brix, and 4x10⁻⁵ m³/s, respectively is shown in Fig. 8.9.

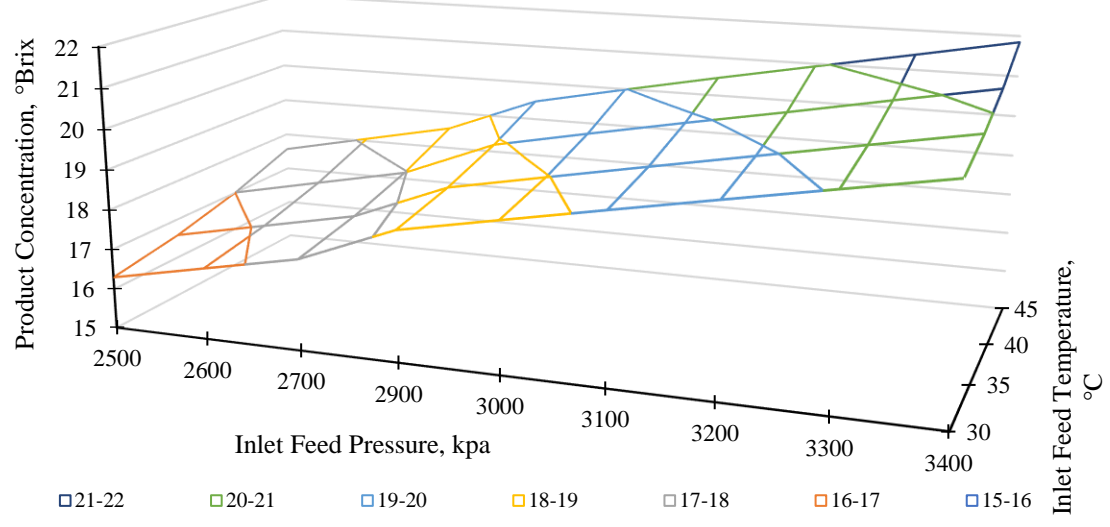


Fig. 8.9. Impact of variation in inlet feed pressure and temperature on product concentration at fixed inlet feed concentration and flow rate of 10.5 °Brix, and 4x10⁻⁵ m³/s

Fig. 8.9 shows that the temperature variation has inconsiderable impact on product concentration in comparison with the operating pressure. Interestingly, Figs 8.10 and 8.11 clearly show that the rejection of all sugar species decreases due to an increase in the operating temperature in two different feed flow rates, which is quite similar to the findings of aroma compounds retention in the case 1 of this chapter (Fig. 3.6 in Chapter 3). Moreover, Chou et al. (1991) observed that an increase in operating temperature from 20 °C to 40 °C tends to increase the permeation rate at the penalty of lowering the retention of volatiles compounds. The probable explanation for this can be that by increasing feed temperature, density and viscosity decrease and water permeation rate through membrane and diffusivity parameter increase. Also, the solubility of sugar species increases and higher diffusion rate of sugar through the membrane is possible due to the variation of pore size of the polymeric membrane, which ultimately reduces the rejection parameter and reduces the retentate flow rate with somehow elevated product concentration. Zainal et al. (2000) studied the impact of operating temperature on the physical properties of pink guava juice and showed that increasing the temperature causes a decrease in consistency coefficient, which result in an increase in the flow behaviour index due to less resistance flow.

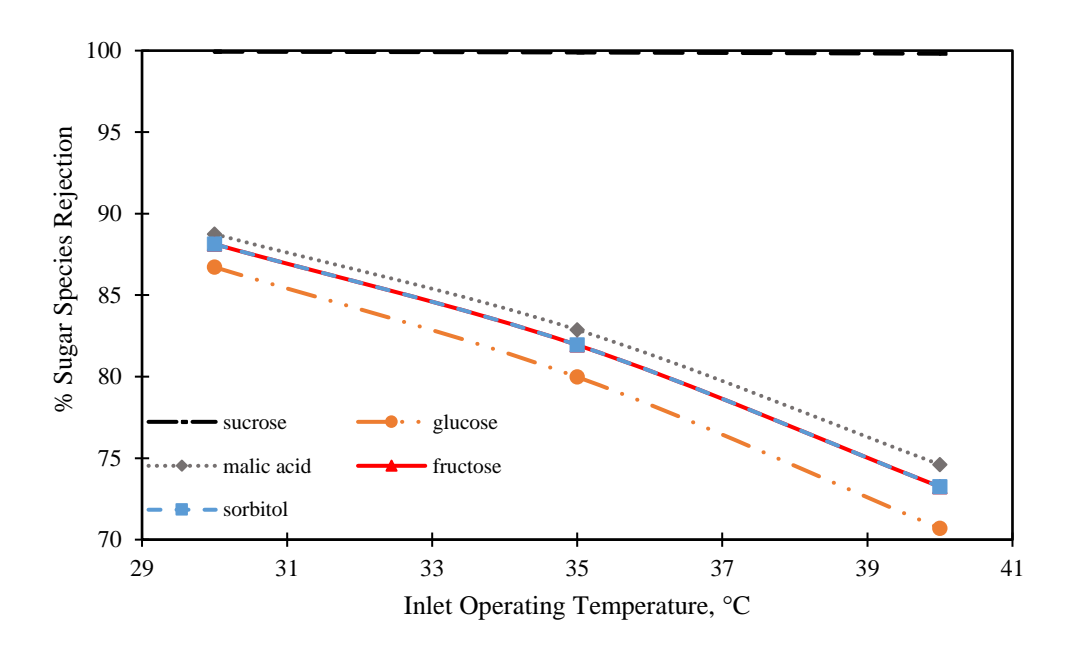


Fig. 8.10. Sugar species rejection as a function to operating feed temperature at inlet feed concentration and flow rate of 10.5 Brix, and 3.68x10⁻⁵

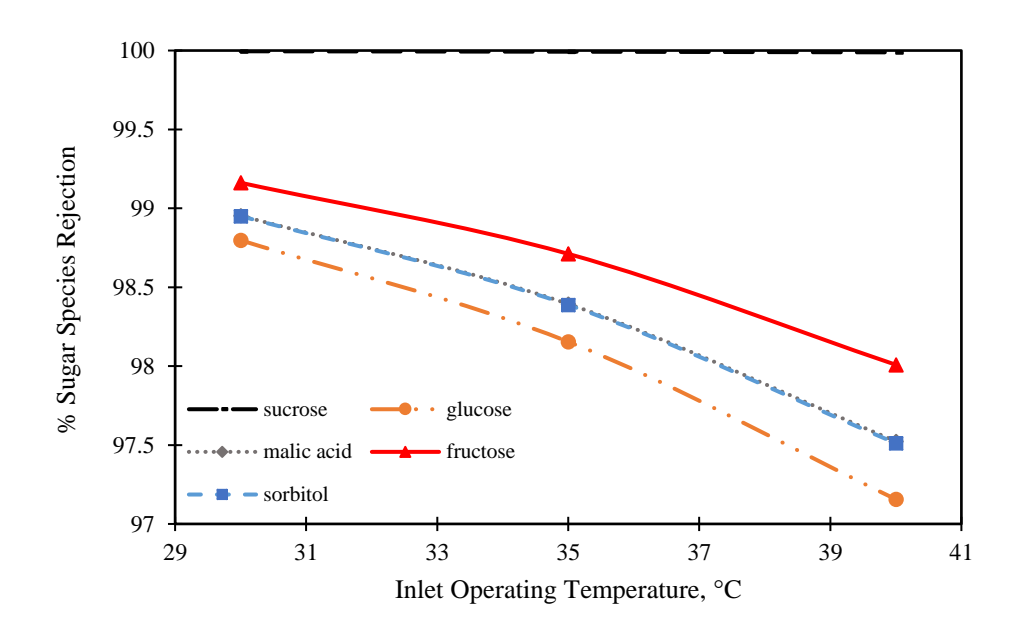


Fig. 8.11. Sugar species rejection as a function to operating feed temperature at inlet feed concentration and flow rate of 10.5 Brix, and 1x10-3

8.4 Conclusions

This chapter shows the use of Model Type_6 presented in Chapter 3 to simulate an individual spiral wound RO process from the apple juice concentration. This in turn investigates the influence of various operating conditions on permeate flux and aroma compounds rejection.

Secondly, the simulation and optimisation of multi-stage RO process based on a spiral wound module for the apple juice concentration juice considering the limits of operation and the constraints of both the module and RO layout is carried out using the lumped Model Type_7 presented in Chapter 3. The study revealed that the multi-stage series RO process can optimise the product concentration of apple juice better than other configurations. It has been concluded that the series configuration of twelve elements of 1.03 m² area improves the product apple juice concentration by about 142% compared to one element. Furthermore, the impact of the main operating parameters of feed pressure, flow rate, and temperature on the product specification were investigated for the optimum RO network. It is concluded that the feed pressure and flow rate have weighty impact on apple juice concentration in comparison to inconsiderable impact of feed temperature.

Chapter 9

Conclusions and Recommendations for Future Research

9.1 Conclusions

Reverse Osmosis (RO) is now recognised as the most promising technology for water recycling and reuse. The main aim of this research was to develop an efficient method of RO process for the removal of high-toxic organic compounds from wastewater and concentrating apple juice by improving the reliability and efficiency of the underlying separation and concentration process. The research is mainly exhibited the developing of the RO process by improving the performance of removing special organic compounds from wastewater, which in turn aids to produce good quality water for several industries. Unquestionably, the removal of high toxicological organic compounds from wastewater poses various complex challenges, which are explored in detail in this research. The research provides a one-stop-shop for RO outlining its scope and limitations for the removal of highly-toxic compounds from wastewater.

The research starts by highlighting the challenges posed by a significant increase in demand of fresh water and the urgent need to recycle wastewater at minimum cost. The research then addresses and discusses specific high-toxic organic phenolic and N-nitrosamine compounds that can be found in the wastewater of several industrial applications and raises awareness about increased and tighter legislation. Broadly speaking, the existence of a small trace amount of such harmful compounds in industrial effluents can prohibit the reuse of water in many applications. Also, the research investigates the complexities of removing pollutants together with advantages and limitations of different conventional treatment methods. RO process is then presented in some considerable detail covering process operation and feasibility for wastewater treatment.

For this purpose, a reliable process model is the first step before achieving effective simulation and optimisation for the RO process that aid to generate alternative design and high-efficient process. Therefore, several models were developed for the spiral wound RO process for both the removal of high toxic compounds from wastewater and apple juice concentration as an example of food processing. Most importantly, the research explores other attempts, which explored distributed spiral wound RO process models used especially for wastewater treatment and apple juice concentration. Then, current feasible

solutions are discussed in respect of their amenability for improving process performance and energy consumption based on process simulation using a wide range of operating parameters. Process optimisation yields best operating parameters, which can achieve the objective functions of maximising the process performance and energy consumption given the constraints set by the manufacturer's specification. More specifically, the research provides illustrative examples of the various model-based simulation and optimisation studies used to explore several conceptual designs of multi-stage RO wastewater system for permeate and retentate reprocessing and two-pass configuration for the removal of pollutants from wastewater. Also, the research highlights the successful techniques for reducing the energy consumption required in the RO process. This has been typically achieved by optimising the operating conditions, module configurations, and implementing energy recovery devices.

Moreover, a case of multicomponent wastewater is further modelled and the total rejection of each compound is optimised at a maximum recovery rate. Lastly, the simulation and optimisation of apple juice process are presented in detail.

The net result of this research has confirmed the applicability and suitability of the RO process for treating secondary effluents at low energy. The methods suggested in this research has made a significant reduction of the probability of accidental release of the harmful compounds into the recycled water by implementing different techniques and improved design of the RO process. This in turn can be served as an elaborated guide for water treatment approaches in many indirect potable water reuse schemes. However, the performance of RO process to remove N-nitrosodimethylamine-D6 (NDMA) has been a challenge. Whilst the concentration of these micro-pollutants is relatively low in wastewater, it will continue to challenge future research for developing an improved separation process. The direction of travel for providing a sustainable solution for treating these highly toxic compounds will continue to attract RO researchers for many reasons, not least because of the tightening regulation for lower recommended concentrations in both drinking water and wastewater.

In this research, the gPROMS software is used to create several models-based simulation and optimisation. Specifically, the parameter estimation tool of the gEST in the gPROMS is also used to predict the unknown parameters of the models developed. Whilst, the optimisation problem is posed as a Non-Linear Programming (NLP) problem and is solved using a Successive Quadratic

Programming (SQP) method. The following detailed conclusions can be drawn from this research.

In Chapter 3, the development of several mathematical and computational models (steady state, dynamic, lumped and distributed) for the individual spiral wound and multi-stage RO process for the removal of selected high-toxic organic compounds from wastewater in addition to the apple juice concentration process are presented. The two and one-dimensional distributed models presented go a long way to realising the improvement required to achieving a better and cheaper solution. This is evidenced by the very small margin of error between the experimental data gathered from the literature and the model predictions for a number of process parameters. This is also involved the parameter estimation approach for the model parameters based on the experimental data. Also, a comprehensive detail was given for the gPROMS software used for the modelling, simulation and optimisation. This also involved the parameter estimation technique and the explanation of the optimisation tool used.

In Chapter 4, the impact of several operating parameters on the performance of an individual spiral wound RO process to remove chlorophenol from wastewater was explored in detail. In line with this case, it is recognised that there is a room to improve the performance of RO process to remove chlorophenol. Therefore, the research shows the merits of a hypothetical two-stage/two-pass RO design process for improving low chlorophenol rejection rates via simulation and optimisation. The requirements of reducing the total energy consumption and at the same time elevating the rejection parameter has been achieved using an optimisation study manipulating the process parameters within allowed operational limits. A maximum of 93.3% chlorophenol rejection has been obtained for the proposed configuration 12.4% higher than the latest published work in the literature. The results also show that a significantly higher recovery rate of 40% at a lower energy consumption of 1.949 kWh/m³ is possible to the proposed RO network.

In Chapter 5, the dynamic simulation of 2D model for an individual spiral wound RO process is presented. The dynamic simulation has facilitated the investigation of the impact of a step change of the operating parameters on the process performance to remove dimethylphenol from wastewater. It is concluded that the process requires a specific finite time to settle after imposing a step change on several operating parameters. Also, the settling time is dependent on the type of

the operating parameters. Additionally, the results show that a ramped change of operating pressure yields a different process settling time.

In Chapter 6, the multistage spiral wound RO process of two configurations of with and without energy recovery device was simulated considering the rejection of NDMA from wastewater, total water recovery, and specific energy consumption. In the line of this research, it is recognised that the performance of RO process to remove N-nitrosodimethylamine-D6 (NDMA) has been a challenge. Therefore, the research has presented methodologies of process simulation and optimisation for improving the RO performance and energy consumption for the removal of selected high-toxic pollutants. In other words, this research has evaluated several conceptual designs of multi-stage and multi-pass designs for RO processes for NDMA rejection using model-based techniques and compute the total recovery rate and energy consumption. Moreover, the research has suggested a new proposed RO network, which has been specifically designed to include the permeate processing for high NDMA rejection and yet achieve an acceptable permeate recovery rate. The research results clearly show that the proposed adaptive RO design with permeate reprocessing was able to solve the issue of low NDMA rejection. Specifically, it has been found the optimisation of the proposed design yields a competitive value of 92.487% rejection and a practicable permeate recovery of 40% at an all-time low 2.664 kWh/m³ total energy consumption. This is compared to the maximum NDMA rejection of 80% that can be found in the literature.

In Chapter 7, the case of a realistic wastewater of multi compounds is suggested for an individual spiral wound RO process where the modelling, simulation, and process optimisation are given in detail. The multi-objective optimisation problem has elaborated the maximum values of the rejection of all the compounds and permeate recovery.

In Chapter 8, the apple juice concentration using spiral wound and multistage RO processes is presented. This includes the studying of the process performance under the impact of the operating parameters and to investigate the proper RO network that commensurate with high concentrated product using an enhanced optimisation technique. It is concluded that the multi-stage series RO process can optimise the product concentration of apple juice better than other configurations. Statistically, the product apple juice concentration has improved by about 142% compared to one element.

To sum up, the delivered solutions in this research affirmed that the RO is not only yields a much cheaper solution in terms of energy consumption, but it can readily be used to achieve the stringent limits of highly toxic compounds concentration, which are set to increase in the future. However, the research highlights the fact that more work is still required for developing rigorous models, which resolve substantial approximations made in such previous studies. Moreover, there is still room for improvement the multi stage RO process for achieving a better solution especially for NDMA.

9.2 Recommendations for future research

- The models developed in this research have not referred to the fouling impact on the process performance. Therefore, the incorporation of fouling parameter will ultimately enhance the model prediction of the process rejection and recovery rate especially using the high-concentration wastewater for a long time of operation. However, the enhanced models should be validated against experimental data of removing organic compound from wastewater alongside the operation time for the spiral wound RO process.
- The use of an automatic control for the RO process is both critical and important for maintaining process performance within a specified level. The dynamic Model Type_2 developed and presented in Chapter 3 has a promising potential for improved control and optimisation, which can be explored further in upcoming research. Therefore, the control efficiency of different types of controller scheme such as PID (proportional-integral-derivative) and MPC (model predictive control) has to be examined for the wastewater RO process taking into consideration a constant performance of organic compound removal (lower release of pollutants to the environment) under a realistic water recovery. Additionally, one of the advantages of the control system is to maintain a lower permeate recovery with the lowest operating pressure in order to reduce the operation cost and prolong the membrane life.
- To the best of the author's knowledge, the abilities and indeed possibilities
 of the RO process for removing NDMA are yet to be fully explored or
 realised with many opportunities and challenges for optimising the
 underlying operating conditions, superstructure, and membrane

synthesis. Further work is required to investigate the optimal design of a RO network using the MINLP (Mixed Integer Non-linear Programming) optimisation for pollutants of high solute transport values such as N-nitrosodimethylamine (NDMA) nitrosamine when implementing the multistage arrangement that could involve permeate reprocessing required for improving the purity of the permeate.

- The results of this research are encouraging in that the performance of the RO system investigated can be enhanced further by testing the models developed on the RO process of a high permeability membrane type, one that can save both energy and money and impact more positively on the environmental. However, this is required a full experimental data for model validation.
- It is recommended to continue the investigation of several RO process configurations with a higher organic compounds concentration, with the objective of a reduced energy cost per volume of produced permeate.
- Further work is essential to optimise the apple juice concentration by weighing the impact of the high module area and different layouts of recycled RO network.

References

- Abbas, A. (2005) Simulation and analysis of an industrial water desalination plant. Chemical Engineering and Processing: Process Intensification 44 (9) 999-1004.
- Ahmad, A. L., Chong, M. F. and Bhatia, S. (2007) Mathematical modeling of multiple solutes system for reverse osmosis process in palm oil mill effluent (POME) treatment. *Chemical Engineering Journal* 132 (1) 183-193.
- Ahmed, S., Rasul, M. G., Martens, W. N., Brown, R. and Hashib, M. A. (2010) Heterogeneous photocatalytic degradation of phenols in wastewater: A review on current status and developments. *Desalination* 261 (1) 3-18.
- Akin, O. and Temelli, F. (2011) Probing the hydrophobicity of commercial reverse osmosis membranes produced by interfacial polymerization using contact angle, XPS, FTIR, FE-SEM and AFM. *Desalination* 278 (1) 387-396.
- Al-Bastaki, N. (2004) Removal of methyl orange dye and Na 2 SO 4 salt from synthetic waste water using reverse osmosis. *Chemical Engineering and Processing: Process Intensification* 43 (12) 1561-1567.
- Al-Bastaki, N. and Abbas, A. (2003) Permeate recycle to improve the performance of a spiral-wound RO plant. *Desalination* 158 (1) 119-126.
- Alvarez, S., Riera, F., Alvarez, R., Coca, J., Cuperus, F., Bouwer, S. T., Boswinkel, G., Van Gemert, R., Veldsink, J. and Giorno, L. (2000) A new integrated membrane process for producing clarified apple juice and apple juice aroma concentrate. *Journal of Food Engineering* 46 (2) 109-125.
- Álvarez, S., Riera, F. A., Álvarez, R. and Coca, J. (1998) Permeation of apple aroma compounds in reverse osmosis. *Separation and Purification Technology* 14 (1) 209-220.
- Álvarez, S., Riera, F. A., Álvarez, R. and Coca, J. (2001) Prediction of Flux and Aroma Compounds Rejection in a Reverse Osmosis Concentration of Apple Juice Model Solutions. *Industrial & Engineering Chemistry Research* 40 (22) 4925-4934.
- Álvarez, S., Riera, F. A., Álvarez, R. and Coca, J. (2002) Concentration of Apple Juice by Reverse Osmosis at Laboratory and Pilot-Plant Scales. *Industrial & Engineering Chemistry Research* 41 (24) 6156-6164.
- Alvarez, V., Alvarez, S., Riera, F. A. and Alvarez, R. (1997) Permeate flux prediction in apple juice concentration by reverse osmosis. *Journal of Membrane Science* 127 (1) 25-34.
- Amar, N. B., Kechaou, N., Palmeri, J., Deratani, A. and Sghaier, A. (2009) Comparison of tertiary treatment by nanofiltration and reverse osmosis for water reuse in denim textile industry. *Journal of Hazardous Materials* 170 (1) 111-117.
- Anderson, W., Stover, R. and Martin, J. (2009) Keys to High Efficiency, Reliable Performance and Successful Operation of SWRO Processes. *Proceedings of the IDA World Congress, Dubai UAE.*
- Andrea, I. S., William, M., Sophie, W., Albert, M., Emma, T., Martin, R. and (2010) Drinking water as a source of human exposure to xenobiotics: The case of disinfection by-product N-nitrosodimethylamine (NDMA). Published as 'Micropollutants in Water Recycling: A Case Study of N-Nitrosodimethylamine (NDMA) Exposure from Water versus Food' Sustainability Science and Engineering, Sustainable Water for the Future: Water Recycling versus Desalination 2 203-228.

- Araujo, W. and Maciel, M. R. W. (2009) Reverse osmosis concentration of orange juice using spiral wound membranes. *Alimentos e Nutrição Araraquara* 16 (3) 213-219.
- Arsuaga, J. M., Sotto, A., López-Muñoz, M. J. and Braeken, L. (2011) Influence of type and position of functional groups of phenolic compounds on NF/RO performance. *Journal of Membrane Science* 372 (1) 380-386.
- ATSDR (2015) ASTDR's substance priority list, https://www.atsdr.cdc.gov/spl/index.html). (Accessed, 10. 14. 2016).
- Avlonitis, S., Hanbury, W. T. and Boudinar, M. B. (1991) Spiral wound modules performance. An analytical solution, part I. *Desalination* 81 (1–3) 191-208.
- Avlonitis, S., Hanbury, W. T. and Boudinar, M. B. (1993) Spiral wound modules performance an analytical solution: Part II. *Desalination* 89 (3) 227-246.
- Avlonitis, S. A., Pappas, M. and Moutesidis, K. (2007) A unified model for the detailed investigation of membrane modules and RO plants performance. *Desalination* 203 (1–3) 218-228.
- Baker, R. W., (2004) Membrane technology and applications, 2nd edition. Membrane Technology and Research, Inc. California.
- Balannec, B., Vourch, M., Rabiller-Baudry, M. and Chaufer, B. (2005) Comparative study of different nanofiltration and reverse osmosis membranes for dairy effluent treatment by dead-end filtration. Separation and Purification Technology 42 (2) 195-200.
- Barger, M. and Carnahan, R. P. (1991) Fouling prediction in reverse osmosis processes. *Desalination* 83 (1) 3-33.
- Bhattacharya, P., Roy, A., Sarkar, S., Ghosh, S., Majumdar, S., Chakraborty, S., Mandal, S., Mukhopadhyay, A. and Bandyopadhyay, S. (2013) Combination technology of ceramic microfiltration and reverse osmosis for tannery wastewater recovery. *Water Resources and Industry* 3 (Supplement C) 48-62.
- Blandin, G., Verliefde, A., Comas, J., Rodriguez-Roda, I. and Le-Clech, P. (2016) Efficiently Combining Water Reuse and Desalination through Forward Osmosis—Reverse Osmosis (FO-RO) Hybrids: A Critical Review. *Membranes* 6 (3) 37.
- Bódalo, A., Gómez, J. L., Gómez, E., León, G. and Tejera, M. (2004a) Sulfonated polyethersulfone membranes in the desalination of aqueous solutions. *Desalination* 168 (Supplement C) 277-282.
- Bódalo-Santoyo, A., Gómez-Carrasco, J. L., Gómez-Gomez, E., Maximo-Martin,
 M. F. and Hidalgo-Montesinos, A. M. (2004b) Spiral-wound membrane reverse osmosis and the treatment of industrial effluents. *Desalination* 160 (2) 151-158.
- Bódalo, A., Gómez, J.-L., Gómez, E., León, G. and Tejera, M. (2004c) Reduction of sulphate content in aqueous solutions by reverse osmosis using cellulose acetate membranes. *Desalination* 162 55-60.
- Bodalo, A., Gomez, J.-L., Gomez, E., Leon, G. and Tejera, M. (2005) Ammonium removal from aqueous solutions by reverse osmosis using cellulose acetate membranes. *Desalination* 184 (1-3) 149-155.
- Bolong, N., Ismail, A. F., Salim, M. R. and Matsuura, T. (2009) A review of the effects of emerging contaminants in wastewater and options for their removal. *Desalination* 239 (1) 229-246.
- Bond, T., Huang, J., Templeton, M. R. and Graham, N. (2011) Occurrence and control of nitrogenous disinfection by-products in drinking water A review. *Water Research* 45 (15) 4341-4354.

- Boudinar, M. B., Hanbury, W. T. and Avlonitis, S. (1992) Numerical simulation and optimisation of spiral-wound modules. *Desalination* 86 (3) 273-290.
- Brisson, I. J., Levallois, P., Tremblay, H., Sérodes, J., Deblois, C., Charrois, J., Taguchi, V., Boyd, J., Li, X. and Rodriguez, M. J. (2013) Spatial and temporal occurrence of N-nitrosamines in seven drinking water supply systems. *Environmental Monitoring and Assessment* 185 (9) 7693-7708.
- Busca, G., Berardinelli, S., Resini, C. and Arrighi, L. (2008) Technologies for the removal of phenol from fluid streams: A short review of recent developments. *Journal of Hazardous Materials* 160 (2) 265-288.
- Charrois, J. W. A., Boyd, J. M., Froese, K. L. and Hrudey, S. E. (2007) Occurrence of N-nitrosamines in Alberta public drinking-water distribution systems. *Journal of Environmental Engineering and Science* 6 (1) 103-114.
- Chen, K. L., Song, L., Ong, S. L. and Ng, W. J. (2004) The development of membrane fouling in full-scale RO processes. *Journal of Membrane Science* 232 (1) 63-72.
- Chen-Jen, L., You-Syuan, C. and Gow-Bin, W. (2010) a dynamic simulation model of reverse osmosis desalination systems. *The 5th International Symposium on Design, Operation and Control of Chemical Processes, PSE ASIA, Singapore.*
- Cheong, K. W., Tan, C. P., Mirhosseini, H., Hamid, N. S. A., Osman, A. and Basri, M. (2010) Equilibrium headspace analysis of volatile flavor compounds extracted from soursop (Annona muricata) using solid-phase microextraction. *Food Research International* 43 (5) 1267-1276.
- Choi, J. and Valentine, R. L. (2002) Formation of N-nitrosodimethylamine (NDMA) from reaction of monochloramine: a new disinfection by-product. *Water Research* 36 (4) 817-824.
- Chou, F., Wiley, R. C. and Schlimme, D. V. (1991) Reverse osmosis and flavor retention in apple juice concentration. *Journal of food science* 56 (2) 484-487.
- Constenla, D., Lozano, J. and Crapiste, G. (1989) Thermophysical properties of clarified apple juice as a function of concentration and temperature. *Journal of Food Science* 54 (3) 663-668.
- Da Costa, A. R., Fane, A. G. and Wiley, D. E. (1993) Ultrafiltration of whey protein solutions in spacer-filled flat channels. *Journal of Membrane Science* 76 (2) 245-254.
- Da Costa, A. R., Fane, A. G. and Wiley, D. E. (1994) Spacer characterization and pressure drop modelling in spacer-filled channels for ultrafiltration. *Journal of Membrane Science* 87 (1) 79-98.
- Dickson, J., Matsuura, T., Blais, P. and Sourirajan, S. (1975) Reverse osmosis separations of some organic and inorganic solutes in aqueous solutions using aromatic polyamide membranes. *Journal of Applied Polymer Science* 19 (3) 801-819.
- Du, Y., Liu, Y., Zhang, S. and Xu, Y. (2016) Optimization of Seawater Reverse Osmosis Desalination Networks with Permeate Split Design Considering Boron Removal. *Industrial & Engineering Chemistry Research* 55 (50) 12860-12879.
- Du, Y., Xie, L., Liu, J., Wang, Y., Xu, Y. and Wang, S. (2014) Multi-objective optimization of reverse osmosis networks by lexicographic optimization and augmented epsilon constraint method. *Desalination* 333 (1) 66-81.
- Edgar, T. F., Himmelblau, D. M. and Lasdon, L. S. (2001) *Optimization of chemical processes*. McGraw-Hill.

- EFSA (2013) Scientific opinion on the toxicological evaluation of phenol. *EFSA Journal* 11 (4) 3189.
- El-halwagi, M. M. (1992) Synthesis of reverse osmosis networks for waste reduction. *AIChe J.* 38 1185-1198.
- Evangelista, F. (1988) An improved analytical method for the design of spiral-wound modules. *The Chemical Engineering Journal* 38 33-40.
- Farhat, A., Ahmad, F., Hilal, N. and Arafat, H. A. (2013) Boron removal in new generation reverse osmosis (RO) membranes using two-pass RO without pH adjustment. *Desalination* 310 (Supplement C) 50-59.
- Farré, M. J., Döderer, K., Hearn, L., Poussade, Y., Keller, J. and Gernjak, W. (2011) Understanding the operational parameters affecting NDMA formation at Advanced Water Treatment Plants. *Journal of Hazardous Materials* 185 (2) 1575-1581.
- Fowler, R. and Guggenheim, E. A. (1965) Statistical thermodynamics: a version of statistical mechanics for students of physics and chemistry.
- Fritzmann, C., Löwenberg, J., Wintgens, T. and Melin, T. (2007) State-of-the-art of reverse osmosis desalination. *Desalination* 216 (1) 1-76.
- Fujioka, T., Nghiem, L. D., Khan, S. J., McDonald, J. A., Poussade, Y. and Drewes, J. E. (2012) Effects of feed solution characteristics on the rejection of N-nitrosamines by reverse osmosis membranes. *Journal of Membrane Science* 409-410 (Supplement C) 66-74.
- Fujioka, T., Khan, S. J., McDonald, J. A., Roux, A., Poussade, Y., Drewes, J. E. and Nghiem, L. D. (2013) N-nitrosamine rejection by nanofiltration and reverse osmosis membranes: The importance of membrane characteristics. *Desalination* 316 (Supplement C) 67-75.
- Fujioka, T. (2014a) Assessment and optimisation of N-nitrosamine rejection by reverse osmosis for planned potable water recycling applications. Ph.d Theses. University of Wollongong.
- Fujioka, T., Khan, S. J., McDonald, J. A., Roux, A., Poussade, Y., Drewes, J. E. and Nghiem, L. D. (2014b) Modelling the rejection of N-nitrosamines by a spiral-wound reverse osmosis system: Mathematical model development and validation. *Journal of Membrane Science* 454 (Supplement C) 212-219.
- Fujioka, T., Ishida, K. P., Shintani, T. and Kodamatani, H. (2018) High rejection reverse osmosis membrane for removal of N-nitrosamines and their precursors. *Water research* 131 45-51.
- Gami, A. A., Shukor, M. Y., Khalil, K. A., Dahalan, F. A., Khalid, A. and Ahmad, S. A. (2014) Phenol and its toxicity *Journal of Environmental Microbiology and Toxicology* 2 (1) 11-24.
- Geraldes, V., Pereira, N. E. and Norberta de Pinho, M. (2005) Simulation and Optimization of Medium-Sized Seawater Reverse Osmosis Processes with Spiral-Wound Modules. *Industrial & Engineering Chemistry Research* 44 (6) 1897-1905.
- Ghobeity, A. and Mitsos, A. (2010) Optimal time-dependent operation of seawater reverse osmosis. *Desalination* 263 (1) 76-88.
- Gholami, M., Mirzaei, R., Kalantary, R. R., Sabzali, A. and Gatei, F. (2012) Performance evaluation of reverse osmosis technology for selected antibiotics removal from synthetic pharmaceutical wastewater. *Iranian Journal of Environmental Health Science & Engineering* 9 (1) 19.
- Girard, B., Fukumoto, L. R. and Sefa Koseoglu, S. (2000a) Membrane Processing of Fruit Juices and Beverages: A Review. *Critical Reviews in Biotechnology* 20 (2) 109-175.

- Girard, B., Fukumoto, L. and Sefa Koseoglu, S. (2000b) Membrane processing of fruit juices and beverages: a review. *Critical reviews in biotechnology* 20 (2) 109-175.
- Gladdon, J. and Dole, M. (1953) Diffusivity determination of sucrose and glucose solutions. *J. Am. Chem. Soc* 75 3900-3904.
- Gómez, J. L., León, G., Hidalgo, A. M., Gómez, M., Murcia, M. D. and Griñán, G. (2009) Application of reverse osmosis to remove aniline from wastewater. *Desalination* 245 (1) 687-693.
- Goosen, M. F., Sablani, S. S., Al-Maskari, S. S., Al-Belushi, R. H. and Wilf, M. (2002) Effect of feed temperature on permeate flux and mass transfer coefficient in spiral-wound reverse osmosis systems. *Desalination* 144 (1-3) 367-372.
- Gostoli, C., Bandini, S., Di Francesca, R., Zardi, G. and Bandini, S. (1995) Concentrating fruit juices by reverse osmosis. The low retention/high retention method. *Fruit Processing* 6 417-421.
- Greenlee, L. F., Lawler, D. F., Freeman, B. D., Marrot, B. and Moulin, P. (2009) Reverse osmosis desalination: Water sources, technology, and today's challenges. *Water Research* 43 (9) 2317-2348.
- Gupta, S. K. (1985) Analytical design equations for reverse osmosis systems. Industrial and Engineering Chemistry Process Design and Development 24 (4) 1240-1244.
- Guria, C., Bhattacharya, P. K. and Gupta, S. K. (2005) Multi-objective optimization of reverse osmosis desalination units using different adaptations of the non-dominated sorting genetic algorithm (NSGA). *Computers & Chemical Engineering* 29 (9) 1977-1995.
- Hafez, A. and El-Mariharawy, S. (2004) Design and performance of the two-stage/two-pass RO membrane system for chromium removal from tannery wastewater. Part 3. *Desalination* 165 141-151.
- Henze, M., van Loosdrecht, M. C. M., Ekama, G. A. and Brdjanovic, D. (2008) Biological Wastewater Treatment. IWA Publishing.
- Hidalgo, A., León, G., Gómez, M., Murcia, M., Bernal, M. and Ortega, S. (2014) Polyamide nanofiltration membranes to remove aniline in aqueous solutions. *Environmental technology* 35 (9) 1175-1181.
- Hsieh, F.-M., Huang, C., Lin, T.-F., Chen, Y.-M. and Lin, J.-C. (2008) Study of sodium tripolyphosphate-crosslinked chitosan beads entrapped with Pseudomonas putida for phenol degradation. *Process Biochemistry* 43 (1) 83-92.
- Irfanudeen, N. M., Prakash, I. A., Saundaryan, R., Alagarraj, K., Goel, M. and Ravi Kumar, K. (2015) The potential of using low cost naturally available biogenic substrates for biological removal of chlorophenol. *Bioresource Technology* 196 (Supplement C) 707-711.
- Jain, S. and Gupta, S. K. (2004) Analysis of modified surface force pore flow model with concentration polarization and comparison with Spiegler– Kedem model in reverse osmosis systems. *Journal of Membrane Science* 232 (1–2) 45-62.
- Jiang, A., Wang, J., Biegler, L. T., Cheng, W., Xing, C. and Jiang, Z. (2015) Operational cost optimization of a full-scale SWRO system under multiparameter variable conditions. *Desalination* 355 124-140.
- Jiang, H., Fang, Y., Fu, Y. and Guo, Q.-X. (2003) Studies on the extraction of phenol in wastewater. *Journal of Hazardous Materials* 101 (2) 179-190.

- Jiao, B., Cassano, A. and Drioli, E. (2004) Recent advances on membrane processes for the concentration of fruit juices: a review. *Journal of Food Engineering* 63 (3) 303-324.
- Jiménez, B. and Asano, T. (2008) Water reuse: an international survey of current practice, issues and needs / edited by Blanca Jiménez and Takashi Asano. London: IWA Publishing,.
- Jonsson, G. (1980) Overview of theories for water and solute transport in UF/RO membranes. *Desalination* 35 (Supplement C) 21-38.
- Kaghazchi, T., Mehri, M., Ravanchi, M. T. and Kargari, A. (2010) A mathematical modeling of two industrial seawater desalination plants in the Persian Gulf region. *Desalination* 252 (1) 135-142.
- Kamble, S. P., Mangrulkar, P. A., Bansiwal, A. K. and Rayalu, S. S. (2008) Adsorption of phenol and o-chlorophenol on surface altered fly ash based molecular sieves. *Chemical Engineering Journal* 138 (1) 73-83.
- Karigar, C., Mahesh, A., Nagenahalli, M. and Yun, D. J. (2006) Phenol Degradation by Immobilized Cells of Arthrobacter citreus. *Biodegradation* 17 (1) 47-55.
- Kedem, O. and Katchalsky, A. (1958) Thermodynamic analysis of the permeability of biological membranes to non-electrolytes. *Biochimica et Biophysica Acta* 27 (Supplement C) 229-246.
- Khazaali, F., Kargari, A. and Rokhsaran, M. (2014) Application of low-pressure reverse osmosis for effective recovery of bisphenol A from aqueous wastes. *Desalination and Water Treatment* 52 (40-42) 7543-7551.
- Kiss, I., Vatai, G. and Bekassy-Molnar, E. (2004) Must concentrate using membrane technology. *Desalination* 162 295-300.
- Koroneos, C., Dompros, A. and Roumbas, G. (2007) Renewable energy driven desalination systems modelling. *Journal of Cleaner Production* 15 (5) 449-464.
- Koyuncu, I., Turan, M., Topacik, D. and Ates, A. (2000) Application of low pressure nanofiltration membranes for the recovery and reuse of dairy industry effluents. *Water Science and Technology* 41 (1) 213-221.
- Kozák, Á., Bánvölgyi, S., Vincze, I., Kiss, I., Békássy-Molnár, E. and Vatai, G. (2008) Comparison of integrated large scale and laboratory scale membrane processes for the production of black currant juice concentrate. Chemical Engineering and Processing: Process Intensification 47 (7) 1171-1177.
- Krauss, M., Longrée, P., Dorusch, F., Ort, C. and Hollender, J. (2009) Occurrence and removal of N-nitrosamines in wastewater treatment plants. *Water Research* 43 (17) 4381-4391.
- Krauss, M., Longrée, P., van Houtte, E., Cauwenberghs, J. and Hollender, J. (2010) Assessing the Fate of Nitrosamine Precursors in Wastewater Treatment by Physicochemical Fractionation. *Environmental Science & Technology* 44 (20) 7871-7877.
- Kujawski, W., Warszawski, A., Ratajczak, W., Porbski, T., Capała, W. and Ostrowska, I. (2004) Removal of phenol from wastewater by different separation techniques. *Desalination* 163 (1) 287-296.
- Lee, C.-J., Chen, Y.-S. and Wang, G.-B. (2010) A dynamic simulation model of reverse osmosis desalination systems. *The 5 th International Symposium on Design, Operation and Control of Chemical Processes, PSE Asia, Singapore.*
- Lee, S. and Lueptow, R. M. (2001) Rotating reverse osmosis: a dynamic model for flux and rejection. *Journal of Membrane Science* 192 (1–2) 129-143.

- Li, M. (2011) Reducing specific energy consumption in Reverse Osmosis (RO) water desalination: An analysis from first principles. *Desalination* 276 (1) 128-135.
- Li, Y., Wei, J., Wang, C. and Wang, W. (2010) Comparison of phenol removal in synthetic wastewater by NF or RO membranes. *Desalination and Water Treatment* 22 (1-3) 211-219.
- Lonsdale, H. K., Merten, U. and Riley, R. L. (1965) Transport properties of cellulose acetate osmotic membranes. *Journal of Applied Polymer Science* 9 (4) 1341-1362.
- Loutatidou, S., Liosis, N., Pohl, R., Ouarda, T. B. and Arafat, H. A. (2017) Wind-powered desalination for strategic water storage: Techno-economic assessment of concept. *Desalination* 408 36-51.
- Lu, Y.-y., Hu, Y.-d., Xu, D.-m. and Wu, L.-y. (2006) Optimum design of reverse osmosis seawater desalination system considering membrane cleaning and replacing. *Journal of Membrane Science* 282 (1–2) 7-13.
- Madaeni, S. S. and Koocheki, S. (2006) Application of taguchi method in the optimization of wastewater treatment using spiral-wound reverse osmosis element. *Chemical Engineering Journal* 119 (1) 37-44.
- Madaeni, S. S. and Koocheki, S. (2010) Influence of di-hydrogen phosphate ion on performance of polyamide reverse osmosis membrane for nitrate and nitrite removal. *Journal of Porous Materials* 17 (2) 163-168.
- Magara, Y., Tabata, A., Kohki, M., Kawasaki, M. and Hirose, M. (1998)

 Development of boron reduction system for sea water desalination.

 Desalination 118 (1) 25-33.
- Malaiyandi, P., Matsuura, T. and Sourirajan, S. (1982) Predictability of membrane performance for mixed solute reverse osmosis systems. System cellulose acetate membrane-D-glucose-D, L-malic acid-water. *Industrial & Engineering Chemistry Process Design and Development* 21 (2) 277-282.
- Mane, P. P., Park, P.-K., Hyung, H., Brown, J. C. and Kim, J.-H. (2009) Modeling boron rejection in pilot- and full-scale reverse osmosis desalination processes. *Journal of Membrane Science* 338 (1–2) 119-127.
- Marcovecchio, M. G., Aguirre, P. A. and Scenna, N. J. (2005) Global optimal design of reverse osmosis networks for seawater desalination: modeling and algorithm. *Desalination* 184 (1) 259-271.
- Marriott, J. (2001) Detailed modelling and optimal design of membrane separation systems. Ph.D Thesis. Department of Chemical Engineering, University College London.
- Marriott, J. and Sørensen, E. (2003) A general approach to modelling membrane modules. *Chemical Engineering Science* 58 (22) 4975-4990.
- Mason, E. A. and Lonsdale, H. K. (1990) Statistical-mechanical theory of membrane transport. *Journal of Membrane Science* 51 (1) 1-81.
- Matsuura, T. and Sourirajan, S. (1973) Physicochemical criteria for reverse osmosis separation of monohydric and polyhydric alcohols in aqueous solutions using porous cellulose acetate membranes. *Journal of Applied Polymer Science* 17 (4) 1043-1071.
- Matsuura, T., Bednas, M., Dickson, J. and Sourirajan, S. (1974) Polar and steric effects in reverse osmosis. *Journal of Applied Polymer Science* 18 (9) 2829-2846.
- Matsuura, T., Baxter, A. and Sourirajan, S. (1975a) Reverse osmosis recovery of flavor components from apple juice waters. *Journal of Food Science* 40 (5) 1039-1046.

- Matsuura, T., Bednas, M., Dickson, J. and Sourirajan, S. (1975b) Reverse osmosis separations of aldehydes, ketones, and ethers in aqueous solutions using porous cellulose acetate membranes. *Journal of Applied Polymer Science* 19 (9) 2473-2484.
- Matsuura, T., Dickson, J. and Sourirajan, S. (1976) Free energy parameters for reverse osmosis separations of undissociated polar organic solutes in dilute aqueous solutions. *Industrial & Engineering Chemistry Process Design and Development* 15 (1) 149-161.
- Matta, V., Moretti, R. and Cabral, L. (2004) Microfiltration and reverse osmosis for clarification and concentration of acerola juice. *Journal of Food Engineering* 61 (3) 477-482.
- Ministry of the Environment of Ontario (2009) Technical support document for Ontario Drinking Water Standards, objectives and guidelines. as of January, http://www.ene.gov.on.ca/envision/techdocs/4449e.htm.
- Miyawaki, O., Gunathilake, M., Omote, C., Koyanagi, T., Sasaki, T., Take, H., Matsuda, A., Ishisaki, K., Miwa, S. and Kitano, S. (2016) Progressive freeze-concentration of apple juice and its application to produce a new type apple wine. *Journal of Food Engineering* 171 153-158.
- Mohammadi, H., Gholami, M. and Rahimi, M. (2009) Application and optimization in chromium-contaminated wastewater treatment of the reverse osmosis technology. *Desalination and Water Treatment* 9 (1-3) 229-233.
- Mohammed, A. E., Jarullah, A. T., Gheni, S. A. and Mujtaba, I. M. (2016) Optimal design and operation of an industrial three phase reactor for the oxidation of phenol. *Computers & Chemical Engineering* 94 (Supplement C) 257-271.
- Mohsen-Nia, M., Montazeri, P. and Modarress, H. (2007) Removal of Cu2+ and Ni2+ from wastewater with a chelating agent and reverse osmosis processes. *Desalination* 217 (1) 276-281.
- Moles, C., Mendes, P. and Banga, J. (2003) Parameter Estimation in Biochemical Pathways: A Comparison of Global Optimization Methods. *Genome Research* 2467-2474. http://www.genome.org/cgi/doi/10.1101/gr.1262503.
- Mujtaba, I. M. (2004) *Batch distillation: Design and operation.* Imperial College Press, London, UK.
- Mujtaba, I. M. (2012) The role of PSE community in meeting sustainable freshwater demand of tomorrow's world via desalination. In: Karimi, I.A., Srinivasan, Rajagopalan(Eds.). *Computer Aided Chemical Engineering* 31 91–98.
- Muldowney, G. P. and Punzi, V. L. (1988) A comparison of solute rejection models in reverse osmosis membranes for the system water-sodium chloride-cellulose acetate. *Industrial & engineering chemistry research* 27 (12) 2341-2352.
- Murthy, Z. V. P. and Gupta, S. K. (1998) Thin Film Composite Polyamide Membrane Parameters Estimation for Phenol-Water System by Reverse Osmosis. Separation Science and Technology 33 (16) 2541-2557.
- Murthy, Z. V. P. and Gupta, S. K. (1999) Sodium cyanide separation and parameter estimation for reverse osmosis thin film composite polyamide membrane. *Journal of Membrane Science* 154 (1) 89-103.
- Murthy, Z. V. P. and Vengal, J. C. (2006) Optimization of a Reverse Osmosis System Using Genetic Algorithm. Separation Science and Technology 41 (4) 647-663.

- Nabetani, H., Nakajima, M., Watanabe, A., Ikeda, S.-i., Nakao, S.-i. and Kimura, S. (1992a) Development of a new type of membrane osmometer. *Journal of chemical engineering of Japan* 25 (3) 269-274.
- Nabetani, H., Nakajima, M., Watanabe, A., Nakao, S.-i. and Kimura, S. (1992b) Prediction of the flux for the reverse osmosis of a solution containing sucrose and glucose. *Journal of chemical engineering of Japan* 25 (5) 575-580.
- Nabetani, H. (1996) Development of a membrane system for highly concentrated fruit juice. *Membrane* 21 (2) 102-108.
- Najm, I. and Trussell, R. R. (2001) NDMA formation in water and wastewater. Journal (American Water Works Association) 93 (2) 92-99.
- Oh, H.-J., Hwang, T.-M. and Lee, S. (2009) A simplified simulation model of RO systems for seawater desalination. *Desalination* 238 (1) 128-139.
- Olsson, J. and Trägårdh, G. (1999) Influence of feed flow velocity on pervaporative aroma recovery from a model solution of apple juice aroma compounds. *Journal of Food Engineering* 39 (1) 107-115.
- Patroklou G., Sassi, K. M. and Mujtaba, I. M. (2013) Simulation of boron rejection by seawater reverse osmosis desalination. *Chemical Engineering Transaction* 32 1873-1878.
- Peñate, B., Castellano, F., Bello, A. and García-Rodríguez, L. (2011) Assessment of a stand-alone gradual capacity reverse osmosis desalination plant to adapt to wind power availability: A case study. *Energy* 36 (7) 4372-4384.
- Pepper, D. (1990) RO for improved products in the food and chemical industries and water treatment. *Desalination* 77 (Supplement C) 55-71.
- Pereira, E. N., Matsuura, T. and Sourirajan, S. (1976) Reverse osmosis separations and concentrations of food sugars. *Journal of Food Science* 41 (3) 672-680.
- Plumlee, M. H., López-Mesas, M., Heidlberger, A., Ishida, K. P. and Reinhard, M. (2008) N-nitrosodimethylamine (NDMA) removal by reverse osmosis and UV treatment and analysis via LC–MS/MS. *Water Research* 42 (1) 347-355.
- Pomiès, M., Choubert, J. M., Wisniewski, C. and Coquery, M. (2013) Modelling of micropollutant removal in biological wastewater treatments: A review. *Science of The Total Environment* 443 (Supplement C) 733-748.
- Pozderović, A., Moslavac, T. and Pichler, A. (2006a) Concentration of aqueous solutions of organic components by reverse osmosis: II. Influence of transmembrane pressure and membrane type on concentration of different alcohol solutions by reverse osmosis. *Journal of Food Engineering* 77 (4) 810-817.
- Pozderović, A., Moslavac, T. and Pichler, A. (2006b) Concentration of aqua solutions of organic components by reverse osmosis. I: Influence of transmembrane pressure and membrane type on concentration of different ester and aldehyde solutions by reverse osmosis. *Journal of Food Engineering* 76 (3) 387-395.
- Process System Enterprise Ltd, P. S. E. L., London. (2001) gPROMS Introductory User Guide.
- Qdais, H. A. and Moussa, H. (2004) Removal of heavy metals from wastewater by membrane processes: a comparative study. *Desalination* 164 (2) 105-110.
- Qi, B., Wang, Y., Xu, S., Wang, Z. and Wang, S. (2012) Operating energy consumption analysis of RO desalting system: effect of membrane

- process and energy recovery device (ERD) performance variables. *Industrial & Engineering Chemistry Research* 51 (43) 14135-14144.
- Qin, J.-J., Htun Oo, M., Nyunt Wai, M., Lee, H., Hong, S. P., Kim, J. E., Xing, Y. and Zhanga, M. (2005) Pilot study for reclamation of secondary treated sewage effluent. *Desalination* 171 (3) 299-305.
- Redondo, J., Busch, M. and De Witte, J.-P. (2003) Boron removal from seawater using FILMTECTM high rejection SWRO membranes. *Desalination* 156 (1) 229-238.
- Reverberi, A. P., Fabiano, B., Cerrato, C. and Dovì, V. G. (2014) Concentration Polarization in Reverse Osmosis Membranes: Effect of Membrane Splitting. *Chemical Engineering Transactions*, 39 763-768.
- Sagne, C., Fargues, C., Broyart, B., Lameloise, M.-L. and Decloux, M. (2009) Modeling permeation of volatile organic molecules through reverse osmosis spiral-wound membranes. *Journal of Membrane Science* 330 (1–2) 40-50.
- Sagne, C., Fargues, C., Lewandowski, R., Lameloise, M.-L., Gavach, M. and Decloux, M. (2010) A pilot scale study of reverse osmosis for the purification of condensate arising from distillery stillage concentration plant. *Chemical Engineering and Processing: Process Intensification* 49 (4) 331-339.
- Sapienza, F. J., Gill, W. N. and Soltanieh, M. (1990) Separation of ternary salt/acid aqueous solutions using hollow fiber reverse osmosis. *Journal of Membrane Science* 54 (1) 175-189.
- Sarkar, P., Goswami, D., Prabhakar, S. and Tewari, P. K. (2008) Optimized design of a reverse osmosis system with a recycle. *Desalination* 230 (1) 128-139.
- Sassi, K. M. (2012) Optimal Scheduling, Design, Operation and Control of Reverse Osmosis based Desalination,. Doctor of Philosophy University of Bradford
- Schäfer, A. I., Mitch, W., Walewijk, S., Munoz, A., Teuten, E. and Reinhard, M. (2010) Chapter 7 Micropollutants in Water Recycling: A Case Study of N-Nitrosodimethylamine (NDMA) Exposure from Water versus Food. In Escobar, I. C. and Schäfer, A. I. (editors) Sustainability Science and Engineering. Vol. 2. Elsevier. 203-228.
- Schock, G. and Miquel, A. (1987) Mass transfer and pressure loss in spiral wound modules. *Desalination* 64 339-352.
- Schoeman, J. J. and Steyn, A. (2003) Nitrate removal with reverse osmosis in a rural area in South Africa. *Desalination* 155 (1) 15-26.
- Schwinge, J., Wiley, D. E. and Fletcher, D. F. (2002) A CFD study of unsteady flow in narrow spacer-filled channels for spiral-wound membrane modules. *Desalination* 146 (1) 195-201.
- Schwinge, J., Neal, P., Wiley, D., Fletcher, D. and Fane, A. (2004) Spiral wound modules and spacers: review and analysis. *Journal of membrane science* 242 (1) 129-153.
- Selbes, M., Glenn, M. and Karanfil, T. (2015) The Role of Pre-Oxidation in Controlling NDMA Formation: A Review. Recent Advances in Disinfection By-Products.ACS Symposium Series. Vol. 1190. American Chemical Society. 151-172.
- Senthilmurugan, S., Ahluwalia, A. and Gupta, S. K. (2005) Modeling of a spiral-wound module and estimation of model parameters using numerical techniques. *Desalination* 173 (3) 269-286.

- Sharma, R. R., Agrawal, R. and Chellam, S. (2003) Temperature effects on sieving characteristics of thin-film composite nanofiltration membranes: pore size distributions and transport parameters. *Journal of Membrane Science* 223 (1) 69-87.
- Sharma, V. K. (2012) Kinetics and mechanism of formation and destruction of Nnitrosodimethylamine in water – A review. *Separation and Purification Technology* 88 1-10.
- Sheu, M. and Wiley, R. (1983) Preconcentration of apple juice by reverse osmosis. *Journal of Food Science* 48 (2) 422-429.
- Soltanieh, M. and Gill, W. N. (1981) Review of reverse osmosis membranes and transport models. *Chemical Engineering Communications* 12 (4-6) 279-363.
- Souza, A. L., Pagani, M. M., Dornier, M., Gomes, F. S., Tonon, R. V. and Cabral, L. M. (2013) Concentration of camu–camu juice by the coupling of reverse osmosis and osmotic evaporation processes. *Journal of Food Engineering* 119 (1) 7-12.
- Spiegler, K. S. and Kedem, O. (1966) Thermodynamics of hyperfiltration (reverse osmosis): criteria for efficient membranes. *Desalination* 1 (4) 311-326.
- Srinivasan, G., Sundaramoorthy, S. and Murthy, D. V. R. (2009) Separation of dimethyl phenol using a spiral-wound RO membrane Experimental and parameter estimation studies. *Desalination* 243 (1) 170-181.
- Srinivasan, G., Sundaramoorthy, S. and Murthy, D. V. R. (2010) Spiral wound reverse osmosis membranes for the recovery of phenol compounds-experimental and parameter estimation studies. *American J. of Engineering and Applied Sciences* 3 (1) 31-36.
- Srinivasan, G., Sundaramoorthy, S. and Murthy, D. V. R. (2011) Validation of an analytical model for spiral wound reverse osmosis membrane module using experimental data on the removal of dimethylphenol. *Desalination* 281 (Supplement C) 199-208.
- Steinle-Darling, E., Zedda, M., Plumlee, M. H., Ridgway, H. F. and Reinhard, M. (2007) Evaluating the impacts of membrane type, coating, fouling, chemical properties and water chemistry on reverse osmosis rejection of seven nitrosoalklyamines, including NDMA. *Water Research* 41 (17) 3959-3967.
- Sundaramoorthy, S., Srinivasan, G. and Murthy, D. V. R. (2011a) An analytical model for spiral wound reverse osmosis membrane modules: Part I Model development and parameter estimation. *Desalination* 280 (1–3) 403-411.
- Sundaramoorthy, S., Srinivasan, G. and Murthy, D. V. R. (2011b) An analytical model for spiral wound reverse osmosis membrane modules: Part II Experimental validation. *Desalination* 277 (1–3) 257-264.
- Sutzkover, I., Hasson, D. and Semiat, R. (2000) Simple technique for measuring the concentration polarization level in a reverse osmosis system. *Desalination* 131 (1) 117-127.
- Tabassi, D., Mnif, A. and Hamrouni, B. (2014) Influence of operating conditions on the retention of phenol in water by reverse osmosis SG membrane characterized using Speigler–Kedem model. *Desalination and Water Treatment* 52 (7-9) 1792-1803.
- Taniguchi, Y. (1978) An analysis of reverse osmosis characteristics of ROGA spiral-wound modules. *Desalination* 25 (1) 71-88.
- Thirugnanasambandham, K., Sivakumar, V., Loganathan, K., Jayakumar, R. and Shine, K. (2016) Pilot scale evaluation of feasibility of reuse of wine

- industry wastewater using reverse osmosis system: modeling and optimization. *Desalination and Water Treatment* 57 (53) 25358-25368.
- Thomson, M., Miranda, M. S. and Infield, D. (2003) A small-scale seawater reverse-osmosis system with excellent energy efficiency over a wide operating range. *Desalination* 153 (1-3) 229-236.
- US EPA (2009a) Contaminant Information Sheets for the Final CCL 3 Chemicals, EPA.
- US EPA (2009b) United States Environmental Protection Agency IRIS database, https://www.epa.gov/iris.
- Van Gauwbergen, D. and Baeyens, J. (1998) Modelling reverse osmosis by irreversible thermodynamics. *Separation and Purification Technology* 13 (2) 117-128.
- Verliefde, A. R. D., Cornelissen, E. R., Heijman, S. G. J., Verberk, J. Q. J. C., Amy, G. L., Van der Bruggen, B. and van Dijk, J. C. (2009) Construction and validation of a full-scale model for rejection of organic micropollutants by NF membranes. *Journal of Membrane Science* 339 (1) 10-20.
- Villafafila, A. and Mujtaba, I. M. (2003) Fresh water by reverse osmosis based desalination: simulation and optimisation. *Desalination* 155 (1) 1-13.
- Wade Miller, G. (2006) Integrated concepts in water reuse: managing global water needs. *Desalination* 187 (1) 65-75.
- Walker, J. B. (1990) Reverse osmosis concentration of juice products with improved flavor. Google Patents.
- Wankat, P. C. (1990) Rate-controlled separations.
- Water U.K. (2011) National guidance for healthcare waste water discharges, hospitals, http://www.water.org.uk/publications/water-industry-guidance/national-guidance-healthcare-waste-water-discharges). (Accessed, 10, 14, 2016).
- Wei, Q. J. and McGovern, R. K. (2017) Saving energy with an optimized twostage reverse osmosis system. *Environmental Science: Water Research* & *Technology*.
- Wijmans, J. G. and Baker, R. W. (1995) The solution-diffusion model: a review. *Journal of Membrane Science* 107 (1–2) 1-21.
- Wilke, C. and Chang, P. (1955) Correlation of diffusion coefficients in dilute solutions. *AIChE Journal* 1 (2) 264-270.
- Xijun, C., Guohua, C., Po-Lock, Y. and Yongli, M. (1997) Pilot scale membrane separation of electroplating waste water by reverse osmosis. *Journal of Membrane Science* 123 (2) 235-242.
- Zainal, B., Rahman, R. A., Ariff, A., Saari, B. and Asbi, B. (2000) Effects of temperature on the physical properties of pink guava juice at two different concentrations. *Journal of Food Engineering* 43 (1) 55-59.
- Zelman, A. (1972) Membrane Permeability: Generalization of the Reflection Coefficient Method of Describing Volume and Solute Flows. *Biophysical Journal* 12 (4) 414-419.
- Zhu, A., Christofides, P. D. and Cohen, Y. (2009) Effect of Thermodynamic Restriction on Energy Cost Optimization of RO Membrane Water Desalination. *Industrial & Engineering Chemistry Research* 48 (13) 6010-6021.

Appendix (A)

Table A.1. Model Equations of Srinivasan et al. (2009) and Srinivasan et al. (2010)

Title	The Mathematical Expression	Eq.
Title	The Mathematical Expression	no.
The water flux	$J_{w}=A_{w}(\Delta P-\Delta \pi)$	1
The trans-membrane pressure	$\Delta P_{b} = ((P_{b(0)} + P_{b(L)})/2) - P_{p}$	2
The solute flux	$J_{s} = B_{s} (C_{w} - C_{p})$	3
The osmotic pressure	$\Delta \pi = R(T_b + 273.15)(C_w - C_p)$	4
The concentration at membrane wall	$\frac{C_{\mathbf{w}} - C_{\mathbf{p}}}{C_{\mathbf{b}} - C_{\mathbf{p}}} = e^{\frac{\mathbf{J}_{\mathbf{w}}}{\mathbf{k}}}$	5
The rejection parameter	$Rej = 1 - \frac{c_p}{c_w}$	6
The bulk concentration	$C_{b} = \frac{C_{b(0)}}{(1-\tau)+\tau M(1-Rej)}$	7
parameter τ in Eq. (7)	$\tau = \frac{F_{\rm p}}{F_{\rm b(0)}}$	8
parameter M in Eq. (7)	$M = \frac{\frac{J_W}{e^{\frac{J}{k}}}}{Rej + (1 - Rej)e^{\frac{J}{k}}}$	9
The permeate concentration	$C_p = M C_{b(0)} (1 - Rej)$	10

Table A.2. Equations describing the spiral-wound RO modelling of Sundaramoorthy et al. (2011a)

'	,	
Title	The Mathematical Expression	Eq.
The water flux at any point along the x-axis	$J_{w(x)} = \frac{\emptyset}{A \sinh \emptyset} \left[\left(F_{b(0)} \cosh \emptyset \left(1 - \frac{x}{L} \right) - F_{b(L)} \cosh \frac{\emptyset x}{L} \right) \right]$	1
The parameter Ø in Eq. (1)	$\emptyset = L \left(\frac{WbA_w}{\left(1 + A_w \frac{R}{B_S} T C_p \right)} \right)^{0.5}$	2
The feed pressure at any point along the x-axis	$\begin{aligned} P_{b(x)} &= P_{b(0)} - \frac{bL}{\emptyset \sinh \emptyset} \left[F_{b(L)} \left(\cosh \frac{\emptyset x}{L} - 1 \right) - F_{b(0)} \left(\cosh \emptyset \left(1 - \frac{x}{L} \right) - \cosh \emptyset \right) \right] \end{aligned}$	3
The retentate pressure	$P_{b(L)} = P_{b(0)} - \frac{bL}{\emptyset \sinh \emptyset} [(F_{b(0)} + F_{b(L)})(\cosh \emptyset - 1)]$	4
The osmotic pressure at any point along the x-axis	$\Delta \pi_{(x)} = R(T_b + 273.15)(C_{b(x)} - C_p)$	5
The feed concentration at any point along the x-axis	$C_{b(x)} = C_p + \frac{F_{b(0)}(C_{b(0)} - C_p)}{F_{b(x)}}$	6
The rejection parameter	$Rej = 1 - \frac{c_p}{c_{b(L)}}$	7
The mass transfer coefficient of dimethylphenol at any point along the x-axis	$k_{(x)}de_b = 246.9 D_{b(x)} Re_{b(x)}^{0.101} Re_{p(x)}^{0.803} C_{m(x)}^{0.129}$	8
The mass transfer coefficient of chlorophenol at any point along the x-axis	$k_{(x)}de_b = 147.4 D_{b(x)} Re_{b(x)}^{0.13} Re_{p(x)}^{0.739} C_{m(x)}^{0.135}$	9
The permeate concentration at any point along the permeate channel	$C_{p} = \frac{C_{b(x)}}{\begin{pmatrix} \frac{J_{w(x)}}{B_{S}} \\ 1 + \frac{J_{w(x)}}{B_{K}} \\ \frac{J_{w(x)}}{e^{k_{(x)}}} \end{pmatrix}}$	10

Table A.3. Equations describing the spiral wound RO modelling of Fujioka et al. (2014b)

Title	The Mathematical Expression	Eq.
Calculate water flux at each point along the x-axis	$J_{w(x)} \texttt{=} L_{p} \big[\big(P_{b(x)} - P_{p} - \sigma \Delta \pi_{(x)} \big) \big]$	1
Calculate the total permeate flux per each slide	$Q_{p(x)} = J_{w(x)} \Delta S$	2
Calculate the total permeate flux of membrane	$Q_{p,t} = \sum Q_{p(x)}$	3
Calculate the osmotic pressure at each point along the x-axis	$\pi_{(x)} = 1.19(T + 273.15) \sum C_{b(x)}$	4
Calculate the progress of feed concentration at each point along the x-axis	$C_{b(x+1)} = \frac{F_{b(x)}C_{b(x)} - C_{p(x)}Q_{p(x)}}{F_{b(x+1)}}$	5
Calculate the sub-section feed flow rate at each point along the x-axis	$F_{b(x+1)} = F_{b(x)} - Q_{p(x)}$	6
Calculate the pressure drop at each point along the membrane length	$\Delta P_{b(x)} = 0.5 b \rho_{b(x)} U_{b(x)}^2 \frac{\Delta x}{d_h}$	7
Calculate the total pressure drop per each element	$\Delta P_{b.t} = \sum \Delta P_{b(x)}$	8
Calculate the progress of feed pressure at each sub-section	$P_{b(x+1)} = P_{b(x)} - \Delta P_{b(x)}$	9
Calculate the density parameter		10
Calculate the parameter M_f in Eq. (8)	$m_f = 1.0069 - 2.757.10^{-4} T_b$	11
Calculate the rejection parameter at each point along the membrane length	$Rej_{(x)} = \frac{\sigma(1-F_{(x)})}{(1-\sigma F_{(x)})}$	12
Calculate the observed rejection parameter	$Rej_{obs(x)} = \frac{Rej_{(x)}}{(1-Rej_{(x)})x \exp\left(\frac{J_{w(x)}}{k_{(x)}}\right) + Rej_{(x)}}$	13
Calculate the parameter $(F_{(x)})$ in Eq. (10)	$F_{(x)} = \exp\left[-\frac{(1-\sigma)}{B_s}J_{w(x)}\right]$	14
Calculate mass transfer coefficient. K , $\mu_{b(x)}$ and $\rho_{b(x)}$ are the efficiency of mixing (K = 0.5)	$\begin{array}{c} k_{(x)} \! = \! 0.753 \\ \left(\frac{K}{2\text{-}K}\right)^{0.5} \left(\frac{D_{b(x)}}{t_f}\right) \left(\frac{\mu_{b(x)}\rho_{b(x)}}{D_{b(x)}}\right)^{0.1666} \left(\frac{2t_f^2 U_{b(x)}}{D_{b(x)}\Delta L}\right)^{0.5} \end{array}$	15
Calculate the viscosity parameter	$\mu = 2.141E - 5x \times 10^{\frac{247.8}{T-140}}$	16
Calculate the permeate concentration at each point along the permeate channel	$C_{p(x)} = C_{b(x)}(1 - Rej_{obs})$	17
Calculate the overall permeate concentration	$C_{p(av)} = \frac{\sum C_{p(x)}Q_{p(x)}}{\sum Q_{p(x)}}$	18

Table A.4. Equations describing the spiral wound RO modelling of Alvarez et al. (2002)

Title	The Mathematical Expression	Eq.
Title	The Mathematical Expression	no.
Calculate water flux	$J_{w}=A_{w}[(\Delta P_{b}-\Delta \pi_{Total})]$	1
Calculate solute flux	$J_{s} = B_{s} (C_{w} - C_{p})$	2
Calculate permeate	$C_{\rm p} = \frac{J_{\rm s}}{I_{\rm res}}$	3
concentration	$G_{\rm p} = I_{\rm w}$	
Wall membrane	$\frac{(C_{\rm w})}{(C_{\rm h})} = \exp\left(\frac{J_{\rm w}}{k}\right)$	4
concentration	(C_b) (k)	1
Rejection	$Rej = \frac{c_b - c_p}{c_b} x100$	5
Water permeability	$A_{\rm w} = 9.059 \times 10^{-7} \left(\frac{T_{\rm b}}{25}\right)^{0.62} \left(\frac{36.0 \times 10^5 \rm Q_f}{400}\right)^{-0.1447}$	6
constant	$A_{W} = 3.033 \text{ All } \left(\frac{1}{25}\right) \left(\frac{1}{400}\right)$	
Total osmotic pressure	$\Delta \pi_{Total} = \pi_{C_{\mathbf{w}}} - \pi_{C_{\mathbf{p}}}$	7
	$\pi_{\text{su,w}} + \pi_{\text{g,w}} + \pi_{\text{ma,w}} =$	
Total osmotic pressure	$-\frac{R\left(T_{b}+273.15\right)}{V_{w}} \ln \left\{ \!\! \frac{\left[\!\! \frac{\left(1000-C_{SU,w}-C_{g,w}\right)}{M_{wb}} \!\! -\! \frac{\left[\!\! \frac{\left(4C_{SU,w}\right)}{M_{SU}} \!\! -\! \frac{\left[\!\! \frac{\left(2C_{g,w}\right)}{M_{g}} \!\! \right]}{M_{g}} \!\! \right]}{\left[\!\! \frac{\left(1000-C_{SU,w}-C_{g,w}\right)}{M_{wb}} \!\! -\! \frac{\left[\!\! \frac{\left(4C_{SU,w}\right)}{M_{SU}} \!\! -\! \frac{\left[\!\! \frac{\left(2C_{g,w}\right)}{M_{g}} \!\! \right]}{M_{g}} \!\! \right]}{M_{g}} \!\! \right\} + $	8
	$\frac{R (T_b + 273.15) C_{ma,w}}{M_{ma}}$	

The physical properties equations are similar to what mentioned Model Type_7 in Chapter 3

Table A.5. Dynamic 1D model equations (Model Type_1)

Title	The Mathematical Expression	Eq. no.
Dynamic axial water flux,	$\frac{\mathrm{d}J_{w(x)}}{\mathrm{d}t} = \left\{ \left(A_w \left((P_{b(x)} - P_p) - RT_{b(x)} \left(C_{w(x)} - P_p \right) \right) \right\} \right\}$	
m/s²	at (('	1
	$C_{p(x)}))$ $-J_{w(x)}$ $\left(\frac{F_{b(x)}}{t_f W \Delta x}\right)$	
Dynamic axial solute flux,	$\frac{\mathrm{d}J_{s(x)}}{\mathrm{d}t} = \left\{ \left(B_{s} \exp\left(\frac{J_{w(x)}}{k_{(x)}}\right) \left(C_{b(x)} - C_{p(x)} \right) \right) - \right.$	
kmol/m² s²	$\frac{1}{dt} = \left\{ \left(\sum_{k=0}^{\infty} e^{kx} p \left(\frac{1}{k(x)} \right) \left(C_{b(x)} - C_{p(x)} \right) \right) - \frac{1}{k(x)} \right\}$	2
	$J_{S(x)} \left\{ \frac{F_{b(x)}}{t_{f} W \Delta x} \right\}$	
	$\int S(x) \int \left(t_f W \Delta x \right)$	
Dynamic axial membrane	$\frac{dC_{w(x)}}{dt} = \left\{ \left(C_{p(x)} + \exp\left(\frac{J_{w(x)}}{k_{(x)}}\right) \left(C_{b(x)} - C_{p(x)} \right) \right) - \right.$	
wall concentration, kmol/m³ s	$dt = \left(\left(\frac{op(x) + exp}{k_{(x)}} \right) \left(\frac{op(x)}{op(x)} \right) \right)$	3
	$C_{w(x)} \left\{ \left(\frac{F_{b(x)}}{f_{t} W \Delta x} \right) \right\}$	
) (1 ===)	
Pressure difference along the	$\Delta P_{b(x)} = (P_{b(x)} - P_{p})$	4
membrane, atm Dynamic axial feed flow rate,		
m ² /s ²	$\left \frac{dF_{b(x)}}{dt} = \right \left -W \left(A_w \left((P_{b(x)} - P_p) - \right) \right) \right $	
	at [(("(* Jos)	
	$\left R T_{b(x)} \exp \left(\frac{J_{w(x)}}{k_{(x)}} \right) \left(C_{b(x)} - C_{p(x)} \right) \right) \right -$	5
	$\left\{\begin{array}{ccc} K & I_{b(x)} & CAP \\ k_{(x)} & J & CB(x) & CB(x) \end{array}\right\}$	
	$\left[\frac{dF_{b(x)}}{dx}\right]\left(\frac{F_{b(x)}}{t_{c}W}\right)$	
	$\left \frac{b(x)}{dx} \right \left(\frac{b(x)}{t_f W} \right)$	
Dynamic axial feed pressure,	$dP_{b(x)}$ $dP_{b(x)}$ $dP_{b(x)}$	
atm/s	$\left \frac{dP_{b(x)}}{dt} = \left[-b F_{b(x)} - \frac{dP_{b(x)}}{dx} \right] \left(\frac{F_{b(x)}}{t_f W} \right)$	6
Axial permeated flow rate,	$F_{p(x)} = J_{w(x)} W \Delta x$	7
m³/s		
Dynamic axial molar flux of	$\frac{dC_{b(x)}}{dt} = -\frac{C_{b(x)}}{t_f W} \frac{dF_{b(x)}}{dx} - \frac{F_{b(x)}}{t_f W} \frac{dC_{b(x)}}{dx} +$	
feed, kmol/m³ s	$\frac{d}{d} \left[D_{x} - \frac{dC_{b(x)}}{dx} \right] - \frac{J_{w(x)} C_{p(x)}}{J_{w(x)} C_{p(x)}}$	8
Described to the second	$ \frac{\frac{d}{dx} \left[D_{b(x)} \frac{dC_{b(x)}}{dx} \right] - \frac{J_{w(x)} C_{p(x)}}{t_{f}} }{\frac{dC_{p(x)}}{dt} = -\frac{C_{p(x)}}{t_{p} W} \frac{dF_{p(x)}}{dx} - \frac{F_{p(x)} dC_{p(x)}}{t_{p} W} \frac{dC_{p(x)}}{dx} + $	
Dynamic axial molar flux of permeate, kmol/m³ sec	$\frac{d\mathbf{c}\mathbf{p}(\mathbf{x})}{dt} = -\frac{\mathbf{c}\mathbf{p}(\mathbf{x})}{t_{\mathbf{p}}} \frac{d\mathbf{r}\mathbf{p}(\mathbf{x})}{d\mathbf{x}} - \frac{\mathbf{r}\mathbf{p}(\mathbf{x})}{t_{\mathbf{p}}} \frac{d\mathbf{c}\mathbf{p}(\mathbf{x})}{d\mathbf{x}} +$	
permeate, kino//iii- sec	$\frac{d}{dx} \left[D_{p(x)} \frac{dC_{p(x)}}{dx} \right] + \frac{J_{w(x)} C_{p(x)}}{t_f}$	9
Dynamic axial feed	$\left \frac{dT_{b(x)}}{dt} = \left[\frac{F_{b(x)} \left(T_{b(x-1)} - T_{b(x)} \right)}{t_f W \Delta x} \right] - \left[\frac{J_{w(x)} \left(T_{b(x)} - T_{p(x)} \right)}{t_f} \right]$	10
temperature, °C/s Dynamic axial permeated		
temperature, °C/s	$ \frac{dT_{p(x)}}{dt} = \left[\frac{J_{w(x)} \left(T_{b(x)} - T_{p(x)} \right)}{t_f} \right] $	11
Total permeated flow rate,	$F_{p(Total)} = \sum F_{p(x)}$	12
m³/s		12
Total recovery,	$Rec_{(Total)} = \frac{F_{p(Total)}}{F_{b(0)}} X100$	13
dimensionless Average solute rejection	Ch(Y-1)=Cn(yy)	-
Average solute rejection, dimensionless	$Rej_{(av)} = \frac{c_{b(X=L)} - c_{p(av)}}{c_{b(X=L)}} X100$	14
Average permeated	$C_{p(av)} = \sum C_{p(x)}/n$. sub – divisions	4.5
concentration, kmol/m³		15
Axial mass transfer	$k_{(x)} de_b = 147.4 D_{b(x)} Re_{b(x)}^{0.13} Re_{p(x)}^{0.739} C_{m(x)}^{0.135}$	16
coefficient, m/s	Chris	+
Axial Dimensionless solute concentration, dimensionless	$C_{m(x)} = \frac{C_{b(x)}}{\rho_w}$	17
Axial feed diffusivity, m ² /s		
	$D_{b(x)} = 6.725E - 6 \exp \{0.1546E - $	18
	$D_{b(x)} = 6.725E - 6 \exp \left\{ 0.1546E - 3 C_{b(x)} x18.01253 - \frac{2513}{T_{b(x)} + 273.15} \right\}$	10
	T 1272.15	1
	$1_{b(x)+2/3.15}$	1

Table A.5. Dynamic	1D model equations (Model Type_1) (Continued)		
Title	The Mathematical Expression	Eq.	
Axial permeated diffusivity, m²/s	$\begin{split} D_{p(x)} &= 6.725E - 6 \exp \left\{ 0.1546E - 3 \ C_{p(x)} \ x18.01253 - \frac{2513}{T_{p(x)} + 273.15} \right\} \end{split}$	19	
Axial feed viscosity, kg /m s	$\begin{split} \mu_{b(x)} &= 1.234E - 6 \ exp \left\{ 0.0212E - \right. \\ &\left. 3 \ C_{b(x)} \ x18.0153 + \frac{_{1965}}{_{T_{b(x)} + 273.15}} \right\} \end{split}$	20	
Axial permeated viscosity, kg /m s	$\begin{split} \mu_{p(x)} &= 1.234E - 6 \ exp \left\{ 0.0212E - \right. \\ &\left. 3 \ C_{p(x)} \ x18.0153 + \frac{^{1965}}{^{T}_{p(x)} + 273.15} \right\} \end{split}$	21	
Axial feed density, kg/m³	$\rho_{b(x)} = 498.4 \text{ m}_{f(x)} + \sqrt{\left[248400 \text{ m}_{f(x)}^2 + 752.4 \text{ m}_{f(x)} \text{ C}_{b(x)} \text{ x} 18.0153\right]}$	22	
Axial permeated density, kg/m³	$\begin{split} \rho_{p(x)} &= 498.4 \; m_{p(x)} \; + \\ \sqrt{\left[248400 \; m_{p(x)}^2 + 752.4 \; m_{p(x)} \; \; C_{p(x)} \; x18.0153 \right]} \end{split}$	23	
Axial variable in Eq. (22)	$m_{f(x)} = 1.0069 - 2.757E - 4 T_{b(x)}$	24	
Axial variable in Eq. (23)	$m_{p(x)} = 1.0069 - 2.757E - 4 T_{p(x)}$	25	
Axial feed channel Reynolds number, dimensionless	$Re_{b(x)} = \frac{\rho_{b(x)} de_b F_{b(x)}}{t_f W \mu_{b(x)}}$	26	
Axial permeate channel Reynolds number, dimensionless	$Re_{p(x)} = \frac{\rho_{p(x)} de_p J_{w(x)}}{\mu_{p(x)}}$	27	
The equivalent diameter of feed channel, m	$de_b = 2t_f$	28	
The equivalent diameter of permeated channel, m Total number of equations is 2	$de_p = 2t_p$	29	
Total Hambol of Oquationio to 20			

Table A.6. Specifications of variables

	Total
Variables:	
$J_{w(x)}, J_{s(x)}, P_{p(x)}, T_{b(x)}, T_{p(x)}, C_{w(x)}, C_{b(x)}, C_{p(x)}, F_{b(x)}, F_{p(x)}, k_{(x)}, F_{p(Total)},$	39
$Rec_{(Total)}, Rej_{(av)}, C_{p(av)}, de_b, de_p, C_{m(x)}, D_{b(x)}, D_{p(x)}, \mu_{b(x)}, \mu_{p(x)}, \rho_{b(x)},$	
$\rho_{p(x)}, m_{f(x)}, m_{p(x)}, Re_{b(x)}, Re_{p(x)}, \Delta P_{b(x)}, A_w, B_s, L,$	
W , ρ_w , b , P_p , t_f , t_p and ρ_w	
Differential variables at t = 0:	9
$\frac{dJ_{w(x)}}{dx}, \frac{dJ_{s(x)}}{dx}, \frac{dC_{w(x)}}{dx}, \frac{dF_{b(x)}}{dx}, \frac{dP_{b(x)}}{dx}, \frac{dC_{b(x)}}{dx}, \frac{dC_{p(x)}}{dx}, \frac{dT_{b(x)}}{dx}, \frac{dT_{p(x)}}{dx}$	
dt dt dt dt dt dt dt dt	
t is independent variable	1
Total	49

The specification of the dynamic model (Table A.6) shows that the total number of variables is 49, while the number of equations is 29 as can be seen in Table A.5, so:

D.F. = Total number of variables – Total number of equations

$$D.F. = 49 - 29 = 20$$

The number of parameters is 10 (Table A.7) and assigned initial values of differential variables at t = 0 are 9 (Table A.2) and independent variable =1, (time, t). So, this specification counts 20 variables.

Table A.7. Specifications of constant parameters and differential variables at t = 0

Parameter	Value
Feed spacer thickness (t _f)	0.8 mm
Permeate channel thickness (t _p)	0.5 mm
Module length (L)	0.934 m
Module width (W)	8.4 m
Molal density of water, (ρ_w)	55.56 kmol/m³
Gas law constant, (R)	0.082 (atm m ³ /°K kmol)
Permeate pressure (P _p)	1 atm
Feed channel friction parameter, (b)	$8529.45 \left(\frac{\text{atm s}}{\text{m}^4}\right)$
Solvent transport coefficient, (A _w)	$9.5188 \times 10^{-7} \left(\frac{m}{a tm s}\right)$
Solute transport coefficient, (B _s) (chlorophenol)	$8.468 \times 10^{-8} \left(\frac{m}{s}\right)$

Differential variables at t = 0

$$\begin{split} J_{w(0)} &= A_w \left((P_{b(0)} - P_p) - RT_{b(0)} \left(C_{w(0)} - C_{p(0)} \right) \right) \\ J_{s(0)} &= B_s \, \exp \left(\frac{J_{w(0)}}{k_{(0)}} \right) \left(C_{b(0)} - C_{p(0)} \right) \\ &\frac{\left(C_{w(0)} - C_{p(0)} \right)}{\left(C_{b(0)} - C_{p(0)} \right)} = \exp \left(\frac{J_{w(0)}}{k_{(0)}} \right) \end{split}$$

Assigned variables at t = 0:

 $C_{b(0)}, F_{b(0)}, C_{p(0)}, F_{p(0)}, T_{b(0)}$ and $T_{p(0)}$ [These are same as x = 0]

Table A.8. Dynamic 2D model equations (Model Type_2)

No	Title	The Mathematical Expression
140	TIUC	17
1	Dynamic axial and vertical water flux	$\frac{\mathrm{d}_{\mathrm{w}(x,y)}}{\mathrm{dt}} = \left\{ \left(A_{\mathrm{w}} \left((P_{\mathrm{b}(x,y)} - P_{\mathrm{p}(x,y)}) - RT_{\mathrm{b}(x,y)} \left(C_{\mathrm{w}(x,y)} - P_{\mathrm{b}(x,y)} \right) \right) \right\} \right\}$
	יטונוסמו שמנטו וועג	$C_{p(x,y)})) - J_{w(x,y)} \left\{ \begin{pmatrix} F_{b(x,y)} \\ t_f \Delta x \Delta y \end{pmatrix} \right\}$
2	Dynamic axial and vertical solute flux	$\frac{\mathrm{d}J_{s(x,y)}}{\mathrm{d}t} = \left\{ \left(B_s \exp\left(\frac{J_{w(x,y)}}{k_{(x,y)}}\right) \left(C_{b(x,y)} - C_{p(x,y)} \right) \right) - J_{s(x,y)} \right\} \left(\frac{F_{b(x,y)}}{t_f \Delta x \Delta y}\right)$
3	Dynamic axial and vertical membrane wall concentration	$ \frac{dc_{w(x,y)}}{dt} = \left\{ \left(C_{p(x,y)} + exp\left(\frac{J_{w(x,y)}}{k_{(x,y)}} \right) \left(C_{b(x,y)} - C_{p(x,y)} \right) \right) - C_{w(x,y)} \right\} \left(\frac{F_{b(x,y)}}{t_f \Delta x \Delta y} \right) $
4	Pressure difference along the two dimensions of the membrane	$\Delta P_{b(x,y)} = \left(P_{b(x,y)} - P_{p(x,y)}\right)$
5	Dynamic axial and vertical feed flow rate	$\begin{split} &\frac{\mathrm{d} F_{b(x,y)}}{\mathrm{d} t} = \left\{ \left[- (\Delta y) \left(J_{w(x,y)} \right) \right] - \left(\frac{\mathrm{d} F_{b(x,y)}}{\mathrm{d} x} \right) \right\} \left\{ \frac{F_{b(x,y)}}{t_f \Delta y} \right\} + \\ &\left\{ \left[- (\Delta x) \left(J_{w(x,y)} \right) \right] - \left(\frac{\mathrm{d} F_{b(x,y)}}{\mathrm{d} y} \right) \right\} \left\{ \frac{F_{b(x,y)}}{t_f \Delta x} \right\} \end{split}$
6	Dynamic axial and vertical feed pressure	$\begin{split} \frac{\mathrm{d}P_{b(x,y)}}{\mathrm{d}t} &= \left[\left[\left(\left(-b \; F_{b(x,y)} \right) \right) \left(\frac{F_{b(x,y)}}{\Delta x \; t_f} \right) \right] - \left[\left(\frac{\mathrm{d}P_{b(x)}}{\mathrm{d}x} \right) \left(\frac{F_{b(x,y)}}{\Delta y \; t_f} \right) \right] - \left[\left(\frac{\mathrm{d}P_{b(y)}}{\mathrm{d}y} \right) \left(\frac{F_{b(x,y)}}{\Delta x \; t_f} \right) \right] \right] \end{split}$
7	Dynamic axial and vertical permeated pressure	$\frac{dP_{p(x,y)}}{dt} = \left[\left[\left(\left(-b \ F_{p(x,y)} \right) \right) \left(\frac{F_{p(x,y)}}{\Delta y \ t_p} + \frac{F_{p(x,y)}}{\Delta x \ t_p} \right) \right] - \left[\left(\frac{dP_{p(x,y)}}{dx} \right) \left(\frac{F_{p(x,y)}}{\Delta y \ t_p} \right) \right] - \left[\left(\frac{dP_{p(x,y)}}{dy} \right) \left(\frac{F_{p(x,y)}}{\Delta x \ t_p} \right) \right] \right]$
8	Axial and vertical permeated flow rate	$F_{p(x,y)} = J_{w(x,y)} \Delta x \Delta y$
9	Dynamic axial and vertical molar flux of feed	$\begin{split} \frac{dC_{b(x,y)}}{dt} &= -\frac{C_{b(x,y)}}{t_f \Delta y} \frac{dF_{b(x,y)}}{dx} - \frac{F_{b(x,y)}}{t_f \Delta y} \frac{dC_{b(x,y)}}{dx} + \frac{d}{dx} \left[D_{b(x,y)} \frac{dC_{b(x,y)}}{dx} \right] - \\ \frac{C_{b(x,y)}}{t_f \Delta x} \frac{dF_{b(x,y)}}{dy} - \frac{F_{b(x,y)}}{t_f \Delta x} \frac{dC_{b(x,y)}}{dy} + \frac{d}{dy} \left[D_{b(x,y)} \frac{dC_{b(x,y)}}{dy} \right] - \frac{J_{s(x,y)}}{t_f} \end{split}$
10	Dynamic axial and vertical molar flux of permeate	$ \frac{\frac{C_{b(x,y)}}{t_f \Delta x}}{\frac{dF_{b(x,y)}}{dy}} - \frac{F_{b(x,y)}}{t_f \Delta x} \frac{dC_{b(x,y)}}{dy} + \frac{d}{dy} \left[D_{b(x,y)} \frac{dC_{b(x,y)}}{dy} \right] - \frac{J_{s(x,y)}}{t_f} \frac{dC_{p(x,y)}}{dy} - \frac{J_{b(x,y)}}{t_f} \frac{dC_{p(x,y)}}{dx} - \frac{J_{b(x,y)}}{t_f \Delta y} \frac{J_{b(x,y)}}{dx} + \frac{J_{b(x,y)}}{dx} \frac{J_{b(x,y)}}{dx} - \frac{J_{b(x,y)}}{dx} \frac{J_{b(x,y)}}{dx} - \frac{J_{b(x,y)}}{dx} \frac{J_{b(x,y)}}{dx} - \frac{J_{b(x,y)}}{dx} \frac{J_{b(x,y)}}{dy} - \frac{J_{b(x,y)}}{t_f \Delta x} \frac{J_{b(x,y)}}{dy} + \frac{J_{b(x,y)}}{dy} \frac{J_{b(x,y)}}{dy} + \frac{J_{b(x,y)}}{dy} + \frac{J_{b(x,y)}}{dy} \frac{J_{b(x,y)}}{dy} + J_{b(x,y$
11	Dynamic axial and vertical feed temperature	$\frac{\mathrm{dT_{b(x,y)}}}{\mathrm{dt}} = \left[\frac{F_{b(x,y)}\left(T_{b(x-1,y)} - T_{b(x,y)}\right)}{t_f \Delta x \Delta y}\right] - \left[\frac{J_{w(x,y)}\left(T_{b(x,y)} - T_{p(x,y)}\right)}{t_f}\right]$
12	Dynamic axial and vertical permeated temperature	$\frac{dT_{p(x,y)}}{dt} = \left[\frac{J_{w(x,y)} \left(T_{b(x,y)} - T_{p(x,y)} \right)}{t_f} \right]$
13	Total permeated flow rate	$F_{p(Total)} = \sum F_{p(x,y)}$
14	Total water recovery	$Rec_{(Total)} = \frac{F_{p(Total)}}{F_{b(0,y)}} x100$
15	Average solute rejection	$Rej_{(av)} = \frac{C_{b(x=L,y)} - C_{p(av)}}{C_{b(x=L,y)}} x100$
16	Average permeated concentration	$C_{p(av)} = \sum C_{p(x,y)}/n. \text{ sub } - \text{ divisions}$
17	Axial and vertical mass transfer coefficient	$k_{(x,y)} de_b = 246.9 D_{b(x,y)} Re_{b(x,y)}^{0.101} Re_{p(x,y)}^{0.803} C_{m(x,y)}^{0.129}$
18	Axial and vertical dimensionless solute concentration	$C_{m(x,y)} = \frac{C_{b(x,y)}}{\rho_w}$

Table A.8. Dynamic 2D model equations (Model Type_2) (Continued)

	Table 7.0. Byflamie 2B model equations (woder Type_2) (Gontinded)				
No	Title	The Mathematical Expression			
19	Axial and vertical feed diffusivity	$D_{b(x,y)} = 6.725 \times 10^{-6} \exp \left\{ 0.1546 \times 10^{-3} C_{b(x,y)} \times 18.01253 - \frac{2513}{T_{b(x,y)} + 273.15} \right\}$			
20	Axial and vertical permeated diffusivity	$D_{p(x,y)} = 6.725 \times 10^{-6} \exp \left\{ 0.1546 \times 10^{-3} C_{p(x,y)} \times 18.01253 - \frac{2513}{T_{p(x,y)+273.15}} \right\}$			
21	Axial and vertical feed viscosity	$ \mu_{b(x,y)} = 1.234 x 10^{-6} \exp \left\{ 0.0212 \ C_{b(x,y)} \ x 18.0153 + \frac{1965}{T_{b(x,y)} + 273.15} \right\} $			
22	Axial and vertical permeated viscosity	$\begin{split} &\mu_{p(x,y)} = 1.234 x 10^{-6} \ exp \bigg\{ 0.0212 \ C_{p(x,y)} \ x 18.0153 \ + \\ &\frac{_{1965}}{_{T_{p(x,y)}+273.15}} \bigg\} \end{split}$			
23	Axial and vertical feed density	$\begin{split} &\rho_{b(x,y)} = \\ &498.4 \; m_{f(x,y)} \sqrt{\left[248400 \; m_{f(x,y)}^2 + 752.4 \; m_{f(x,y)} \; C_{b(x,y)} \; x18.0153\right]} \end{split}$			
24	Axial and vertical permeated density	$\begin{split} &\rho_{p(x,y)} = \\ &498.4 \; m_{p(x,y)} \sqrt{\left[248400 \; m_{p(x,y)}^2 + 752.4 \; m_{p(x,y)} \; C_{p(x,y)} \; x18.0153\right]} \end{split}$			
25	Axial and vertical variable in Eq. (24)	$m_{f(x,y)} = 1.0069 - 2.757x10^{-4} T_{b(x,y)}$			
26	Axial and vertical variable in the above Equation	$m_{p(x,y)} = 1.0069 - 2.757x10^{-4} T_{p(x,y)}$			
27	Axial and vertical feed channel Reynolds number	$Re_{b(x,y)} = \frac{\rho_{b(x,y)} de_b F_{b(x,y)}}{t_f W \mu_{b(x,y)}}$			
28	Axial and vertical permeate channel Reynolds number	$Re_{p(x,y)} = \frac{\rho_{p(x,y)} de_{p} J_{w(x,y)}}{\mu_{p(x,y)}}$			
29	The equivalent diameter of feed channel	$de_b = 2t_f$			
30	The equivalent diameter of permeated channel	$de_p = 2t_p$			
Tota	Total number of equations is 30				

Table A.9. Specifications of variables

Items	Total
Variables:	
$J_{w(x,y)}, J_{s(x,y)}, P_{b(x,y)}, P_{p(x,y)}, T_{b(x,y)}, T_{p(x,y)}, C_{w(x,y)}, C_{b(x,y)}, C_{p(x,y)},$	
$F_{b(x,y)}, F_{p(x,y)}, k_{(x,y)}, F_{p(Total)}, \%Rec_{(Total)}, \%Rej_{(av)}, C_{p(av)}, de_b, de_p,$	39
$C_{m(x,y)}, D_{b(x,y)}, D_{p(x,y)}, \mu_{b(x,y)}, \mu_{p(x,y)}, \rho_{b(x,y)}, \rho_{p(x,y)}, m_{f(x,y)}, m_{p(x,y)},$	
$Re_{b(x,y)}$, $Re_{p(x,y)}$, $\Delta P_{b_{(x,y)}}$, A_w , B_s , L , W , ρ_w , b , t_f , t_p and ρ_w	
Differential variables at $t = 0$:	
$ \frac{dJ_{w(x,y)}}{dJ_{w(x,y)}} \cdot \frac{dJ_{s(x,y)}}{dJ_{s(x,y)}} \cdot \frac{dC_{w(x,y)}}{dF_{b(x,y)}} \cdot \frac{dP_{b(x,y)}}{dP_{b(x,y)}} \cdot \frac{dC_{b(x,y)}}{dQ_{b(x,y)}} $	10
dt dt dt dt dt dt dt dt	10
$\frac{dC_{p(x,y)}}{dt}$, $\frac{dT_{b(x,y)}}{dt}$ and $\frac{dT_{p(x,y)}}{dt}$	
t is independent variable	1
•	<u> </u>
Total	50

The specification of the dynamic model (Table A.9) shows that the total number of variables is 50, while the number of equations is 30 as can be seen in Table A.8, so:

D.F. = Total number of variables - Total number of equations

D.F. = 50 - 30 = 20

The number of parameters is 9 (Table A.10) and assigned initial values of differential variables at t=0 are 10 and independent variable =1, (time, t). So, this specification counts 20 variables.

Table A.10. Specifications of constant parameters and differential variables at t = 0

Parameter	Value
Feed spacer thickness (t _f)	0.8 mm
Permeate channel thickness (t _p)	0.5 mm
Module length (L)	0.934 m
Module width (W)	8.4 m
Molal density of water (ρ_w)	5.56 kmol/m³
Gas law constant (R)	0.082 (atm m³/K kmol)
Feed channel friction parameter (b)	9400.9 $\left(\frac{\text{atm s}}{\text{m}^4}\right)$
Solvent transport coefficient (A _w)	$9.42009 \times 10^{-7} \left(\frac{m}{a \text{tm s}}\right)$
Solute transport coefficient (B _s) (Dimethylphenol)	$2.22577 \times 10^{-8} \left(\frac{\text{m}}{\text{s}}\right)$
Differential variables at t = 0	

$$\begin{split} & J_{w(0,y)} \text{ from: } J_{w(0,y)} = A_w \left((\Delta P_{b(0,y)}) - RT_{b(0,y)} \left(C_{w(0,y)} - C_{p(0,y)} \right) \right) \\ & J_{s(0,y)} \text{ from: } J_{s(0,y)} = B_s \cdot \exp \left(\frac{J_{w(0,y)}}{k_{(0,y)}} \right) \left(C_{b(0,y)} - C_{p(0,y)} \right) \\ & C_{w(0,y)} \text{ from: } \frac{\left(C_{w(0,y)} - C_{p(0,y)} \right)}{\left(C_{b(0,y)} - C_{p(0,y)} \right)} = \exp \left(\frac{J_{w(0,y)}}{k_{(0,y)}} \right) \end{split}$$

$$J_{s(0,y)} \text{ from: } J_{s(0,y)} = B_s \cdot exp \left(\frac{J_{w(0,y)}}{k_{(0,y)}} \right) \left(C_{b(0,y)} - C_{p(0,y)} \right)$$

$$C_{w(0,y)} \text{ from: } \frac{(c_{w(0,y)} - c_{p(0,y)})}{(c_{b(0,y)} - c_{p(0,y)})} = exp\left(\frac{J_{w(0,y)}}{k_{(0,y)}}\right)$$

$$C_{p(0,y)} = 0$$

Assigned variables at t = 0:

 $C_{b(0,y)}$, $F_{b(0,y)}$, $C_{p(0,y)}$, $F_{p(0,y)}$, $T_{b(0,y)}$ and $T_{p(0,y)}$ [These are same as x=0]

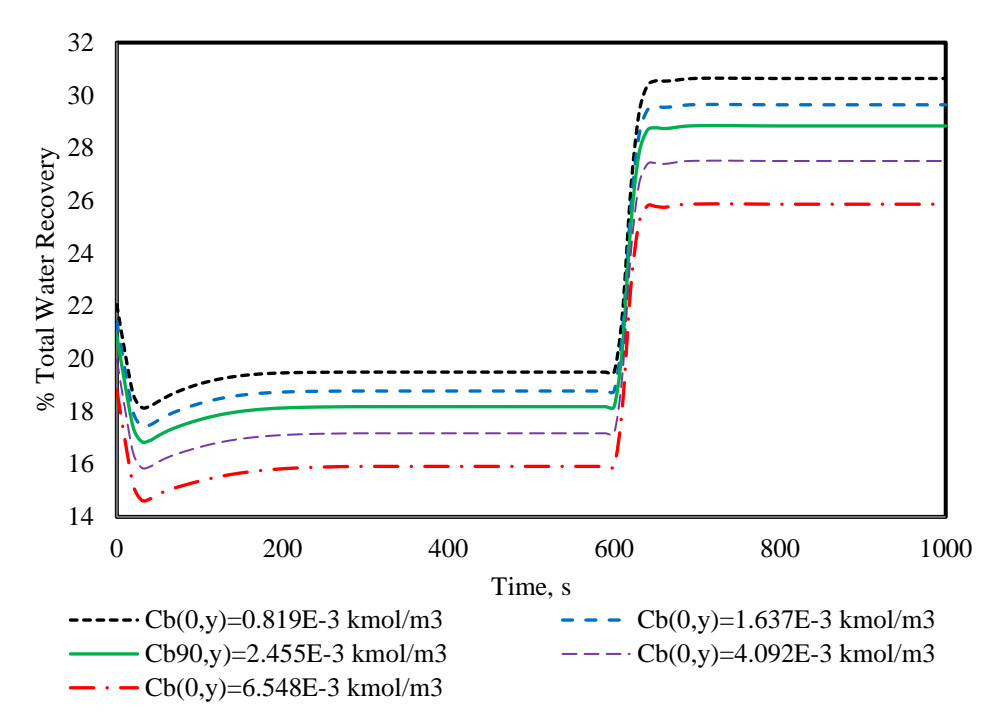


Fig. A.1. The result of the step change of operating pressure on total water recovery for several operating concentrations at operating conditions of 2.583x10⁻⁴ m³/s, 9.71 atm, and 31.5 °C

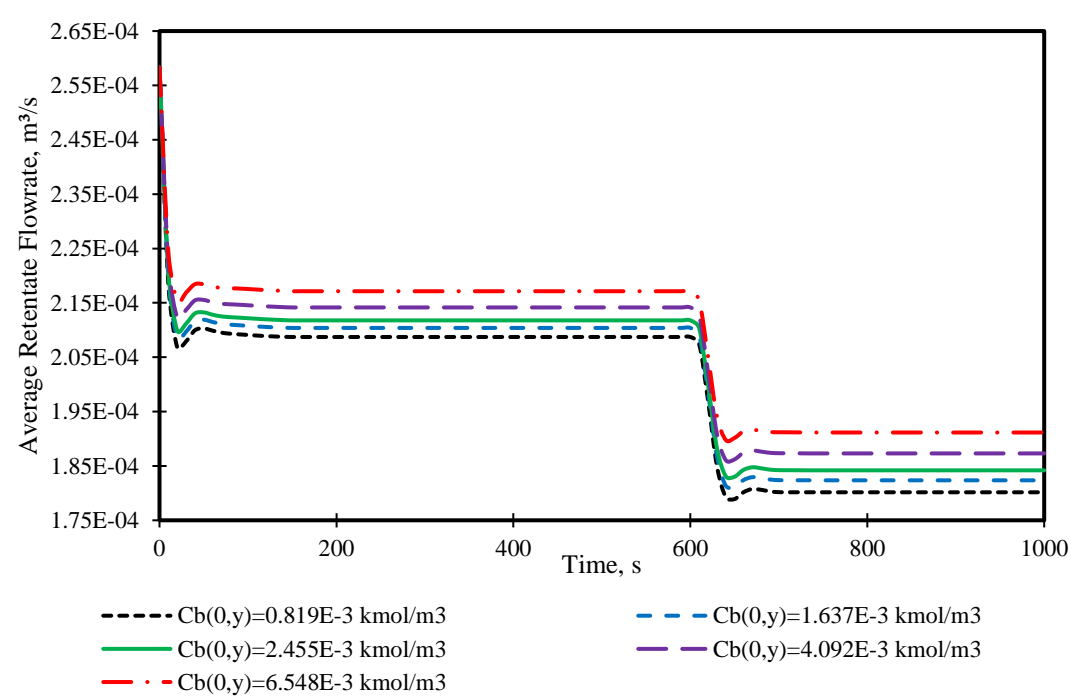


Fig. A.2. The result of the step change of operating pressure on retentate flow rate for several operating concentrations at operating conditions of 2.583x10⁻⁴ m³/s, 9.71 atm, and 31.5 °C

List of publications out of the author's PhD project Journals

- Al-Obaidi M.A., Mujtaba I.M., 2016. Steady state and dynamic modeling of spiral wound wastewater reverse osmosis process. Computers and Chemical Engineering, 90, 278–299. Impact Factor: 3.113.
- Al-Obaidi M.A., Kara-Zaïtri C., Mujtaba I.M., 2017. Development of a mathematical model for apple juice compounds rejection in a spiral-wound reverse osmosis process. Journal of Food Engineering, 192, 111–121. Impact Factor: 3.197.
- Al-Obaidi M.A., Kara-Zaïtri C., Mujtaba I.M., 2017. Wastewater treatment by spiral wound reverse osmosis: Development and validation of a two dimensional process model. Journal of Cleaner Production, 140, 1429– 1443. Impact Factor: 5.651.
- Al-Obaidi M.A., Li J-P., Kara-Zaïtri C., Mujtaba I.M., 2017. Optimisation of reverse osmosis based wastewater treatment system for the removal of chlorophenol using genetic algorithms. Chemical Engineering Journal, 316, 91–100. Impact Factor: 6.735.
- Al-Obaidi M.A., Kara-Zaitri C., Mujtaba I.M., 2017. Scope and limitations
 of the irreversible thermodynamics and the solution diffusion models for
 the separation of binary and multi-component systems in reverse osmosis
 process. Computers and Chemical Engineering, 100, 48–79. Impact
 Factor: 3.113.
- 6. Al-Obaidi M.A., Kara-Zaitri C., Mujtaba I.M., 2017. Modeling of a spiral-wound reverse osmosis process and parameter estimation. Desalination and Water Treatment, 69, 93–101. Impact Factor: 1.631.
- Al-Obaidi M.A., Kara-Zaïtri C., Mujtaba I.M., 2017. Optimum design of a multi-stage reverse osmosis process for the production of highly concentrated apple juice. Journal of Food Engineering, 214, 47–59. Impact Factor: 3.197.
- 8. Al-Obaidi M.A., Kara-Zaïtri C., Mujtaba I.M., 2017. Removal of phenol from wastewater using spiral-wound reverse osmosis process: Model development based on experiment and simulation. Journal of Water Process Engineering, 18, 20–28. Impact Factor: 3.61.
- 9. Al-Obaidi M. A., Kara-Zaïtri C., Mujtaba I.M., 2017. Simulation of full-scale reverse osmosis filtration system for the removal of N-

- nitrosodimethylamine from wastewater. Asia-Pacific Journal of Chemical Engineering, e2167, 1–13. Impact Factor: 1.238.
- Al-Obaidi M.A., Kara-Zaïtri C., Mujtaba I.M., 2018. Optimal reverse osmosis network configuration for the rejection of dimethylphenol from wastewater. Journal of Environmental Engineering, 144(1), (04017080-1) (04017080-9). Impact Factor: 1.541.
- 11. Al-Obaidi M.A., Kara-Zaïtri C., Mujtaba I.M., 2018. Significant energy savings by optimising membrane design in multi-stage reverse osmosis wastewater treatment process. Environmental Science: Water Research and Technology, 4, 449–460. Impact Factor: 3.649.
- 12. Al-Obaidi M.A., Kara-Zaïtri C., Mujtaba I.M., 2018. Simulation and optimisation of a two-stage/two-pass reverse osmosis system for improved removal of chlorophenol from wastewater. Journal of Water Process Engineering, 22, 131–137. Impact Factor: 3.61.
- 13. Al-Obaidi M.A., Kara-Zaïtri C., Mujtaba I.M., 2018. Simulation and optimisation of spiral-wound reverse osmosis process for the removal of N-nitrosamine from wastewater. Chemical Engineering Research and Design, 133, 168–182. Impact factor: 2.795.
- 14. Al-Obaidi M.A., Jarullah A.T., Kara-Zaïtri C., Mujtaba I.M., 2018. Simulation of hybrid trickle b e d reactor—reverse osmosis process for the removal of phenol from wastewater. Computers and Chemical Engineering, 113, 264–273. Impact Factor: 3.113.
- 15. Al-Obaidi M.A., Kara-Zaïtri C., Mujtaba I.M., 2018. Simulation and sensitivity analysis of spiral wound reverse osmosis process for the removal of dimethylphenol from wastewater using 2-D dynamic model. Journal of Cleaner Production, 193, 140–157. Impact Factor: 5.651.
- 16. Al-Obaidi M.A., Kara-Zaïtri C., Mujtaba I.M., 2018. Performance evaluation of multi-stage and multi-pass reverse osmosis networks for the removal of N-nitrosodimethylamine -D6 (NDMA) from wastewater using model-based techniques. Journal of Environmental Chemical Engineering, 6(4), 4797–4808. Impact Factor: 3.42.
- 17. Al-Obaidi M.A., Li J-P., Alsadaie S., Kara-Zaïtri C., Mujtaba I.M., 2018. Modelling and optimisation of a multistage reverse osmosis processes with permeate reprocessing and recycling for the removal of N-nitrosodimethylamine from wastewater using species conserving genetic

- algorithms. Chemical Engineering Journal, 350, 824–834. Impact Factor: 6.735.
- Al-Obaidi M.A., Alsarayreh A.A., Al-Hroub A.M., Alsadaie S., Mujtaba I.M., 2018. Performance analysis of a medium-sized industrial reverse osmosis brackish water desalination plant. Desalination, 443, 272–284. Impact Factor: 6.603.
- 19. Dhorat A., Al-Obaidi M.A., Mujtaba I.M., 2018. Numerical modelling and sensitivity analysis of natural draft cooling towers. Chemical Product and Process Modeling. Impact Factor: 0.44. DOI: https://doi.org/10.1515/cppm-2017-0078. https://www.degruyter.com/view/j/cppm.ahead-of-print/cppm-2017-0078.xml.
- 20. Filippini G., Al-Obaidi M.A., Manenti F., Mujtaba I.M., 2018. Performance analysis of hybrid system of multi effect distillation and reverse osmosis for seawater desalination via modeling and simulation. Desalination, 448, 21–35. Impact Factor: 6.603.
- 21. Al-Obaidi M.A., Kara-Zaïtri C., Mujtaba I.M., 2018. Performance evaluation of multi-stage reverse osmosis process with permeate and retentate recycling strategy for the removal of chlorophenol from wastewater. Accepted in Computer and Chemical Engineering (In press). Impact Factor: 3.113.
- 22. Dhorat A., Al-Obaidi M.A., Mujtaba I.M. Dynamic Modelling and Operational Optimisation of Natural Draft Cooling Towers. Accepted in Applied Thermal Engineering Journal (In press). Impact Factor: 3.771.

Conferences

- Al-Obaidi M.A., Kara-Zaïtri C., Mujtaba I.M, 2016. Development and validation of N-nitrosamine rejection mathematical model using a spiralwound reverse osmosis process. Chemical Engineering Transactions, 52, 1129–1134.
- M.A. Al-Obaidi, C. Kara-Zaïtri, I.M. Mujtaba, 2017. Optimisation of membrane design parameters of a spiral-wound reverse osmosis module for high rejection of dimethylphenol from wastewater at low energy consumption. Editor(s): Antonio Espuña, Moisès Graells, Luis Puigjaner. Computer Aided Chemical Engineering, Elsevier, Volume 40, Pages 2713-

- 2718, ISSN 1570-7946, ISBN 9780444639653, https://doi.org/10.1016/B978-0-444-63965-3.50454-2. (https://doi.org/10.1016/B978-0-444-63965-3.50454-2. (https://doi.org/10.1016/B978-0-444-63965-3.50454-2. (https://www.sciencedirect.com/science/article/pii/B978044463965350454. 2).
- Mudhar A. Al-Obaidi, Chakib Kara-Zaïtri, Iqbal M. Mujtaba, 2018. Modeling the performance of low pressure reverse osmosis membrane system for N-nitrosamine rejection. Editor(s): Anton Friedl, Jiří J. Klemeš, Stefan Radl, Petar S. Varbanov, Thomas Wallek. Computer Aided Chemical Engineering, Elsevier, Volume 43, Pages 19-24, ISSN 1570-7946, ISBN 9780444642356, https://doi.org/10.1016/B978-0-444-64235-6.50006-1 (https://doi.org/10.1016/B978-0-444-64235-6.50006-1
- Al-Obaidi M.A., Kara-Zaïtri C., Mujtaba I.M, 2018. Simultaneous removal of organic compounds from wastewater using reverse osmosis process: Modelling, simulation, and optimisation. Mario R. Eden, Marianthi lerapetritou and Gavin P. Towler (Editors) Proceedings of the 13th International Symposium on Process Systems Engineering – PSE 2018, July 1-5, 2018, San Diego, California, USA.
- Al-Obaidi M.A., Kara-Zaïtri C., Mujtaba I.M, 2018. Statistical-based modeling and optimization of chlorophenol removal from wastewater using reverse osmosis process. Chemical Engineering Transactions, 70. ISBN 978-88-95608-67-9; ISSN 2283-9216.

Books Chapters

- Mujtaba I.M., Alsadai S.M., Al-Obaidi M.A., Patel R., Sowgath M.T., Manca D., Desalination, Model-Based Techniques in Desalination Processes: A Review, in: I. M. Mujtaba, R. Srinivasan, N. Elbashir (Eds.), The Water-Food-Energy Nexus, Processes, Technologies, and Challenges, CRC Press, Taylor & Francis Group, Boca Raton, 2018, pp. 3-40.
- Mujtaba I.M., Al-Obaidi M.A., Kara-Zaïtri C. Applications of reverse osmosis for the removal of organic compounds from wastewater: A stateof-the-art from process modelling to simulation. Organic Pollutants in Wastewater II Methods of Analysis, Removal and Treatment Eds. Inamuddin, Mohd Imran Ahamed, Shadi Wajih Hasan Materials Research

- Foundations Volume 32. Publication Date 2018, 203 Pages Print ISBN 9781945291708 (release date May 15th, 2018).
- 3. Al-Obaidi M.A., Kara-Zaïtri C., Mujtaba I.M. RO process for the removal of phenol and phenolic compounds from wastewater: Process modelling, simulation and optimisation. Accepted chapter in the book titled "Water Management: social and technological perspective" (In press).